Unclassified **NEA/CSNI/R(2009)3**

Organisation de Coopération et de Développement Économiques
Organisation for Economic Co-operation and Development

03-Aug-2009

English text only

NUCLEAR ENERGY AGENCY
COMMITTEE ON THE SAFETY OF NUCLEAR INSTALLATIONS

NEA/CSNI/R(2009)3
Unclassified

ABILITY OF CURRENT ADVANCED CODES TO PREDICT CORE DEGRADATION, MELT PROGRESSION AND REFLOODING

Benchmark Exercise on an Alternative TMI-2 Accident Scenario

JT03268437

English text only

Ability of Current Advanced Codes to Predict Core Degradation, Melt Progression and Reflooding

Benchmark Exercise on an Alternative TMI-2 Accident Scenario

Participating Organizations and Authors

ENEA	Giacomino Bandini
GRS	Henrique Austregesilo
IKE	Michael Buck
IRSN	Olivier Marchand & Florian Fichot
IVS	Miro Branak & Peter Matejovic
SNL	Larry Humphries
SNU	Kune Suh
UPI	Sandro Paci

TABLE OF CONTENTS

1. ABBREVIATIONS

AFW	Auxiliary Feed Water
CCFL	Counter Current Flow Limitation
CL	Cold Leg
CSNI	Committee on the Safety of Nuclear Installations
DC	Downcomer
DOE	Department of Energy
EC	European Community
ECCS	Emergency Core Coolant System
GAMA	Working Group on Accident Management and Analysis
GRS	Gesselschaft für Anlagen und Reaktorsicherheit mbH (Germany)
HL	Hot Leg
HPI	High Pressure Injection
IKE	Institut für Kernenergetik und Energiesysteme - Universität Stuttgart
IRSN	Institut de Radioprotection et de Sûreté Nucléaire (France)
ISP	International Standard Problem
IVS	Inzinierska Vypoctova Spolocnost (Slovakia)
LOCA	Loss Of Coolant Accident
LOFT	Loss-of-Fluid Test (experimental facility at Idaho National Engineering Laboratory, USA)
MATPRO	Materials Properties correlations and computer subcodes
NPP	Nuclear Power Plant
NRC	U.S. Nuclear Regulatory Commission
PHÉBUS	Experimental facility at Cadarache, France
PWR	Pressurized Water Reactor
QUENCH	Experimental facility at Forschungszentrum Karlsruhe, Germany
SAM	Severe Accident Management
SARNET	Severe Accident Research Network
SB-LOCA	Small Break-Loss of Coolant Accident
SG	Steam Generator
SGTR	Steam Generator Tube Rupture
SNU	Seoul National University (Korea)
TMI-2	Three Mile Island – Unit 2
TSO	Technical Support Organisation
UPI	University of Pisa (Italy)
US	United States of America

2. LIST OF FIGURES

3. EXECUTIVE SUMMARY

3.1 Background

The experimental database on core degradation and melt relocation (and their consequences on hydrogen production, vessel rupture) is limited to small-scale experiments which are only partially representative of what could occur in a reactor. As a consequence, there is uncertainty in the capability of codes to predict core degradation in postulated severe accident transients of nuclear power plants. The GAMA has launched an action in order to determine the ability of current advanced codes to predict core degradation in nuclear reactors. The TMI-2 scenario was selected as the case to analyze since it concerns the only full scale Pressurized Water Reactor to have experienced core degradation. Data from the code calculations were compared to the TMI-2 end-state to determine the codes' predictive capability. The study was completed in 2004, and is documented in ref. 2. One conclusion of the study is that variability in the codes predictions existed in part because initial conditions of the tMI-2 scenario were not well defined. It was concluded that code variability could be better evaluated if these conditions were better defined. Therefore, an additional task was proposed to benchmark the codes. This phase II study evaluates the variability in the codes' results using a postulated core degradation scenario of the TMI-2 reactor. The scenario was specified with simple initial and boundary conditions so that the influence of uncertainty of these conditions was minimized and the variability in the codes' results is more readily determined.

3.2 Objectives

This phase II exercise is the first benchmarking of severe accident codes promoted by NEA in almost 20 years. The objective of Phase II of the exercise was to perform a code benchmark on a well-defined plant (similar to TMI-2) and with prescribed boundary conditions. Therefore, the benchmark avoided additional and unwanted sources of discrepancies between code calculations, so as to focus on the variability of the codes calculations of core degradation. This report includes all the information concerning the preparation of the benchmark, the results, and the conclusions of the exercise.

3.3 Definition of the Alternative Scenario and Analysis of Benchmark Results

The first meeting of the group of participants in Phase II was held in November 2005 and the final results were received in January 2008, which gives a total duration of slightly more than 2 years for this phase. For the new benchmark exercise, an alternative scenario was proposed. The standard TMI-2 plant is modelled, with the complete primary circuit (loops A and B) and a simplified secondary circuit. The initial plant state corresponds to the standard TMI-2 accident sequence. The accident is initiated by a small break located at 4m along the hot leg A. It is followed by a stop of primary pumps when the mass of water contained in the primary system is lower than 85 tons. The HPI operation is delayed until 5000s after the stop of primary pumps. This scenario leads to a significant degradation and core melting before the reflooding of the core. The complete sequence was thus divided in three phases. Participants met and had group discussions between each phase. Relevant variables were selected for comparison, and benchmark results were assessed. Previous benchmark exercises on TMI-2, and other benchmarks and

International Standard Problems (ISP) were taken into account in the assessment too. Sensitivity analysis of some input and model parameters were performed by participants.

3.4 Main Results

At the end of this exercise, it is possible to conclude that:

- A reference severe accident scenario, initiated by a SB-LOCA, based on a TMI-2 plant model, and with prescribed boundary conditions was defined.
- A set of output variables was proposed and accepted by the participants, which allowed the assessment of the quality of the calculation results.
- This scenario can be used as a reference calculation to assess the agreement between current codes or even for an adequate training of a code user.

The main results of the exercise, regarding the ability of the participating codes' calculations of severe accidents are the following:

- For the initial transient, up to the primary system pumps trip, the calculated results are in good agreement. The states of the core and the primary circuit calculated by all codes are very similar at the time of pump trip. The main discrepancies are in the calculation of the void fraction in the core, and the calculation of the time of pump stop, but those discrepancies are considered acceptable.
- For the degradation phase, up to the reflooding of the core, the results show a rather good agreement between all participants for global calculation of results such as total hydrogen production and total mass of molten materials. The variability in these results is not only much better than the results obtained in the benchmark exercise performed 20 years ago, but is also comparable or even better than the variability obtained in recent benchmarks on integral tests (PHEBUS-FPT1 and QUENCH-11). This result shows a significant improvement of the codes in the last two decades.
- For the reflooding phase, there is a general agreement on the calculated pressure increase, on the total hydrogen mass produced during this phase, and on the increased rate of core degradation. However, although all codes agree, some results may be questionable as they are apparently in contradiction with experimental observations (LOFT and QUENCH for example) and with the TMI-2 assumed evolution. In addition, there is a lack of agreement on the calculated efficiency of quenching. It can be concluded that, despite considerable improvement in codes abilities, more modelling and assessment should be done before codes can be considered reliable enough to calculate the reflooding phase.
- Sensitivity studies performed by participants have shown that variations of some key empirical model (such as the cladding failure criteria) could induce a variation in some calculation results (such as hydrogen production) obtained by a single participant, which is of the same order of magnitude as the variation obtained when comparing different codes and/or participants. This indicates that some physical processes are still poorly known and inadequately modeled.

3.5 Conclusions and recommendations

The surprisingly reduced scatter of the global calculation results is probably due to the fact that code models have been assessed globally and adjusted on the same basis of integral tests but also to the participation of very experienced code users. Such conclusion raises again the issue of the importance of adequate user training, in particular for utilities and TSOs who submit safety studies to regulatory

bodies. Also it raises the issue of having good user manuals and guidelines, which must reduce to a minimum user's uncertainty and "guessing" when building inputs.

Overall, the results of this exercise are quite encouraging. First, all the codes succeeded in calculating the scenario from the beginning to the end, with very little tuning of parameters or optimization of input decks. This shows the robustness of current codes, which is a great progress compared to the state of codes 20 years ago when several codes could not calculate the complete TMI-2 sequence. Moreover, it appears that the codes' global results are significantly more consistent than they were 20 years ago.

The code scattering in the calculation of some phenomena revealed some model weaknesses. Three major phenomena are concerned. The first one is oxidation of molten mixtures and their relocation. The second one is the prediction of UO2 melting and its interaction with molten corium. The third one is the core coolability and the behaviour of hot corium when the vessel is entirely reflooded. The weaknesses of codes in the prediction of those phenomena are not surprising because experimental data are scarce and the physical understanding is still incomplete.

The benchmark exercise involved some of the most important system codes which are currently used by utilities, TSO's, and regulatory agencies. Because of that, the benchmark has provided substantial and important insights. However, due to the limited number of participants and the fact that only one scenario was calculated, the conclusions of this benchmark exercise must be considered with caution.

4. INTRODUCTION

The experimental database on core degradation and melt relocation (and their consequences on hydrogen production, vessel rupture) is limited to small-scale experiments which are only partially representative of what could occur in a reactor. As a consequence, there is uncertainty in the capability of codes to predict core degradation in postulated severe accident transients of nuclear power plants.

A first benchmark exercise was conducted 20 years ago by OECD/NEA and US/DOE, involving participants from several countries and various codes to calculate the TMI-2 accident transient. The results were made available in 1988. This was followed by other reactor benchmarks, mainly in the framework of EC programs.

The GAMA has launched an action in order to determine the ability of current advanced codes to predict core degradation in nuclear reactors. The TMI-2 scenario was selected as the case to analyze since it concerns the only full scale Pressurized Water Reactor to have experienced core degradation. Data from the code calculations were compared to the TMI-2 end-state to determine the codes' predictive capability. The study was completed in 2004, and is documented in ref. 2. One conclusion of the study is that variability in the codes predictions existed in part because initial conditions of the tMI-2 scenario were not well defined. It was concluded that code variability could be better evaluated if these conditions were better defined. Therefore, an additional task was proposed to benchmark the codes. This phase II study evaluates the variability in the codes' results using a postulated core degradation scenario of the TMI-2 reactor. The scenario was specified with simple initial and boundary conditions so that the influence of uncertainty of these conditions was minimized and the variability in the codes' results is more readily determined. Considering the interest of this Phase 2, it was decided to open the exercise also to organizations which were not directly involved with GAMA but belonged to the EC SARNET network where a similar activity on reactor benchmarks was also planned.

Several participants (from GAMA and SARNET), all of them experts in using severe accident codes, have been involved in the activity. The codes used are the most widely used system codes throughout the world, with maybe the only exception of the SCDAP/RELAP code. The strategy of the project was to first define a schematic scenario or "alternative TMI-2 scenario" that would lead to core uncovery and a large degradation before reflooding the vessel. Then, this initial scenario was slightly refined in order to obtain the expected state of degradation and to allow a proper comparison of all results. It was also an opportunity for all participants to review extensively their input decks for the TMI-2 reactor and to update them.

In this report, complete descriptions of the modelling of the core, the steady state, the initiating event, the boundary conditions and the transient scenario are provided. The physical parameters selected for comparison, and the criteria used to judge the quality of the comparisons are also listed and discussed. The results are compared and conclusions about the predictive qualities of the codes are drawn. Sensitivity studies were also made and their results are discussed. Finally, general conclusions of this exercise are drawn and proposals to continue this benchmark activity are given. In the Appendix to this report, all participants have provided their complete individual results and their views and opinions about the comparisons.

Twenty years ago, one of the conclusions of the first benchmark exercise was the expectation that "significant progress in the severe accident code capabilities could be achieved in the future". The main goal of this report is to measure the progress made in twenty years.

5. PLANT DESCRIPTION AND ALTERNATIVE TRANSIENT DEFINITION

For the accurate prediction of the TMI-2 transient, the proper definition of boundary conditions and plant characteristics is essential. However, some of these data are either unknown or difficult to estimate. In particular, the data for the make-up and let-down flows were not recorded during the accident. Although these data do not bring any improvement in the understanding of severe accident processes, they have required important efforts from code users who have tried to estimate them. To avoid such problems, a new benchmark exercise is proposed, based on an alternative scenario. The objective is to do the calculations on a well-defined plant (similar to TMI-2, for convenience) and with prescribed boundary conditions, in order to avoid additional and unwanted sources of discrepancies between code predictions.

The standard TMI-2 plant is modelled, with the complete primary circuit (loops A and B) and a simplified secondary circuit. The details are given below. The geometry of the circuits is provided in the following section. The initial state corresponds to the standard TMI-2 sequence (see table below for the thermal-hydraulic conditions)

5.1 Initiating Event

Loss of main feedwater.

Opening of a small break on hot leg A:

- size : 0.001 m^2
- position : 4 m along hot leg A

5.2 End of calculation

The calculation is stopped a few thousand seconds after the HPI operation or as soon as the core is completely cooled down.

5.3 Main Assumptions

- No PORV failure.
- Stop of primary pumps when the primary water mass is less than 85 tons.
- Delayed HPI operation: 5000s after the stop of primary pumps. 30 kg/s, per loop (60kg/s total).
- No let-down flow.
- All other parameters are standard TMI-2 parameters (in particular the behaviour of vent valves between the upper plenum and the top of the downcomer: details are provided below).

5.4 Power

- Initial core power = 2700 MW
- Core power transient as shown in the table below
- Thermal heat losses from primary system to containment atmosphere are not taken into account

Time (s)	Power (W)
0	2700e6
1	167.94e6
4	147.96e6
10	130.14e6
40	103.14e6
100	86.13e6
400	65.34e6
800	52.92e6
1000	49.95e6
2000	42.39e6
4000	34.56e6
8000	28.35e6
10000	26.05e6
20000	21.46e6

- Core heat flux profile

– Axial profile:

Z (m)	Factor
0	0
0.15	0
0.302	0.675
0.607	0.857
0.912	1.037
1.217	1.153
1.522	1.202
1.826	1.231
2.131	1.241
2.436	1.209
2.893	1.102
3.503	0.595
3.81	0
4	0

– Radial profile

Ring	Factor
1	1.2572
2	1.2127
3	1.1469
4	1.0596
5	0.951
6	0.8198

5.5 Boundary Conditions

Boundary conditions for primary system make-up flow = 3.0 kg/s (total).

Boundary conditions for secondary system are given by the regulation of steam generator pressures and water levels (see figures 5-1 and 5-2 below).

Figure 5-1 : SG Level regulation

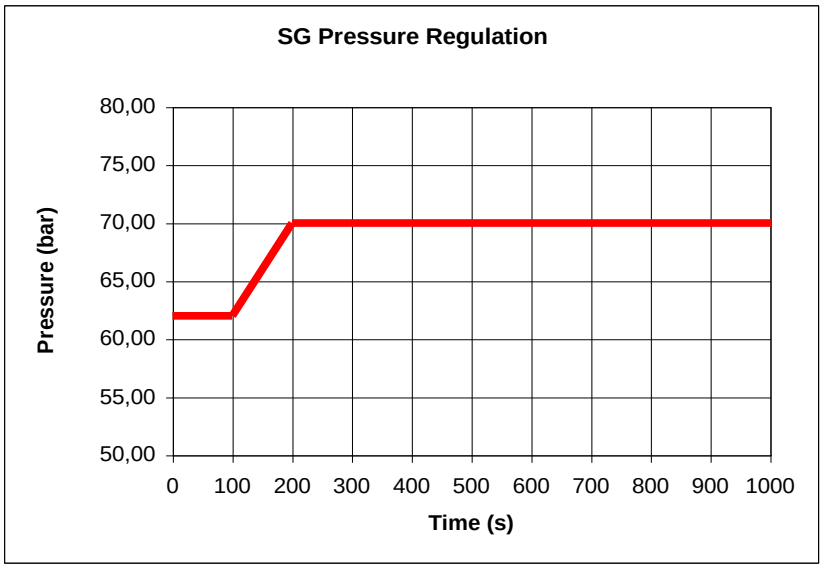

Figure 5-2 : SG Pressure regulation

6. GEOMETRY

6.1 Free volumes

- Primary system volume without the pressurizer = 294.6 m^3
- Pressurizer volume = 43 m^3
- RPV volume = 116.5 m^3
- Secondary side free volume of 1 SG (up to the SG exit) = 34.4 m^3

6.2 Heat transfer with secondary side

SG tubes surface (secondary side)/SG = 12302.5 m^2
- Number of tubes/SG = 15530

6.3 Initial core geometry

Main characteristics of the core

- Number of fuel bundles of type 15x15 = 177
- Active core length = 3.66 m
- Total core length = 4.00 m (from core bottom: 0.15+3.66+0.19)
- Type of fuel lattice = square, pitch = 0.01443 m
- Number of fuel rods/assembly = 208
- External diameter of fuel rod = 0.0109 m
- Fuel pellet radius = 0.0047 m
- Fuel rod cladding thickness = 0.000673 m

Initial core material inventory

- UO2 mass = 93650 kg (over the 3.66 m of core active length)
- Zircaloy mass = 23050 kg (H2 total mass if converted from total zircaloy = 1011 kg (mZr/22.8))
- AIC mass (Ag+In+Cd) = 2750 kg
- Core baffle internal diameter = 3.28 m
- Core baffle external diameter = 3.33 m
- Core barrel internal diameter = 3.584 m
- Core barrel external diameter = 3.683 m

Core meshing

- Radial rings = 5 or 6
- Axial meshes (over total core length) = 20 , mesh size = 0.20 m (all meshes with equal height)

6.4 Vent valves

These valves, between the upper plenum and the top of the downcomer, are designed to avoid a direct loss of water by the hot leg. They should be modelled, as they were shown to have an influence on the transient. In the ICARE/CATHARE code model, these valves are modelled as follows:

- If $\Delta p < 414$ Pa, the valves are closed.
- If $\Delta p > 1724$ Pa, the valves are fully open, which corresponds to a total section of 0.794 m^2.
- If $414 < \Delta p < 1724$, the valves are considered partly open, with a cross section area increasing linearly with Δp.

7. CHOICE OF PHYSICAL PARAMETERS TO COMPARE

7.1 Parameters selected for comparison

A selection of parameters to compare was made, according to several criteria. The first criterion is the relevance for safety and/or severe accident management (i.e. primary pressure, hydrogen production, core exit temperature),. The second criterion is the monitoring of the reactor state (i.e. water inventory, mass of molten materials). The third and last criterion is the significance for more detailed comparisons of models (i.e. break flow rate, mass of dissolved UO2). The parameters selected for comparison are listed in the following table, with the criteria for their selection.

Variables	Criterion of selection
Steam Generator A Pressure	Monitoring of circuits
Steam Generator A Level	Monitoring of circuits
Steam Generator B Pressure	Monitoring of circuits
Steam Generator B Level	Monitoring of circuits
Pressuriser Pressure	Accident management
Pressuriser Level	Monitoring of circuits
Loop A Flow Rate	Monitoring of circuits
Loop B Flow Rate	Monitoring of circuits
Pump A void fraction	Comparison of models
Pump B void fraction	Comparison of models
Hot Leg A Temperature (at the position 12m)	Monitoring of circuits
Hot Leg B Temperature (at the position 12m)	Monitoring of circuits
Cold Leg A Temperature	Monitoring of circuits
Cold Leg B Temperature	Monitoring of circuits
Break Flow Rate	Comparison of models
Total Primary Mass	Monitoring of circuits
Swollen Water Level in the Core (2)	Comparison of models
Collapsed Water Level in the Core (2)	Comparison of models
Cumulated Hydrogen production	Accident management
Power exchanged with SG A	Monitoring of circuits

Variables	Criterion of selection
Power exchanged with SG B	Monitoring of circuits
Instantaneous Hydrogen production	Comparison of models
Total mass of molten materials (i.e. materials which have melted but may have frozen at lower levations)	Monitoring of core state
Total mass of molten metals (same as above)	Comparison of models
Total mass of dissolved UO2 (i.e. removed by chemical interaction with molten Zr)	Comparison of models
Fraction of non-oxidized Zr in the molten materials (i.e. ratio between the mass of molten Zr and the molten mass ZR+ZrO2)	Comparison of models
Total mass of debris (if available in the modelling)	Monitoring of core state
Total mass of molten pool (if any, but it may also be approximated as the total mass of liquid materials)	Monitoring of core state
Rod temperature at the bottom of the core	Monitoring of core state
Rod temperature in the middle of the core	Monitoring of core state
Rod temperature at the top of the core	Monitoring of core state
Gas Temperature at the entrance of the Hot Leg	Accident management
Total decay power	Monitoring of core state
Water level in downcomer	Monitoring of circuits
Water level in bypass	Monitoring of circuits
Fraction of non-oxidized Zr in all the core (i.e. ratio between the initial total mass of Zr and the total mass ZR+ZrO2)	Monitoring of core state

7.2 Criteria for the quality of agreement

To be able to claim that a set of results is in good agreement with another one, one has to define subjective criteria reflecting the level of uncertainty that is acceptable for a specific physical parameter calculateed by a code. The choice can be made either from a safety analysis point of view, or with a more pragmatic point of view, by comparing with uncertainties obtained in previous benchmarks. Because there are no regulations or rules which define what can be considered as “acceptable” uncertainty in safety studies, the first criterion was not used. Rather, what is essential from the regulatory point of view is that license applications based on best-estimate calculations, include a thorough and complete evaluation of uncertainties using accepted methods. Because of that, the second option was selected and the following table provides the uncertainty ranges obtained in the current benchmark, to be compared with the uncertainties obtained in the previous TMI-2 benchmark, in the PHEBUS-FPT1 benchmark, which is relevant for late phase degradation and in the QUENCH-11 benchmark, which is relevant for transients involving core dry-out followed by reflooding. For some variables, no criteria could be found in previous benchmarks to judge the quality of agreement (they appear with the mention “NA” in the following table). For those variables, the acceptable range of uncertainty was decided among the participants by “expert judgement”.

Variables	Current benchmark	Previous benchmarks
Time of pump stop	+/- 3 %	specified
Minimum Steam Generator Pressure	+/- 11 %	NA
Maximum Steam Generator Level	+/- 11 %	NA
Primary Pressure before reflooding	+/- 14 %	> 30% TMI2
Loop Flow Rate before pump stop	+/- 40 %	NA
Loop Flow Rate during core reflood		> 200% Q11
Pump A void fraction (at pump stop)	+/- 10 %	NA
Maximum Core Temperature	+/- 300K ~11 %	+/- 350K TMI2 +/- 150K FPT1 +/- 500K Q11
Maximum Hot Leg Temperature	+/- 10 %	NA
Break Flow Rate	+/- 30 %	NA
Total Primary Mass at pump stop	+/- 28 %	+/- 50% Q11
Swollen Water Level in the Core (before HPI operation)	+/- 10 %	NA
Collapsed Water Level in the Core		NA
Time of oxidation runaway	+/- 42 %	17% TMI2
Cumulated Hydrogen production	+/- 18 %	+/- 33% TMI2 +/- 10% FPT1 +/- 20% Q11
Power exchanged with SG		NA
Max. Instantaneous Hydrogen production	+/- 30 %	NA
Total mass of molten materials	+/- 35 %	+/- 67% FPT1 +/- 100% Q11
Total mass of molten metals	+/- 16 %	NA
Total mass of dissolved UO2	+/- 80 %	NA
Fraction of non-oxidized Zr in the molten materials	+/- 100 %	NA
Fraction of non-oxidized Zr (total)	+/- 10 %	NA

8. COMPARISONS BETWEEN PARTICIPANTS RESULTS

The main objective of the benchmark exercise was to compare the calculations of core degradation and reflooding. However, any severe accident sequence starts with an initial, purely thermalhydraulic, transient phase which can last a significant time, depending on the scenario. The impact of that initial transient on the subsequent degradation is quite important because it determines the time of core uncovery and heat-up. Therefore the comparisons include that phase too. The sequence was divided into 3 phases: initial thermalhydraulic phase (until main pumps stop), core degradation phase and reflooding phase. Calculation of the sequence was preceded by the calculation of an "Initial Steady State".

8.1 Initial Steady State

The steady state is calculated by all codes. Differences in the calculated values are not significant and can be considered as acceptable. The following table indicates the steady-state values obtained by each participant and also for comparison the "reference values" obtained from TMI-2 measurements.

		ENEA	GRS	DIMNP	SNL	IRSN	IVS	SNU	IKE	**TMI-2**
		ASTEC 1.3	ATHLET-CD	MELCOR 1.8.5	MELCOR 1.8.6	ICARE/ CATHARE	ASTEC 1.3	MAAP4	ATHLET/ MEWA	
Reactor Power	W	2700	2663	2770	2700	2700	2700	2700		**2700**
Primary Pressure	MPa	15.2	14.9	15.2	15.0	15.02	15.32	15.2		**15.2**
Temperature Hot Leg A	K	592.1	592.2	592	592	592.3	592.9	579		**592**
Temperature Hot Leg B	K	592.1	592.2	592	592	592.3	592.9	579		**592**
Temperature Cold Leg A	K	563.8	564.8	563.6	564	566.3	565.1	559		**548-561**
Temperature Cold Leg B	K	564.1	564.8	563.6	564	564.7	565.1	559		**565**
Mass Flow Rate – Loop A	kg/s	8290	8638	8520	8737	8805	8501	?		**8280**
Mass Flow Rate – Loop B	kg/s	8560	8675	8520	8828	8846	8498	?		**8560**
Pressurizer Level	M	5.78	5.78	5.68	5.77	5.60	5.69	6.78		**5.77**
Total Primary Mass	ton	225120	223300	230850	231273	23038	221515	211170		-
Pressure SG A	MPa	6.80	6.34	6.41	6.42	6.38	6.247	6.38		**7.31**
Pressure SG B	MPa	6.80	6.20	6.41	6.27	6.24	6.246	6.38		**7.24**

		ENEA	GRS	DIMNP	SNL	IRSN	IVS	SNU	IKE	**TMI-2**
		ASTEC 1.3	ATHLET-CD	MELCOR 1.8.5	MELCOR 1.8.6	ICARE/ CATHARE	ASTEC 1.3	MAAP4	ATHLET/ MEWA	
Steam Temperature SG A	K	574	568	569.5	568	584.9	578.8	508		**586**
Steam Temperature SG B	K	575	568	569.5	567	583.6	578.0	508		**586**
Collapsed Level SG A	M	3.7	4.03	?	5.6	5.26	3.81	3.28		-
Collapsed Level SG B	M	3.5	3.54	?	5.1	5.39	3.65	3.28		-
Liquid Mass SG A	Kg	19210	14630	?	18700	18425	15303	17506		-
Liquid Mass SG B	Kg	18410	13140	?	16900	18989	14409	17506		-
Feedwater Flow SG A	Kg/s	742	743.7	761.6	750	700	746.5	756		**723**
Feedwater Flow SG B	Kg/s	759	738.5	761.6	770	742	737.2	756		**717**
SG Feedwater Temperature	K	513	503	510.9	513	513	513	508		-

8.2 Initial thermal-hydraulic phase up to the stop of main pumps (~5000s)

The first phase is governed mainly by the mass flow rate at the break and the heat transfer to the secondary circuit.

8.2.1 Mass flow rate at the break

Looking at the curves, we can observe a very good coincidence of the results for most of the codes. Five of the curves are almost identical. Discharge from the break can be divided in thre phases: liquid discharge up to the reaching of saturated conditions at about 200 sec, two-phase discharge until about 4500 or 5000 sec when the main pumps are stopped, and steam discharge up to the start of the reflooding phase at about 10000 sec. The UPI-MELCOR calculation shows a slightly different behaviour of the break mass flow rate during the two-phase discharge, which becomes constant after some time, instead of slowly decreasing like the other ones. This leads to reach earlier the criterion for the stop of pumps. The SNU-MAAP4 calculation shows a slightly lower flow rate after the initial rapid depressurization and the latest time for pump stop.

8.2.2 Primary mass

As a result of the agreement for the previous parameter, there is a very similar evolution of the primary mass calculated by all participants. This is a surprisingly good result because larger discrepancies were expected, considering that there was almost no “tuning” of the codes or the input decks, and the slight discrepancies in the break flow rate for some codes. Five calculations indicate almost the same time of pump stop, just before 5000s. The UPI-MELCOR calculation predicts it 500s earlier and the SNU-MAAP4 calculation predicts it 400s later.

8.2.3 Heat transfers with secondary side

Again, most of the curves coincide, indicating that the energy balance of the primary circuit is very similar for all calculations. However, the ASTEC calculations (ENEA and IVS) show a higher value of the heat transfers (approximately 100% higher than the others, at the end of the thermal hydraulics phase). This is probably due to the overestimation of pump heat loss into the primary coolant. The SNU-MAAP4 results show very strong oscillations which do not appear in the other calculations. No explanation of that behaviour has been provided, but it seems related to oscillations which appear also in SG A pressure and SG A level until the pumps stop.

8.2.4 Water levels in the core

More significant differences appear when comparing the water levels. Most codes calculate that the core remains wet during all the thermal hydraulics phase (swollen level at the top of the core) although the GRS-ATHLET calculation shows an early and steady decrease of the dry-out level. However, this may just be a misinterpretation of the parameter because the core remains at saturation temperature for all codes, indicating that the core is not dry. The comparison of the collapsed level shows more discrepancies, indicating that the calculated average core void fractions are different for each code. This may be due to several differences in the modelling of heat transfers between coolant and assemblies, of pump behaviour or of fluid stratification in the primary circuit.

8.2.5 SG behaviour

The SG water level and pressure were controlled by regulations in that phase, therefore no significant differences are observed, except for the water level calculated by SNU-MAAP4 calculations which increases instead of remaining constant. It may be due to an improper regulation.

8.2.6 Core temperatures

The core remains at saturation temperature everywhere, for all codes, indicating that the core is not dry.

8.2.7 Pressurizer level

Most codes calculate a fast decrease of the pressurizer level down to a minimum value, close to zero. The UPI-MELCOR results show very strong oscillations which do not appear in the other calculations. These oscillations are due to the loop-seal configuration of the pressurizer surge line (a key issue to predict how the pressurizer water level was maintained during the TMI-2 accident). The surge line at TMI-2 drops down from the bottom of the pressurizer, traverses several meters, and then rises to where it connects to hot-leg piping. This downward and then upward routing of the surge line is captured in the UPI MELCOR model with the inclusion of a control volume representing the surge line and capturing the hydrostatic characteristics of the water loop seal. Following the complete emptying of the pressurizer, some water is trapped inside the loop-seal up to the first 4500 s of this benchmark and very small oscillations in the primary pressure cause the oscillations in the pressuriser level

Overall, the states of the core and the primary circuit calculated by all codes are very similar at the time of pumps stop. The main discrepancies are in the void fraction in the core and the time of pump stop itself but those discrepancies are considered acceptable.

8.3 Core degradation phase (up to reflooding)

When the pumps stop, the mass flow rate at the break is significantly reduced due to the separation of steam and liquid, and the primary mass decreases more slowly. The heat transfer to the secondary side is strongly reduced and the evolution of the primary pressure becomes independent of the secondary pressure. This phase is characterized by a progressive dry-out and uncovery of the core, followed by the

increase of temperature of the rods and oxidation of the claddings. The details of the degradation processes are given below.

8.3.1 Water levels in the core

After the pumps stop, water in the loops is drained down into the vessel, which leads to the increase of water volume in the vessel. All codes calculate this increase of the collapsed level. Following this rapid variation of the level, a progressive decrease of the water level is calculated, corresponding to the dry-out and core uncovery. The curves calculated by each code are very similar, in particular the slope (which is approximately proportional to the steam production in the core) and the final value of the water level. Despite differences in the time of beginning of core uncovery, most codes calculate a stabilization of the water level around 60-70 cm above the bottom of the core. The SNU-MAAP4 calculation shows a remarkably different behaviour, probably due to the fact that the MAAP4 swollen core level is of parametric nature. The UPI-MELCOR calculation calculates a complete dry-out of the active part of the core. In general, all the results agree on the prediction of the core dry-out.

8.3.2 Mass flow rate at the break

All results show a slow decrease of the mass flow rate at the break, from a value of approximately 10 kg/s to a rather stable value of approximately 4 kg/s before reflooding. SNU-MAAP4 drops to zero and remains to the end of the calculation. However, the shapes of the curves are different and, during the transient, the calculated mass flow rate can differ by a factor 2 between the minimum estimated value and the maximum one.

8.3.3 Primary mass

As a result of the previous observation, the decrease of primary mass differs from one result to the other. Looking at the absolute value of the primary mass calculated just before reflooding, the relative discrepancy is limited to 9%. However, it is more relevant to compare the relative decrease with respect to the value at the time of pumps stop (limit of 85 tons in the primary system). In this case, the relative discrepancy between the calculated values is 28%, which is quite significant.

8.3.4 Primary pressure

There are significant discrepancies in the evolution in the primary pressure calculated by the participants. Some results indicate that the primary pressure decreases continuously after pump stop whereas other codes show a transient increase of the primary pressure (between 8 and 15 bars) during approximately 1000s, due to the fact that heat transfer to the secondary system is greatly reduced. The time when this pressure increase starts also vary from one result to the other, due to the differences in the calculation of the time when pumps stop. The SNL-MELCOR calculation shows a swelling in pressuriser level when the pumps stop, probably due to flashing, although calculated primary pressure remains constant. Other participants calculate an increase in pressure, but without any swelling.Those discrepancies were not clearly explained. They could depend on the efficiency of decay heat removal by the secondary side through residual natural circulation of steam in the primary circuit and condensation in the steam generators.

The average final primary pressure (before reflooding) is predicted at 57 bars, with a variance of 14%, which is acceptable.

8.3.5 Core temperatures

The evolution of core temperatures calculated by participants show several differences. The curves may be divided into three parts: heat-up before oxidation, oxidation runaway and “late-phase” heat-up following the first relocation of molten materials.

For the heat-up phase before oxidation, the slope is very similar for all curves, except for the IVS-ASTEC and the ENEA-ASTEC calculations which show a delayed but steep heat up, in particular at the top of the core (the IVS-ASTEC middle core temperature is in fact maximum core temperature). The main discrepancy is the time of beginning of heat-up which varies (in the middle of the core) from 500s to 1800s after pump stop, with a variance of 40%. Discrepancies are smaller for the evolution of temperatures at the top of the core. The delay between curves is partly due to the delay of core uncovery (discussed previously). Another cause is probably the differences in the melt relocation models which lead to a different velocity of propagation of the "hot" oxidation front.

For the oxidation run-away, we can observe a surprising agreement between several results which predict it between 7500s and 8000s. One calculation predicts it earlier (IVS-ASTEC at 6500s) and one predicts it later (IRSN-ICARE/CATHARE at 9500s). The increase of temperature due to temperature escalation is very comparable for most results. The maximum calculated temperature after escalation is approximately 2300K.

The heat-up calculated after the temperature escalation has approximately the same slope as before the escalation, as shown in almost all curves. The main difference between results in that phase is the maximum temperature reached, which is closely related to the choice of the melting temperature of UO2.

8.3.6 Hydrogen production

The calculated rate of hydrogen production is very similar for most results (approximately 0.6 kg/s in average) and the main differences are the times of maximum production. This is of course linked to the delays observed in the core temperature curves.

As a result, the shapes of the cumulated hydrogen mass curves are very similar, in particular the slope at the oxidation runaway. Once again, it is interesting to notice that 5 out of 7 results calculate the oxidation runaway approximately at the same time (around 8000s). The main differences are observed after the oxidation runaway where some results show a continuation of oxidation whereas other codes show a clear reduction of the oxidation after the runaway. The SNU-MAAP4 calculation shows, a continuation of oxidation after the runaway. There is a rather good agreement on the cumulated hydrogen production calculated before reflooding, with a lower than 20% variation.

The fraction of non-oxidized Zr, which was another parameter chosen for comparison, shows inconsistencies with the cumulated hydrogen mass. The curves should be almost symmetrical because hydrogen is mainly produced from Zr oxidation. Those inconsistencies need to be explained. Despite of that, the agreement between calculations is very good with an average oxidized fraction of 0.43 with a variation of only 10% between all results.

In contrast, the fraction of oxidized Zr in the melt (which could not be provided by all participants) shows an extreme variability: from 0.18 to 0.96. This indicates that models for oxidation of melts are significantly different from one code to the other.

8.3.7 Cladding failure and melt relocation

The cladding failure and first melt relocation are also calculated at approximately the same time for most codes. This is a direct consequence of the good agreement on the time of oxidation run-away.

8.3.8 Fuel melting and relocation

The evolution of the total mass of molten materials shows interesting differences. For some participants, the calculated molten mass increases simultaneously and almost proportionally to the cumulated hydrogen mass, which means that the energy brought by oxidation is directly converted into latent heat

to melt the oxides. For other participants, the molten mass increases smoothly, even a long time after the oxidation runaway, which indicates that the oxidation energy is "stored" in the core materials and does not cause a rapid melting. One reason for such discrepancy is the choice of melting temperature of the oxides. If this temperature is far from the temperature reached after the end of the oxidation runaway (approximately 2300K), then the melting must occur later than the oxidation. Despite the differences in the history of melting, there is a rather good agreement on the final mass of molten materials. The maximum variation obtained is 35%, which is surprisingly low considering that the molten mass depends on many uncertain phenomena: core heat-up, Zr oxidation, melting of oxides, etc. This may indicate that there is some sort of compensation between all the phenomena leading to core melting and that the calculated global energy balance of the core is approximately the same for all participants.

The SNU-MAAP4 calculation is a surprising exception: it predicts the maximum hydrogen mass but also the minimum molten mass. This apparently contradictory result was not explained.

There is an even better agreement on the calculated mass of molten metal with a variation of only 16%. This could be explained by the fact that the melting temperatures of metals are known with less uncertainty than those of the oxides.

8.3.9 State of the core

The states of the core calculated by the participants at the beginning of the oxidation runaway appear to be rather consistent. The temperature distributions are similar, the core is divided into a cold lower part and a hot upper part which is uncovered. The radial variations of temperature are consistent and the most external ring is calculated to be colder than the other ones by all participants. The main difference is the position of the maximum temperature. Some participants calculate it at the top of the core and others calculate it slightly below the top (approximately 50cm below).

The states of the core calculated at the beginning of melt relocation, show greater differences, and the location of the first damages or melting varies significantly from one calculation to the other. Some participants calculate the first melting at the top (3.66m) while others calculate it closer to the middle (between 2.5m and 3m). In addition to that, a difference is also observed in the calculated level of the "cold" zone (covered with water): most participants calculate it around 1m but some participants calculate it up to 1.5m. Such differences are quite significant and are likely due to the modelling of thermalhydraulics in the core. Differences in pressure drops or heat transfer coefficients and flow distribution (axial/radial) are probably the main causes for the observed discrepancies.

The states of the core calculated just before the reflooding, show both a very different distribution of materials and a very different temperature field. Some calculations show a large empty area at the top of the core, resulting from the collapse or melting of fuel rods. Other calculations show standing rods at the top of the core with a more limited molten area in the center of the core. Almost all calculations show a very compact region of accumulated materials at approximately 1m elevation. This may be interpreted as a "crust" or "crucible" made of relocated materials. The elevation of that crust varies significantly from one calculation to the other, between 0.6m to 2m. Some calculations predict high temperatures in the "crust" region, while other calculations predict the maximum at the center of the core. The ASTEC-IVS calculation shows the formation of a molten pool before reflooding while the MELCOR-SNL calculation shows the formation of a large debris bed.

8.4 Reflooding phase

8.4.1 Water levels in the core

All codes calculate a fast increase of the water level in the core and the core by-pass, with approximately the same velocity. In some calculations, discontinuities in the increase of the water level are observed

(MELCOR-SNL, ICARE/CATHARE-IRSN and ASTEC-ENEA) but they are probably due to the numerical tracking of the water level. In comparison, the increase of water level in the by-pass is smoother and continuous. At the end of the calculation, most calculations indicate a stable water level in the core but the ASTEC-ENEA calculation shows a surprising decrease of the water level (this is likely due to some flow instabilities in the primary loops during reflooding with subsequent redistribution of voids in the primary circuit). The stabilized level differs from one calculation to the other (from 3m to 4m). This was not explained.

8.4.2 Primary pressure

The average calculated pressure increase is 50 bars, with a variance of 38%. In the real TMI-2 scenario, the pressure increase after the restart of pumps was also of the order of 50 bars, but it was attributed to both a strong steam generation and a strong oxidation which produced a lot of non-condensable hydrogen. In the present exercise, participants calculate a small amount of hydrogen generated during reflood and therefore the increase of pressure results mainly from the strong steam formation.

8.4.3 Core temperatures

Most codes calculate a fast quenching of the core, at all elevation. However, the ATHLET/CD-GRS calculation predicts the non coolability of the inner ring (central part) at the bottom of the core and both ASTEC-IVS and ICARE/CATHARE-IRSN predict the non coolability of the middle of the core. The reasons for such non coolability should be investigated more thoroughly. The issue of coolability is crucial for safety studies and the existence of such discrepancies between code calculations reveals a weakness of current models dealing with reflooding of a degraded core.

8.4.4 Hydrogen production- Melt oxidation

A few codes calculate some hydrogen production during reflooding but it is quite limited. The largest amount is calculated by ASTEC-ENEA (approx. 29 kg) while ATHLET/CD-GRS and ICARE/CATHARE-IRSN calculate a slow continuation of oxidation for a long time after reflooding, because of the existence of non-quenched areas in the higher temperature areas of the core as explained above. For the other calculations, oxidation is predicted to stop as soon as the reflooding starts and no additional hydrogen is produced during reflooding.

For all codes, those calculations are obviously wrong as it was demonstrated by QUENCH program that the reflooding of a very hot but still undestroyed core (i.e. a core with a maximum temperature above 2100K but below 2500K) should lead to a large hydrogen production. And the same observation was made during the TMI-2 accident where half of the total hydrogen output (160kg out of 300kg) was supposedly produced during reflooding. Recent studies suggest that hydrogen produced during reflooding mainly comes from the oxidation of melt containing Zr. Therefore we may assume that there is an inadequate modelling of this phenomenon in current codes. This may be amplified by an inaccurate modelling of melt formation and relocation.

8.4.5 State of the core

For almost all the participants, the final calculated state of the core is very similar to the state before reflooding. There is no significant increase of the degradation or core melting during reflooding. Such result might not be conservative at all, as it was observed in QUENCH program that the reflooding of a very hot core (i.e. the maximum temperature is above 2000K) could lead to the melting of the claddings and a significant relocation of materials. However, QUENCH tests are not fully representative of a core since there are no UO2 pellets. Moreover, the average calculated core temperature in this scenario is approximately 2500K, i.e. much higher than the temperature obtained in QUENCH tests. Therefore it is not possible to conclude, solely on the basis of experimental results, that code calculations are wrong.

8.5 Figures for comparison

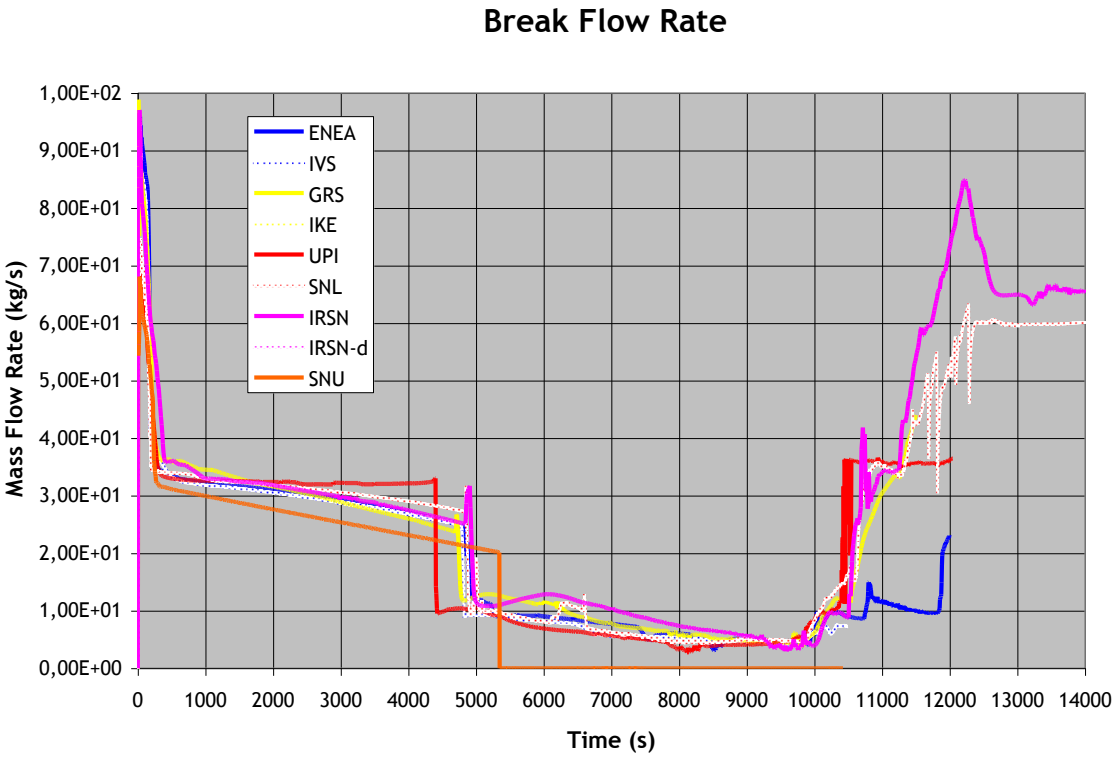

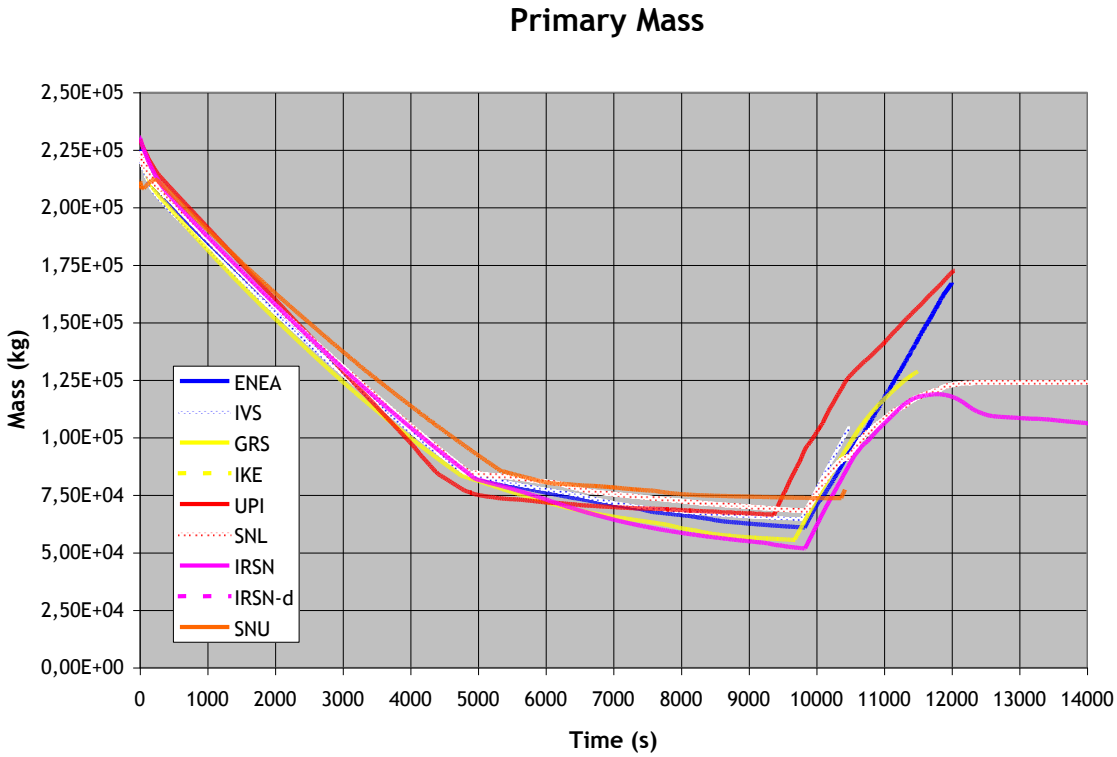

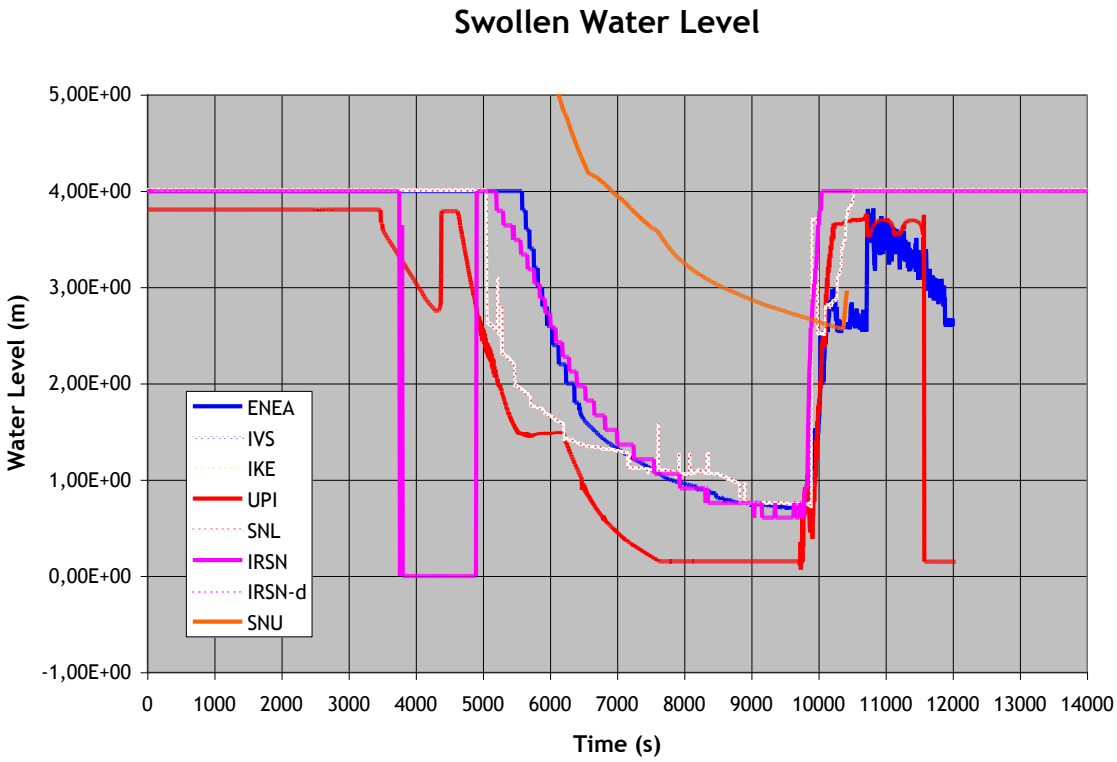
Swollen Water Level
Water Level (m)
5,00E+00
4,00E+00
3,00E+00
2,00E+00
1,00E+00
0,00E+00
-1,00E+00
0
1000
2000
3000
4000
5000
6000
7000
8000
9000
10000
11000
12000
13000
14000
Time (s)
ENEA
IVS
IKE
UPI
SNL
IRSN
IRSN-d
SNU

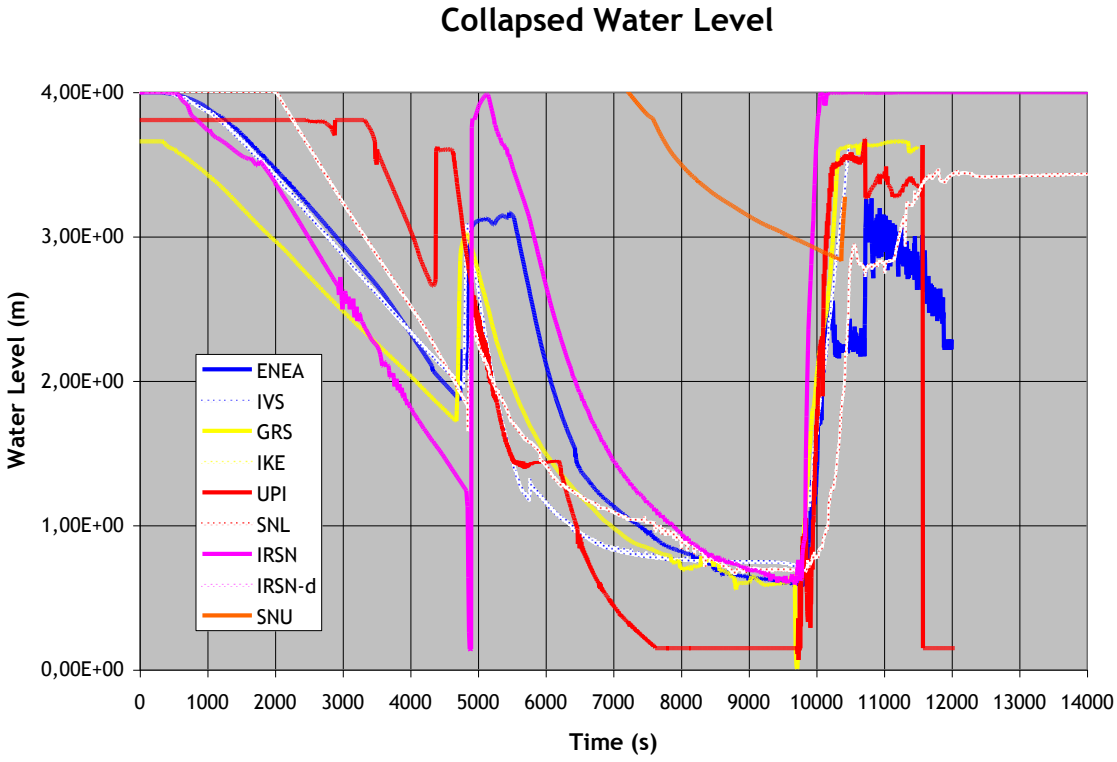
Collapsed Water Level
Water Level (m)
4,00E+00
3,00E+00
2,00E+00
1,00E+00
0,00E+00
0
1000
2000
3000
4000
5000
6000
7000
8000
9000
10000
11000
12000
13000
14000
Time (s)
ENEA
IVS
GRS
IKE
UPI
SNL
IRSN
IRSN-d
SNU

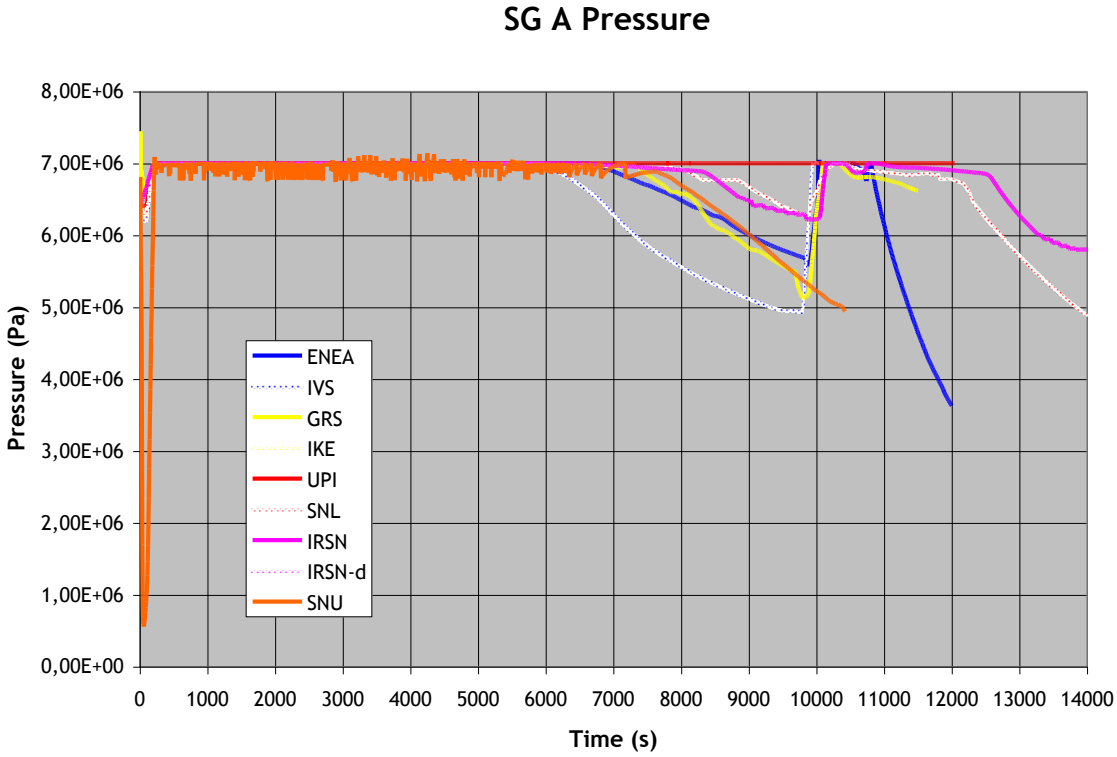
SG A Pressure
Pressure (Pa)
8,00E+06
7,00E+06
6,00E+06
5,00E+06
4,00E+06
3,00E+06
2,00E+06
1,00E+06
0,00E+00
0
1000
2000
3000
4000
5000
6000
7000
8000
9000
10000
11000
12000
13000
14000
Time (s)
ENEA
IVS
GRS
IKE
UPI
SNL
IRSN
IRSN-d
SNU

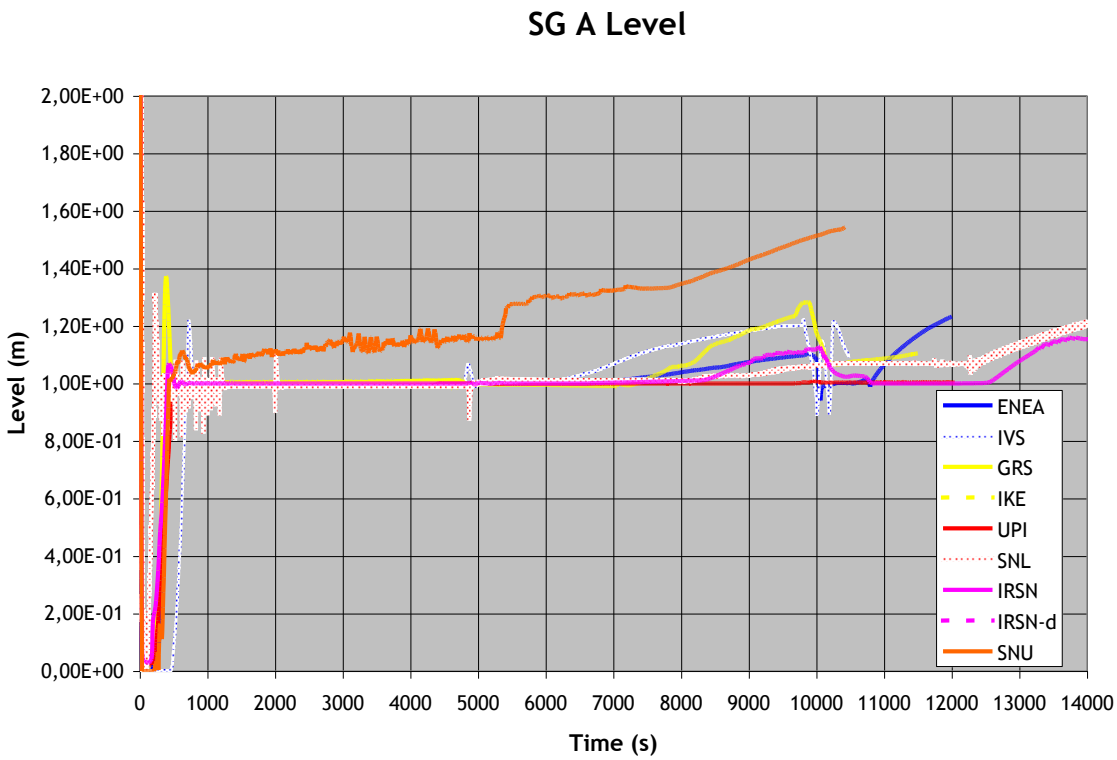
SG A Level
Level (m)
2,00E+00
1,80E+00
1,60E+00
1,40E+00
1,20E+00
1,00E+00
8,00E-01
6,00E-01
4,00E-01
2,00E-01
0,00E+00
0
1000
2000
3000
4000
5000
6000
7000
8000
9000
10000
11000
12000
13000
14000
Time (s)
ENEA
IVS
GRS
IKE
UPI
SNL
IRSN
IRSN-d
SNU

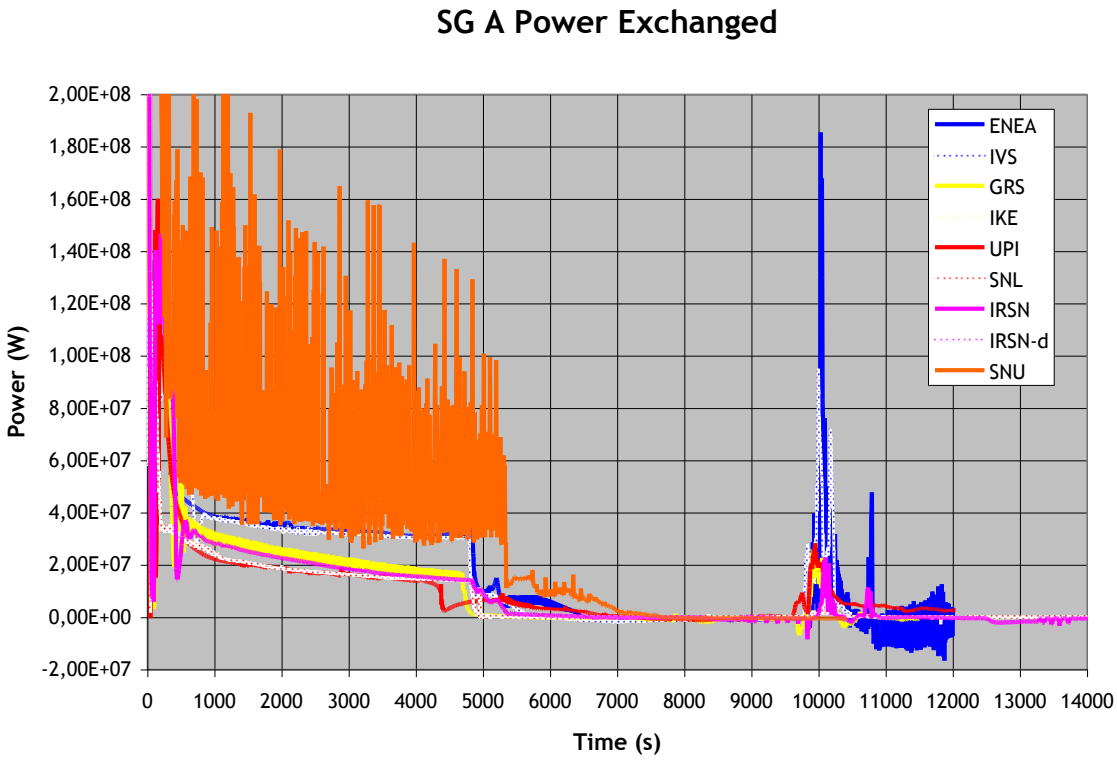
SG A Power Exchanged
Power (W)
2,00E+08
1,80E+08
1,60E+08
1,40E+08
1,20E+08
1,00E+08
8,00E+07
6,00E+07
4,00E+07
2,00E+07
0,00E+00
-2,00E+07
0
1000
2000
3000
4000
5000
6000
7000
8000
9000
10000
11000
12000
13000
14000
Time (s)
ENEA
IVS
GRS
IKE
UPI
SNL
IRSN
IRSN-d
SNU

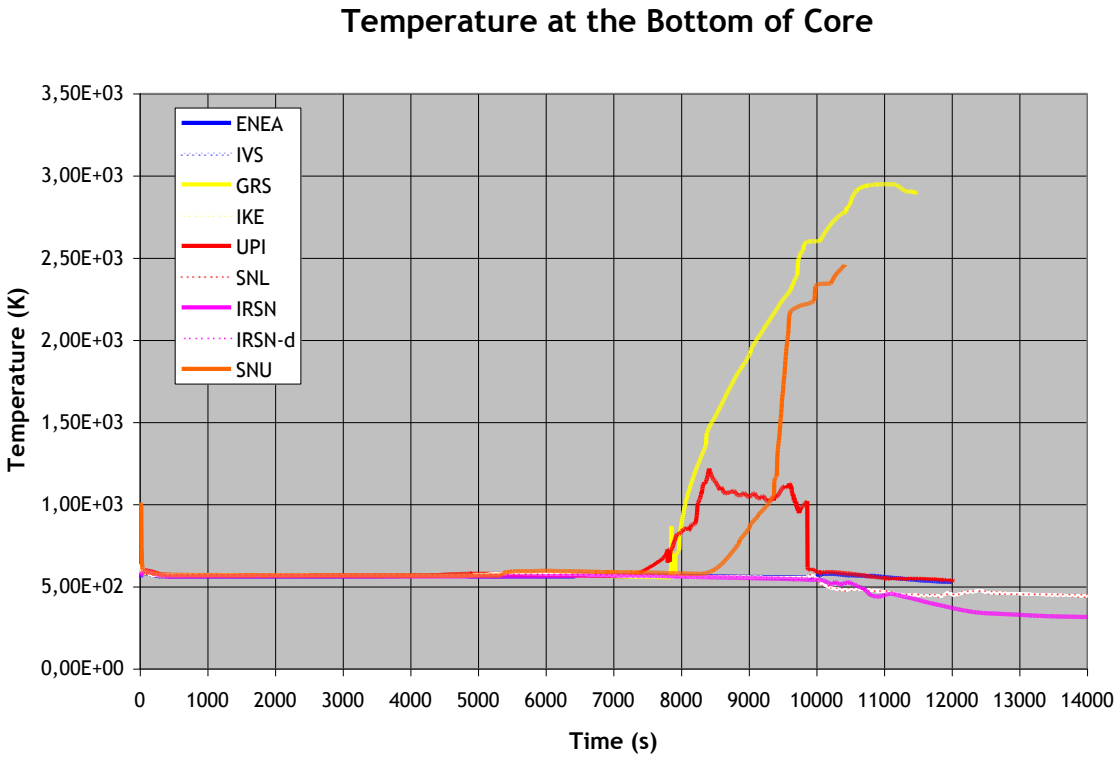
Temperature at the Bottom of Core
Temperature (K)
3,50E+03
3,00E+03
2,50E+03
2,00E+03
1,50E+03
1,00E+03
5,00E+02
0,00E+00
0
1000
2000
3000
4000
5000
6000
7000
8000
9000
10000
11000
12000
13000
14000
Time (s)
ENEA
IVS
GRS
IKE
UPI
SNL
IRSN
IRSN-d
SNU

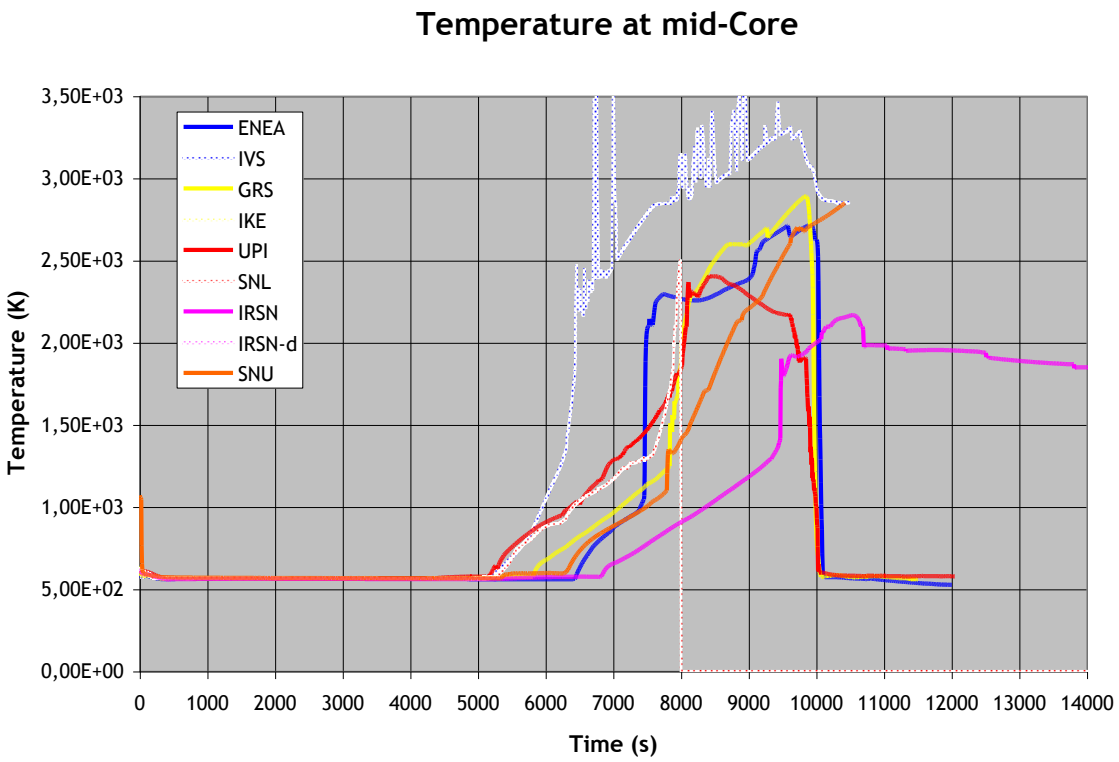
Temperature at mid-Core
Temperature (K)
Time (s)
ENEA
IVS
GRS
IKE
UPI
SNL
IRSN
IRSN-d
SNU
3,50E+03
3,00E+03
2,50E+03
2,00E+03
1,50E+03
1,00E+03
5,00E+02
0,00E+00
0
1000
2000
3000
4000
5000
6000
7000
8000
9000
10000
11000
12000
13000
14000

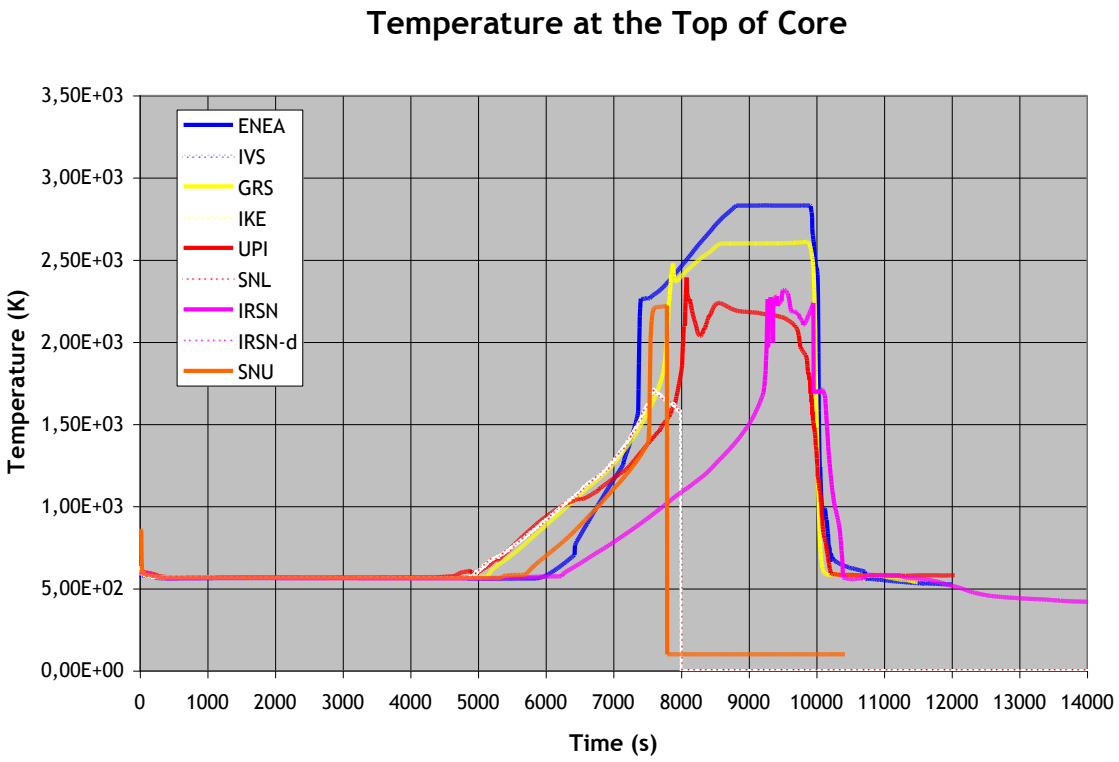
Temperature at the Top of Core
Temperature (K)
Time (s)
ENEA
IVS
GRS
IKE
UPI
SNL
IRSN
IRSN-d
SNU
3,50E+03
3,00E+03
2,50E+03
2,00E+03
1,50E+03
1,00E+03
5,00E+02
0,00E+00
0
1000
2000
3000
4000
5000
6000
7000
8000
9000
10000
11000
12000
13000
14000

Pressurizer Pressure

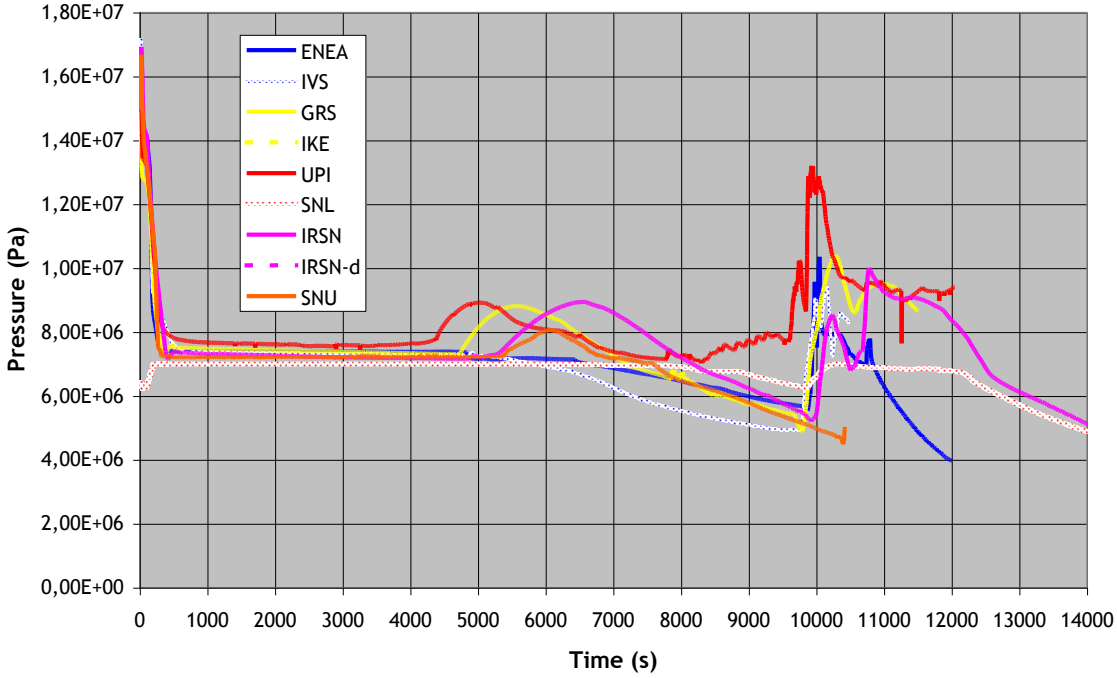

Pressurizer Level

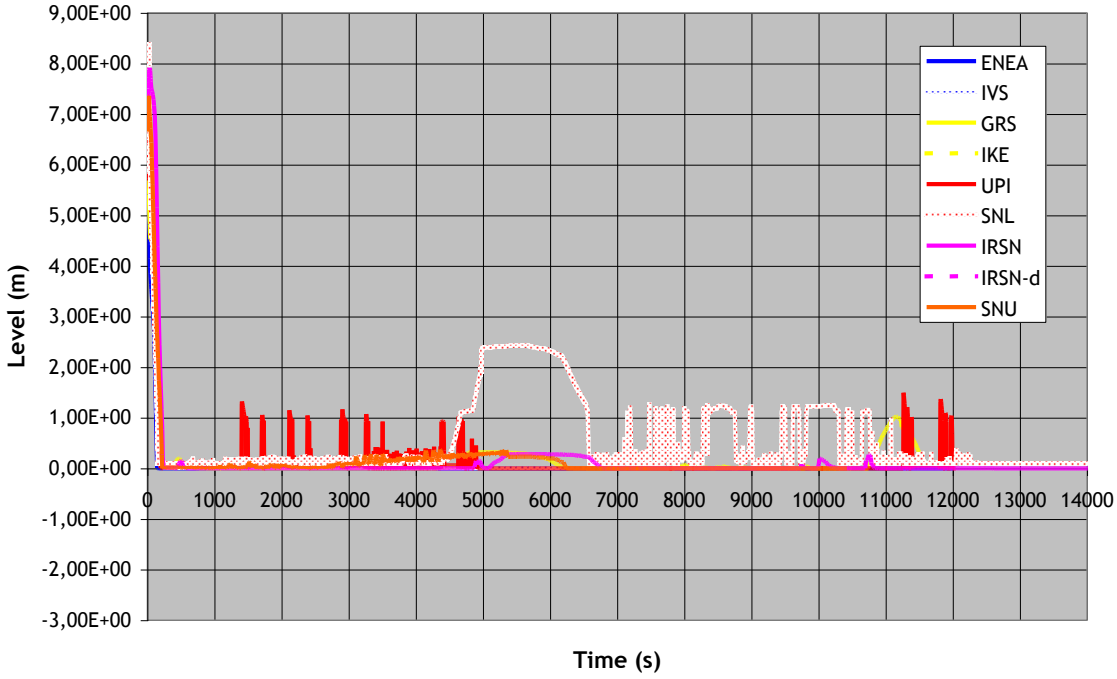

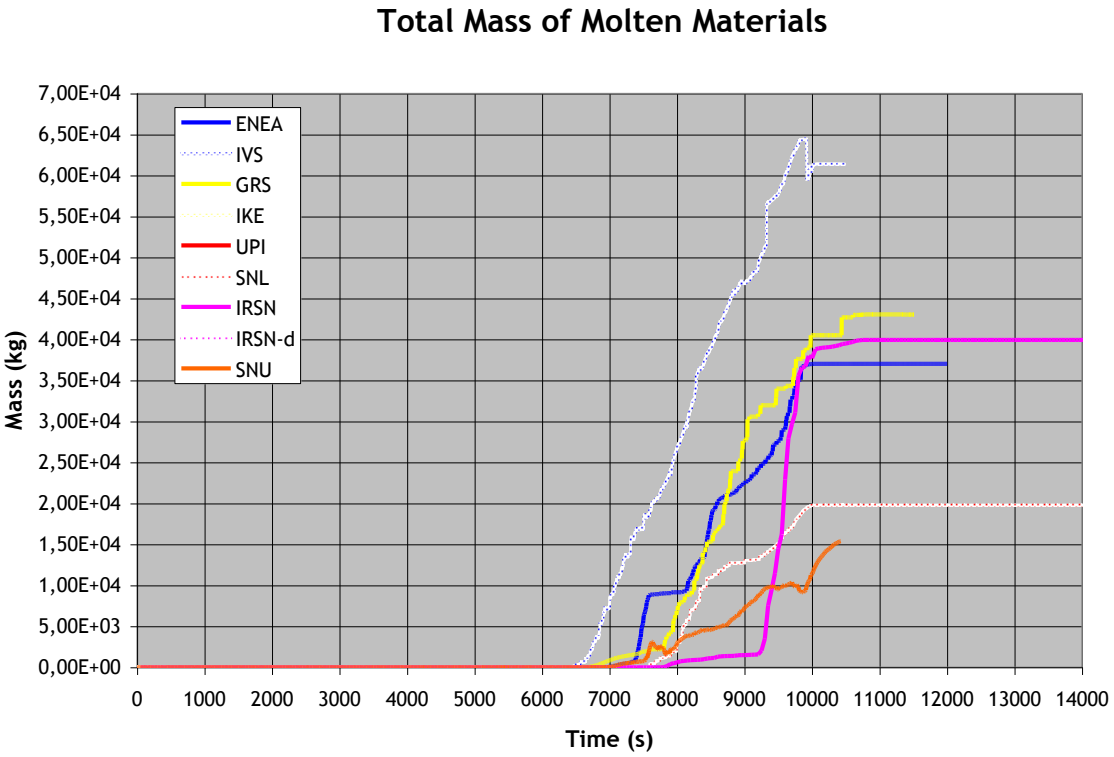
Total Mass of Molten Materials
Mass (kg)
Time (s)
ENEA
IVS
GRS
IKE
UPI
SNL
IRSN
IRSN-d
SNU
7,00E+04
6,50E+04
6,00E+04
5,50E+04
5,00E+04
4,50E+04
4,00E+04
3,50E+04
3,00E+04
2,50E+04
2,00E+04
1,50E+04
1,00E+04
5,00E+03
0,00E+00
0
1000
2000
3000
4000
5000
6000
7000
8000
9000
10000
11000
12000
13000
14000

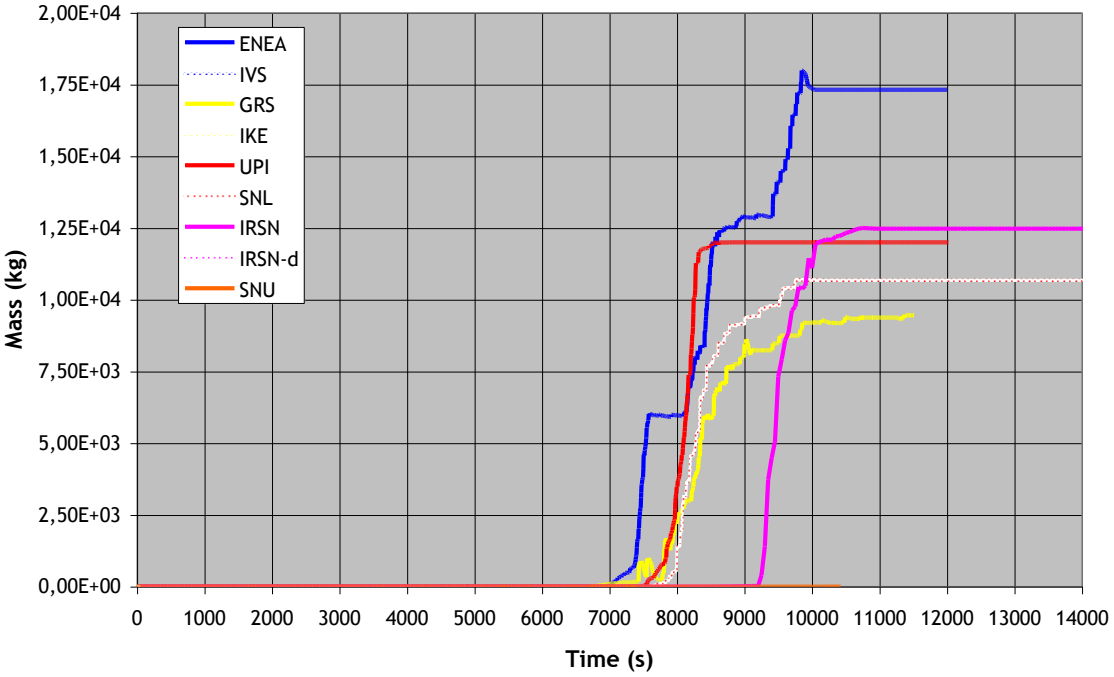
Total Mass of Molten Metal
Mass (kg)
Time (s)
ENEA
IVS
GRS
IKE
UPI
SNL
IRSN
IRSN-d
SNU
2,00E+04
1,75E+04
1,50E+04
1,25E+04
1,00E+04
7,50E+03
5,00E+03
2,50E+03
0,00E+00
0
1000
2000
3000
4000
5000
6000
7000
8000
9000
10000
11000
12000
13000
14000

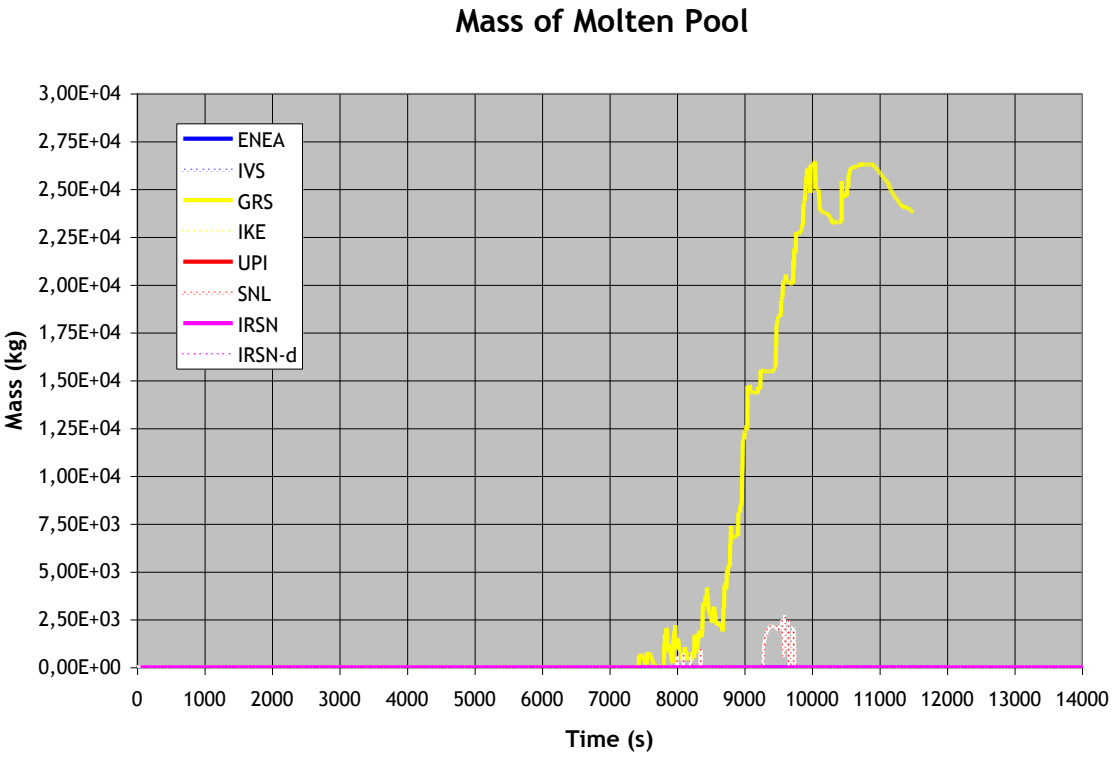
Mass of Molten Pool
3,00E+04
2,75E+04
2,50E+04
2,25E+04
2,00E+04
1,75E+04
1,50E+04
1,25E+04
1,00E+04
7,50E+03
5,00E+03
2,50E+03
0,00E+00
Mass (kg)
ENEA
IVS
GRS
IKE
UPI
SNL
IRSN
IRSN-d
0
1000
2000
3000
4000
5000
6000
7000
8000
9000
10000
11000
12000
13000
14000
Time (s)

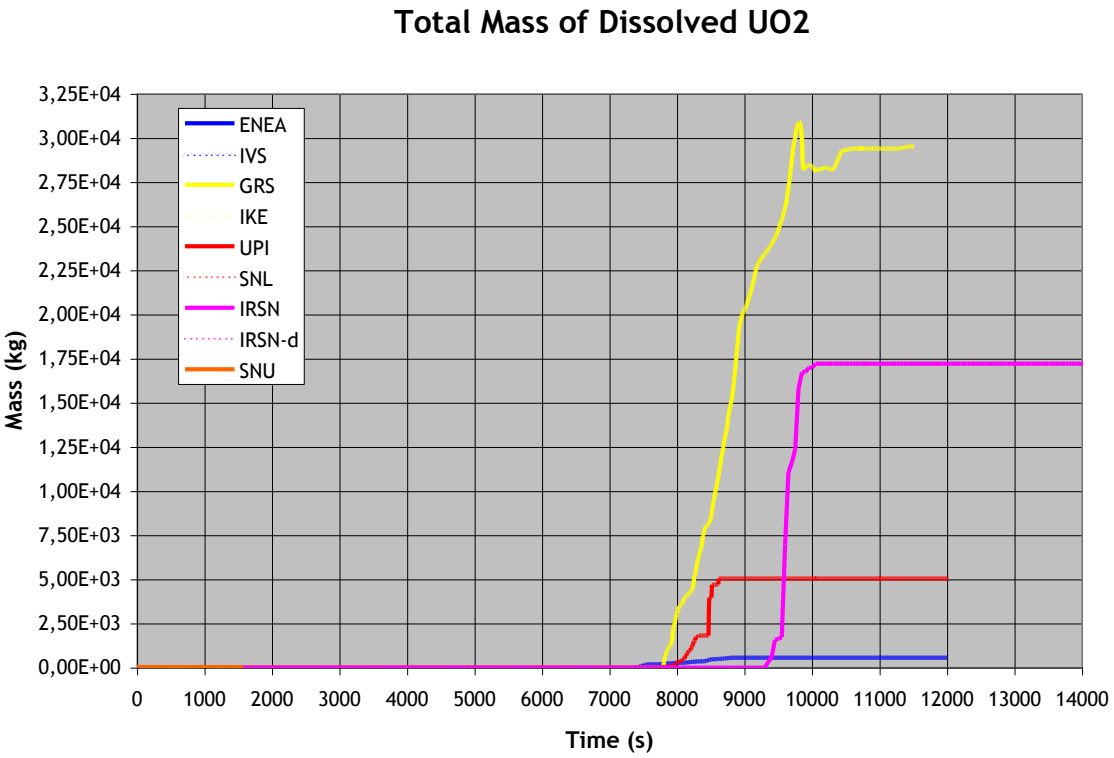
Total Mass of Dissolved UO2
3,25E+04
3,00E+04
2,75E+04
2,50E+04
2,25E+04
2,00E+04
1,75E+04
1,50E+04
1,25E+04
1,00E+04
7,50E+03
5,00E+03
2,50E+03
0,00E+00
Mass (kg)
ENEA
IVS
GRS
IKE
UPI
SNL
IRSN
IRSN-d
SNU
0
1000
2000
3000
4000
5000
6000
7000
8000
9000
10000
11000
12000
13000
14000
Time (s)

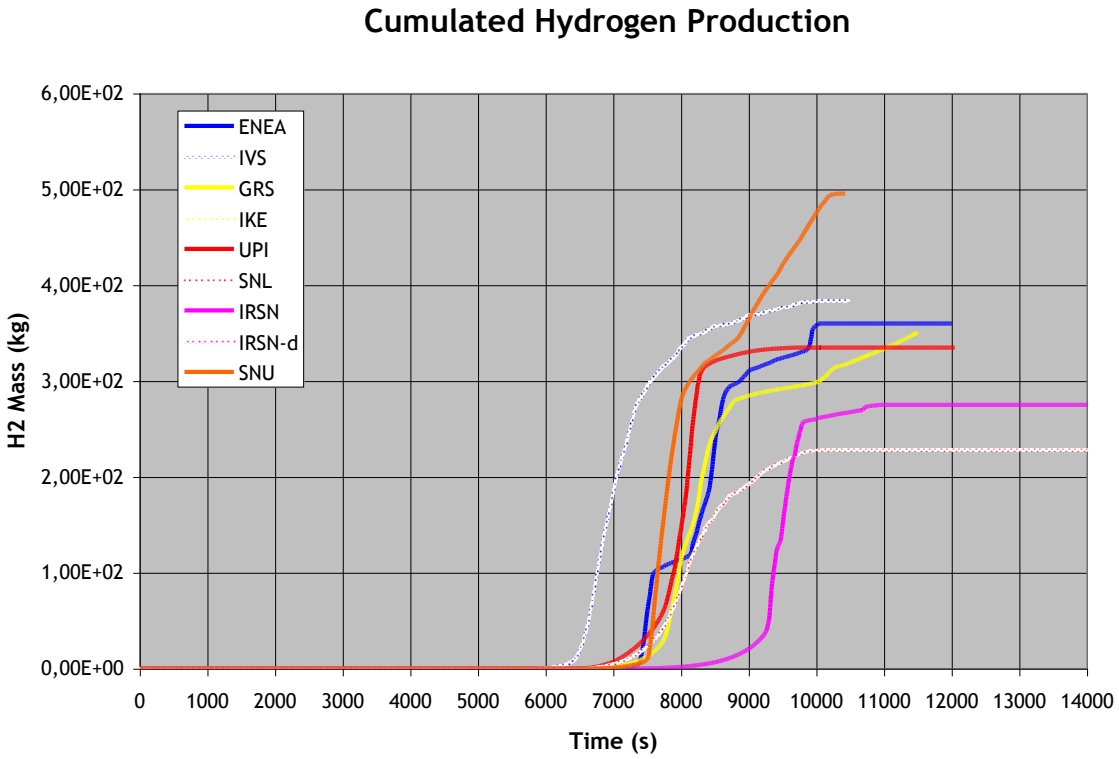
Cumulated Hydrogen Production
H2 Mass (kg)
6,00E+02
5,00E+02
4,00E+02
3,00E+02
2,00E+02
1,00E+02
0,00E+00
0
1000
2000
3000
4000
5000
6000
7000
8000
9000
10000
11000
12000
13000
14000
Time (s)
ENEA
IVS
GRS
IKE
UPI
SNL
IRSN
IRSN-d
SNU

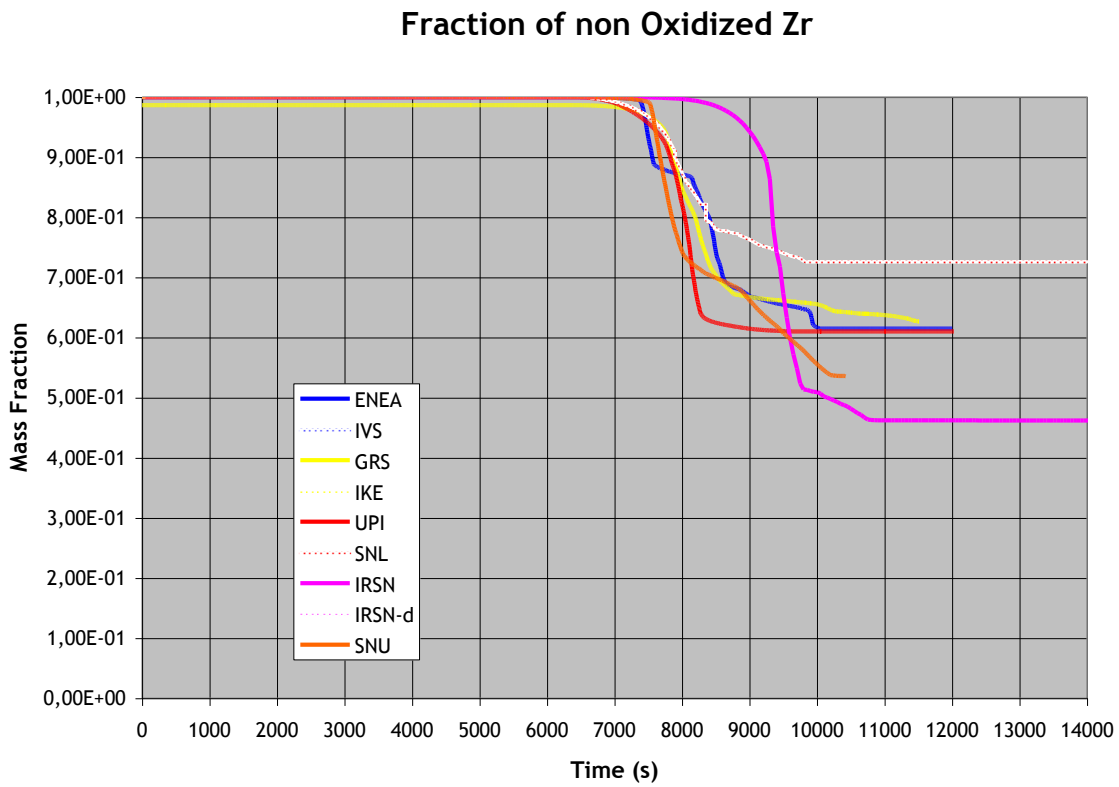
Fraction of non Oxidized Zr
Mass Fraction
1,00E+00
9,00E-01
8,00E-01
7,00E-01
6,00E-01
5,00E-01
4,00E-01
3,00E-01
2,00E-01
1,00E-01
0,00E+00
0
1000
2000
3000
4000
5000
6000
7000
8000
9000
10000
11000
12000
13000
14000
Time (s)
ENEA
IVS
GRS
IKE
UPI
SNL
IRSN
IRSN-d
SNU

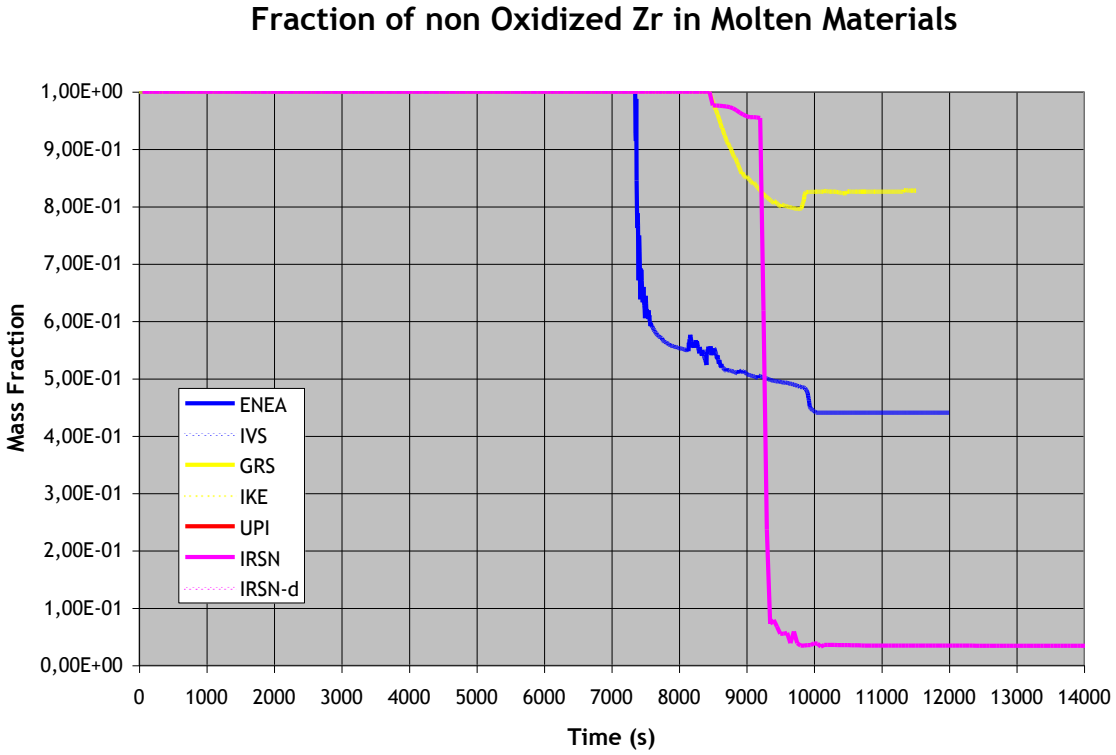
Fraction of non Oxidized Zr in Molten Materials
Mass Fraction
1,00E+00
9,00E-01
8,00E-01
7,00E-01
6,00E-01
5,00E-01
4,00E-01
3,00E-01
2,00E-01
1,00E-01
0,00E+00
0
1000
2000
3000
4000
5000
6000
7000
8000
9000
10000
11000
12000
13000
14000
Time (s)
ENEA
IVS
GRS
IKE
UPI
IRSN
IRSN-d

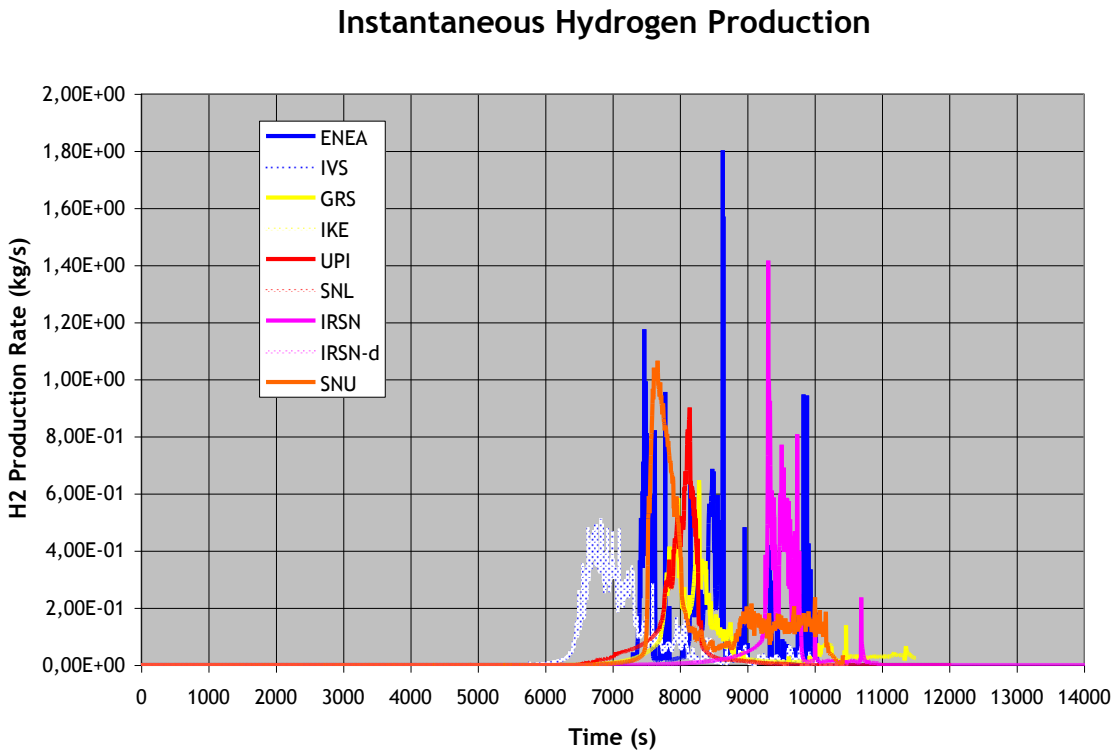
Instantaneous Hydrogen Production
H2 Production Rate (kg/s)
2,00E+00
1,80E+00
1,60E+00
1,40E+00
1,20E+00
1,00E+00
8,00E-01
6,00E-01
4,00E-01
2,00E-01
0,00E+00
0
1000
2000
3000
4000
5000
6000
7000
8000
9000
10000
11000
12000
13000
14000
Time (s)
ENEA
IVS
GRS
IKE
UPI
SNL
IRSN
IRSN-d
SNU

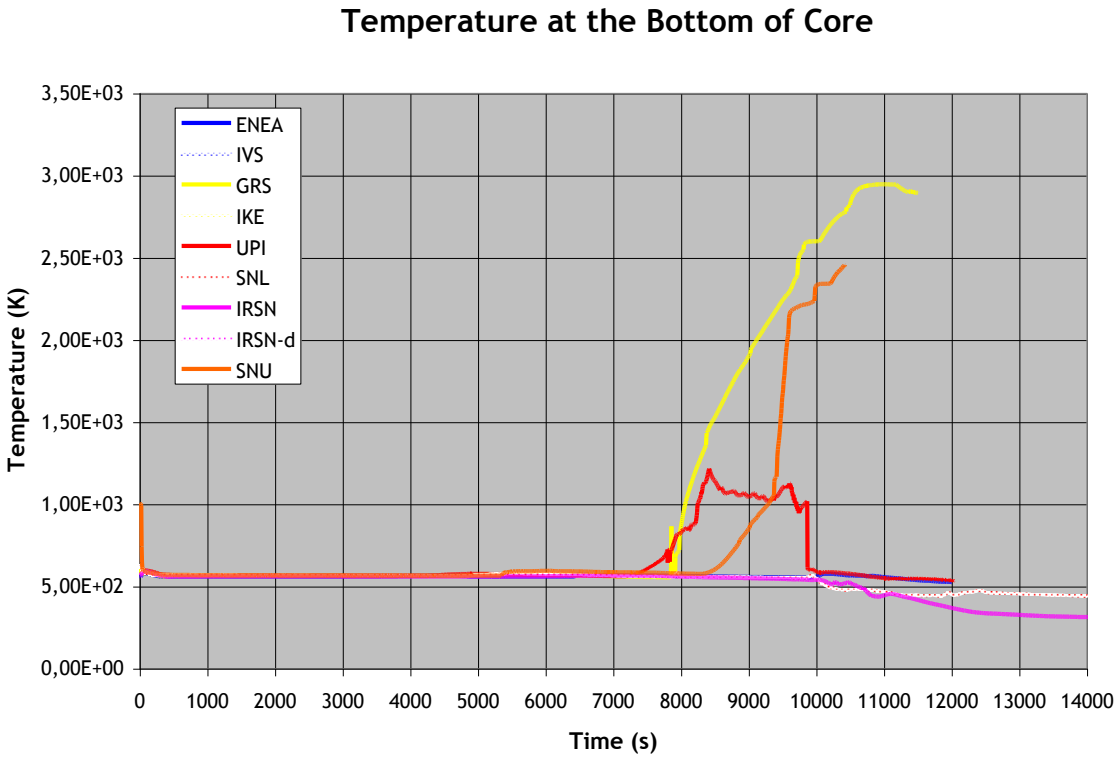
Temperature at the Bottom of Core
3,50E+03
3,00E+03
2,50E+03
2,00E+03
1,50E+03
1,00E+03
5,00E+02
0,00E+00
Temperature (K)
0
1000
2000
3000
4000
5000
6000
7000
8000
9000
10000
11000
12000
13000
14000
Time (s)
ENEA
IVS
GRS
IKE
UPI
SNL
IRSN
IRSN-d
SNU

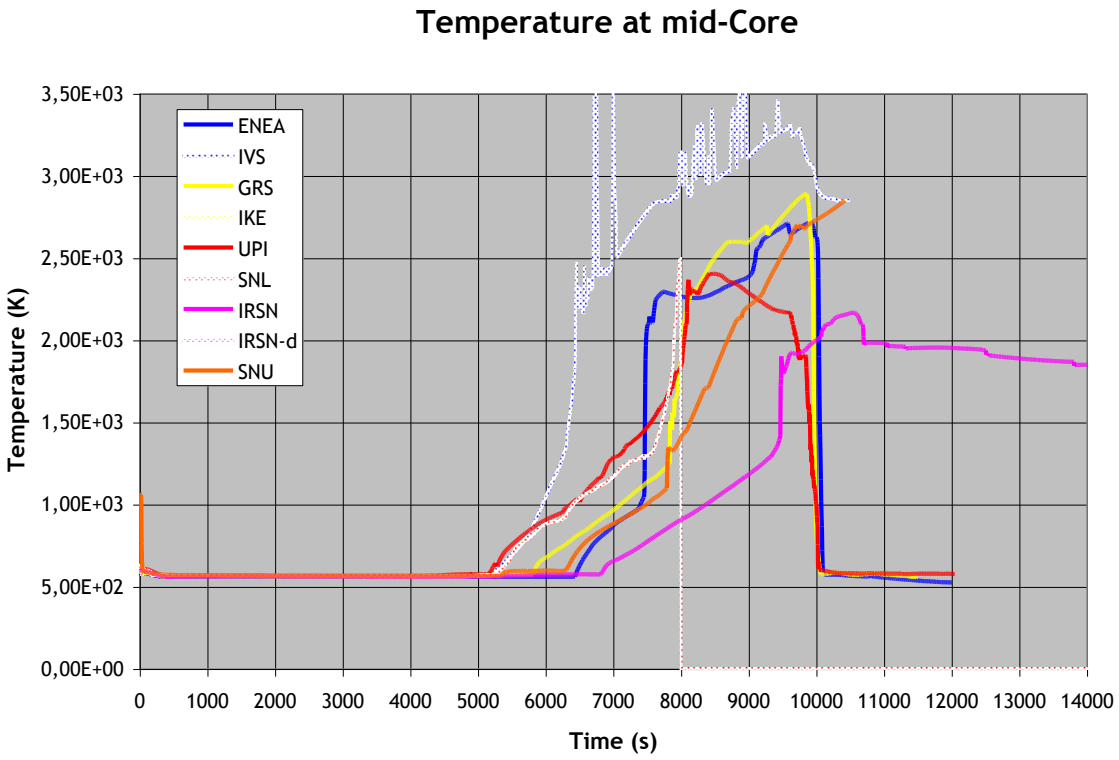
Temperature at mid-Core
3,50E+03
3,00E+03
2,50E+03
2,00E+03
1,50E+03
1,00E+03
5,00E+02
0,00E+00
Temperature (K)
0
1000
2000
3000
4000
5000
6000
7000
8000
9000
10000
11000
12000
13000
14000
Time (s)
ENEA
IVS
GRS
IKE
UPI
SNL
IRSN
IRSN-d
SNU

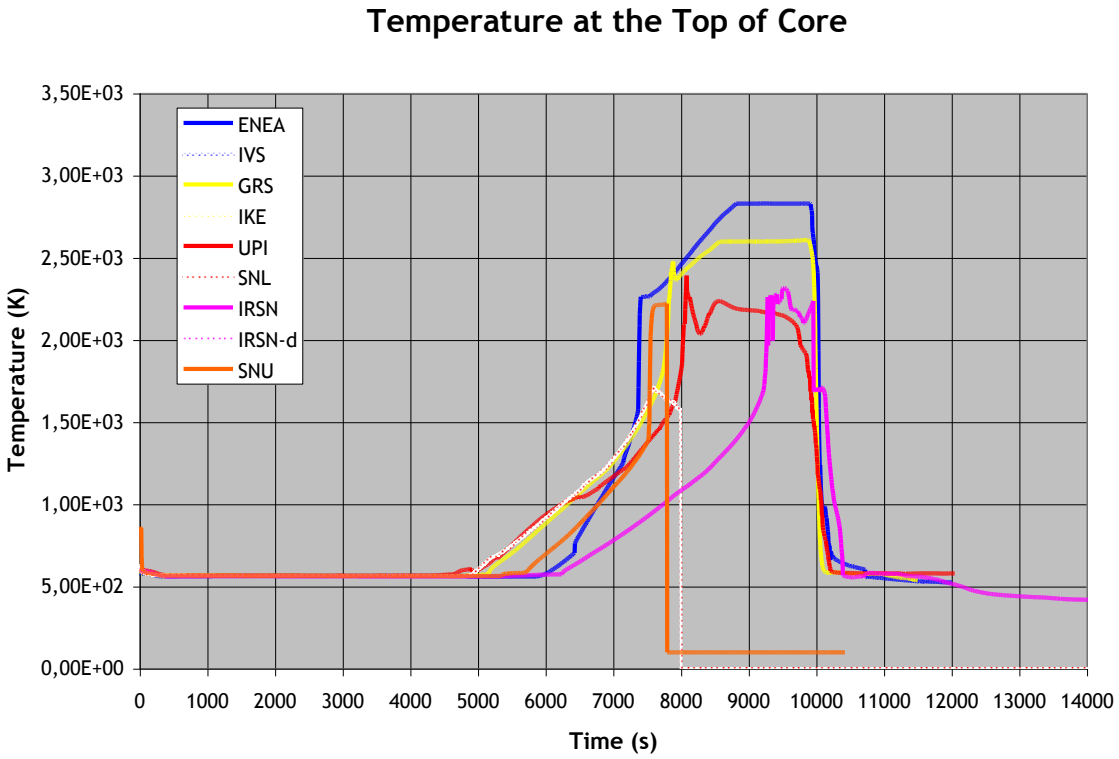
Temperature at the Top of Core
Temperature (K)
3,50E+03
3,00E+03
2,50E+03
2,00E+03
1,50E+03
1,00E+03
5,00E+02
0,00E+00
0
1000
2000
3000
4000
5000
6000
7000
8000
9000
10000
11000
12000
13000
14000
Time (s)
ENEA
IVS
GRS
IKE
UPI
SNL
IRSN
IRSN-d
SNU

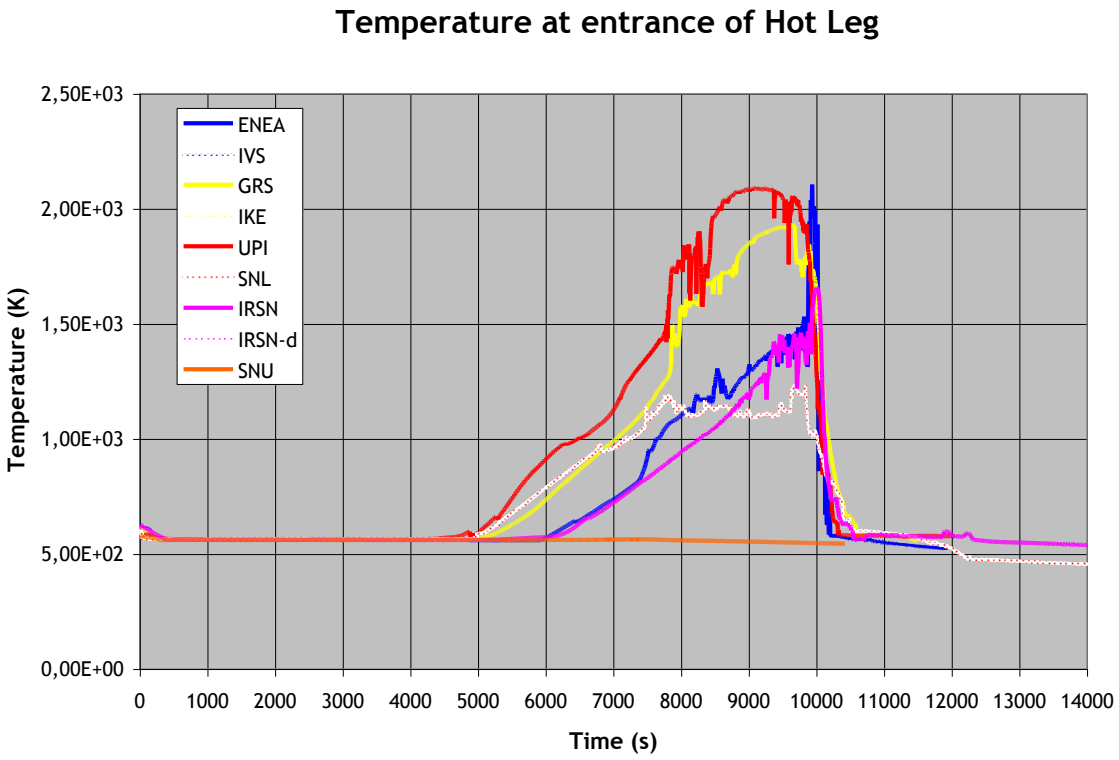
Temperature at entrance of Hot Leg
Temperature (K)
2,50E+03
2,00E+03
1,50E+03
1,00E+03
5,00E+02
0,00E+00
0
1000
2000
3000
4000
5000
6000
7000
8000
9000
10000
11000
12000
13000
14000
Time (s)
ENEA
IVS
GRS
IKE
UPI
SNL
IRSN
IRSN-d
SNU

9. SENSITIVITY STUDIES

Discrepancies between code results may have different origins. One of them is the so-called "user effect". This has been observed in several previous benchmarks, in particular in the frame of OECD International Standard Problems (ISP). User effect may result from an improper checking of the data (plant data are particularly complex) or from a wrong use of the code by an insufficiently trained user. In order to avoid the user effect, recommended values of the parameters used in the models are usually provided to code users in calculation benchmarks. All the reference calculations of this benchmark were done with the recommended values of physical parameters. Taking into account the differences which were observed in the results of the reference calculation, especially in the core degradation phase, it was decided to perform a second calculation with the same core degradation parameters for all codes. Thus, a set of parameters known to have a significant impact on degradation calculations were selected and given to participants. Those will be called "alternative physical parameters". They were chosen from the conclusions of ISP46 (PHEBUS-FPT1) and from the latest findings on core degradation phenomena. Those parameters are listed in the next section.

9.1 Selection of parameters

- Zr oxidation correlation : Urbanic-Heidrick correlation was the most widely used by participants of ISP46. Although there are better alternatives now (following Volchek and Schanz work), it is decided to choose Urbanic correlation for this sensitivity calculation.
- Cladding failure criteria : these criteria have a tremendous impact on the hydrogen production because they control the release and relocation of molten Zr towards lower and colder elevations. Based on PHEBUS analysis, it was found that relevant criteria for the failure of cladding are, under steam starved conditions :
  - $T > 2280K$ and $e(ZrO2) < 0.2mm$ (thickness of zirconia layer)
  - $T > 2450K$ and $e(ZrO2) < 0.3mm$
- Melting temperature of oxides (UO2 and ZrO2) : this parameter also has a strong impact on the results. While it is theoretically around 2800K, it was found that the best agreement with FPT1 was obtained with a greatly reduced relocation temperature of 2500K.
- Debris formation criteria : there are very few data about this parameter (and no information from PHEBUS FPT1). It may be assumed that debris is formed during reflooding, because of the thermal shock. A simple criterion based on temperature is chosen, with a threshold value of 2000K.
- Debris porosity and diameter : once again, there are very few data about these parameters. Based on the analysis of TMI-2 debris, a diameter of 2 mm and a porosity of 0.4 are chosen.

The values used by each participant are summarized in the table below:

	Zr Oxidation correlation
ENEA ASTEC 1.3	Correlations proposed by Schanz et al. (2001) o Cathcart correlation if T < 1800 K o Prater correlation if T > 1900 K Linear interpolation between 1800 – 1900 K
GRS ATHLET-CD	o Cathcart correlation if T < 1800 K o Urbanic correlation if T > 1900 K Linear interpolation between 1800 – 1900 K
DIMNP MELCOR 1.8.5	Urbanic-Heidrick
SNL MELCOR 1.8.6	Urbanic Heidrick
IVS ASTEC 1.3	Urbanic-Heidrick
IRSN ICARE/CATHARE	Correlations proposed by Schanz et al. (2001) o Cathcart correlation if T < 1800 K o Prater correlation if T > 1900 K Linear interpolation between 1800 – 1900 K
SNU MAAP4	Baker-Just model (Tclad > 1875 K) Cathcart model (Tclad < 1850 K) Interpolated inbetween
IKE ATHLET-CD/MEWA	

	Cladding failure criteria
ENEA ASTEC 1.3	o T > 2300 K and e(ZrO2) < 300 μm o T > 2500 K
GRS ATHLET-CD	o T > 2300 K and e(ZrO2) < 300 μm o T > 2500 K
DIMNP MELCOR 1.8.5	o T > 2400 K and e(ZrO2) < 100 μm
SNL MELCOR 1.8.6	o T > 2500 K and e(ZrO2) < 100 μm o T > 2800 K
IVS ASTEC 1.3	o T > 2260K and e(ZrO2) < 160 μm o T > 2280K and e(ZrO2) < 200 μm o T > 2340K and e(ZrO2) < 220 μm o T > 2380K and e(ZrO2) < 240 μm o T > 2450K and e(ZrO2) < 300 μm

IRSN ICARE/CATHARE	o T > 2300 K and e(ZrO2) < 300 μm o T > 2500 K
SNU MAAP4	o T > 2500 K or o e(ZrO2) > 400 μm
IKE ATHLET-CD/MEWA	

	UO2-ZrO2 melting temperature
ENEA ASTEC 1.3	2830K
GRS ATHLET-CD	2600K
DIMNP MELCOR 1.8.5	UO2: 3113K and ZrO2: 2990K
SNL MELCOR 1.8.6	2800K
IVS ASTEC 1.3	Phase Diagram ?
IRSN ICARE/CATHARE	
SNU MAAP4	2500K
IKE ATHLET-CD/MEWA	

	Debris formation criteria
DIMNP MELCOR 1.8.5	Conglomerate debris forms when molten core material resolidifies
SNL MELCOR 1.8.6	Debris forms when clad fails
IVS ASTEC 1.3	code default criteria, debris models and reflooding model in ASTEC are still under development
IRSN ICARE/CATHARE	
SNU MAAP4	
IKE ATHLET-CD/MEWA	

	Debris diameter
DIMNP MELCOR 1.8.5	0.5 m is the particular debris equivalent diameter used to calculate total debris surface area during quenching (it is applied to the zircaly resolified in the colder zones)
SNL MELCOR 1.8.6	Core – 10mm Lower Plenum - 2 mm
IVS ASTEC 1.3	5 % of 2 mm diameter 15 % of 4 mm diameter 60 % of 6 mm diameter 15 % of 8 mm diameter 5 % of 10 mm diameter
IRSN ICARE/CATHARE	
SNU MAAP4	
IKE ATHLET-CD/MEWA	

	Debris porosity
DIMNP MELCOR 1.8.5	0.1
SNL MELCOR 1.8.6	0.4
IVS ASTEC 1.3	0.6
IRSN ICARE/CATHARE	
SNU MAAP4	0.4
IKE ATHLET-CD/MEWA	

9.2 Results of sensitivity studies

The details of sensitivity studies are given in the individual descriptions of calculations provided in the Appendix. Because standard core degradation parameters are somewhat different for each code, the parameters varied in the sensitivity studies performed were not the same for all participants. Therefore,

comparisons between sensitivity calculation results can not be made. But interesting conclusions can be drawn from those studies, in particular to answer the following questions:

- Are the uncertainties in important core degradation results coming from changes in model parameters larger or smaller than the uncertainties coming from the use of different codes?
- Among the parameters chosen, which ones have greater importance, in terms of their impact on significant core degradation results?

To summarize the results obtained by the participants, we can draw the following conclusions:

- The variation of the melting temperature of oxides has a strong impact on the final mass of molten material (which is quite obvious) causing a variation which is of the same order of magnitude as the variation obtained with different codes and/or users. This shows that the physical understanding of fuel rod melting and collapse at is still too limited. Therefore there is no correct mechanistic modelling of the process which relies on user parameters which are very sensitive.
- The hydrogen production is more sensitive to the cladding failure criteria than to the choice of oxidation kinetics. The variation of cladding failure criteria also causes a variation which is comparable to the variation obtained with different codes and/or users. Again, this shows that the physical understanding of cladding failure and liquid Zr relocation is still too limited. Therefore there is no correct mechanistic modelling and the whole process relies on user parameters which are very sensitive.
- The impact of the variation of the selected parameters on the reflooding phase and on the final state of the core seems to be more limited.
- The models involving debris formation introduce an additional criterion for fuel rods collapse which is likely to increase the variability of the results. However, this point was not investigated enough. This is mainly due to the fact that the definition of "debris" differs from one code to the other.

Due to the limited time frame of this exercise, it was not possible to make of thourough analysis of the impact of "debris models" to treat the late phase of degradation. Only two calculations used such models: MELCOR-SNL and ASTEC-IVS. Two more calculations were expected (ATHLET/MEWA-IKE and an alternative ICARE/CATHARE-IRSN) but they could not be performed. Since those models are considered as more advanced than the regular models used up to now in current codes, it would be very interesting, in a further extension of this exercise, to focus on the impact of such "debris models".

It also appears that some model parameters cannot be varied independently because they depend on the same physical processes. For example, if the melting temperature of oxides is reduced to 2400K, the cladding failure criteria should also include a temperature condition lower than 2400K. Sensitivity analyses take into account the combined effect of a consistent set of parameters. This issue should be investigated more thouroughly in the future.

Taking into account that, from the regulatory point of view, it is essential that uncertainties in best-estimate calculations be well studied and assessed, it is suggested that systematic uncertainty analysis be included in future extension of this benchmark, using uncertainty analysis techniques. The BEMUSE program action, which is being carried out in the frame of GAMA, could be a good reference for that.

10. CONCLUSIONS

This phase II exercise is the first benchmarking of severe accident codes promoted by NEA in almost 20 years. The objective of Phase II of the exercise was to perform a code benchmark on a well-defined plant (similar to TMI-2) and with prescribed boundary conditions. Therefore, the benchmark avoided additional and unwanted sources of discrepancies between code calculations, so as to focus on the variability of the codes calculations of core degradation. Although the initial objectives of the Phase 2 of this action were apparently clear, the participants realized that the task needed several preliminary steps and complementary actions:

- Make sure that all participants had a correct input deck for the TMI-2 reactor.
- Define a reasonable scenario that would include a large core degradation followed by a reflooding phase.
- Select the parameters for comparison.
- Analyse the results of the last TMI-2 exercise and of previous benchmarks (the recent PHEBUS-FPT1 and QUENCH-11 benchmarks were chosen) in order to be able to measure the quality of the comparisons made in the present benchmark and the progress made.
- List the physical criteria which are relevant for PSA studies and define the uncertainty ranges which can be considered acceptable for current safety studies.

The first four actions were completed with success and it is possible to conclude that:

- A reference severe accident scenario, initiated by a SB-LOCA, based on a TMI-2 plant model, and with prescribed boundary conditions was defined.
- A set of output variables was proposed and accepted by the participants, which allowed the assessment of the quality of the calculation results.
- This scenario can be used as a reference calculation to assess the agreement between current codes or even for an adequate training of a code user.

The last action was not finished, because there are no regulations or rules which define what can be considered as “acceptable” uncertainty in safet studies. Rather, what is essential from the regulatory point of view is that license applications based on best-estimate calculations, include a thorough and complete evaluation of uncertainties using accepted methods.

The main conclusions of the exercise, regarding the ability of the participating codes to calculate severe accidents are summarized below.

For the initial transient, up to the primary system pumps trip, the calculated results are in good agreement. The states of the core and the primary circuit calculated by all codes are very similar at the time of pump trip. The main discrepancies are in the calculation of the void fraction in the core, and the calculation of the time of pump stop, but those discrepancies are considered acceptable.

For the degradation phase, up to the reflooding of the core, the results show a rather good agreement between all participants for global calculation of results such as total hydrogen production and total mass of molten materials. The variability in these results is not only much better than the results obtained in the benchmark exercise performed 20 years ago, but is also comparable or even better than the variability obtained in recent benchmarks on integral tests (PHEBUS-FPT1 and QUENCH-11). This result shows a significant improvement of the codes in the last two decades. They now include assessed models to describe the main physical processes of degradation as well as robust and consistent numerical schemes which make them reliable to calculate a severe accident sequence with acceptable results. The surprisingly reduced scatter of the global calculation results is probably due to the fact that code models have been assessed globally and adjusted on the same basis of integral tests but also to the participation of very experienced code users. Such conclusion raises again the issue of the importance of adequate user training, in particular for utilities and TSOs who submit safety studies to regulatory bodies. Also it raises the issue of having good user manuals and guidelines, which must reduce to a minimum user's uncertainty and "guessing" when building inputs.

For the reflooding phase, there is a general agreement on the calculated pressure increase, on the total hydrogen mass produced during this phase, and on the increased rate of core degradation. However, although all codes agree, some results may be questionable as they are apparently in contradiction with experimental observations (LOFT and QUENCH for example) and with the TMI-2 assumed evolution. In addition, there is a lack of agreement on the calculated efficiency of quenching. Some codes calculate a fast and complete quenching while other codes calculate the existence of uncoolable regions in the core. Compared to the previous TMI-2 benchmark exercise where almost none of the codes were able to calculate the reflood phase, the abilities and robustness of codes have been considerably improved. However, it is not enough yet to produce reliable predictions. It can be concluded that, despite considerable improvement in codes abilities, more modelling and assessment should be done before codes can be considered reliable enough to calculate the reflooding phase.

Overall, the results of this exercise are quite encouraging. First, all the codes succeeded in calculating the scenario from the beginning to the end, with very little tuning of parameters or optimization of input decks. This shows the robustness of current codes, which is a great progress compared to the state of codes 20 years ago when several codes could not calculate the complete TMI-2 sequence. Moreover, it appears that the codes' global results are significantly more consistent than they were 20 years ago. They are also equally or more consistent than predictions made on integral tests, usually dedicated to the study of specific phenomena. However, this surprising and very positive result must be considered carefully because of the limited number of participants and the fact that they were all very experienced code developers or users, which obviously helped in avoiding to get unphysical or unreasonable results. Despite of that, a few minor physical inconsistencies were observed which indicated that some mistakes may remain in some input decks or some models or in the post-processing of the results. Finally, an unexpected difficulty was met: some codes could not provide plots of the evolution for some requested physical parameters. It is suggested that code developers improve the standard outputs and post-processing of code results in order to help the users to make a sensible and useful analysis of their calculations.

Sensitivity studies performed by participants have shown that variations of some key empirical model (such as the cladding failure criteria) could induce a variation in some calculation results (such as hydrogen production) obtained by a single participant, which is of the same order of magnitude as the variation obtained when comparing different codes and/or participants. This indicates that some physical processes are still poorly known and inadequately modeled. It also appears that some model parameters cannot be varied independently and that sensitivity analyses should look at the combined effect of a consistent set of parameters. This issue was not investigated further.

The code scattering in the calculation of some phenomena revealed some model weaknesses. Three major phenomena are concerned. The first one is oxidation of molten mixtures and their relocation. The second one is the prediction of UO2 melting and its interaction with molten corium. The third one is the core coolability and the behaviour of hot corium when the vessel is entirely reflooded. The weaknesses of codes in the prediction of those phenomena are not surprising because experimental data are scarce and the physical understanding is still incomplete. Experimental programmes are currently under way or planned to provide a better insight of those phenomena. It should help to improve the physical models and the overall quality of prediction of codes.

The benchmark exercise involved some of the most important system codes which are currently used by utilities, TSO's, and regulatory agencies. Because of that, the benchmark has provided substantial and important insights. However, due to the limited number of participants and the fact that only one scenario was calculated, the conclusions of this benchmark exercise must be considered with caution. It is believed that some important codes did not participate in the benchmark. In particular SCDAP/RELAP was absent although it is used in several countries. And also there were many major nuclear actors absent of this exercise (in particular utilities but also TSOs from several countries). Therefore, additional participants are strongly encouraged to join the group of participants if such benchmark action is continued.

11. PROPOSALS FOR FUTURE EXTENSIONS OF THE WORK

The conclusions of this benchmark exercise must be considered with caution because of the limited number of participants and because only one scenario was studied. However, the work performed during this project constitutes a solid basis to continue such benchmark activity in order to confirm the current conclusions. The proposed directions for future work are the following:

1. Improvement of the definition of the boundary conditions and plant description to eliminate any remaining uncertainty and validate this sequence as a reference calculation to be used for further benchmarks or even in training programmes for code users.
2. Extension of the number of parameters to compare, in particular boundary conditions for the containment: hydrogen mass flow rate at the break, mass of non-coolable corium, time of vessel failure (if it happens), etc…
3. Better definition of the criteria to compare and improvement of the outputs of the codes (some comparisons were difficult in the present exercise).
4. Different branch scenarios involving various SAM operations or system failures starting from the same initial conditions: depressurization, delayed start of HPI, loss of AFW, corium relocation into the lower plenum and vessel failure.
5. Taking into account that, from the regulatory point of view, it is essential that uncertainties in best-estimate calculations be well studied and assessed, it is suggested that uncertainty analysis be investigated in future extension of this benchmark, using well known uncertainty analysis methods. The BEMUSE program action, which is being carried out in the frame of GAMA, could be a good reference for that.
6. Extension of the number of participants to involve:
    - More countries
    - More users (in particular utilities and TSO's).

12. REFERENCES

1. TMI-2 Analysis Exercise Final Report, NEA/CSNI/R(91)8, 1991.
2. Progress made in the Last Fifteen Years through Analyses of the TMI-2 Accident performed in Members Countries, NEA/CSNI/R(2005)1, 2005.
3. ISP-46 PHEBUS FPT1, NEA/CSNI/R(2004)18, 2004.
4. SARNET Benchmark on QUENCH-11 – Final Report, FZKA 7368 – SARNET CORIUM P008, 2008.

13. APPENDIX: SCHEDULE OF THE PROJECT

- 1st meeting in November 2005 in Aix en Provence
- 2nd meeting in June 2006 in Aix en Provence
- 3rd meeting in January 2007 in Garching
- 4th meeting in June 2007 in Paris
- 5th meeting in November 2007 in Karlsruhe
- Draft of final report prepared in February 2008
- Final report.

14. APPENDIX: PARTICIPATING ORGANISATIONS AND CODES USED

A few Members Countries have designated experts able to analyze the progress made in the predictions of one or several codes. Each expert is either a code developer or a code user, with a long experience. The operational sequence of events during the TMI-2 accident is well known by all of them. The modelling of the circuits and reactor core has been rather well assessed by all experts. The main uncertainties in the actual TMI2 sequence are the boundary flows, which were not recorded and have been adjusted by each expert independently. Therefore an alternative scenario with fixed boundary conditions has been defined for this benchmark exercise.

All the participants to this analysis are shortly introduced below, with a mention of the code(s) they have used.

14.1 ENEA

ENEA has been involved in several studies of the TMI-2 transient with different codes, since the last OECD benchmark. An important step was the complete transient calculation with SCDAP/RELAP5, which showed a significant progress in the capabilities of a severe accident code. More recently, ENEA particpated to a benchmark exercise in the frame of the COLOSS European Project and calculated the first phases of the transient with ASTEC V1 (developed by GRS and IRSN) and ICARE/CATHARE V1 (developed by IRSN).

In the present exercise, ENEA has used ASTEC V1.3.

14.1.1 Brief Description of the ASTEC V1.3 Code

The European ASTEC code is being jointly developed by IRSN and GRS. It is an integral code able to assess the whole severe accident sequence in a nuclear power plant, from the initiating event up to fission product release and behaviour in the containment.

The code includes several coupled modules that can deal with the different severe accident phenomena: thermal-hydraulics in the reactor system, core degradation and melt release, fission product release and transport, ex-vessel corium interaction, aerosols behaviour and iodine chemistry in the containment, etc. Among them, the CESAR module is used to compute the thermal-hydraulics in the primary and secondary systems of the reactor. Such module is coupled to the DIVA module that computes core degradation, melt relocation and behaviour in the lower head up to vessel failure.

The CESAR module allows a detailed representation of all components of primary and secondary circuits including auxiliary, emergency and control systems. CESAR is a two-phase flow thermal-hydraulic code. The gas phase can be a mixture of steam and hydrogen. The solution of the problem is based on two mass equations, two energy equations, one equation for steam velocity, and a drift flux correlation for water velocity. The state variables computed by CESAR are: total pressure, void fraction, steam and water temperature, steam and water velocity, and partial pressure of hydrogen. All hydraulics components can be discretized by volumes (one mesh) or axial meshed volumes and connected by

junctions. The volumes can be homogeneous or with a swollen level. Thermal structures are used to model the walls of the components, and compute thermal heat exchange between primary and secondary systems and heat losses to the environment.

The DIVA module, which is a simplified version of the ICARE2 core degradation code, can model the thermal-hydraulics in the part of the vessel below the top of the core: downcomer, lower plenum and the core itself including the core bypass. There are simplified thermal-hydraulic models specific for DIVA based on a simplified 2D gas (steam plus non condensable gases) model with water swollen level. The simplified model of the lower head of DIVA has one single mesh for fluids, three layers for corium (pool, metal and debris), and a 2D meshing for the vessel.

The DIVA module is activated to compute core heatup and degradation, in coupled mode with CESAR, at the onset of core uncovery. Before DIVA activation, the thermal-hydraulics in the vessel and the core is computed by CESAR through an automatic vessel model creation based on DIVA input deck.
The convective and radiative heat exchanges between core components and structures are computed by DIVA. Most important core degradation phenomena are dealt with in DIVA including: (1) core material oxidation and hydrogen generation, (2) control rod material interaction, melting and relocation, (3) zircaloy clad melting and fuel dissolution, (4) fuel rod clad failure and metallic melt relocation, (5) debris bed and molten pool formation and spreading in the late degradation phase (these last models, still under development and qualification, were not applied in the present analysis; therefore, fuel rod melting and relocation in the late phase was calculated by decanting and candling models in rod-like geometry).

14.2 GRS

GRS is developing the code ATHLET-CD with the aim to simulate severe accidents in the reactor cooling system. The TMI-2 accident has been selected to assess the code for plant applications.

14.2.1 Brief Description of the ATHLET-CD Code

The system code ATHLET-CD (**A**nalysis of **TH**ermal-hydraulics of **LE**aks and **T**ransients with **C**ore **D**egradation) is designed to describe the reactor coolant system thermal-hydraulic response during severe accidents, including core damage progression as well as fission product and aerosol behaviour, to calculate the source term for containment analyses, and to evaluate accident management measures. It is being developed by GRS in cooperation with the Institut für Kernenergetik und Energiesysteme (IKE), University of Stuttgart. ATHLET-CD includes also the aerosol and fission product transport code SOPHAEROS which is being developed by the French Institut de Radioprotection et de Sûreté Nucléaire (IRSN).

The ATHLET-CD structure is highly modular in order to include a manifold spectrum of models and to offer an optimum basis for further development. ATHLET-CD contains the original ATHLET models for comprehensive simulation of the thermo-fluid-dynamics in the coolant loops and in the core. The ATHLET code comprises a thermo-fluid-dynamic module, a heat transfer and heat conduction module, a neutron kinetics module, a general control simulation module, and a general-purpose solver of differential equation systems called FEBE. The thermo-fluid-dynamic module is based on a six-equation model, with fully separated balance equations for liquid and vapour, complemented by mass conservation equations for up to 5 different non-condensable gases and by a boron tracking model. Alternatively, a five-equation model, with a mixture momentum equation and a full-range drift-flux formulation for the calculation of the relative velocity between phases is also available. Specific models for pumps, valves, separators, mixture level tracking, critical flow etc. are also included in ATHLET.

The rod module ECORE consists of models for fuel rods, absorber rods (AIC and B_4C) and for the fuel assemblies including BWR-canisters and -absorbers. The module describes the mechanical rod behaviour (ballooning), zirconium and boron carbide oxidation (Arrhenius-type rate equations), Zr-UO_2 dissolution as well as melting of metallic and ceramic components. The melt relocation (candling model) is simulated by rivulets with constant velocity and cross section, starting from the node of rod failure. The model allows oxidation, freezing, re-melting, re-freezing and melt accumulation due to blockage formation. The feedback to the thermal-hydraulics considers steam starvation and blockage formation. Besides the convective heat transfer, energy can also be exchanged by radiation between fuel rods and to surrounding core structures.

The release of fission products is modelled by rate equations or by a diffusion model within the module FIPREM. The release of aerosols is described by rate equations. The release of control rod materials (Ag, In, Cd) is based on temperature functions taking into account the partial pressure of the material gases. The transport and retention of aerosols and fission products in the coolant system are simulated by the code SOPHAEROS.

For the simulation of debris beds a specific model MEWA is under development with its own thermal-hydraulic equation system, coupled to the ATHLET-thermo-fluid-dynamics on the outer boundaries of the debris bed. The transition of the simulation of the core zones from ECORE to MEWA depends on the degree of degradation in the zone. The code development comprises also late phase models for core slumping, melt pool behaviour and vessel failure.

The code system ATHLET/ATHLET-CD is coupled to the containment code system COCOSYS, and it is the main process model within the German nuclear plant analyzer ATLAS. The ATLAS environment allows not only a graphical visualisation of the calculated results but also an interactive control of data processing

The code validation is based on integral tests and separate effect tests, proposed by the CSNI validation matrices, and covers thermal-hydraulics, bundle degradation as well as release and transport of fission products and aerosols. Recent post-test calculations have been performed for the out-of pile bundle experiments QUENCH-07, QUENCH-08, QUENCH-09, QUENCH-10 and QUENCH-11 as well as for the in-pile experiments Phébus FPT2 and FPT3. The TMI-2 accident is used to assess the code for reactor applications.

The development and the validation of ATHLET-CD are sponsored by the German Federal Ministry of Economics and Technology (BMWi).

14.3 IVS

IVS has been involved in TMI-2 study in the frame of bilateral co-operation with IRSN devoted to ASTEC validation. The first TMI-2 calculations were performed with ASTEC V1.0 code in 2002-2003. In the present exercise IVS has used ASTEC V1.3 code.

14.4.1 Brief Description of the ASTEC V1.3 Code

The code is the same as the one used by ENEA. It is described in section 14.1.

14.4 NRC - SNL

The main computational tool for the NRC severe accident analysis studies is MELCOR 1.8.6.

14.4.1 Brief Description of the MELCOR Code

MELCOR is a fully integrated computer code that is capable of modeling the progression of severe accidents in light water reactor nuclear power plants. It has been developed for the USNRC by Sandia Laboratories since 1985. The development of MELCOR fulfills NRC's objective of having an analytical capability for predicting the complete evolution of postulated severe accidents in nuclear power plants in some reasonable level of detail.

MELCOR models a broad spectrum of severe accident phenomena in both boiling and pressurized water reactors is treated in MELCOR in a unified framework. Various code 'packages' models:

- thermal-hydraulic response of the primary reactor coolant system, the reactor cavity, the containment, and the confinement buildings,
- core uncovering (loss of coolant), fuel heatup, cladding oxidation, fuel degradation (loss of rod geometry), and core material melting and relocation,
- heatup of reactor vessel lower head from relocated fuel materials and the thermal and mechanical loading and failure of the vessel lower head, and transfer of core materials to the reactor vessel cavity,
- core-concrete attack and ensuing aerosol generation,
- in-vessel and ex-vessel hydrogen production, transport, and combustion,
- fission product release (aerosol and vapor), transport, and deposition
- behavior of radioactive aerosols in the reactor containment building, including scrubbing in water pools, and aerosol mechanics in the containment atmosphere such as particle agglomeration and gravitational settling, and,
- impact of engineered safety features on thermal-hydraulic and radionuclide behavior

Although MELCOR is modular in structure the code is highly integrated and flexible. For example, there are no models for reactor components such as steam generators and pressurizers. Instead, these components are constructed from control volumes, flow paths, and heat structures. In addition, there is one package for modeling the thermalhydraulics that is used in all aspects of the reactor system.

The governing equations for thermal-hydraulic behavior in MELCOR are the equations of conservation of mass, momentum, and energy. A semi-implicit (linearized) formulation of the governing equations is used to permit timesteps greater than the acoustic Courant limit. Also, MELCOR uses a full two-fluid treatment rather than a drift-flux formulation and the resulting equations are iterated when necessary so that the result is fully implicit with respect to pressures used in the momentum equation. A significant feature of this method is that the resulting equations are exactly conservative (to within machine roundoff) with respect to masses and to thermal energy.

The MELCOR COR package calculates the thermal response of the core and lower plenum structures, including the portion of the lower head directly beneath the core, and models the relocation of core materials during melting, slumping, and formation of molten pool and debris. Fuel pellets, cladding, grid spacers, canister walls (for boiling water reactors [BWRs]), core baffles and formers (for pressurized water reactors [PWRs]), other structures (e.g., control rods or guide tubes), molten pools, and particulate debris are modeled separately within individual cells, the basic nodalization unit in the COR package.

Many new modeling enhancements have been added to the MELCOR 1.8.6 COR package to improve the capabilities of the code to better represent the late-phase behavior of severe accidents. These new

models include hemispherical lower head geometry, models for simulating the formation of molten pools both in the lower plenum and the upper core, crust formation, convection in molten pools, stratification of molten pools into metallic and oxide layers, and partitioning of radionuclides between stratified molten pools.

14.5 University Pisa

The University of Pisa was regularly involved in severe accident studies, mainly using SCDAP/RELAP5 and MELCOR codes. The experience gained from these studies helped to achieve a calculation of the first two phases of the TMI-2 accident. The same nodalisation has been employed, with the obvious modifications to the boundary conditions, for the simulation of this benchmark.

14.5.1 Brief Description of the MELCOR V1.8.5 Code

The code is the same as the one used by NRC-SNL. It is described in section 1.7.1. However, UPI has used the version 1.8.5 which differs from the version 1.8.6, mainly by the modelling of late phase behaviour.

14.6 IRSN

The ICARE/CATHARE system is developed by IRSN to meet requirements in light water reactor safety analysis (PWR1, VVER2, EPR3, etc.) and level 2 probabilistic safety analysis (PSA). This system results from the combination of the ICARE2 mechanistic code for core degradation developed by IRSN and the CATHARE2 thermohydraulic code developed in collaboration by CEA, IRSN, EDF and FRAMATOME-ANP.

This system is also an excellent synthesis tool for all phenomenological knowledge on core degradation. ICARE/CATHARE is designed to :

- evaluate the consequences of a severe accident upon the primary system of a PWR (from the initiating event to vessel failure) ,
- calculate experimental programmes conducted by IRSN and French or international partners.

14.6.1 Brief Description of the ICARE/CATHARE V2 Code

ICARE/CATHARE is composed of a series of modules that each deal with a specific phenomenon : thermohydraulics, thermics, mechanics, chemistry, fission products, movement of materials, debris beds, core meltdown, etc.

The V1 version (released from 1999) has been used for IRSN level 2 PSAs applied to 900 MWe reactors.

The first V2 version (V2.1) combined with a 3D thermohydraulic model has been released in 2007 and simulates all physical phenomena, including vessel failure. The system is designed to facilitate the integration of new models and perform calculations both for experimental programmes and reactors.

The validation phase carried out in partnership with about ten foreign organisations includes :

- approximately one hundred separate effect tests (chemistry, mechanics, reflooding, etc.),
- about thirty integral degradation tests making it possible to validate core & structure degradation models (PHEBUS, MAESTRO, PBF, QUENCH, etc.) and enabling coupling with the primary system (LOFT),
- reactor sequence calculations.

Most of the thermohydraulic models benefit from the validation of the CATHARE code.

Development is achieved in a high-level scientific environment: fundamental research (theses & post doctoral studies), collaboration with universities and French & foreign research organisations [(CEA, IMFT/Toulouse, Kurchatov & IBRAE Institutes (Russia), ENEA (Italy), etc.)], not to mention participation in several European R&TD Framework Programmes and international projects (OECD MASCA). International seminars for the Users' Club are held on a regular occasion and unite about fifty users from various different countries.

14.7 Seoul National University (SNU)

14.7.1 Brief Description of the MAAP4 Code 4.03

The Modular Accident Analysis Program (MAAP4) was developed by Fauske & Associates, Inc. MAAP4.03 is a fast running, integrated severe accident analysis code to simulate a transient and specifically accounts for system events that occur during the transient, including operator actions. MAAP4, as a severe accident code, is most widely used by nuclear utilities and vendors because of its short run time and reduced requirements for code expertise. In addition, MAAP4 can be used by an existing plant to simulate how a proposed modification would affect plant operations. Also, plant designers could use the code to predict the performance of future plants if a certain set of conditions were imposed on those plants.

MAAP4 is a fully integrated severe accident analysis code and includes models for important thermal hydraulic and fission product phenomena which may occur during a postulated accident in a pressurized water reactor plant.

The underlying models for MAAP4 address the following phenomena:

- Reactor coolant system (RCS) thermal hydraulics
- Cladding water reaction
- Reactor core heatup, melting and relocation
- Containment thermal hydraulics
- Fuel coolant interactions
- Molten core concrete interactions
- Hydrogen combustion
- Fission product release, transport and deposition.

MAAP4 has capability to model the following in-vessel recovery and advanced reactor systems:

- Modeling of core melting and relocation; and separately tracking UO2, Zircaloy, ZrO2, and control rod materials
- Reactor vessel cooling by containment water surrounding the vessel
- Reactor vessel lower head creep rupture
- Generalized containment model
- Generalized user-defined event codes.

MAAP4 solves a set of lumped parameter, nonlinear, first order, coupled, ordinary differential equations in time. These equations generally express the conservation of mass and energy. Momentum balances in MAAP are assumed to be quasi-steady. MAAP4 then calculates thermal hydraulic and fission product variables at each time step.

The modeling of regions, components, and phenomena is fully integrated into the code. For example, thermal hydraulic and fission product models are generally applicable to such major regions as the reactor coolant system, pressurizer and containment nodes treated in the code. The thermal hydraulic parameters are calculated at each time step, and the fission product parameters are overlaid on the thermal hydraulic models. This feedback permits full interaction between the models. In addition, all of the models are run in parallel. The integrated reactor coolant system and containment modeling is ideal for the passive plant application.

The execution of the MAAP4 code requires the development of two input files: a parameter file and a sequence file. The parameter file describes the nonvariant, plant specific data including geometry, performance data, and system setpoints. The sequence file describes the severe accident sequence to be analyzed including the initiating event, system operability status, and operator actions. MAAP4 automatically initiates system operation, based on system availability described in the sequence file and setpoints described in the parameter file. Similarly, operator actions can be modeled in the sequence file by employing the user-defined event codes to describe the timing and implementation of emergency actions.

The results of the MAAP4 analysis describe the severe accident progression and fission product releases associated with accident sequences analyzed. MAAP4 evaluates the following details of the severe accident:

- Time histories of the important state parameters, such as pressure, temperature, and inventories in each control volume of the reactor coolant system and containment models
- Timing of engineered safety system initiation and termination
- Timing and magnitude of severe accident phenomena predicted to occur in an accident sequence
- Time history for fission product locations and states, including fission product releases to the environment

14.8 IKE

IKE is developing models for the German system code ATHLET-CD, especially for the late phase of core degradation and for the coolability of core debris. In the benchmark calculations, IKE was applying the ATHLET-CD code to model the plant behaviour. Up to the onset of quenching, standard models were used. During the quenching phase, the MEWA module, which is based on a porous medium

approach, was activated, in order to describe the behaviour of a particulate debris bed which was assumed to be formed during flooding.

14.8.1 Brief Description of the ATHLET-CD/MEWA Code

Since the ATHLET-CD code is already described in more detail in the GRS contribution, here only a brief descriptin of the MEWA module is provided.

The MEWA module is being developed and integrated in the German system code ATHLET-CD for the description of late phase core melting. It is developed from a combination of the MESOCO and WABE models. The MEWA model is designed to describe the processes of late phase core degradation with massive melting, melt relocation, molten pool formation and behaviour up to the relocation of melt to the lower head, taking into account the effects of possible core refloding. Emphasis is on the potential accumulation of larger melt masses and on the resulting modes of outflow from the core, which determine the chances of coolability by water injection and the subsequent processes in the lower head.

The processes in a strongly degraded core are described in a quasi-continuum approach in two-dimensional cylindrical geometry. Solid, melt and two-phase fluid (gas/steam) are modelled as separate phases with thermal non-equilibrium between all phases. Several material components can be considered in the solid and melt phase, especially metallic and ceramic components are distinguished. The gas phase can be composed of steam and hydrogen to take into account oxidation of metallic components. Melt velocities are calculated according to the Ergun approach for flow in a porous medium. Formation of a molten pool is detected from the quasi-continuum model based on melt volume fractions. The thermalhydraulics of the molten pool are not simulated directly. The thermal behaviour is described either by empirical correlations or by a representative model assuming an axial temperature profile in the center and a boundary layer flow along the crust of the pool.

Simplified momentum conservation equations are also used for the two-phase fluid, assuming dominant friction between the solid matrix and the phases and neglecting temporal and spatial derivatives of the velocities. For the particle-fluid drag forces the model of Ergun is adapted which is presently extended for two separated fluids by the introduction of relative permeabilities and passabilities according to Reed. Alternatively, a more detailed formulation of drag forces according to Tung and Dhir can be chosen which takes into account flow pattern for bubbly, slug and annular flow and an explicit formulation of interfacial drag between steam and water. The explicit formulation of interfacial drag is considered as essential when multidimensional flow occurs.

In integrated calculations with ATHLET-CD, the modelling can be switched from the description by the rod-oriented ECORE model to the porous media model MEWA, based on user-defined criteria on porosity, melt fraction or temperature. This can be done progressively for parts (groups of meshes) of the core. Since the thermalhydraulics of the coolant in the debris bed is described by MEWA, the ATHLET thermal-hydraulic modelling is switched off in the respective region. The coupling is provided through the exchange of mass and enthalpy flows over the region boundaries.

The development and the validation of the MEWA late phase module for ATHLET-CD are sponsored by the German Federal Ministry of Economics and Technology (BMWi).

15. APPENDIX : ENEA CALCULATION WITH ASTEC V1.3

15.1 TMI-2 Plant Modelling

The TMI-2 plant nodalization scheme employed in this ASTEC V1.3 application is shown in the figure below. The plant nodalization includes a detailed modelling of the primary coolant system with:

- the reactor pressure vessel volumes and structures, including the VENT valve between the cold collector and the hot collector;
- the two primary coolant loops (1 hot leg and 2 cold legs in each loop) with once-through steam generators and main coolant pumps;
- the pressurizer with surge-line, PORV, heaters, spray-line and valve;
- the external walls of the primary circuit;
- main emergency and control systems.

Modelling of the secondary systems is limited to the secondary side of steam generators, the steam lines with isolation valves, and main feedw-ater and auxiliary feedwater injections.

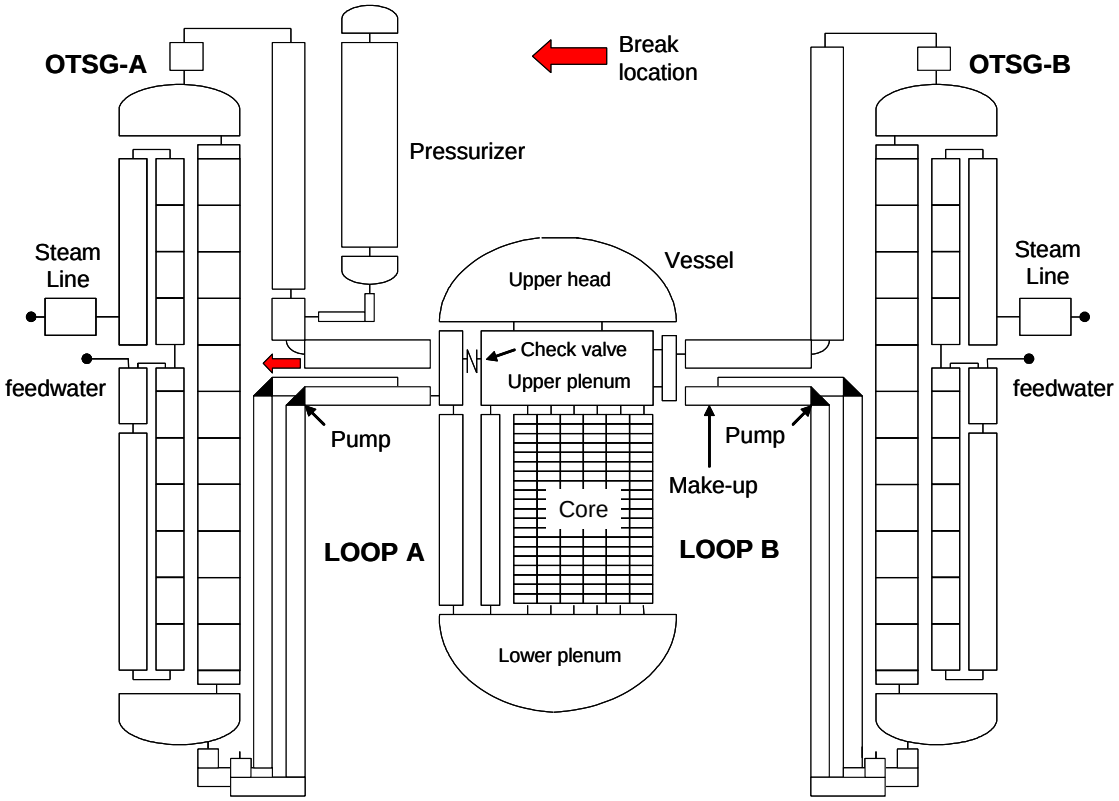

TMI-2 plant nodalization scheme

The core is represented by 6 radial rings plus the by-pass, and axially discretized in 20 equal meshes. The core baffle, the barrel and the thermal shield at the core periphery are also represented. One representative fuel rod component and one control rod component are modelled in each ring. The control rod component simulates all the full and part-length control rods, all the guide tubes (including those containing burnable poison rods) and all the instrument tubes.

The plant geometry, the boundary conditions and the accident scenario have been strictly defined according to alternative TMI-2 scenario benchmark specifications provided by IRSN, as well as recommended values of code physical parameters for the sensitivity study.

15.2 Updated Initial Steady-State Conditions

The TMI2 plant state at transient initiation (initial conditions at t = 0) is obtained by a steady-state code run lasting 500 s and starting from plant thermal-hydraulic parameter values close to the ones specified for TMI-2. During the steady-state calculation, some regulations in the primary and secondary sides are activated to facilitate the achievement of stable conditions, as close as possible to the TMI2 plant state at t = 0 (turbine trip in TMI2 accident).

The regulated parameters are:

- The pressurizer pressure by turning on the heaters when the pressure is lower than the nominal value;
- The pressurizer liquid mass, by water injection or draining, in order to obtain the precise liquid level;
- The feedwater mass flowrate at the steam generator downcomer inlet according to the steam mass flowrate at the dome outlet;
- The primary loop mass flowrate, according TMI2 data, varying the pump rotation speed during the first 100 s of steady-state run.

The TMI2 plant initial conditions calculated by ASTEC V1.3 are compared with TMI2 accident data at turbine trip in the table below. The primary circuit conditions are very well reproduced by ASTEC. Since the turbin trip in TMI2 accident was provoked by instabilities and sudden pressure increase in the secondary circuits, the steady-state conditions calculated by ASTEC for the secondary side cannot precisely match the TMI2 data.

Parameter	Unit	ASTEC V1.3	TMI-2
Reactor Power	W	2700	2700
Primary Pressure	MPa	15.2	15.2
Temperature Hot Leg A	K	592.1	592
Temperature Hot Leg B	K	592.1	592
Temperature Cold Leg A	K	563.8	548-561
Temperature Cold Leg B	K	564.1	565
Mass Flow Rate – Loop A	kg/s	8290	8280
Mass Flow Rate – Loop B	kg/s	8560	8560
Pressurizer Level	M	5.78	5.77

Parameter	Unit	ASTEC V1.3	TMI-2
Total Primary Mass	ton	225120	-
Pressure SG A	MPa	6.80	7.31
Pressure SG B	MPa	6.80	7.24
Steam Temperature SG A	K	574	586
Steam Temperature SG B	K	575	586
Collapsed Level SG A	M	3.7	-
Collapsed Level SG B	M	3.5	-
Liquid Mass SG A	Kg	19210	-
Liquid Mass SG B	Kg	18410	-
Feedwater Flow SG A	Kg/s	742	723
Feedwater Flow SG B	Kg/s	759	717
SG Feedwater Temperature	K	513	-

15.3 Standard Physical Parameters of the Code

Main core degradation physiscal parameters used in the standard calculation with ASTEC are synthetized in the table below. The physical parameters used in this standard calculation are the ones used for the interpretation of the first two phases of the TMI2 accident with ASTEC V1.2 code in the SARNET project

Parameter	ASTEC V1.3
Zr Oxidation correlation	Correlations proposed by Schanz (FZK): Cathcart correlation if T < 1800 K Prater correlation if T > 1900 K Linear interpolation between 1800 – 1900 K
Cadding failure criteria	T > 2300 K and e(ZrO2) < 300 μm T > 2500 K
UO2-ZrO2 melting temperature	2830 K
Debris formation criteria	No debris bed and molten pool formation modelling (standard and sensitivity case)
Debris diameter	-
Debris porosity	-

Clad deformation and burst due to overpressure is calculated by the creep model derived from French EDGAR experiments. The consequent release of fission products from failed pins and their transport through the primary circuit is not addressed in the present analysis.

The Urbanic-Heidrick correlation is used by default in ASTEC V1.3 for zircaloy oxidation. Other correlations (Cathcat-Pawel and Prater-Courtright) can be used or defined by the code user. In this standard calculation, the correlation proposed by Schanz (FZK – Germany) has been defined and applied to compute zircaloy oxidation and hydrogen generation. This correlation is now implemented as default in the ICARE2 code that will be part of the next ASTEC code release.

Control rod failure and relocation occurs at the melting point of stainless steel of absorber rod cladding through dissolution of the zircaloy guide tube by molten steel. Oxidation of steel is modelled by parabolic laws, once the melt relocates downwards on the external surface of zircaloy guide tube.

When fuel rod temperature exceeds the melting point of zircaloy, the Kim-Olander convective model is applied to evaluate the fuel dissolution by molten zircaloy; the simultaneous dissolution of oxide layer is evaluated by the Hofmann diffusive model. The limit in fuel dissolution is based on the liquidus line of ternary U-Zr-O diagram. During this phase, fuel rod clad failure and metallic melt relocation is assumed to occur if clad temperature exceeds 2300 K and oxide layer thickness is lower than 300 μm, or, in any case, when clad temperature exceeds 2500 K. Once the clad fails, the molten U-Zr-O mixture is relocated downwards on the external surface of cladding, at constant velocity (0.6 m/s), until its solidification in a colder region of the core.

Debris bed and magma models are not applied in the late core degradation phase; therefore, fuel rod melting and relocation is computed in rod-like geometry by decanting and candling models. Fuel rod melting is calculated at 2830 K, according to the eutectic temperature of UO_2-ZrO_2 binary phase diagram.

15.4 Chronology of Major Events

The chronology of major events calculated by ASTEC is presented in the table below and discussed in the following section 5.

Event	Time (s)	
	Standard case	Sensitivity case
Break opening and loss of feedwater	0	0
Reactor scram	20	20
Pressurizer is empty	145	145
Primary pump void fraction > 0.6	4740	4740
Primary pump shutdown (M < 85000 kg)	4825	4825
Onset of core uncovery	5580	5580
Onset of core heatup	5950	5950
Beginning of oxidation (DIVA start)	**6431**	**6431**
First fuel rod clad burst	7145	7130
First melt relocation (U-Zr-O)	**7370**	**7428**
First ceramic melting (UO2-ZrO2)	8820	8550
Onset of reflooding	**9825**	**9825**
End of calculation	**12000**	**10928**

15.5 Result Analysis

Despite the hot leg break opening at 0 s, the contemporary feedwater trip with consequent loss of heat removal by the secondary side results in primary pressure increase. The pressure rise leads to reactor scram (P > 16.3 MPa) by the protection system at 20 s. After reactor scram the primary pressure starts to decrease. The primary pressure decrease is accelerated when the pressurizer is empty at 145 s, and the primary pressure approximates the secondary pressure after about 300 s.

Before pump shutdown, a mixture of liquid water and steam circulates in the primary circuit and through the core in saturated conditions, while the void fractions in the primary system increase due to the loss of fluid (mostly liquid) from the hot leg break. In this conditions, the core decay power and pump heat are removed by the steam generators. The primary pump void fraction is greater than 60% after 4740 s. According to benchmark specifications, the primary pumps are shutdown a little bit later at 4825 s, when the total primary mass decreases down below 85000 kg.

After pump shutdown, the liquid water starts to settle down and in the primary circuit and inside the vessel. By this time, the break flow rate quickly reduces, changing from mostly liquid to pure steam flow due to liquid stratification in the primary system with hot leg draining. The core starts to uncover at 5580 s, while core heatup starts at 5950 s at the core top, because the core decay power is no more removed by natural circulation in the primary circuit.

When the maximum core temperature exceeds 773 K at 6431 s, the DIVA module of ASTEC is activated to compute in-vessel core degradation and melt relocation. By this time onwards, the oxidation of the claddings is calculated by DIVA. First fuel rod clad burst due to overpressure is calculated by ASTEC at 7145 s in the standard calculation, when the maximum clad temperature reaches 1250 K at the top of the core centre. In the sensitivity calulation, first clad burst occurs a little bit earlier at 7130 s due to higher oxidation rate below 1200 K with Urbanic-Heidrick correlation. Oxidation runaway with sudden temperature excursion occurs first at the top of the core at 7360 s in the standard calculation. It is followed after few seconds by clad failure (T > 2300 K) and first melt relocation. First clad failure and melt relocation is calculated later on at 7428 s in the sensitivity calculation due to the lower oxidation rate of Urbanic-Heidrick correlation above1200 K.

The different oxidation kinetics is also likeky the main reason for the different ratio of UO2 dissolution in the two ASTEC calculations (565 kg and 1575 kg in standard and sensitivity calculations, respectively). In fact, higher oxidation rate above the melting point of zircaloy in the standard calculation results in earlier clad failure and consequent lower duration of molten zircaloy and UO2 contact. The slightly difference in clad failure criteria does not seem to contribute significantly to the difference in the amount of UO2 dissolved.

Fuel rod melting starts much earlier in the sensitivity calculation, at 8550 s, due to the lower melting point of UO2-ZrO2 considered in this calculation. The total mass of molten UO2 before reflood is 30590 kg (including dissolved UO2), much higher than the one of the standard calculation that is 8900 kg. The total mass of molten metals before reflood (17190 kg and 14510 kg in standard and sensitivity calculations, respectively) is about 15% higher in the standard calculation due to larger axial extent of degradation in the more external core rings, as evidenced in synthetic core degradation views in section 6.

The mass of hydrogen produced before reflood is 331 kg in the standard calculation and 278 kg in the sensitivity calcualtion. The large difference is partly due to different oxidation kinetics and partly caused by different axial extent of oxidized zone at core periphery.

Core reflood by HPI injection is started at 9825 s, 5000 s after pump trip according to benchmark specifications. By this time, the collapsed core water level is about 60 cm above the core bottom in both calculations. The reflood of the core results in sudden primary pressure increase due to steam formation and hydrogen generation. Maximum pressure peak is larger in the standard calculation (10.4 MPa) than in the sensitivity one (9.2 MPa) due to enhanced hydrogen release during reflood.

After reflood, the core is rapidly and completely quenched in about 8 minutes. The hydrogen mass produced during reflood is 29 kg in the standard calculation, about 8% of the total H2 mass release (360 kg), and only 7 kg in the sensitivity calculation (total mass release = 285 kg). The difference seems related to material mixture oxidation, as confirmed by the sharp decrease of the fraction of non-oxidized Zr in the molten material (approximately 5%) observed in the standard calculation during reflood.

Core degradation and increase in the total amount of molten materials during reflood is not very significant in both standard and sensitivity calculations (1960 kg and 520 kg, respectively), as indicated by synthetic core views before and after reflood (see section 6).

Note: The boundary conditions of the steam generators deviate from the specification values after 6700 s and 10700 s (SG pressure decrease and water level increase) owing to steam condensation phenomena in the secondary side in isolated conditions (no auxiliary feedwater injection).

15.6 Major Discrepancies with Other Code Results

In general the thermal-hydraulic behavior of the primary system calculated by ASTEC is consistent with other code results. The main discrepancies concern:

The heat transfer to the secondary side before pump stop, which is much larger with ASTEC likely due to overestimation of total pump heat loss into the primary circuit.

- The primary pressure increase after pump stop, which is avoided in ASTEC calculation by steam circulation in the primary circuit and condensation on steam generators with heat decay heat removal.
- The primary pressure after reflooding that follows the steam generator pressure (heat removal by the secondary side).
- The core uncovery that starts with some delay with respect to other codes (likely much water settle down inside the vessel after primary pump shutdown).
- The rod heatup at core top is larger than other code results, likely due to lower natural circulation calculated by ASTEC inside the core.

Cumulated hydrogen production and total mass of molten materials before and after reflood is consistent with other code results.

15.7 Synthetic Views of the Core at Selected Instants

15.7.1 Standard Case

STANDARD CASE: Beginning of oxidation (6431 s) – Global view

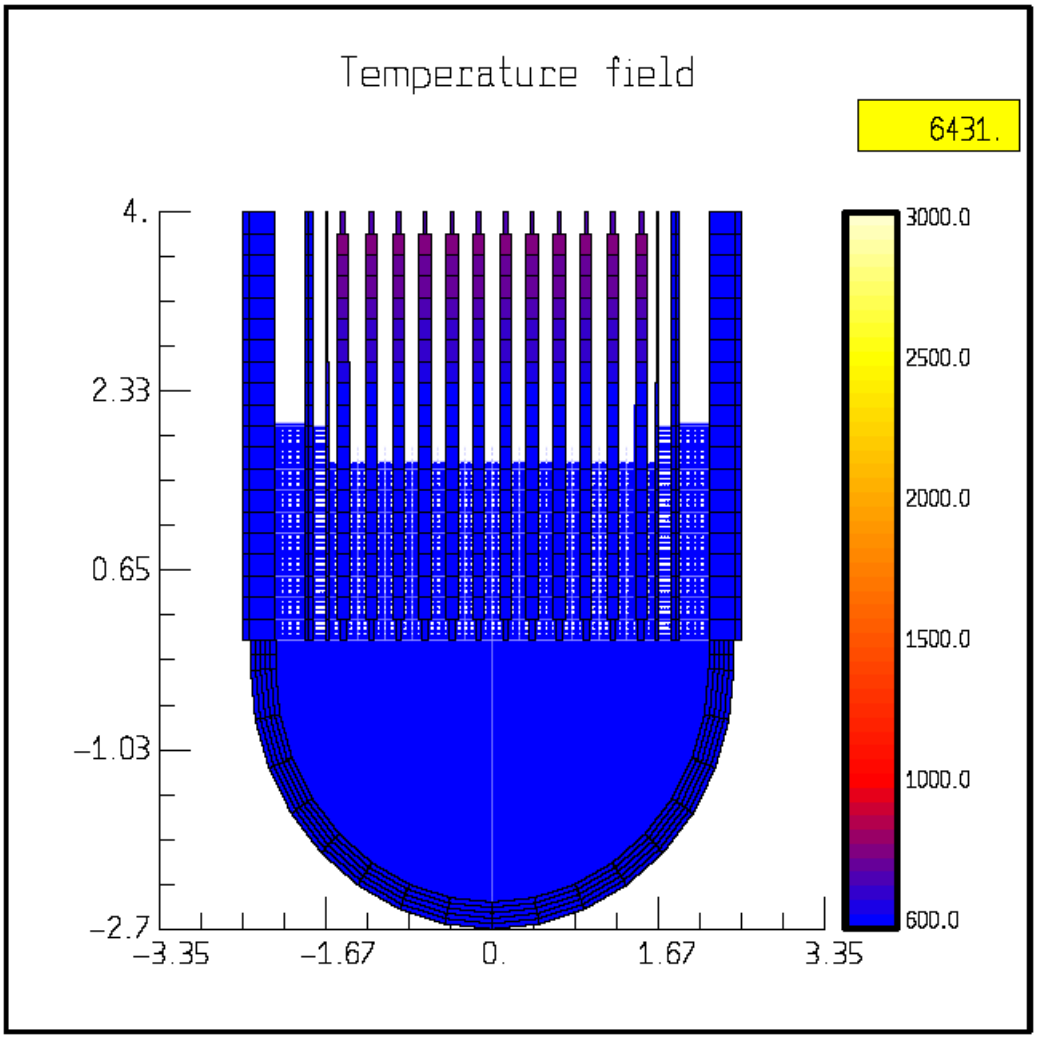

STANDARD CASE: Beginning of oxidation (6431 s)

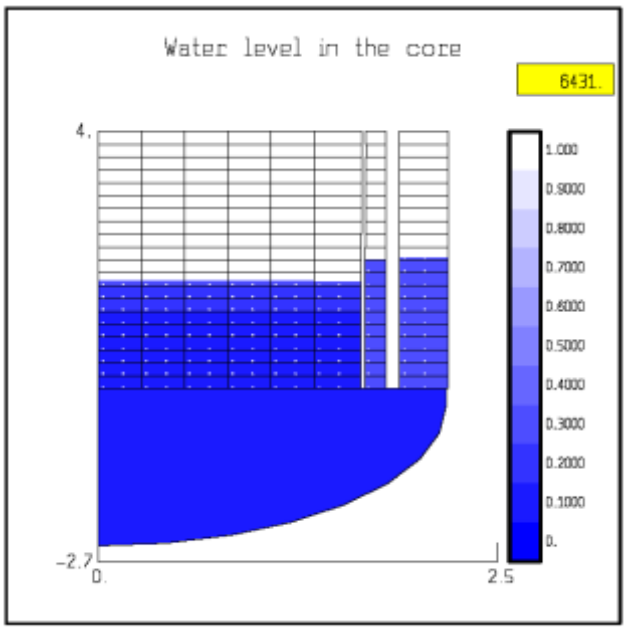

Void fraction distribution

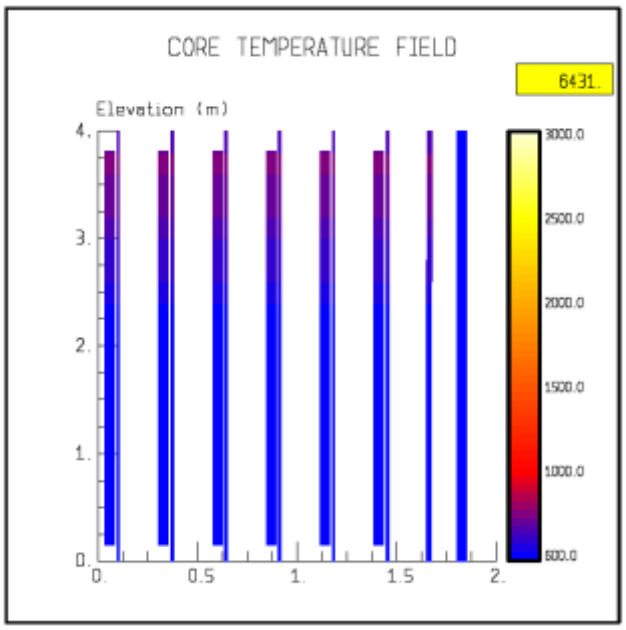

Temperature distribution

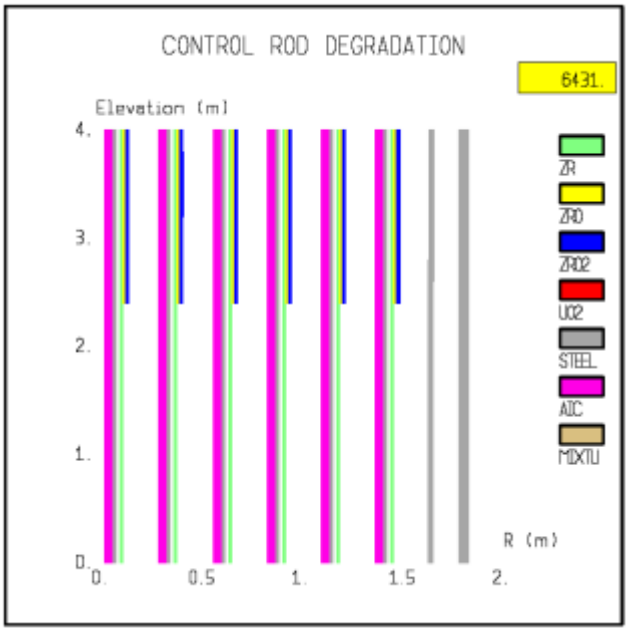

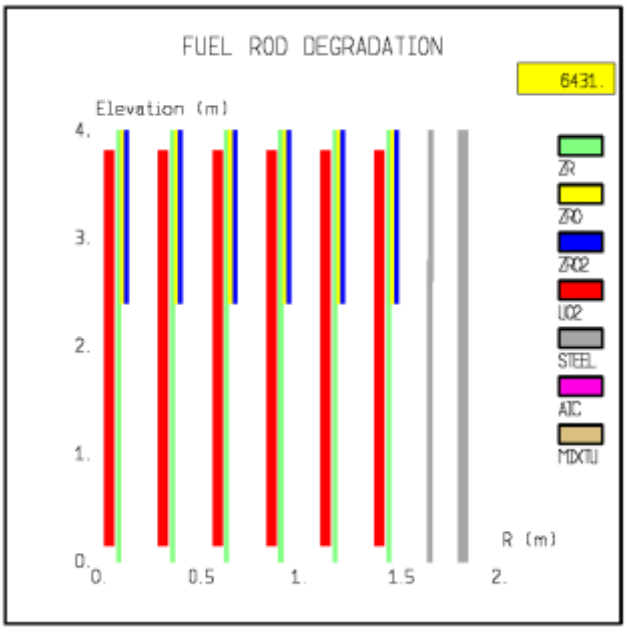

Geometry and degradation

STANDARD CASE: Time of first melt relocation (7370 s) – Global view

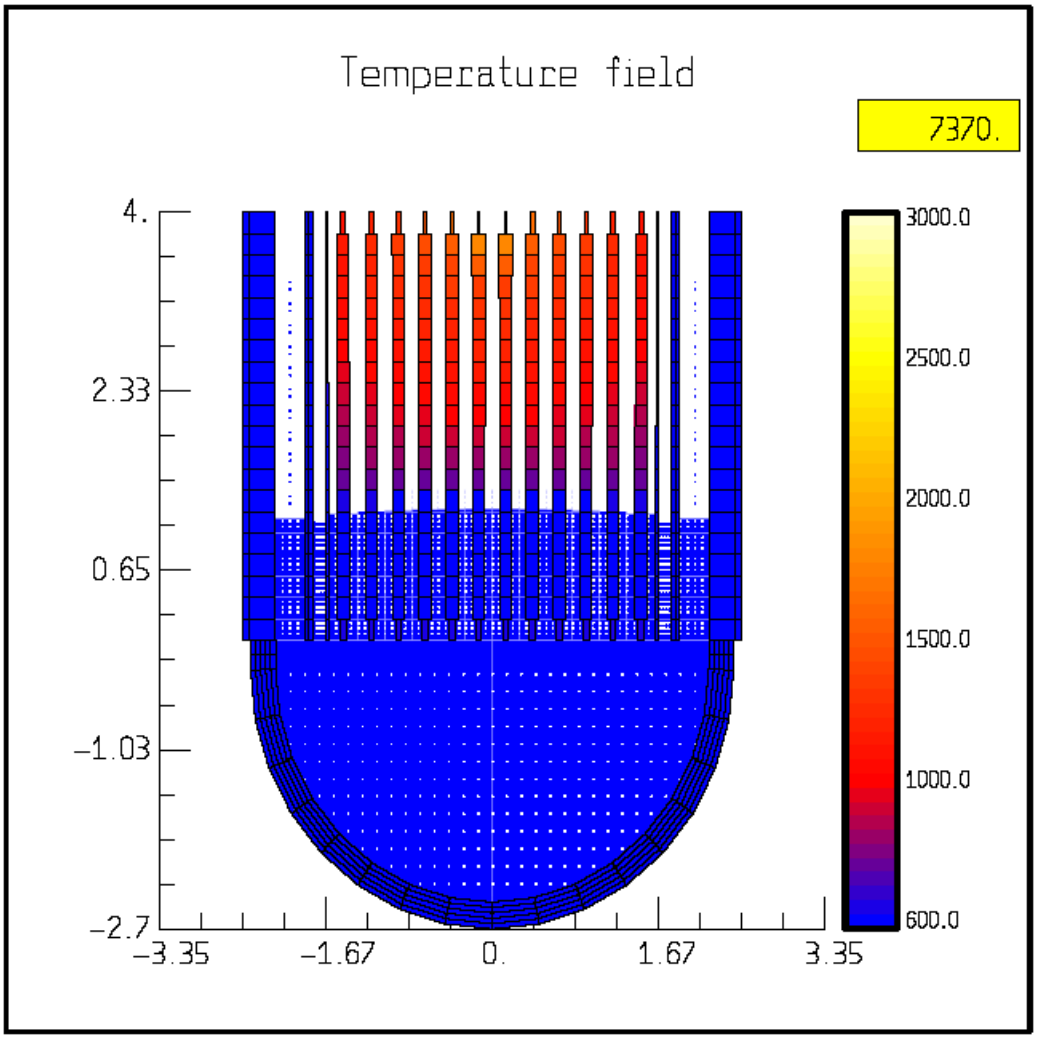

STANDARD CASE: Time of first melt relocation (7370 s)

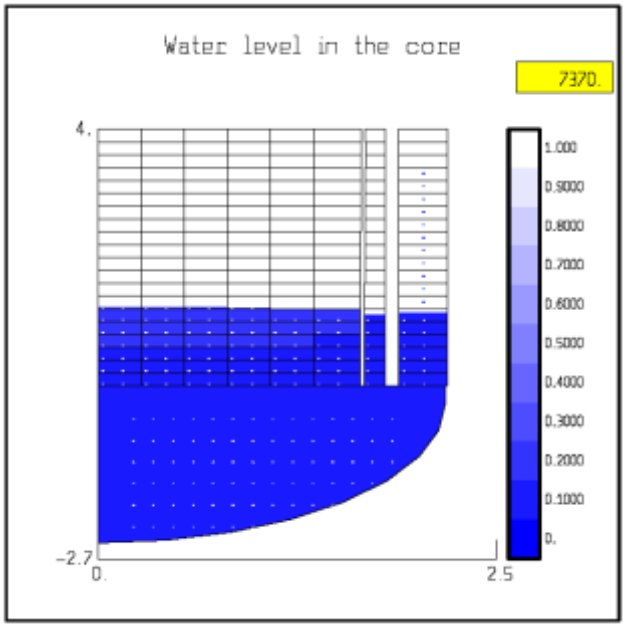

Void fraction distribution

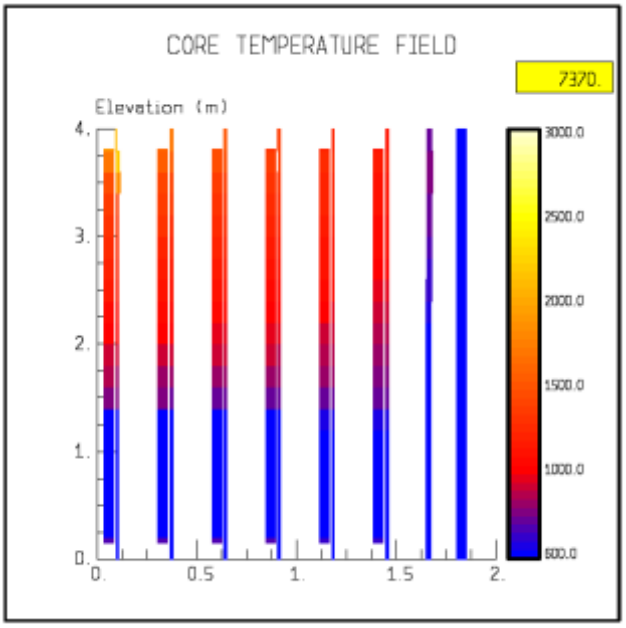

Temperature distribution

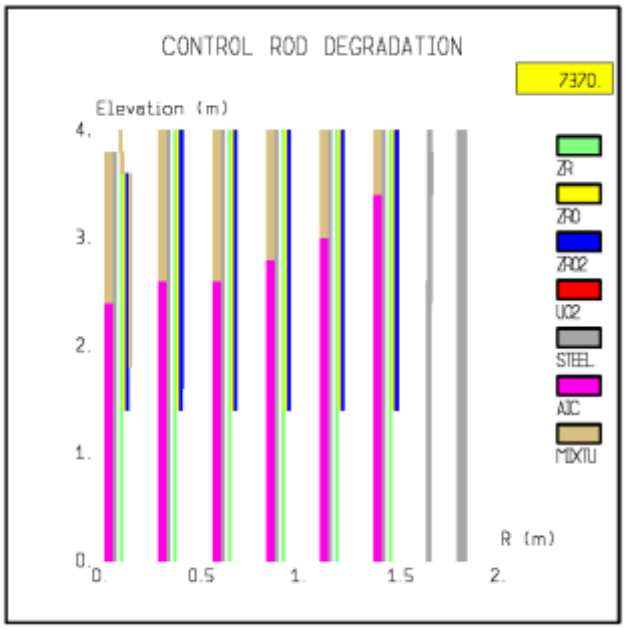

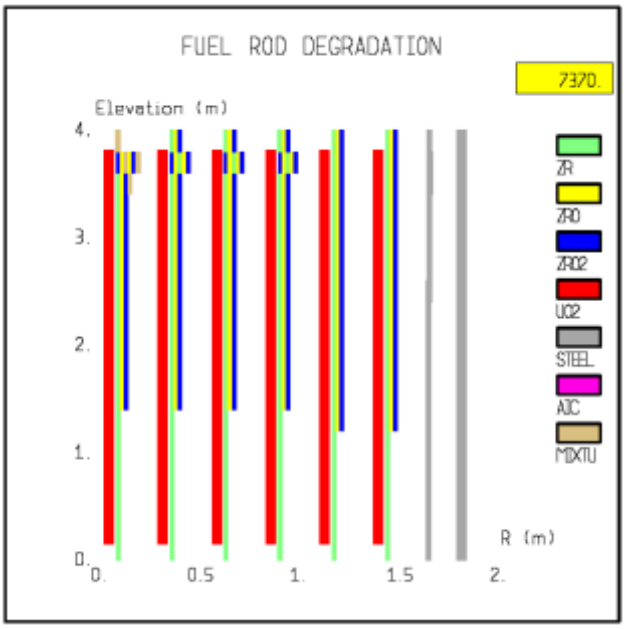

Geometry and degradation

STANDARD CASE: Time of reflooding (9825 s) – Global view

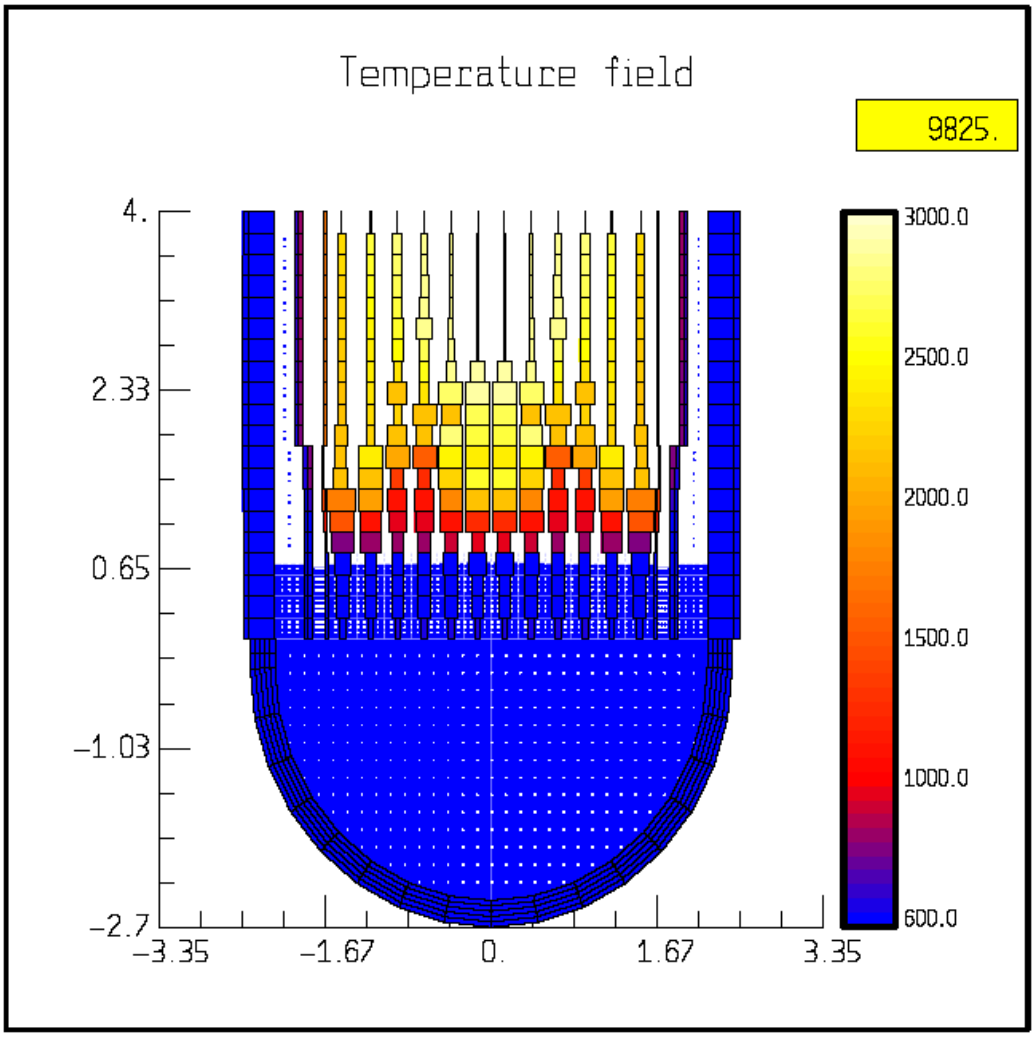

STANDARD CASE: Time of reflooding (9825 s)

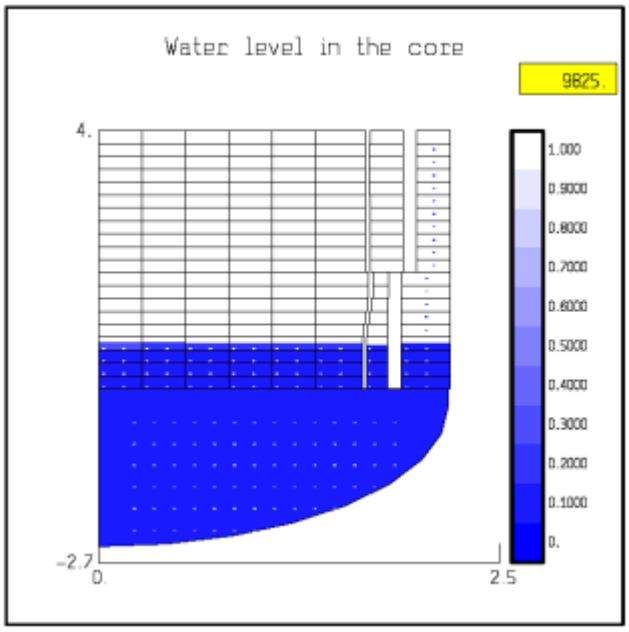

Void fraction distribution

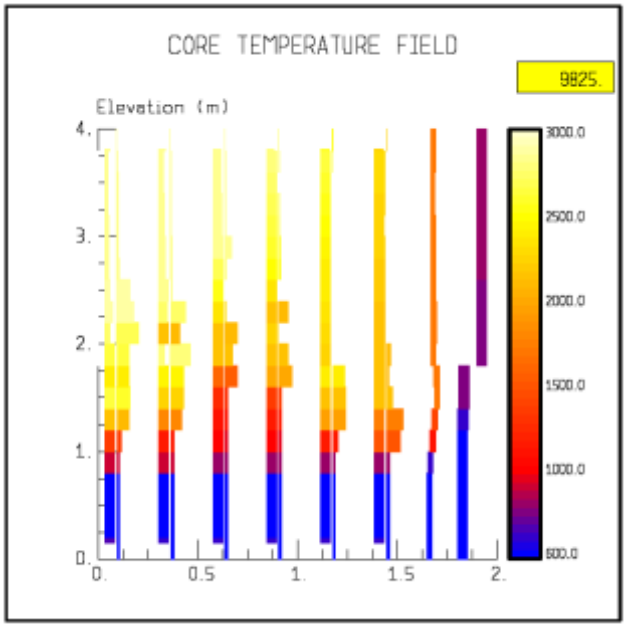

Temperature distribution

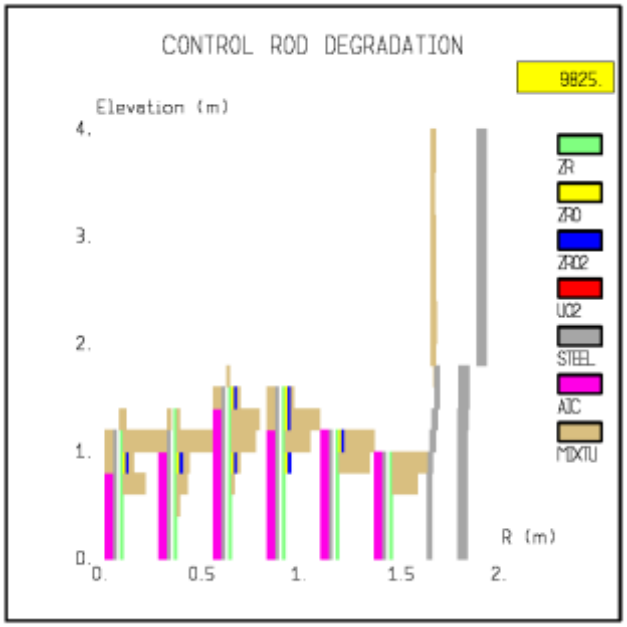

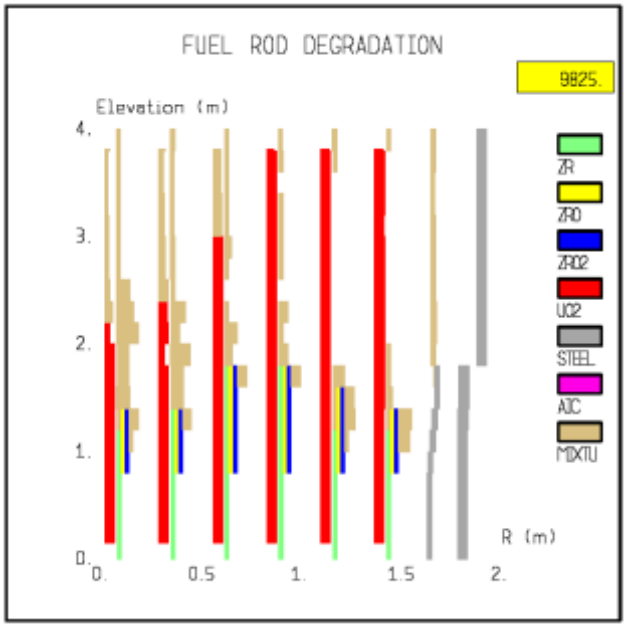

Geometry and degradation

STANDARD CASE: End of calculation (12000 s) – Global view

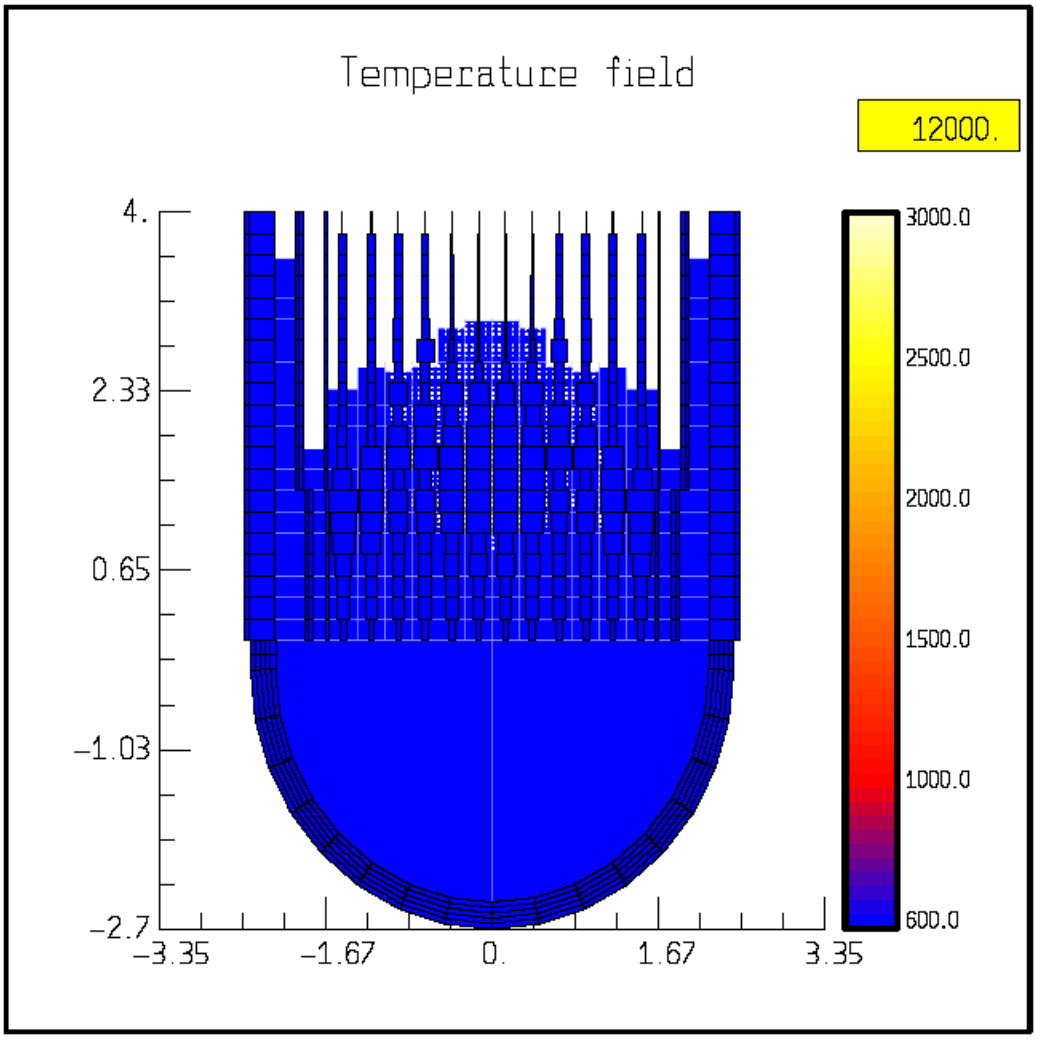

STANDARD CASE: End of calculation (12000 s)

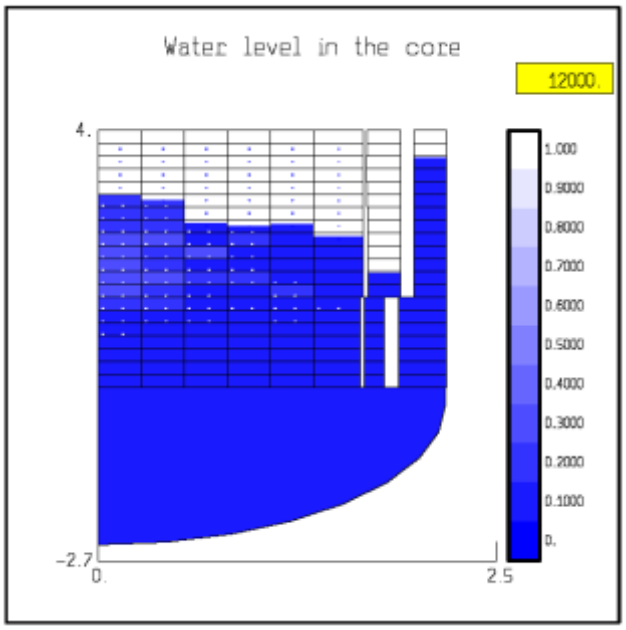

Void fraction distribution

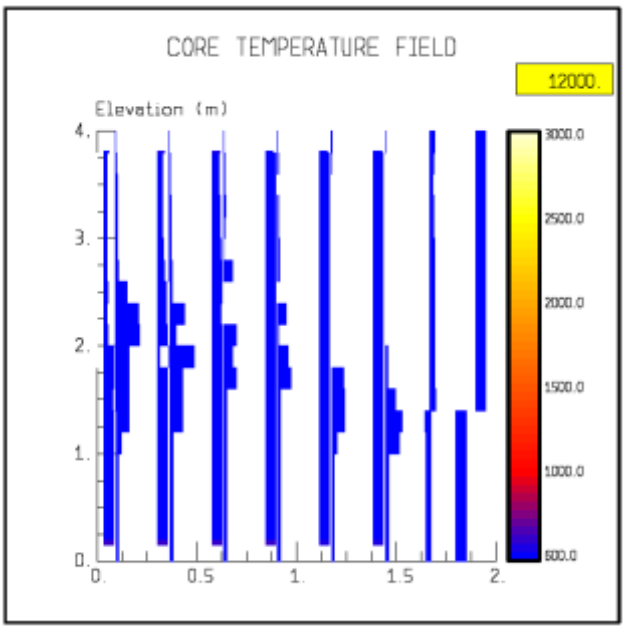

Temperature distribution

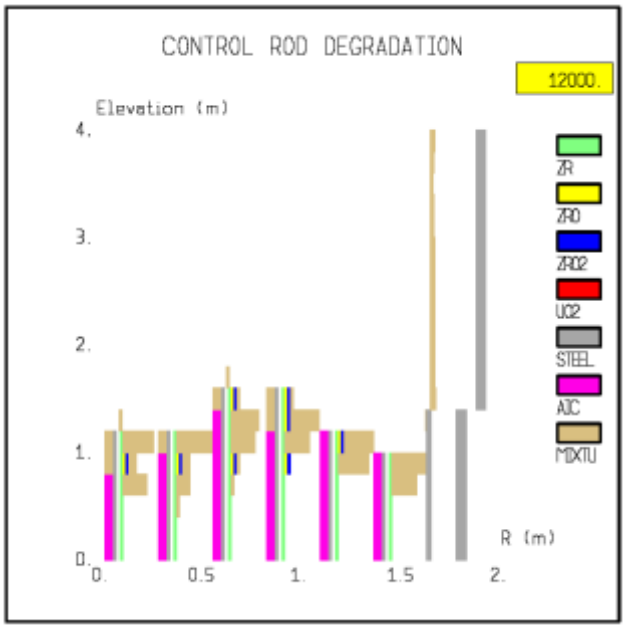

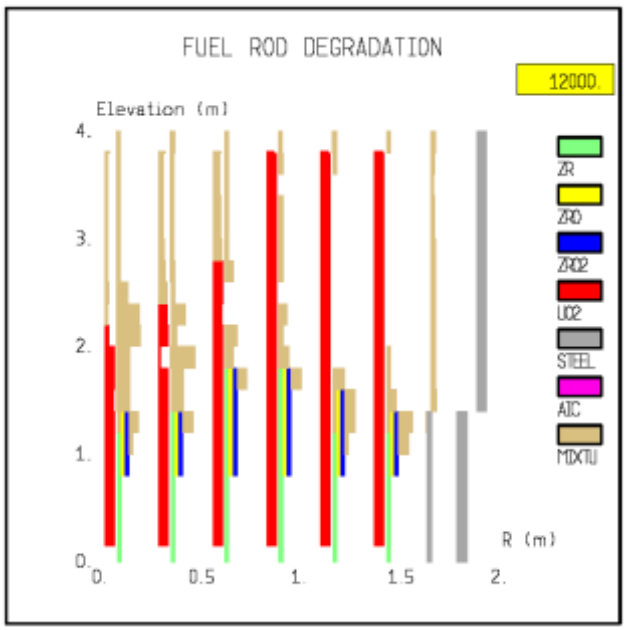

Geometry and degradation

15.7.2 Sensitivity Case

SENSITIVITY CASE: Beginning of oxidation (6431 s) – Global view

Same Results as Standard Case

SENSITIVITY CASE: Time of first melt relocation (7428 s) – Global view

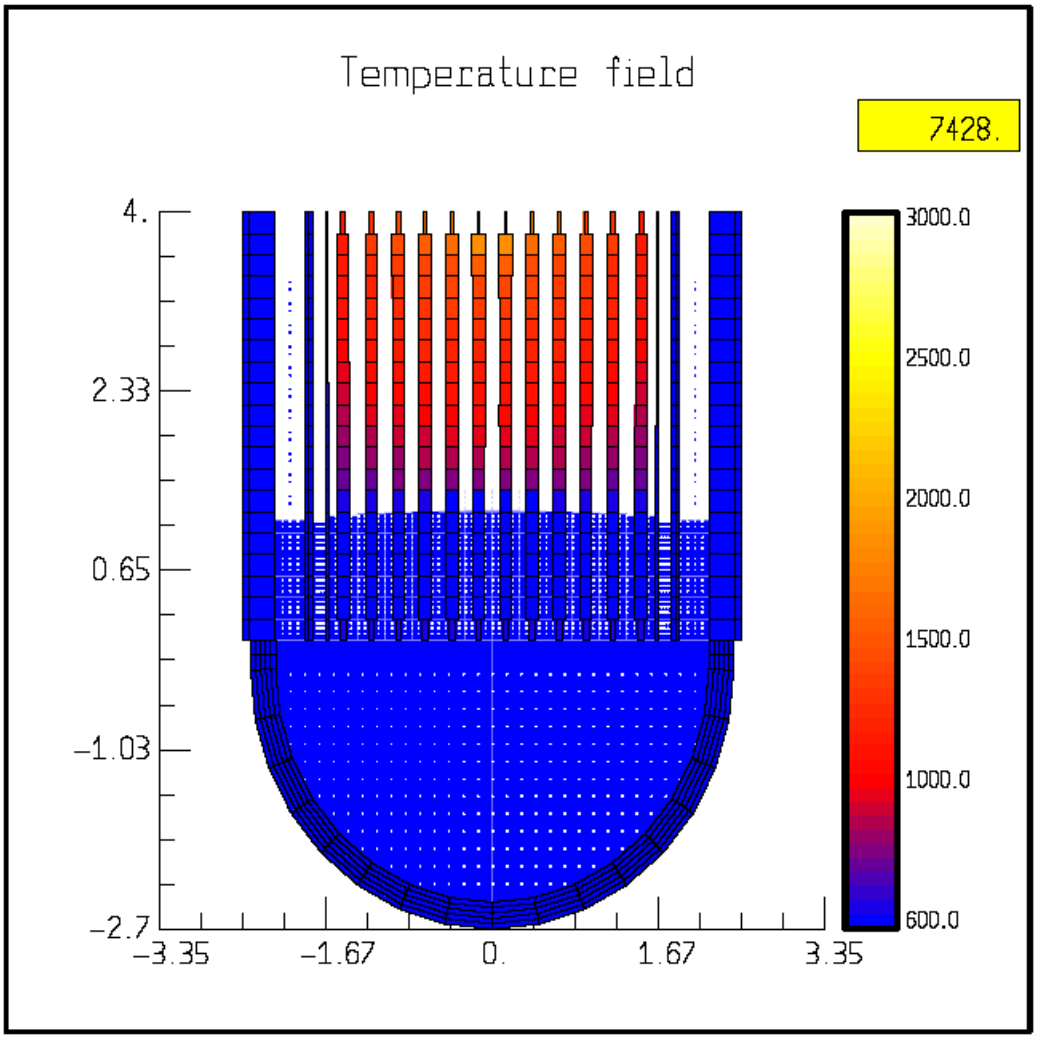

SENSITIVITY CASE: Time of first melt relocation (7428 s)

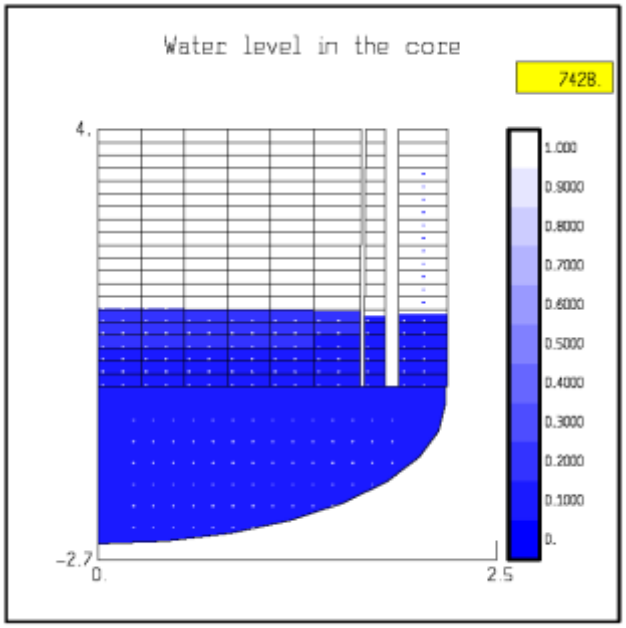

Void fraction distribution

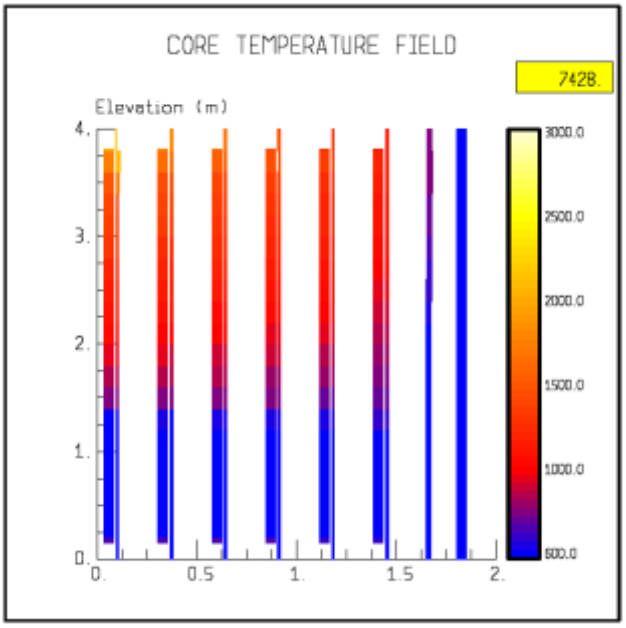

Temperature distribution

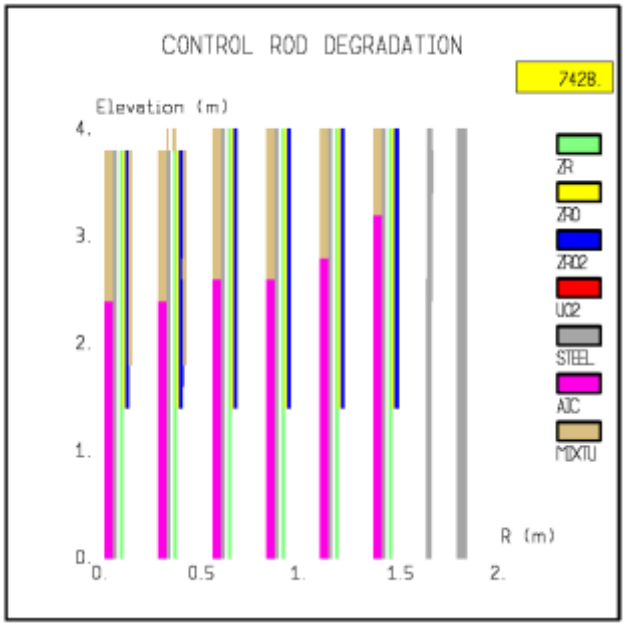

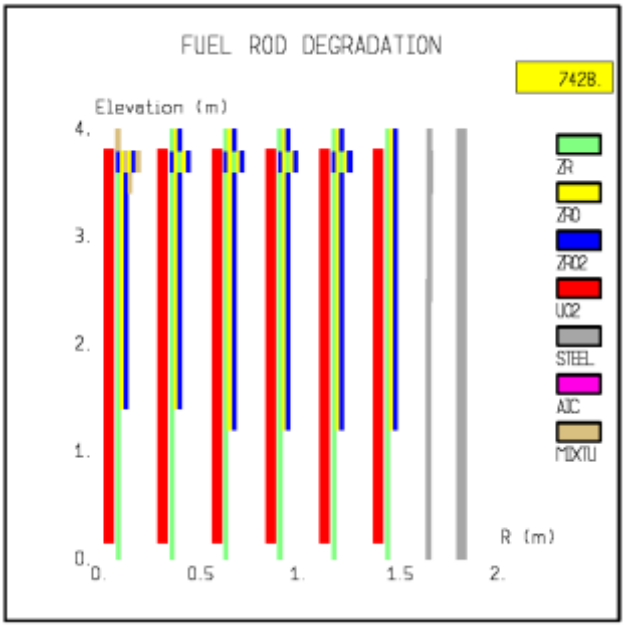

Geometry and degradation

SENSITIVITY CASE: Time of reflooding (9825 s) – Global view

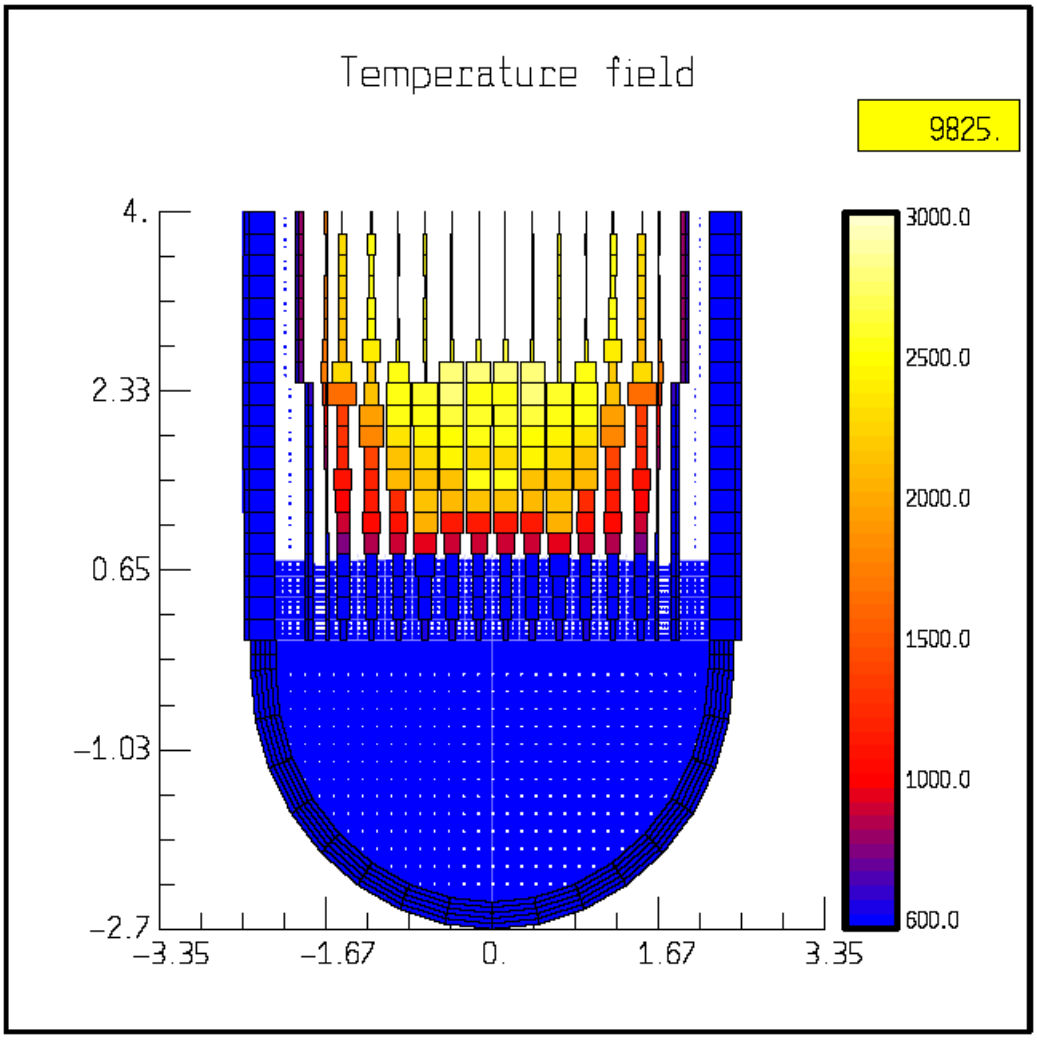

SENSITIVITY CASE: Time of reflooding (9825 s)

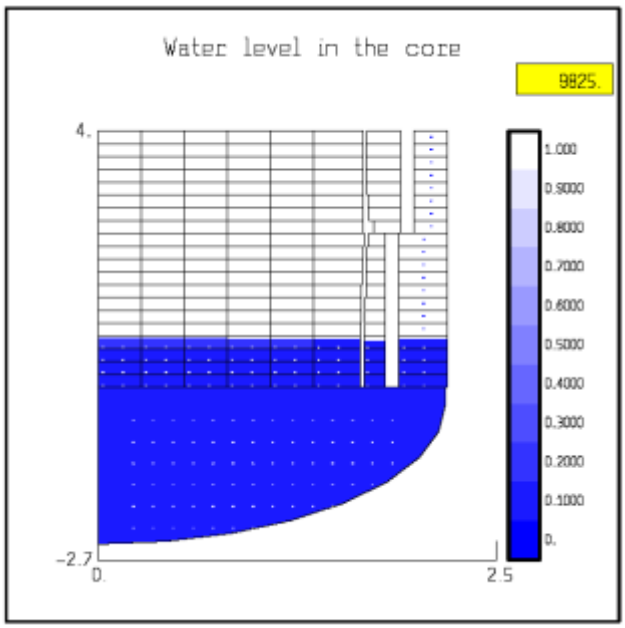

Void fraction distribution

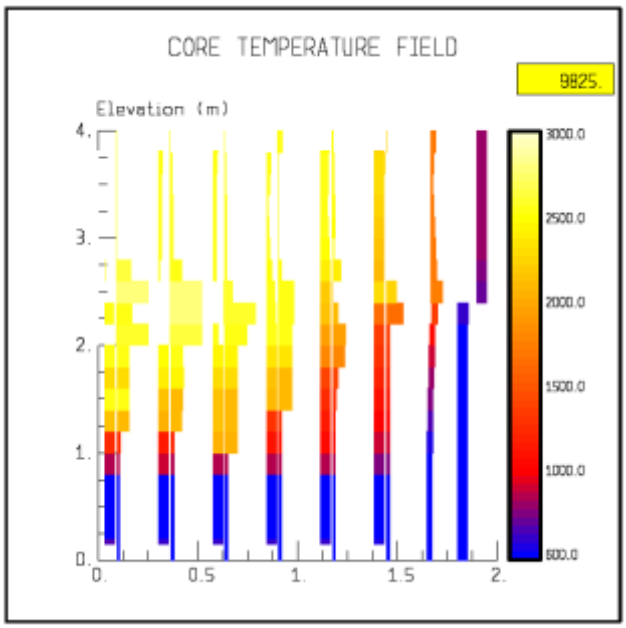

Temperature distribution

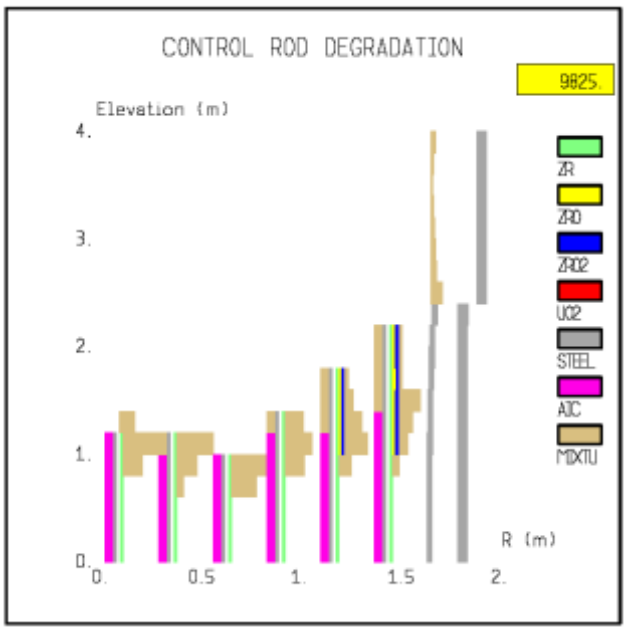

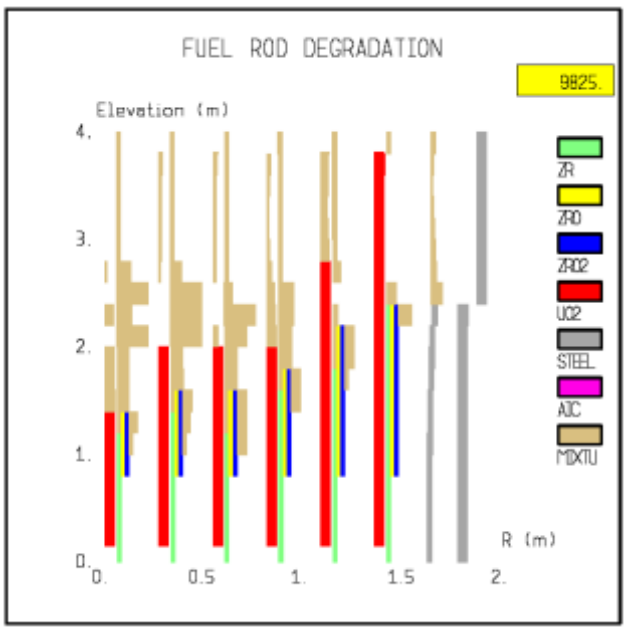

Geometry and degradation

SENSITIVITY CASE: End of calculation (10928 s) – Global view

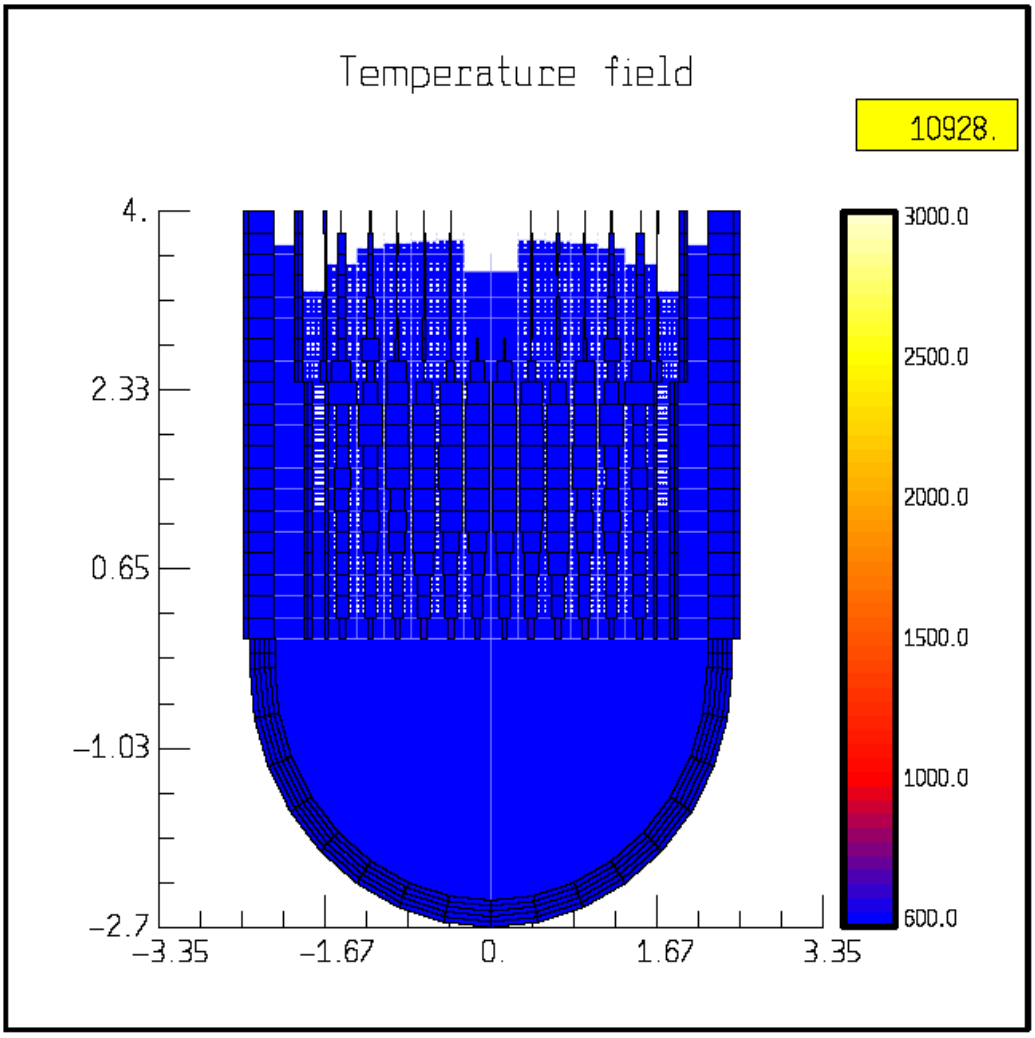

SENSITIVITY CASE: End of calculation (10928 s)

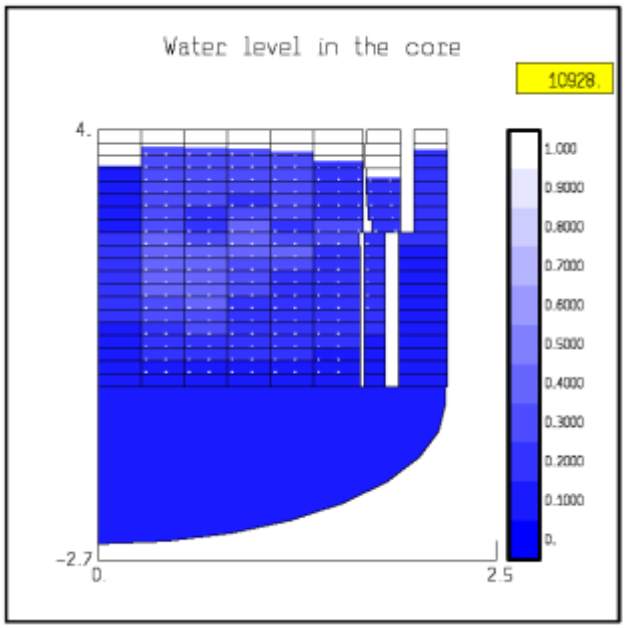

Void fraction distribution

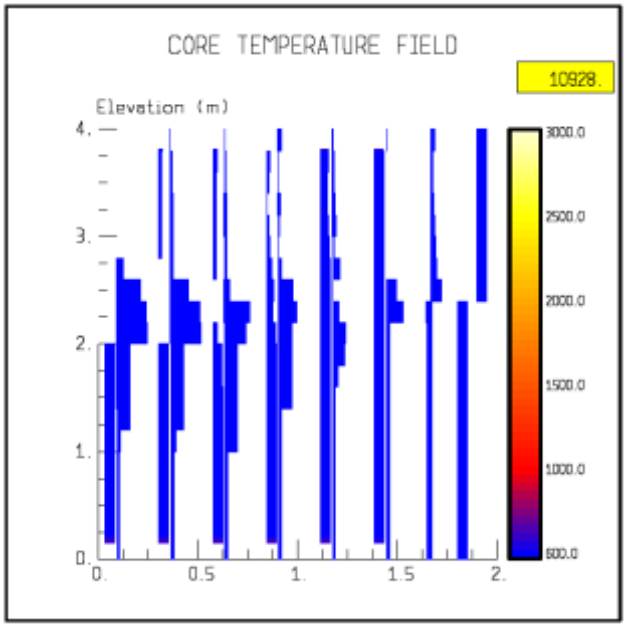

Temperature distribution

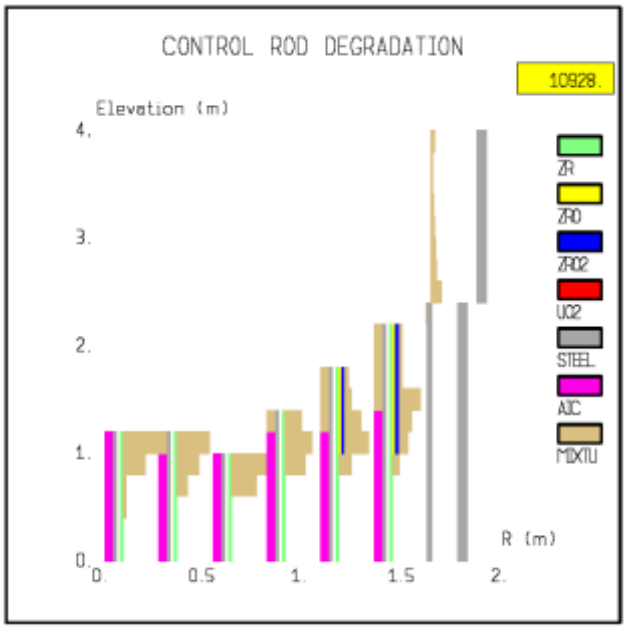

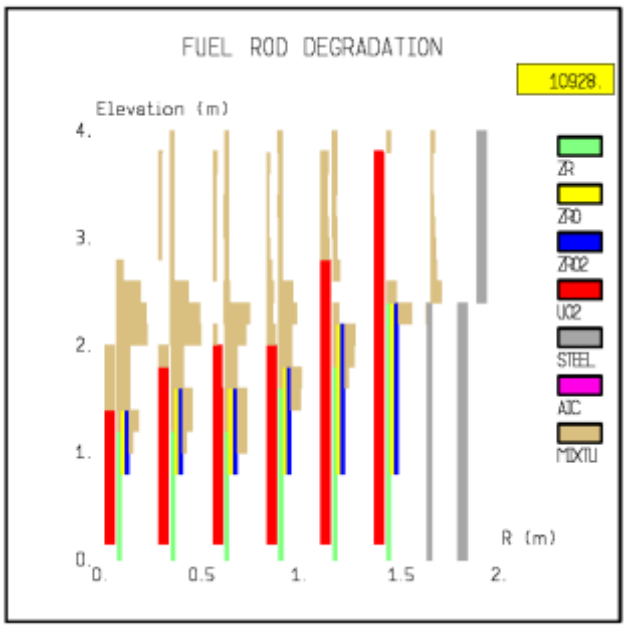

Geometry and degradation

16. APPENDIX : GRS CALCULATION WITH ATHLET-CD

16.1 TMI-2 Plant Modelling

The nodalization adopted for the ATHLET-CD benchmark calculations is shown in Fig. 16-1. It consists of the reactor pressure vessel (RPV), the two coolant loops A and B with the once-through steam generators, four cold legs with main coolant pumps, four high pressure injection lines connected to the cold legs and one let-down in loop A1, as well as the pressurizer with the surge line connected to the hot leg of loop A, heaters, spray line and pilot operated relief valve (PORV).

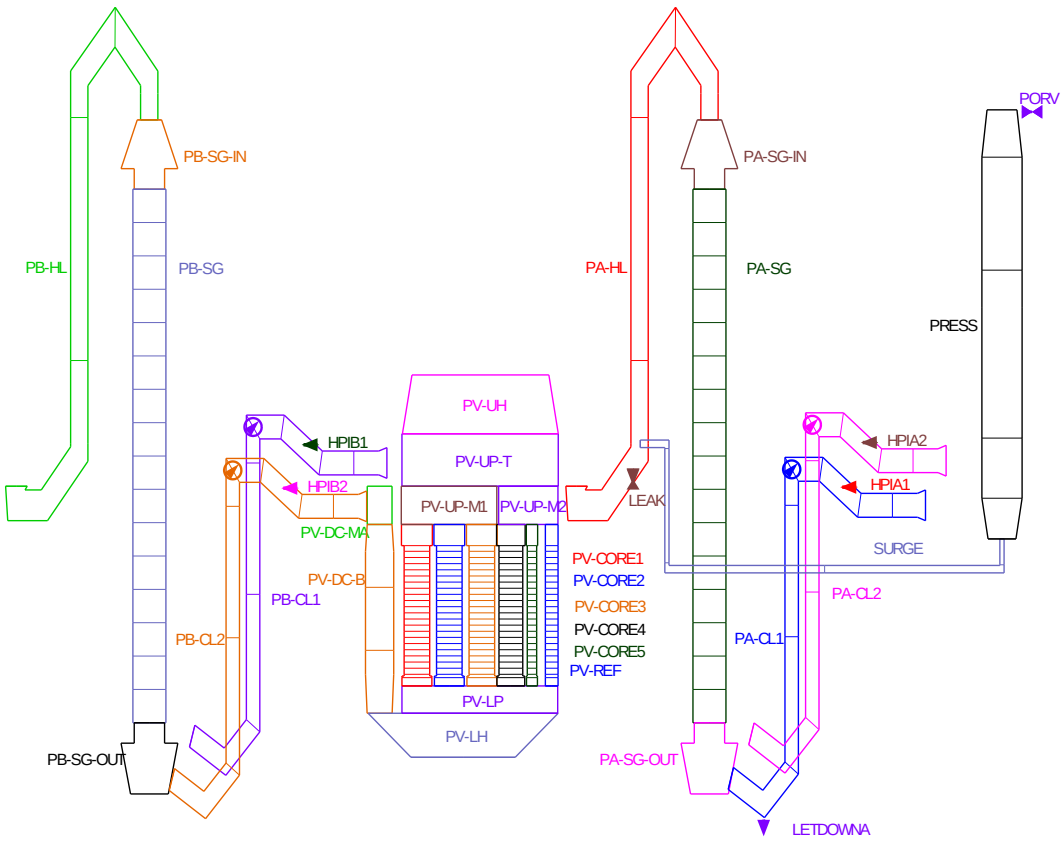

Fig. 16-1: ATHLET-CD nodalization scheme for TMI-2 (primary circuit)

The RPV comprises the downcomer, lower and upper plenum, upper head, the core region and the core bypass. The vent valves between downcomer and upper plenum are modelled as check valves. The core is modelled by five concentric rings with 22 axial nodes (20 within the active core region) and with cross flow connections to allow flow deflection due to fuel rod deformation and blockage formation caused by refreezing of molten material. The three inner core rings include fuel and AIC control rods. The fourth ring contains only fuel rods. The fifth channel contains no rods and is defined to avoid a complete core flow blockage in case of strong melt relocation.

The simplified model of the secondary system consists of two components (loop A and B) simulating the riser, with 16 axial volumes, and steam dome as well as the boundary conditions for feedwater injection and steam outlet flow to control the secondary side water levels and pressures according to the benchmark specifications. In total, the nodalization comprises 376 control volumes, 407 flow paths, as well as 153 heat slabs (not including fuel and control rod components) for the modelling of RPV structures and pipe walls.

16.2 Main modelling options

The benchmark calculations were performed with the code version ATHLET-CD Mod. 2.1 Cycle A, released in August 2006. Only the modules ATHLET (thermal-hydraulics) and ECORE (core degradation) have been applied.

The system thermal-hydraulics was simulated with the six-equation model (fully separated balance equations for liquid and vapour), complemented by an additional mass conservation equation for hydrogen as a non-condensable gas, except for the pressurizer and for the steam generator secondary sides, where the five-equation approach (one mixture momentum equation) together with the mixture level tracking model was used. The quench front model, which takes into account both top and bottom reflooding, has been applied for all rod components.

According to the benchmark specifications, two sets of calculations have been performed, one with input parameters for core degradation as recommended in the code User's Manual (referred as "standard calculation") and the other using values deduced from the analyses of the PHÉBUS experiments (referred as "alternative calculation"). As it can be seen in Table 16-1, both sets of input parameters are very similar, except for a 50 K lower failure criterion for oxidized cladding and a 100 K lower UO2-ZrO2 melting temperature in the alternative calculation.

Fuel rod relocation is simulated in rod-like geometry (candling model) assuming a constant relocation velocity of 6 cm/s for metallic melt and 3 cm/s for ceramic melt, respectively. Radial melt spreading outside a core ring is not taken into account.

Parameter	Unit	Standard Calculation	Alternative Calculation
Start of fuel dissolution by Zirconium	K	2250	2250
Clad failure temperature ($\delta_{ox} < 0.3$ mm)	K	2300	2280
Clad failure temperature ($\delta_{ox} \geq 0.3$ mm)	K	2500	2450
Start of ceramic fuel and Zirconia melting	K	2600	2500
Correlation for cladding oxidation at low temperature range (T<1800 K)	-	Cathcart	Cathcart
Correlation for cladding oxidation at high temperature range (T>1900 K)	-	Urbanic-Heidrick	Urbanic-Heidrick

Tab. 16-1: ATHLET-CD code parameters relevant to core degradation

16.3 Initial steady state conditions

The system code ATHLET/ATHLET-CD provides a steady state calculation capability which initializes the complete system starting from a limited amount of user-supplied initial and boundary conditions. To check the adequacy of this steady state solution, a zero-transient run (without any external disturbances) lasting 100 s was performed. At the end of this period, the main calculated plant parameters were stable and thus this time point was chosen for transient initiation (break opening and loss of main feedwater).

Table 16-2 compares the main plant parameters at transient initiation calculated by ATHLET-CD with TMI-2 accident data at turbine trip. The primary circuit conditions show a good agreement with the plant data. The secondary parameters reflect the estimated plant conditions before turbine trip. Due to the simplified modelling of the steam generator secondary sides, the degree of steam overheating at the steam generator outlets is underestimated, but this does not affect the results of the transient calculations.

Parameter	Unit	GRS (ATHLET-CD)	TMI-2 (Turbine Trip)
Primary System			
Reactor Power	MW	2663	2700
Primary pressure	MPa	14.9	15.2
Temperature Hot Leg A	K	592.2	592
Temperature Hot Leg B	K	592.2	592
Temperature Cold Leg A	K	564.8	548-561
Temperature Cold Leg B	K	564.8	565
Mass Flow Rate - Loop A	kg/s	8638	8280
Mass Flow Rate - Loop B	kg/s	8675	8560
Pressurizer level	m	5.78	5.77
Total primary mass	kg	223300	-
Secondary System			
Pressure SG A	MPa	6.34	7.31
Pressure SG B	MPa	6.20	7.24
Steam temperature SG A	K	568	586
Steam temperature SG B	K	568	586
Collapsed level SG A	m	4.03	-
Collapsed level SG B	m	3.54	-
Liquid mass SG A	kg	14630	-
Liquid mass SG B	kg	13140	-
Feedwater flow SG A	kg/s	743.7	723
Feedwater flow SG B	kg/s	738.5	717
SG feedwater temperature	K	503	-

Tab. 16-2: Initial conditions for TMI-2 benchmark calculation

16.4 Discussion of Results

The main results of the ATHLET-CD calculations are depicted in Figs. 16-2 to 16-18. The blue, solid curves refer to the "standard calculation", the red, dashed ones to the "alternative calculation". A chronology of the main events is presented in Table 16-3. Synthetic views of the core status at selected time points are shown in Section 16.5. The calculations have been performed up to about 30 min after start of ECC injection.

Phase 1: Small break LOCA until start of core heat-up (t = 0 s to t = 5100 s)

The postulated accident starts with the opening of a small break at hot leg A, simultaneously with the complete loss of main feedwater. Due to the strongly reduced heat transfer to the secondary side, primary pressure increases (Fig. 16-2). The pressure set-point for PORV opening is reached within 7 s. Shortly afterwards, reactor scram signal due to high pressure is generated. After reactor scram, primary pressure starts to decrease and the relief valves close (t = 15 s). About 200 s after break opening the pressurizer empties, and the hot legs reach saturation conditions.

At about 250 s flashing starts at the suction lines of the main coolant pumps. In comparison to the other codes, ATHLET-CD predicts a stronger pump performance degradation under two-phase flow conditions and thus considerably lower loop mass flow rates. The void fraction at pump inlet reaches 60% at ca. t = 4000 s (original benchmark criterion for pump trip).

The primary coolant mass inventory reaches 85 ton at t = 4676 s (Fig. 16-4) and the pumps are switched off. With the breakdown of forced circulation, liquid coolant settles down very quickly, mainly in the reactor pressure vessel (Fig. 16-5) and in the pump loop seals. Due to liquid stratification, steam with entrained water flows through the break (Fig. 16-3).

The heat transfer to the secondary side is reduced abruptly, resulting in a considerable primary pressure increase. Two-phase natural circulation is prevented by the liquid accumulation in the loop seals. Afterwards the liquid level within reactor vessel decreases continuously, leading to core depletion (Figs. 16-5, 16-6) and start of core heat-up at t ~ 5100 s (Fig. 16-7), considerably earlier than predicted by other codes (ASTEC, ICARE/CATHARE). In these calculations, the liquid level within reactor vessel remains practically constant for a quite long period (ca. 600 to 800 s) after pump trip. Reasons for such deviations may be found mainly in the different approaches to describe phase separation and counter-current flow phenomena in the core region, but also in the modelling of the vent valves.

Phase 2: Core degradation phase (t = 5100 s to t = 9676 s)

After start of core dryout, fuel cladding temperatures at higher core elevations increase rapidly (Fig. 16-8). First control rod failure through dissolution of the guide tubes by molten steel is predicted to occur at t = 7434 s.

Oxidation runaway with a sudden temperature excursion at the top of the core occurs at about 7700 s (Figs. 16-8 and 16-11). Shortly afterwards first fuel rod clad burst is predicted to occur due to over-pressurization.

Clad melt and relocation starts in the central core ring at about 7800 s in the alternative calculation, slightly earlier than for the standard one, due to the 50 K lower temperature criterion for cladding failure. From this time point on, results of the standard and of the alternative calculation begin to diverge. Due to more metallic Zr available above the core mid-plane, the standard calculation predicts a higher hydrogen production (Fig. 16-11), leading to higher heat generation and higher temperatures (Fig. 16-9) in comparison to the alternative calculation.

In both calculations the metallic melt, mainly formed in the core inner rings, flows downwards and refreezes at an elevation slightly above the liquid surface. The amount of metallic crust, together with the molten control rod materials, is enough to cause a partial channel flow blockage in Ring 1 (Fig. 16-5).

The melt temperature of the UO2-ZrO2 eutectic mixture is reached at 8686 s in the standard calculation, 160 s later than in the alternative one. At this time point ca. 7 ton of metallic melt has been generated and dislocated to the lower core regions. Afterwards ceramic melt becomes the main contributor to the total melt mass (Figs. 16-12 and 16-13). The hot ceramic melt can be only partially cooled in the lower core regions, leading to the inception of a liquid melt pool within the innermost core channel (Fig. 16-14).

At the end of this phase, before the start of ECC injection, the calculated total molten mass amounts to 41 ton (standard calculation) and 31 ton (alternative calculation). The generated H_2 mass is predicted to be 294 kg and 258 kg, respectively. These global values agree satisfactorily with the results of other participants.

However, significant deviations can be observed not only with respect to the melt composition (ATHLET-CD predicts a relatively low fraction of Zr melt, ca. 7 to 8 kg) but also concerning its distribution within the core region.

Both calculations predict a large extent of fuel rod melting mainly in the innermost core channel, creating a cavity between the elevations 1.7 m and 3.0 m above the core bottom, with a maximum diameter of 1.6 m (alternative calculation) and 2.2 m (standard calculation, at elevation 2.3 m), respectively. This fuel melt relocates completely to the lower inner core regions, displacing the water there (Fig. 16-5) and leading to a flow channel blockage. The outer fuel rods (Ring 4) do not melt significantly.

The main parameters concerning core degradation are summarized in Table 16-4 for both calculations. Synthetic views of the core status at the end of the degradation phase are depicted in Fig. 16-21.

Phase 3: Core reflood phase (t = 9676 s to t = 11500 s)

High pressure (HP) injection in the cold legs at a constant, total rate of 60 kg/s is initiated at t = 9676 s, 5000 s after pump trip according to the benchmark specifications. At this time point, the collapsed water level in the outer core rings (Rings 3 to 5) is about 60 cm above core bottom in both calculations (Fig. 16-5). Due to melt accumulation, the inner core channels are blocked.

At reflood initiation ECC water penetrates the core region mainly through the outer channels and through the core bypass. Due to the strong steam formation as well as hydrogen production, primary pressure increases considerably (Fig. 16-2). The pressure peak is higher in the standard calculation (10.4 MPa) as in the alternative one (9.9 MPa) due to the larger amount of hydrogen generated during reflood (Fig. 16-11).

In this phase, the liquid melt pool could only be cooled from the sides, leading to the formation of a crust of refrozen material (Figs. 16-14 and 16-15), which in turn acts as an additional resistance to further melt quenching. At about 10300 s the core water level is high enough to allow water flow into the cavity, partly from the core bypass and upper plenum, partly due to cross-flow from the outer core rings. This water flow partially quenches the melt pool from the top, leading to an enhanced steam generation and to a second primary pressure peak. This behaviour was predicted in both calculations (Figs. 16-2, 16-14 and 16-15), with a considerably slower melt cooling rate in the standard calculation due to the higher temperatures and larger amount of melt. Once again, crust formation inhibits further melt cooling.

Table 16-4 and Fig. 16-22 present the core status at t = 11500 s, 30 min after start of HP injection. At this time point the reactor core was completely refilled. Both calculations show melt accumulation in the lower, central core regions, which could only be partially quenched. The hydrogen generated during reflood amounts to 57 kg (standard calculation) and 19 kg (alternative), respectively. The increase of the total mass of molten materials was about 2 ton during this phase. Fig. 16-16 depicts the average axial mass distribution in the core for both calculations.

For completeness, Figs. 16-17 and 16-18 show the pressure and the water level at the secondary side of the steam generators. It was only possible to control the secondary pressure according to the benchmark specifications as long as the primary pressure remained higher than the secondary pressure, about 7200 s after break opening. Afterwards, heat transfer changed its direction, leading to steam condensation at the secondary side, and to a slight increase of the secondary water level.

Main Events	Time (sec)	
	Standard	**Alternative**
Break opening and loss of main feedwater	0	0
PORV opens	7	7
Reactor scram (primary pressure > 16.35 MPa)	10	10
PORV closes	15	15
Pressurizer empty	200	200
Pumps shutdown (primary inventory reaches 85 ton)	4669	4669
Onset of core heat-up ($T_{UP} > T_{sat}$)	~5100	~5100
Control rod failure	7434	7434
Onset of oxidation runaway (T_{CLAD} ~ 1850 K)	~7700	~7700
First clad perforation/burst	7781	7781
First cladding dislocation	7810	7805
First ceramic melt dislocation	8686	8524
Start of HPI	9669	9669
End of calculation (~ 30 min after start of HPI)	11500	11500

Tab. 16-3: Chronology of main events

Parameter	Start of reflooding (5000 sec after pump trip)		End of calculation (ca. 1800 sec after start of reflooding)	
	Standard	**Alternative**	**Standard**	**Alternative**
Primary mass inventory (ton)	55.5	55.8	128.7	131.8
Generated H_2 mass (ton)	0.29	0.26	0.35	0.28
Mass of molten Zr (ton)	8.2	7.2	9.0	7.2
Mass of molten ZrO_2 (ton)	2.0	1.2	2.0	1.3
Mass of molten UO_2 (ton)	28.0	20.1	29.5	21.7
Mass of molten contr. rods (ton)	2.9	2.7	2.9	2.8
Total magma mass (ton)	41.2	31.2	43.3	33.0

Tab. 16-4: Core status at reflooding phase

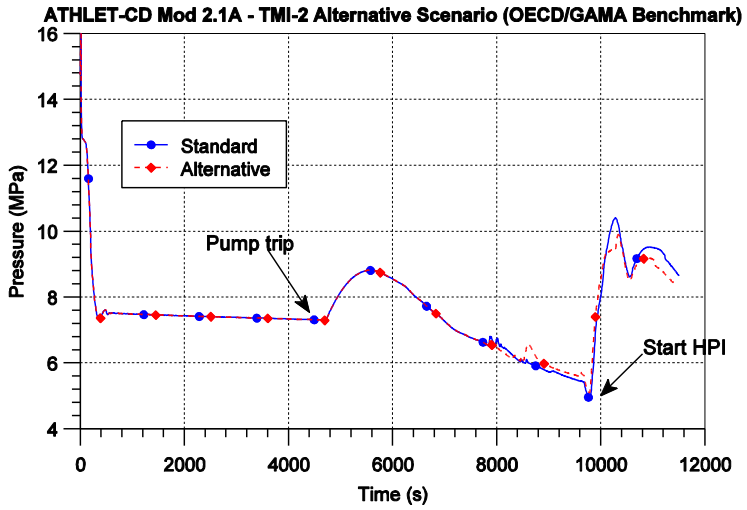

Fig. 16-2: Pressurizer pressure

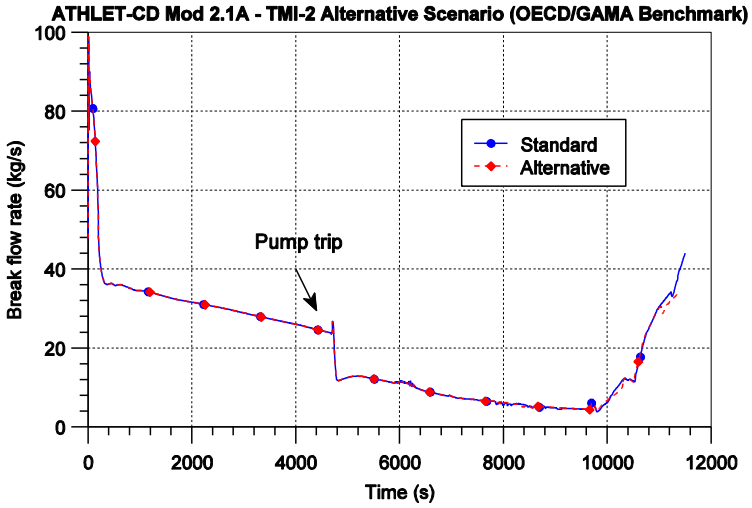

Fig. 16-3: Break mass flow rate

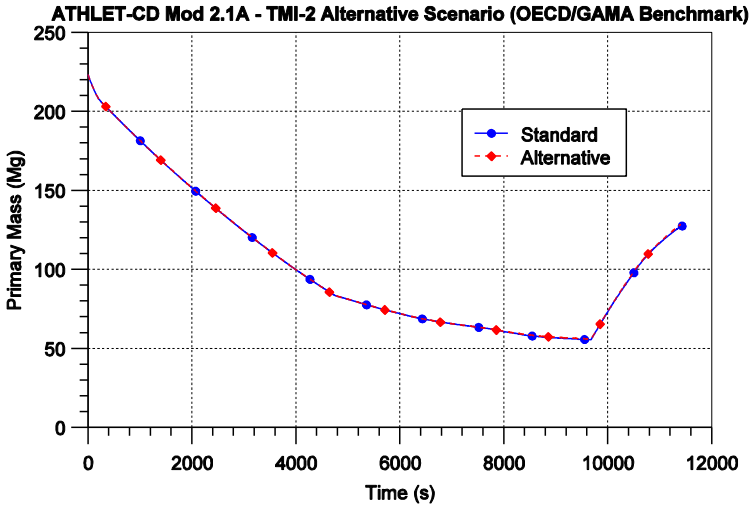

Fig. 16-4: Total primary liquid inventory

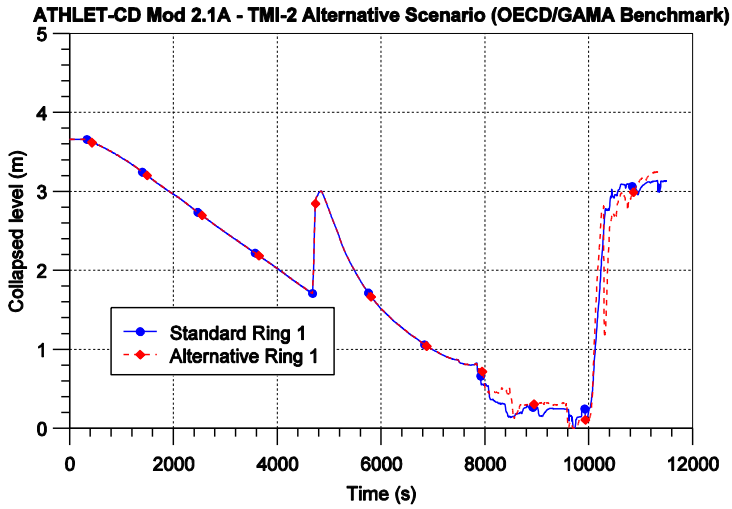

Fig. 16-5: Core collapsed liquid level - inner ring 1

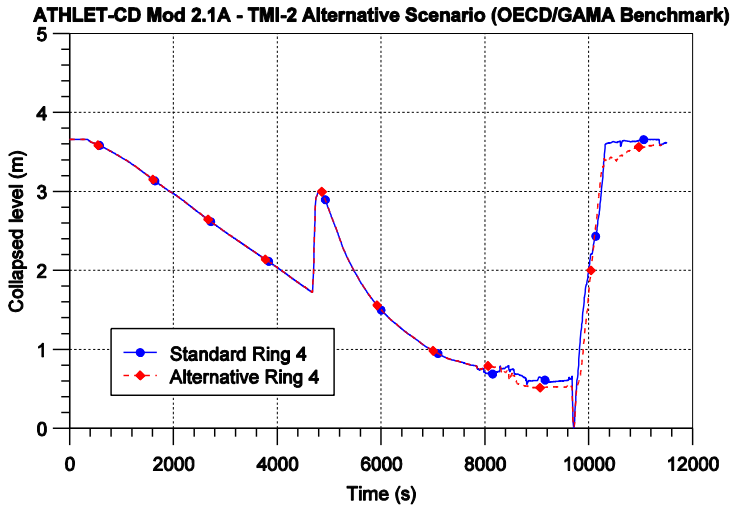

Fig. 16-6: Core collapsed liquid level - outer ring 4

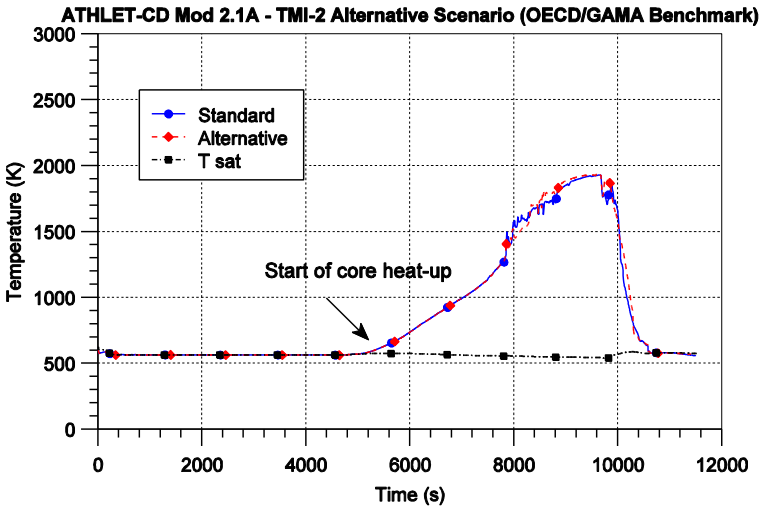

Fig. 16-7: Coolant temperatures in upper plenum

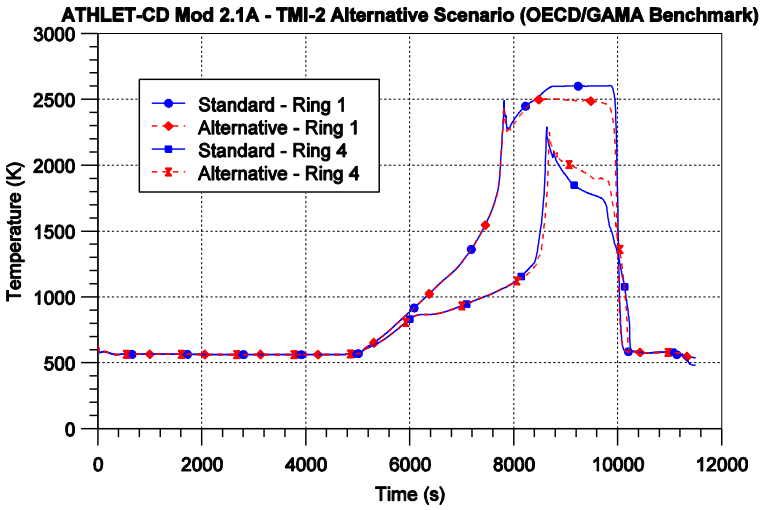

Fig. 16-8: Fuel cladding temperatures at top of core (elevation 3.0 m)

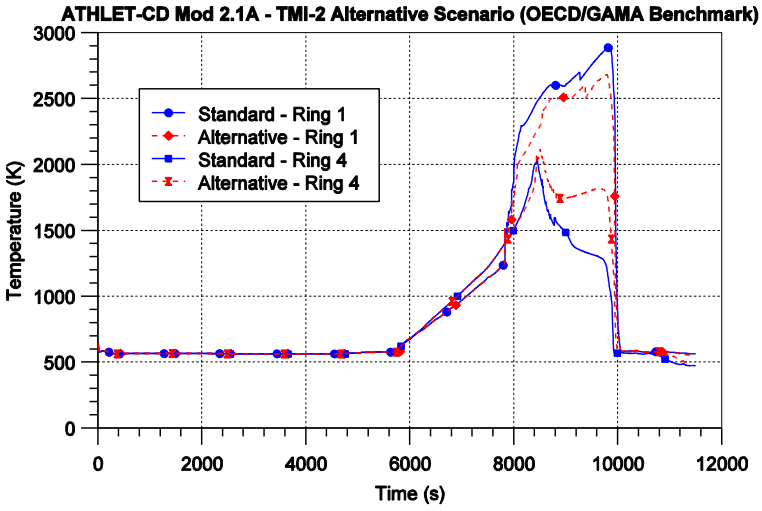

Fig. 16-9: Fuel cladding temperatures at mid-core (elevation 1.7 m)

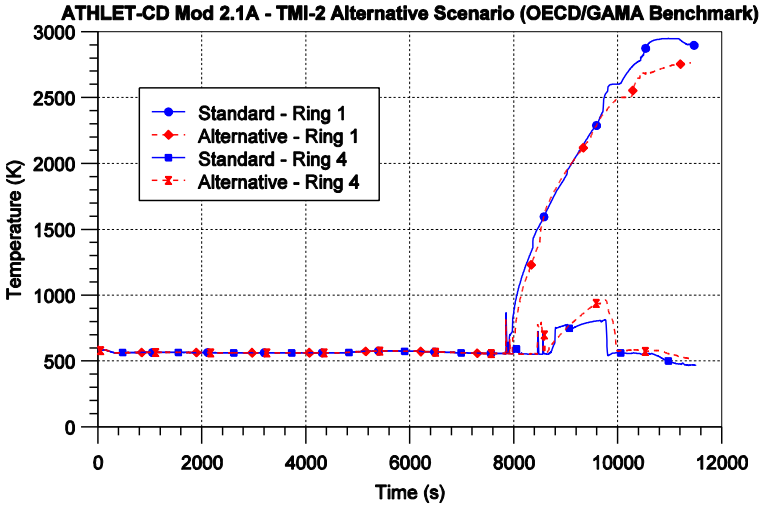

Fig. 16-10: Fuel cladding temperatures at bottom of core (elevation 0.6 m)

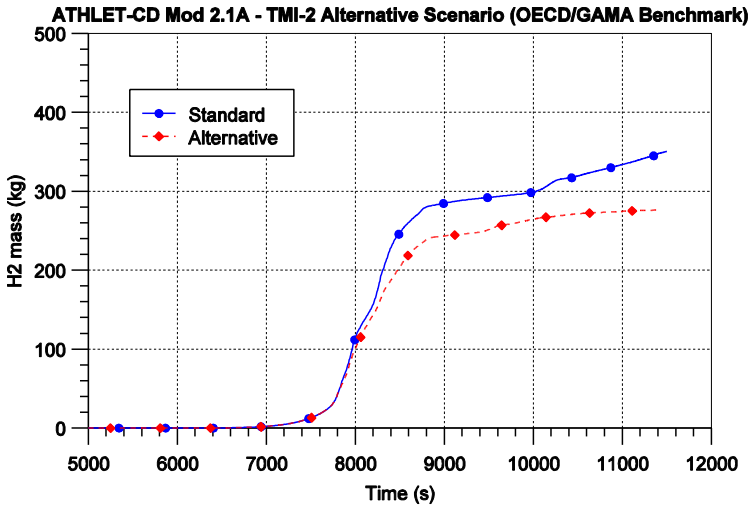

Fig. 16-11: Total hydrogen production

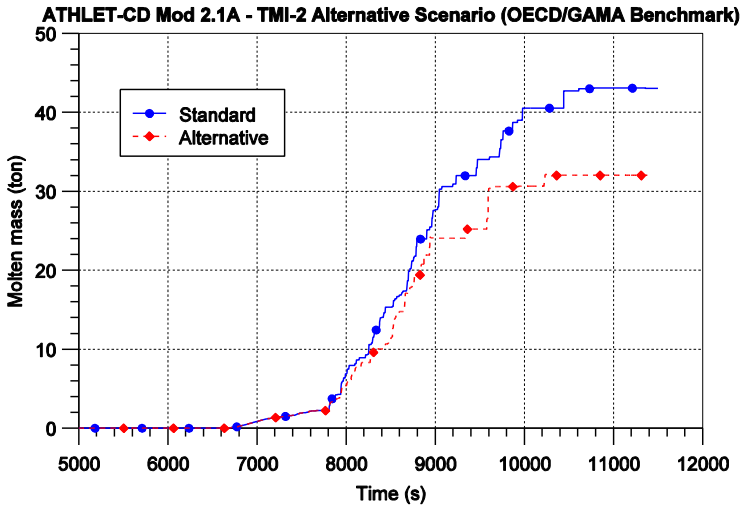

Fig. 16-12: Total mass of molten materials in the core

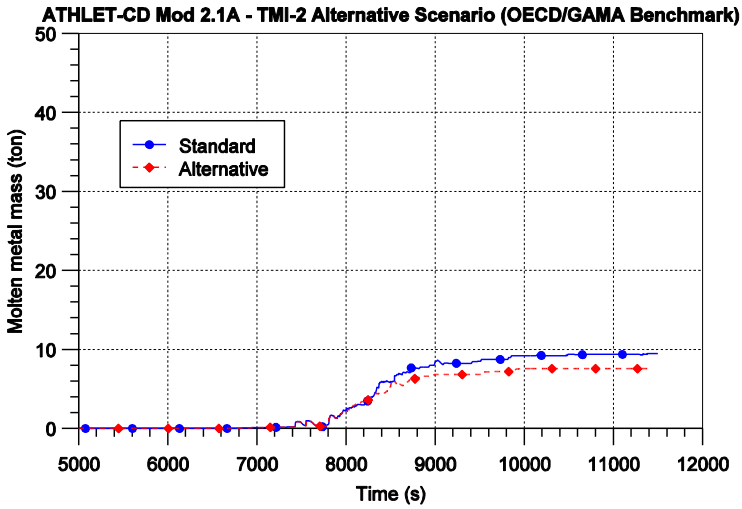

Fig. 16-13: Total mass of molten Zr in the core

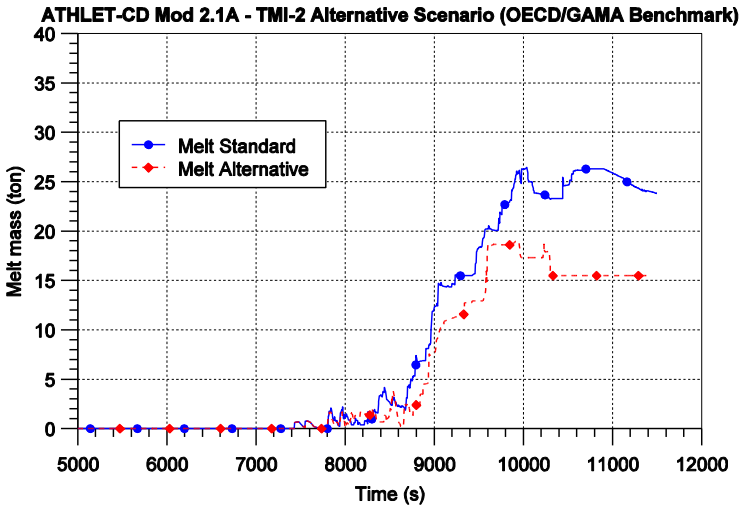

Fig. 16-14: Total mass of liquid melt in the core

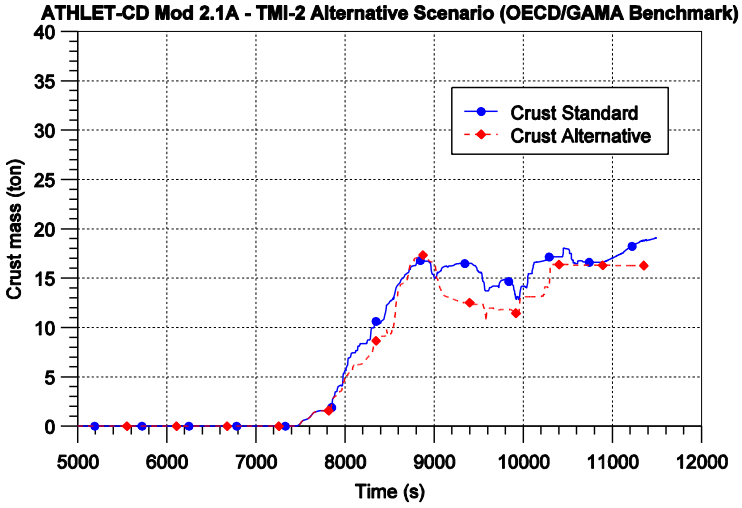

Fig. 16-15: Total mass of refrozen materials in the core

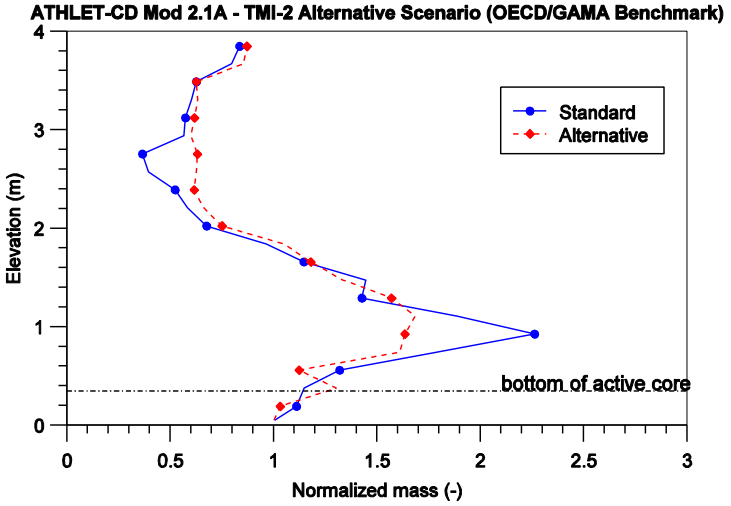

Fig. 16-16: Average axial mass distribution at t = 11500 s

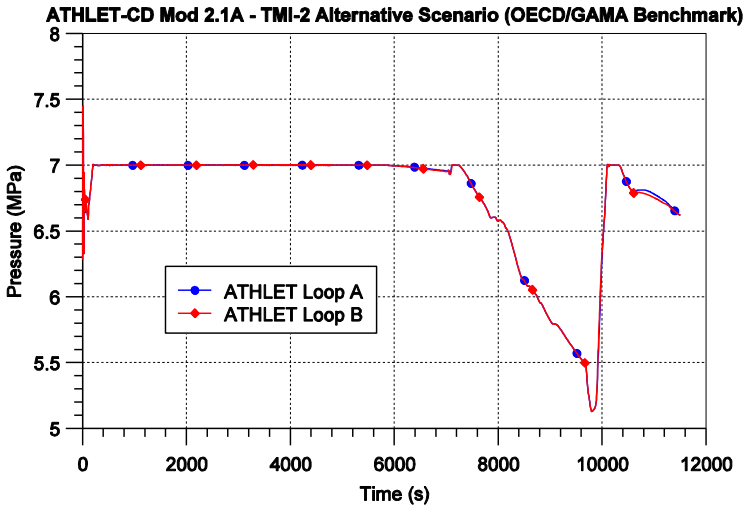

Fig. 16-17: Secondary pressure

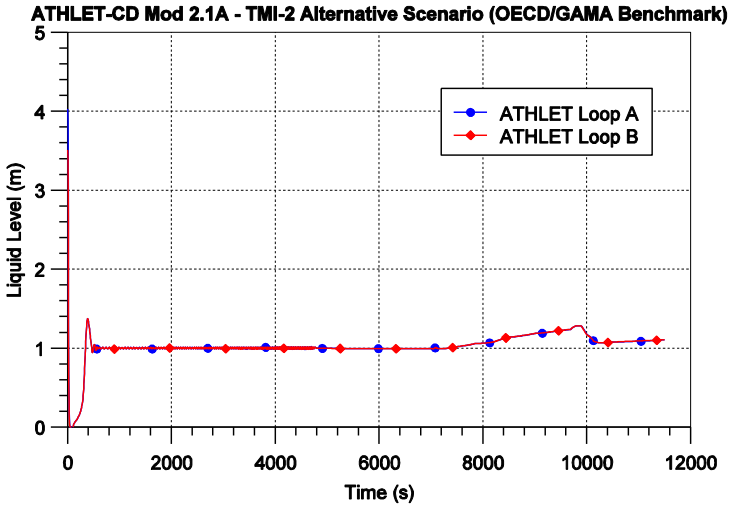

Fig. 16-18: Secondary level

16.5 Synthetic Views of the Core at Selected Instants

Figs. 16-19 to 16-22 show synthetic views of the core status at selected instants for both calculations, obtained with the help of the plant analyzer ATLAS. The pictures show the void distribution (VOID) in the lower plenum (PV-LP), core rings (PV-CORE1…5), core bypass (PV-REF) and upper plenum (PV-UP-M1 and -M2), the cladding temperatures (TCSU) as well as the dislocations of the fuel rods (ROD1 to ROD4) and control rods (at the left hand side of the corresponding fuel rods).

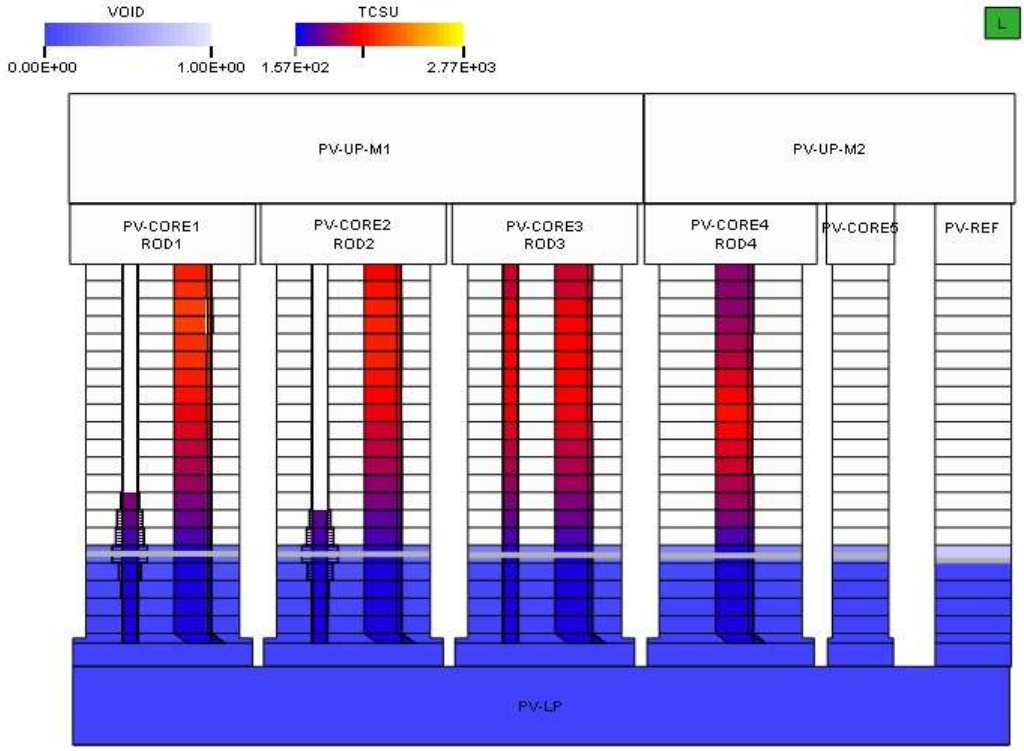

Standard Calculation

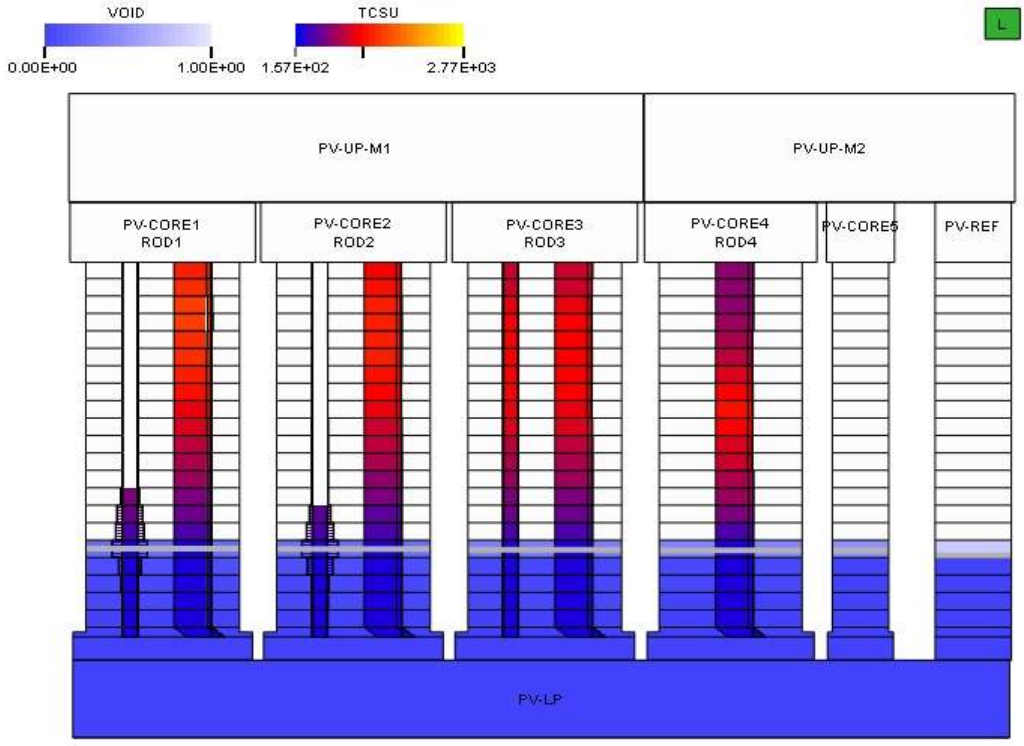

Alternative Calculation

Fig. 16-19: TMI core at beginning of oxidation excursion (T~1850 K)

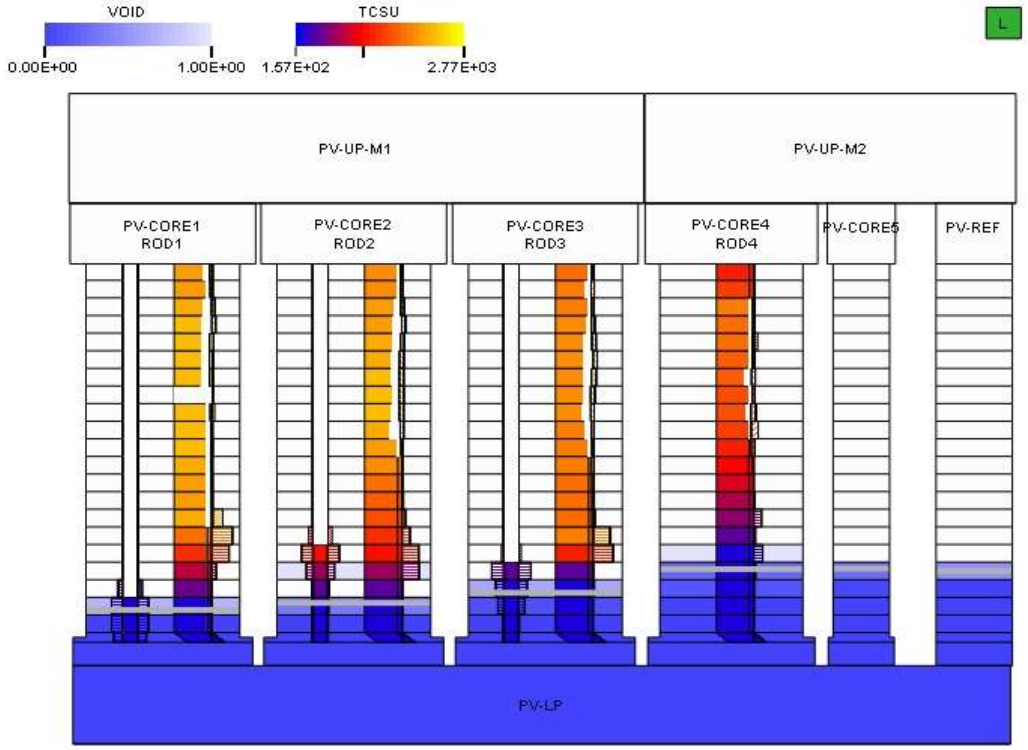

Standard Calculation

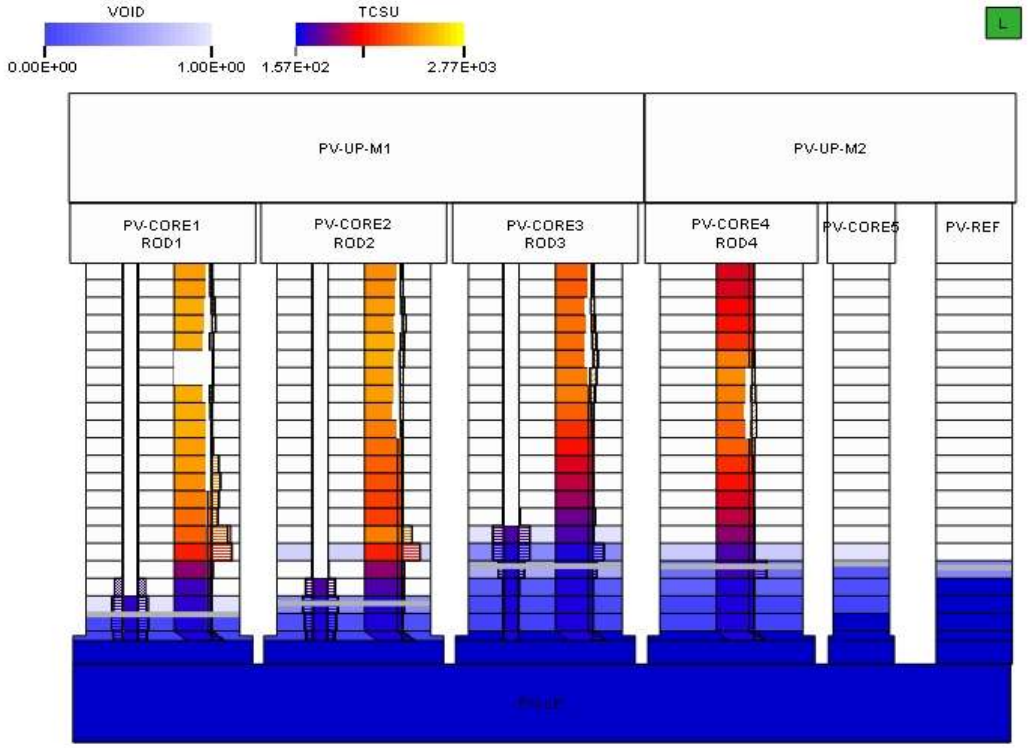

Alternative Calculation

Fig. 16-20: TMI core at time of first ceramic melt relocation

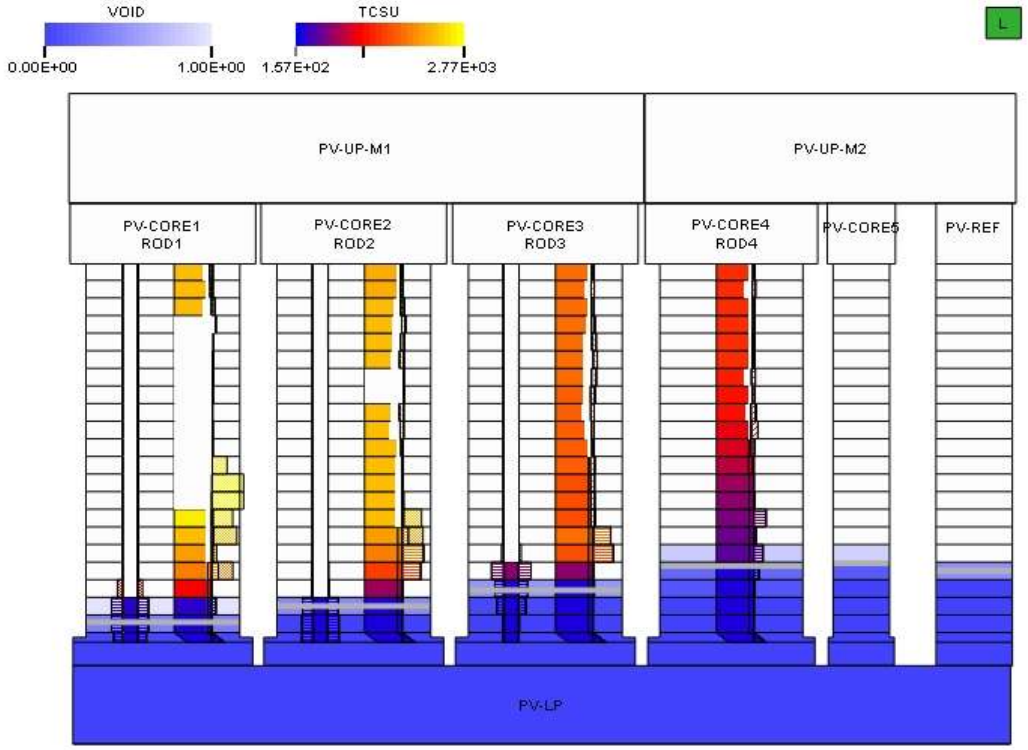

Standard Calculation

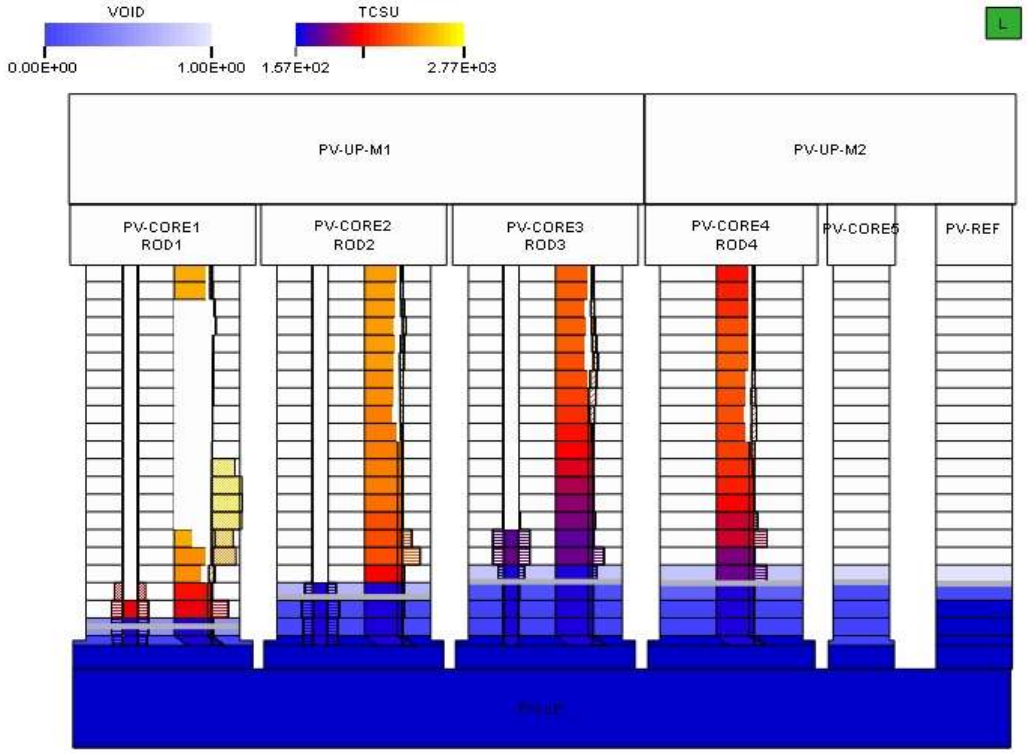

Alternative Calculation

Fig 16-21: TMI core at start of reflooding

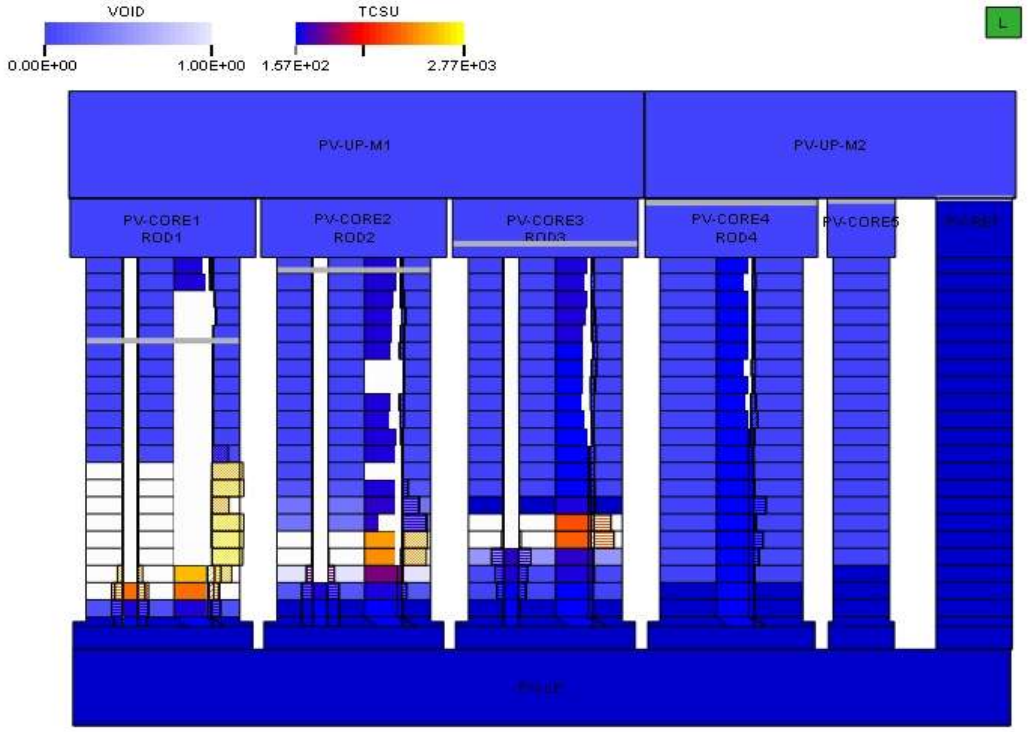

Standard Calculation

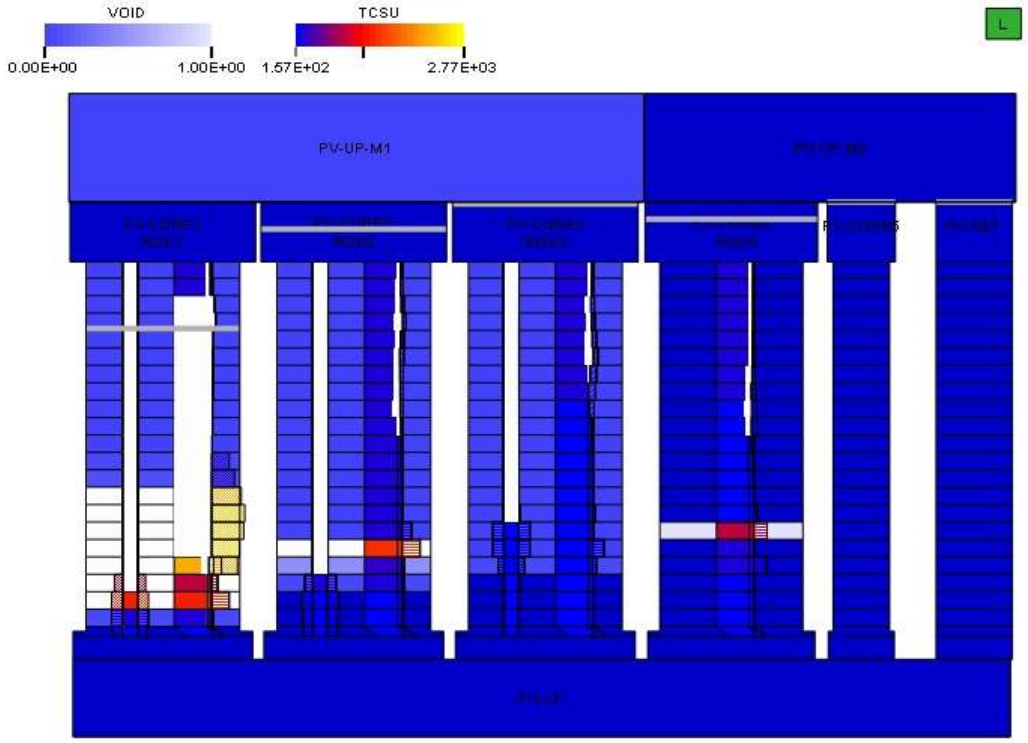

Alternative Calculation

Fig. 16-22: TMI core at the end of calculation (30 min of reflooding)

16.6 Additional calculations

Some additional parametric studies have been performed in the frame of this benchmark. One of them addressed the modelling of Zr oxidation. Using the same set of input parameters as for the "alternative calculation", two additional calculations have been carried out with other correlations available in ATHLET-CD: one with the correlations of Cathcart (low temperature range) and Prater/Courtright (high temperature range), and one with the correlations of Leistikow and Prater/Courtright.

While the results concerning hydrogen production in the low temperature range (T < 1800 K) either with Cathcart or with the Leistikow correlation are very similar, the use of Prater/Courtright in the high temperature range leads to about 20% lower hydrogen production than with the Urbanic-Heidrick correlation, for a similar extent of core degradation.

As shown in Section 16.4, the "standard calculation" predicted about 40% higher mass of UO2-ZrO2 melt than the "alternative calculation", although the temperature criterion for oxide melting was higher (2600 K instead of 2500 K). The reason was the larger extent of oxidation during the degradation phase resulting from the higher temperature criterion for cladding failure (more Zr in metallic form was available at higher elevations) in comparison to the "alternative calculation". An additional calculation shows that, for the same cladding failure temperature criterion, an increase of the ceramic melt temperature from 2500 K to 2600 K leads to a reduction of about 20% of the total ceramic melt mass (ca. 15% of the total melt mass). Thus, analyses of code results should not be based only on single input parameters, but rather take into account the combined influence of them.

Although outside the scope of this benchmark, the ATHLET-CD calculations have been complemented by an estimation of the release of fission products and absorber materials with the code module FIPREM. A surprising outcome is that the relatively small changes on input parameters from the "standard" to the "alternative" calculations yield a considerable reduction of the release rates: about 30% less noble gases and volatiles, 35% less actinides and up to 60% lower Cd release. This illustrates the degree of uncertainty related to source term determination.

16.7 Final remarks

The ATHLET-CD results for the TMI-benchmark are physically reasonable and comparable to the results of other participants, mainly with respect to the thermal-hydraulics of primary system up to the start of ECC injection and to the predicted total mass of hydrogen produced and of molten materials.

The main observed discrepancies are related to core degradation evolution during the reflood phase. ATHLET-CD (without the debris bed module MEWA) was the only code to predict the formation of a melt pool in the lower, central core region, which could not be completely cooled during quenching phase. It is however supposed that the ICARE/CATHARE simulation would also show a similar behaviour, if the HP injection was delayed enough to allow considerable melt relocation and flow blockage. Further investigations should also address the influence of the chosen nodalization on melt progression.

With respect to code performance, the calculations have been performed on a CRAY XD1 Linux Cluster with AMD Opteron 2.4 GHz processors and took about 44000 sec. CPU time, with a ratio CPU to real about 4:1 and an average time step size of 0.1 s. The calculations up to the start of ECC injection were faster than real time, with a considerable increase of processing time during the reflood phase. These figures indicate a rather good and robust code performance and show the adequacy of the coupling technique between the thermal-hydraulics and core degradation models.

Furthermore, one calculation has been repeated in three different platforms, with different operating systems and FORTRAN compilers. The results were practically identical, confirming the good code portability.

Finally, the benchmark calculations showed that the simulation of core degradation phenomena is strongly dependent on the choice of code input parameters like melting temperature criteria or Zr oxidation correlation. Therefore uncertainty evaluations, taking into account the influence of the combined variation of input parameters and modelling options, are recommended to support code applications for deterministic plant analyses.

17. APPENDIX : UPI CALCULATION WITH MELCOR 1.8.5

17.1 TMI-2 Plant Modelling

The same nodalisation used to simulate the first two phase of the TMI-2 accident has been used for this benchmark, with proper boundary conditions. Moreover, minor changes were performed with respect to the first benchmark phase, in order to reduce stratification in the primary side and improve heat transfer through steam generators.

The nodalization of the TMI-2 primary system for the MELCOR 1.8.5 code is presented in the Fig 1. Both primary loops have been modelled simulating each SGs and considering a single equivalent main pump and cold leg. The secondary system is modelled only up to the main feed and isolation valves, while the SGs were modelled with a high level of detail. The secondary side is connected to an imposed pressure control volume and to a "spill&feed" level control, which assure the desired imposed boundary conditions.

Particular care has also been devoted to core simulation (Fig. 2). The core schematization is constituted by five radial rings and twelve axial levels; four thermal-hydraulic levels are used in each ring of the core region, with three core cells axially in each thermal-hydraulic control volume. Radial and axial flow paths in the core region allow for the prediction of 2-D flow patterns. Heat structures representative of the control rod guide tubes and upper tie plate in the upper plenum have been added to the MELCOR model to permit condensation heat transfer and coolant recirculation inside the vessel. The input deck was developed using standard default MELCOR modeling parameters as long as possible, and allows for a complete description of an eventual severe progression of an accidental transient.

The VENT valves are also explicitly modeled between the cold and hot collectors. The plant geometry, the boundary conditions and the accident scenario have been strictly defined according to alternative TMI-2 scenario benchmark specifications provided by IRSN, as well as recommended values of code physical parameters for the sensitivity study.

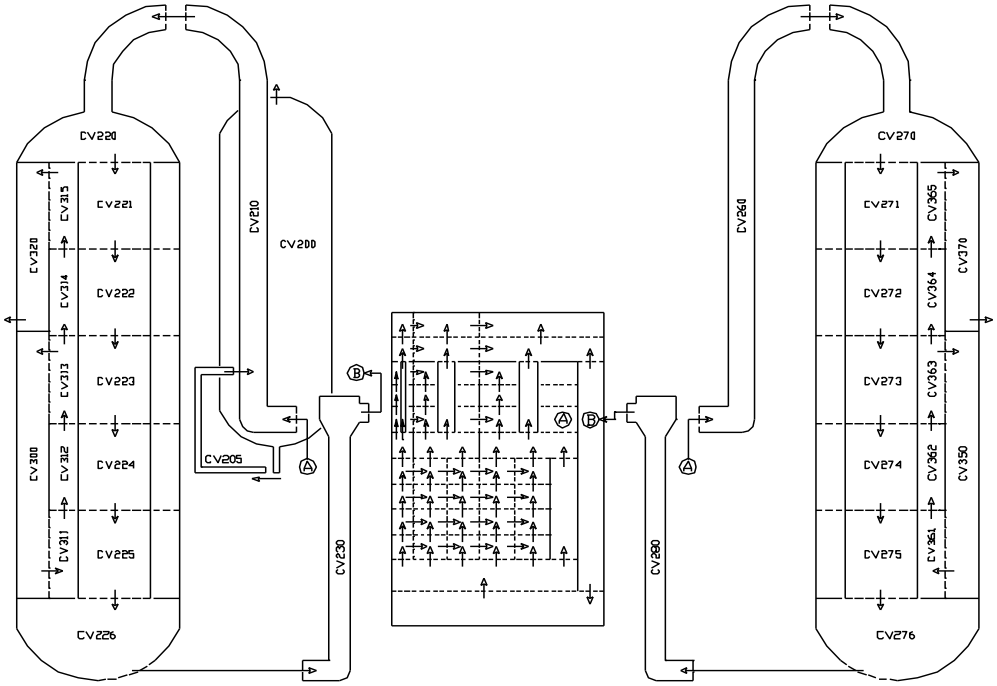

Fig. 1: TMI-2 plant nodalization scheme.

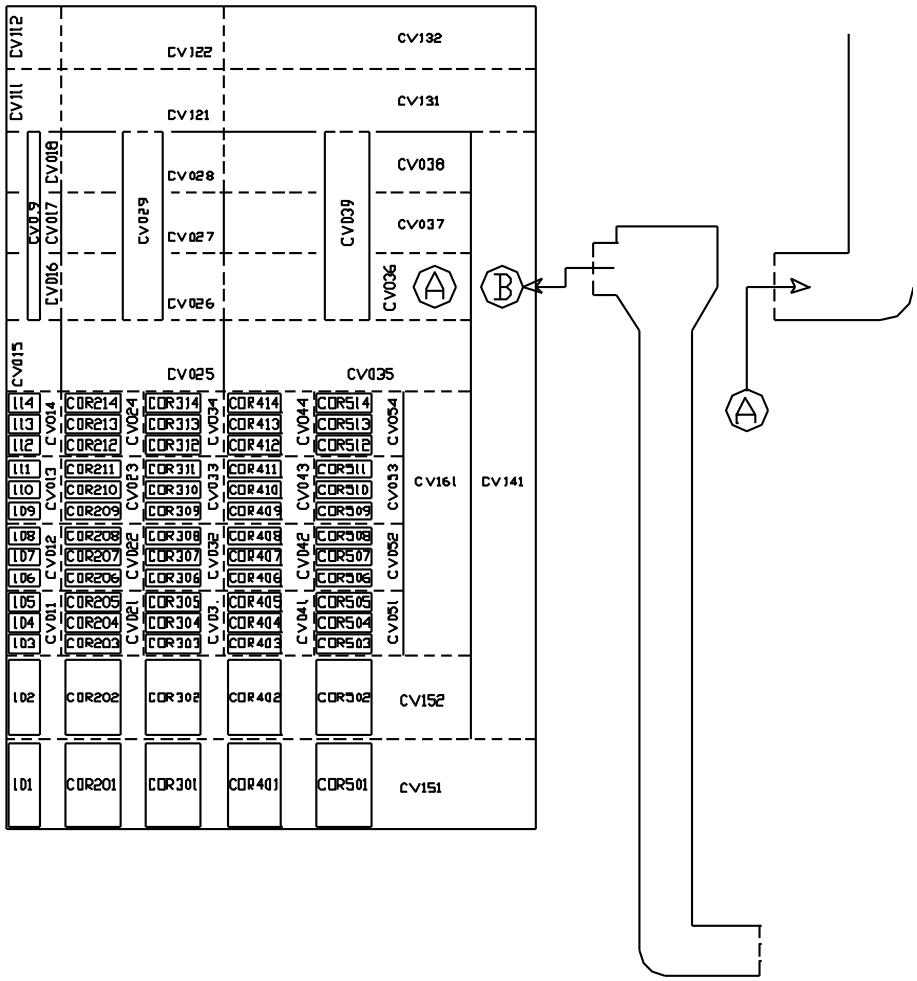

Fig.2: TMI-2 core simulation with MELCOR.

17.2 Updated Initial Steady-State Conditions

The TMI2 initial conditions are obtained by a steady-state code run lasting 2000 s and starting from plant thermal-hydraulic parameter values close to the ones specified for TMI-2. During the steady-state calculation, some regulations in the primary and secondary sides are activated to facilitate the achievement of stable conditions, as close as possible to the TMI2 plant state at t = 0 (turbin trip in TMI2 accident).

The regulated parameters are:

- The pressurizer pressure by turning on the heaters when the pressure is lower than the nominal value;
- The pressurizer liquid mass, by water injection or draining, in order to obtain the precise liquid level.

The TMI2 plant initial conditions calculated by the MELCOR code are compared with TMI-2 accident data at turbine trip in the table below. The primary circuit conditions are very well reproduced by the code, the larger mismatch being the mass core flowrate which resulted about 3% lower with respect to reference plant parameters.

Parameter	Units	Reference value	UPI MELCOR calculation	Difference %
Core power	MWth	2772	2770	0.07
Cold leg temperature	K	563.76	563.6	0.03
Hot leg temperature	K	591.43	592.0	0.08
Lower plenum pressure	MPa	15.36	15.35	0.07
Outlet plenum pressure	MPa	15.17	15.20	0.2
Total RCS flow rate	kg/s	17602.2	17040	3.4
Core flow rate	kg/s	16052.4	15596	2.8
Bypass flow rate	kg/s	1549.8	1504	2.9
Pressuriser level	cm	558.8	568.2	2.0
Feed-water/steam flow	kg/s	761.59	761.59	IMPOSED
OTSG outlet pressure	MPa	6.41	6.41	IMPOSED
OTSG outlet temperature	K	572.63	569.5	0.5
Feed-water temperature	K	510.93	510.93	IMPOSED
Primary mass	kg		230850	-

Table 1: TMI-2 initial conditions as calculated by MELCOR for the alternative scenario.

17.3 Standard Physical Parameters of the Code

Main core degradation physical parameters used in the standard calculation and alternative physical parameters scenario with MELCOR are summarized in the Table 2. The physical parameters used in the standard calculation are the MELCOR default recommended values, while in the sensitivity case they were based on the conclusions of ISP46 (PHEBUS-FPT1) and from the latest findings on core degradation phenomena.

	Reference case	Sensitivity case
Zr oxidation correlation	Urbanic-Heidrick	Urbanic-Heidrick
Cladding failure criteria	ZrO2 thickness < 10 mm and Tclad > 2400 K	ZrO2 thickness < 200 mm and Tclad > 2280 K
UO2-ZrO2 melting temperature	UO2 Tm = 3113 K ZrO2 Tm = 2990 K	UO2 Tm = 2650 K ZrO2 Tm = 2650 K
Debris formation criteria	Rod failure when: Tclad> 2500 K and Zr thickness < 100 mm T_{UO2} > 3100 K	Rod failure when: Tclad> 2500 K and Zr thickness < 100 mm T_{UO2} > 2650 K

Table 2: Main assumptions on main degradation models for the reference and sensitivity calculations.

For Zircalloy oxidation, the solid-state diffusion of oxygen through an oxide layer to unoxidized metal is represented by a parabolic rate equation, whose rate constant is evaluate using the Urbanic-Heidrick correlation. For very low oxidant concentrations, gaseous diffusion may limit the reaction rate, and a mass transfer coefficient is calculated via a heat-mass transfer analogy from the heat transfer correlations.

Candling, that is the downward flow of molten core materials and the subsequent refreezing of these materials as they transfer latent heat to cooler structures below, is addressed with a semi-mechanistic model, based on fundamental thermal/hydraulic principles. Relocation of core materials may result in a reduction of area and increase of flow resistance, or even total blocking of flow, within various parts of the core. A model is also implemented for an oxide shell to hold up molten material until the shell is breached. Molten material is hold up within a component if the oxide thickness is greater than a critical value hold, if the component temperature is less than a critical value, and if no candling from the component in that cell has yet taken place.

MELCOR contains several simple models that consider the structural integrity and support of intact components, and convert them to particulate debris when either is lost. Most are logical models rather than structural models; no stress calculations are performed for any component other than supporting structure. All components other than fuel rods are immediately converted to particulate debris whenever the unoxidized metal thickness is reduced below a user defined minimum value. The thickness criterion is also used for cladding, which is assumed to support fuel pellets, but other criteria are also considered for fuel rods. Oxidized rods are assumed to retain their identity until the cladding reaches 2500 K, and to collapse unconditionally if the fuel temperature reaches 3100 K (the approximate melting temperature of UO2).

17.4 Chronology of Major Events

The chronology of major events calculated by MELCOR is presented in the table below and discussed in the following section 5. Minimum differences are shown only for the first melt relocation that is slightly anticipated in the sensitivity calculation. The other significant difference is related to hydrogen production, as described in the following.

Event	Time (s)	
	Standard case	Sensitivity case
Break opening and loss of feedwater	0	0
Reactor scram	16	16
Pressurizer is empty	215	215
Primary pump void fraction > 0.6	4150	4150
Primary pump shutdown (M < 85000 kg)	4360	4360
Onset of core uncovery	4635	4635
Onset of core heatup	5300	5950
Beginning of oxidation	6800	6800
First fuel rod clad burst	7450	7450
First melt relocation	7510	7470
Onset of reflooding	9360	9360
End of calculation	12000	12000

Table 3: Chronology of major events in the two calculations.

17.5 Result Analysis

The behaviour of the main thermal-hydraulic variables is quite similar in the two MELCOR calculations. Boundary conditions on the SGs secondary side (Figures 3 to 4) are maintained during the whole transient, by connecting each steam generator secondary side to a control volume with imposed pressure and using a "spill&feed" level control. So, changes in pressure and in liquid level due to steam evaporation/condensation taking place during the transient are continuously corrected by injecting/spilling saturated steam and water from/to the two controlled source. The results of this control are particular clear in the long-term comparison of the SGs levels, where the condensation of the steam induced by HPI actuation is compensated by spilling away the condensate water.

The initial feedwater trip and the consequent heat removal loss through the two steam generators causes the primary pressure to rapidly reach the opening PORV set-point and after 16 s the SCRAM is actuated. The primary pressure (Fig. 5) rapidly approaches saturation as a consequence of the break on the hot leg and it remains almost constant at a value of 7.5 MPa (that is a slightly higher value respect to the other codes predictions) up to the trip of the pumps which takes place after 4400 s. Almost at the same time the break uncovers and pressure starts increasing due to reduced removed power through the steam generators and the break. After 10 minutes the pressure decreases again reaching a minimum value of about 7.1 MPa. Finally, core reflood by HPI injection is started at 9400 s, 5000 s after pump trip according to benchmark specifications. By this time, the collapsed core water level is at the core bottom in both calculations. The reflood of the core results in sudden primary pressure increase due to the steep increase in convective heat transfer and steam formation. Maximum pressure peak is about 128 MPa.

Formation of a void fraction is still delayed respect to other code predictions (Fig. 6), due to the slightly higher primary system pressure that delays saturation. This is probably due to the slight under-estimation of heat transfer through the two steam generators (Fig. 7). The removed heat is directly correlated to the primary system saturation temperature up to the trip of the main pumps, when heat removal steeply decreases. The following pressurisation and temperature increase causes a weak heat transfer increment, even though it almost goes to zero at about 8000 s.

The mass of water in the primary system (Fig. 8) decreases with an almost constant rate during liquid flow-rate through the break. The calculation of break mass flow-rate (Fig. 9) is performed using RETRAN correlations for choked flow, that is the Moody model for saturated water and the Henry-

Fauske model for the subcooled phase. The higher primary pressure delays the reaching of saturated conditions in the primary system and this could explain the almost constant break mass flow-rate, compared to the decreasing values of the break flow-rate calculated by the other codes. The larger mass flow-rate through the break leads to a slightly anticipated pump trip, as the total primary mass decreases down below 85000 kg at about 4400 s. After break uncovering the mass inventory decreases more slowly reaching a minimum value of about 68 tons. The actuation of HPI finally causes a steep increase of the primary water mass.

The mass flow-rate through the two primary loops (Fig. 10) is predicted to be rapidly reduced due to void formation inside the primary system. A void degradation factor has been also applied in order to simulate the decrease of pumps head as a function of the void fraction.

The core starts to uncover at 4800 s (Fig. 11), while core heatup starts at 5950 s at the core top, because the decay power is no more removed by natural circulation in the primary circuit. Core level is predicted to reach the bottom of the active fuel after 7800 s and it remains to this level, as also indicated by the analysis of the by-pass, down-comer and lower plenum levels, up to the actuation of the HPI.

The temperature in the cold leg (Fig. 12) remains at saturation during almost the whole transient and undergoes a steep decrease after HPI actuation. The behaviour of the temperature inside the hot leg (Fig. 13) is similar to other code predictions, even though higher values of steam superheating are evaluated during core heatup phase.

Also the fuel rod temperature, as evaluated by MELCOR at three different core elevations (Figures from 14 to 16), shows a good agreement with other code calculations. At the bottom of the core, a weaker fuel rod heat-up is anyway predicted during the phase where the core level goes to zero. The core quenching behaviour is strongly affected by the input value of the hydraulic diameter of the particulate debris (in this calculation the debris is only the refrozen zircalloy in the middle-lower parts of the core and the fuel pellets are still intact). The data presented in the following plots have been obtained using a value of 0.5 m, respect to the previous value of 3.0 m that led to an increase of the core temperatures after the reflood phase, due to a reduction in the predicted heat removal. A further reduction of this value leads to the prediction of a larger core degradation before the reflooding.

Fuel rod melting starts just before the main oxidation phase. Melting of Zircalloy starts at about 7500 s also causing a partial dissolution of the fuel. The total mass of molten metals is predicted to be about 12 tons (Fig. 17), while about 18 tons of material debris (Fig. 18) are calculated by MELCOR.

The main oxidation phase takes place (Figures 19 and 20) between 6700 s and 8500 s since the beginning of the transient. The hydrogen production is different for the reference and alternative calculations (Fig. 21). In the sensitivity calculation cladding failure is anticipated (larger minimum thickness and lower maximum temperature); this causes a larger release and relocation of molten Zr towards lower and colder elevations, reducing available metal for the oxidation process. The final amount of hydrogen is therefore larger (335 kg) during the reference case with respect to the alternative parameter calculation (275 kg). No hydrogen production is calculated during and after core reflooding phase.

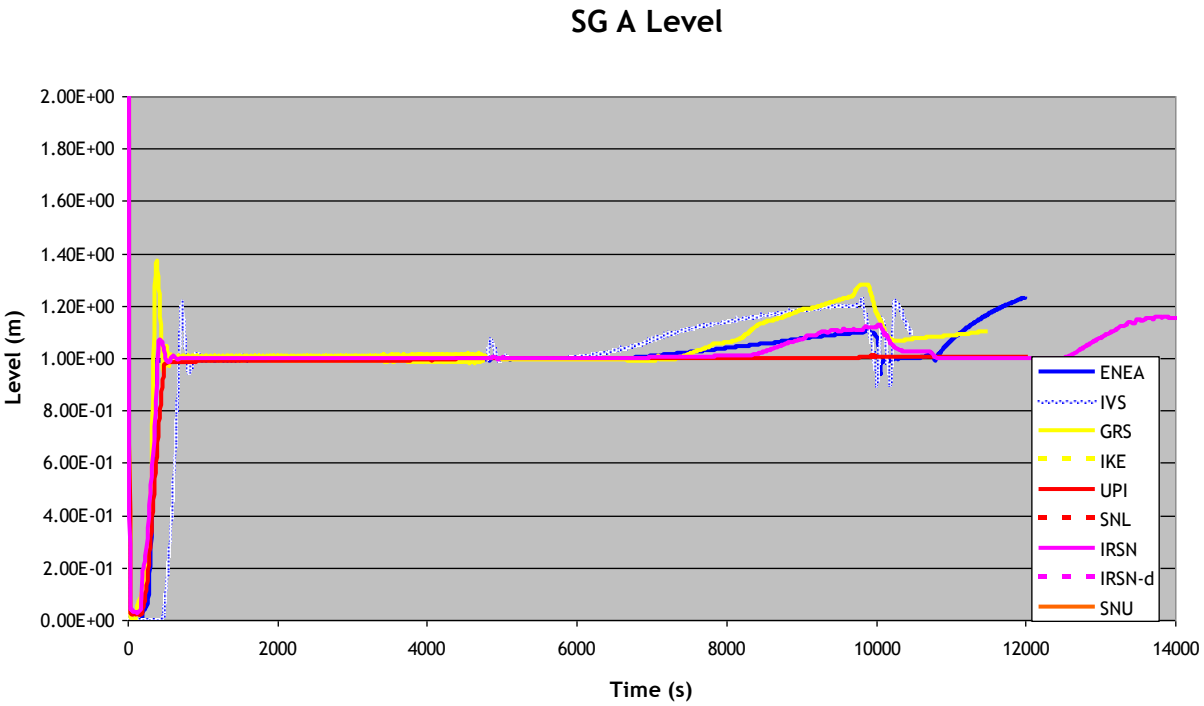

Fig. 3: Steam generator A level

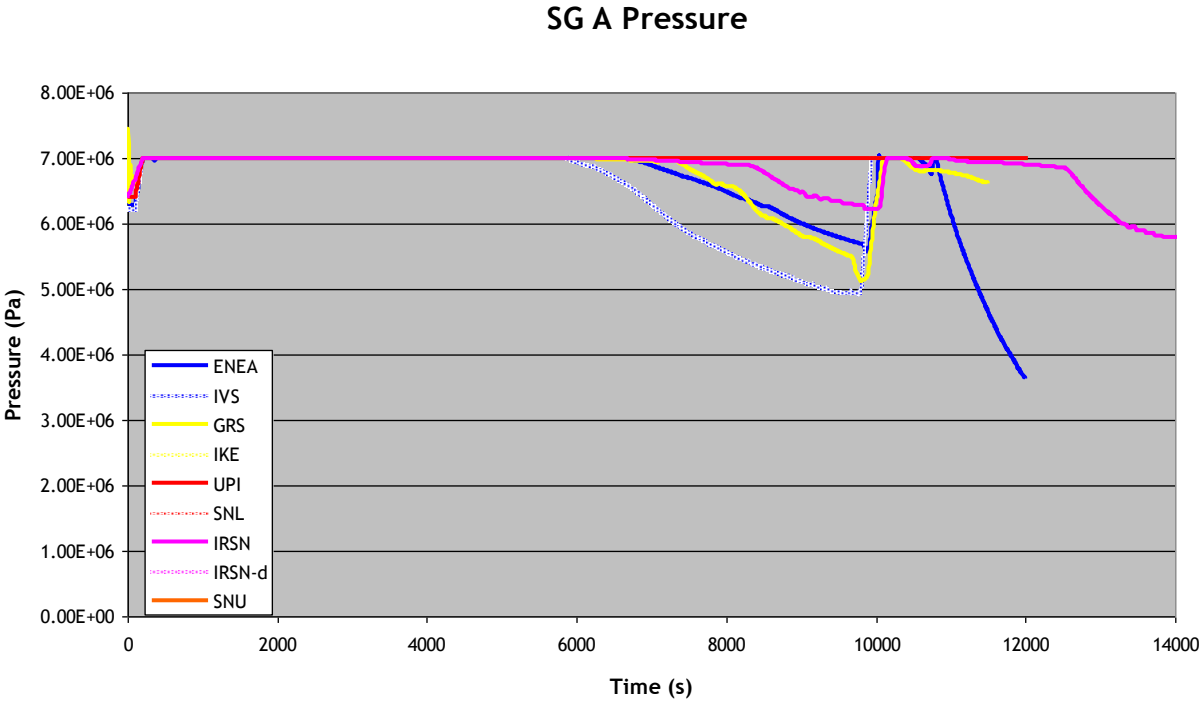

Fig. 4: Steam generator A pressure

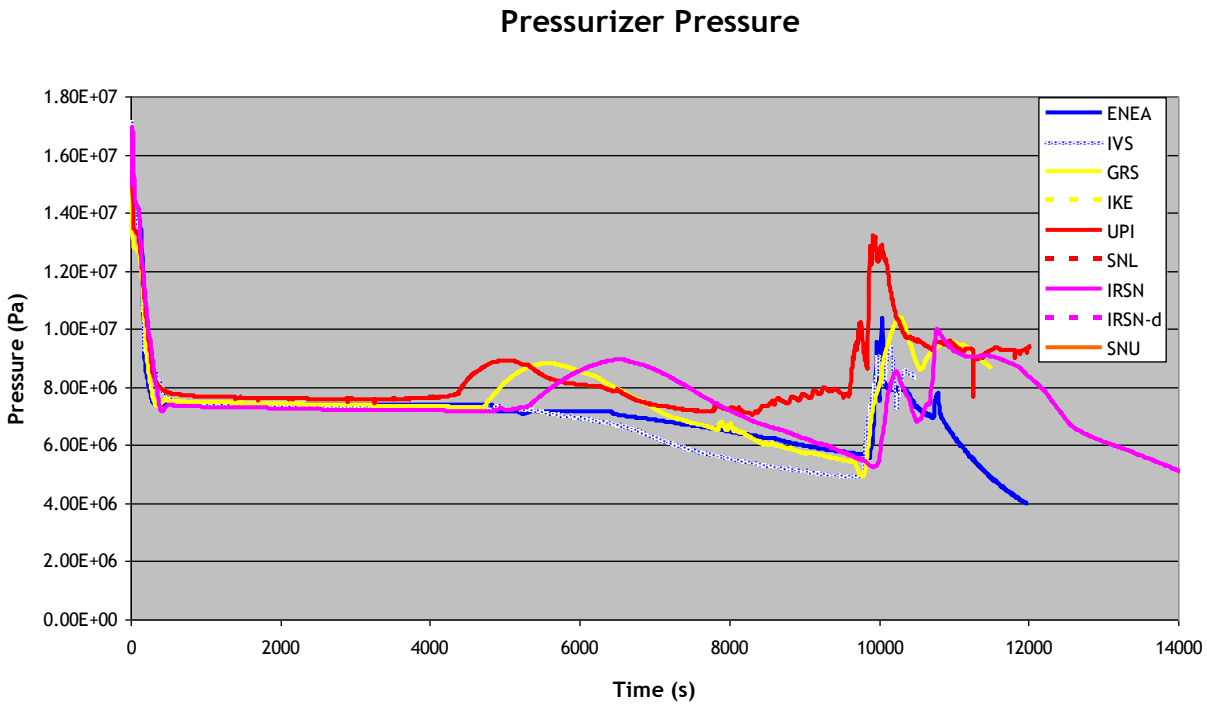

Fig. 5: Pressuriser pressure

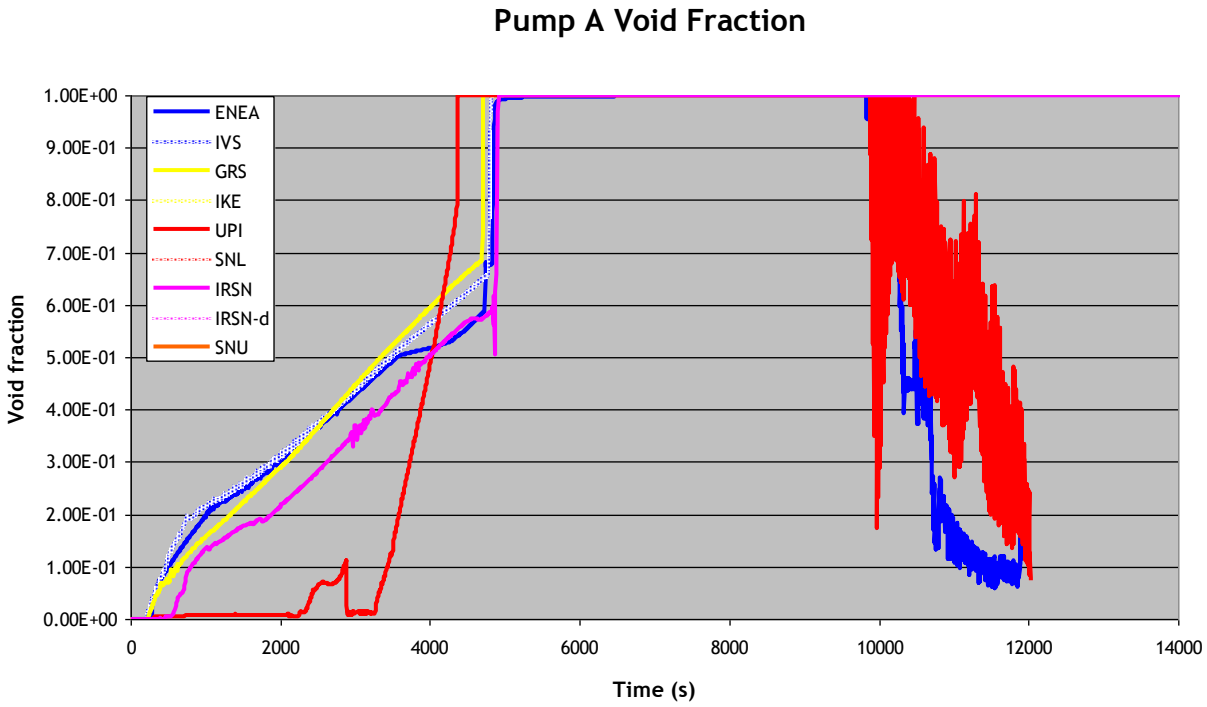

Fig. 6: Main pump A void fraction

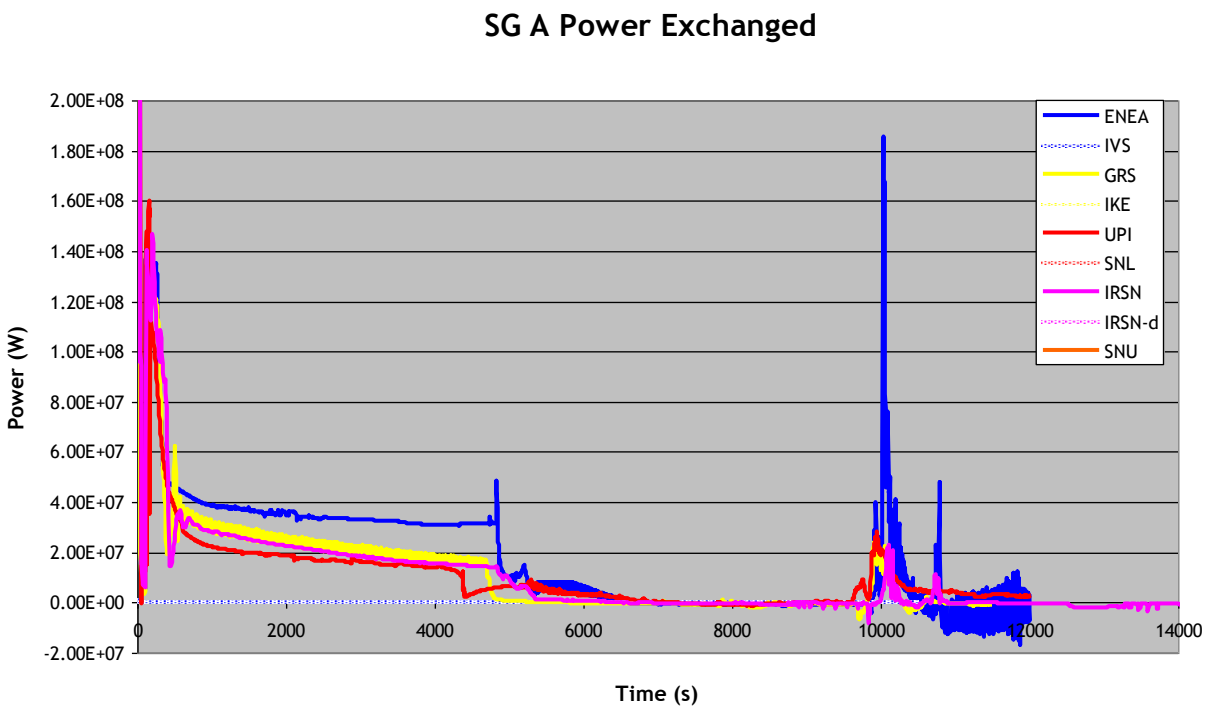

Fig. 7: Steam generator A removed power

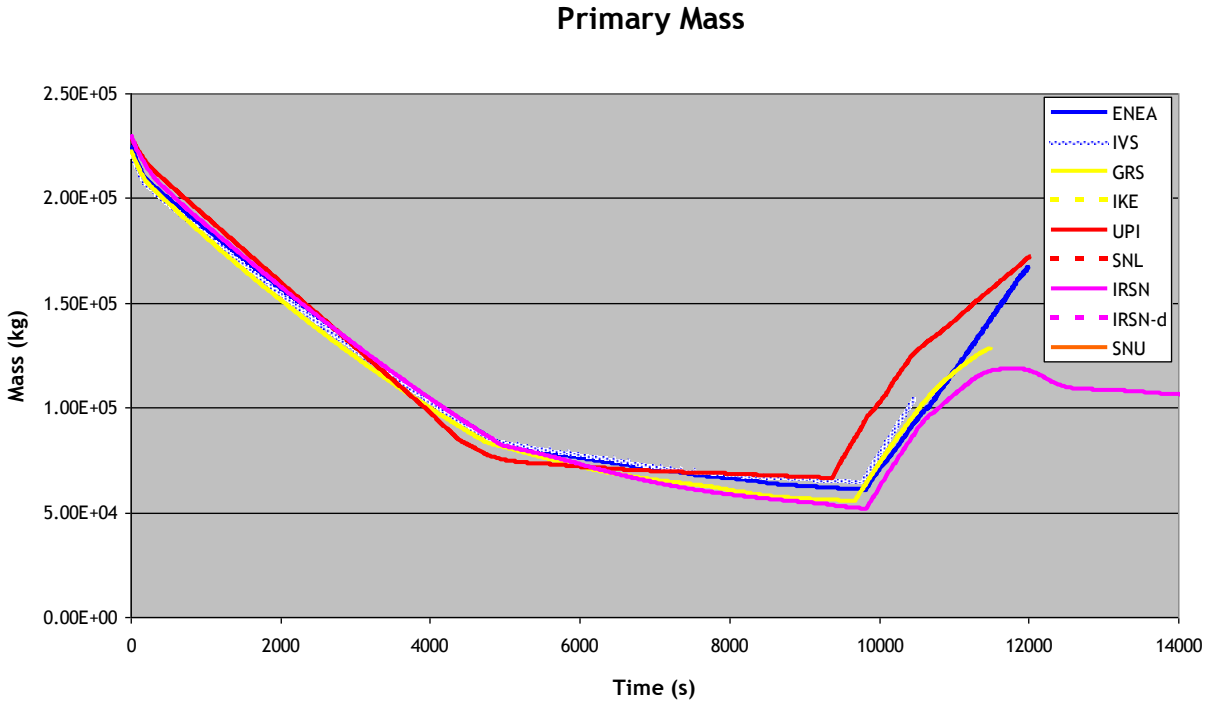

Fig. 8: Total primary water mass

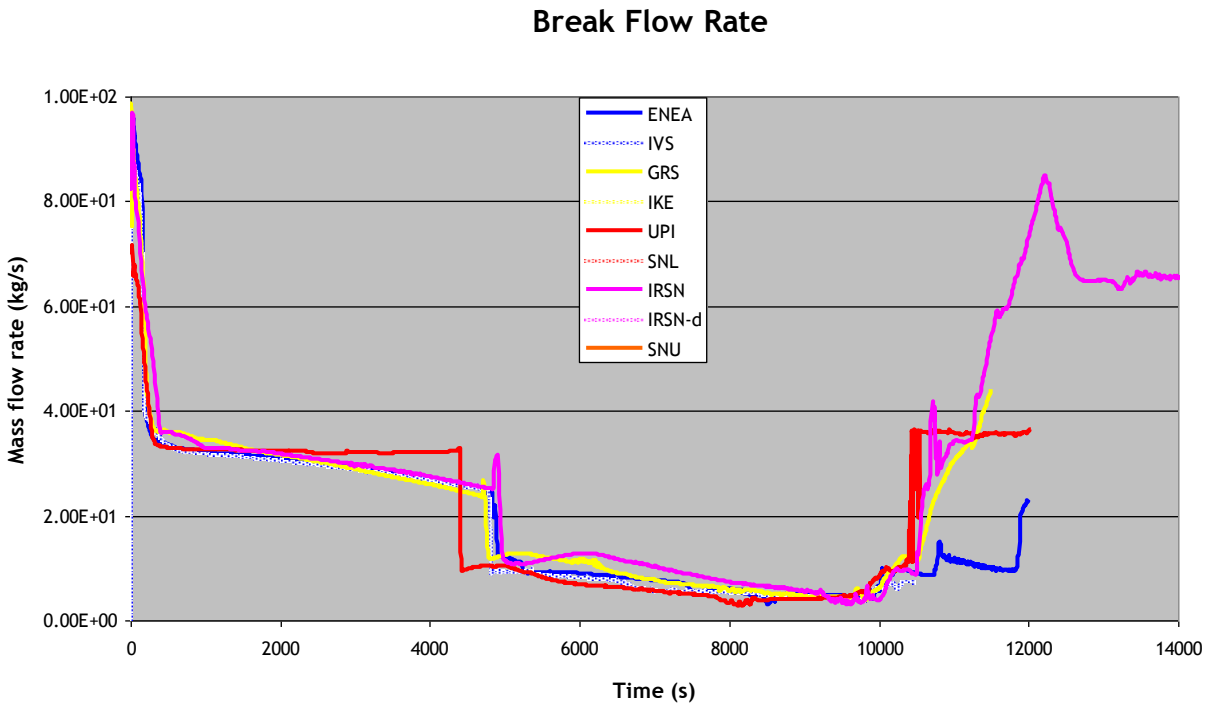

Fig. 9: Break mass flowrate

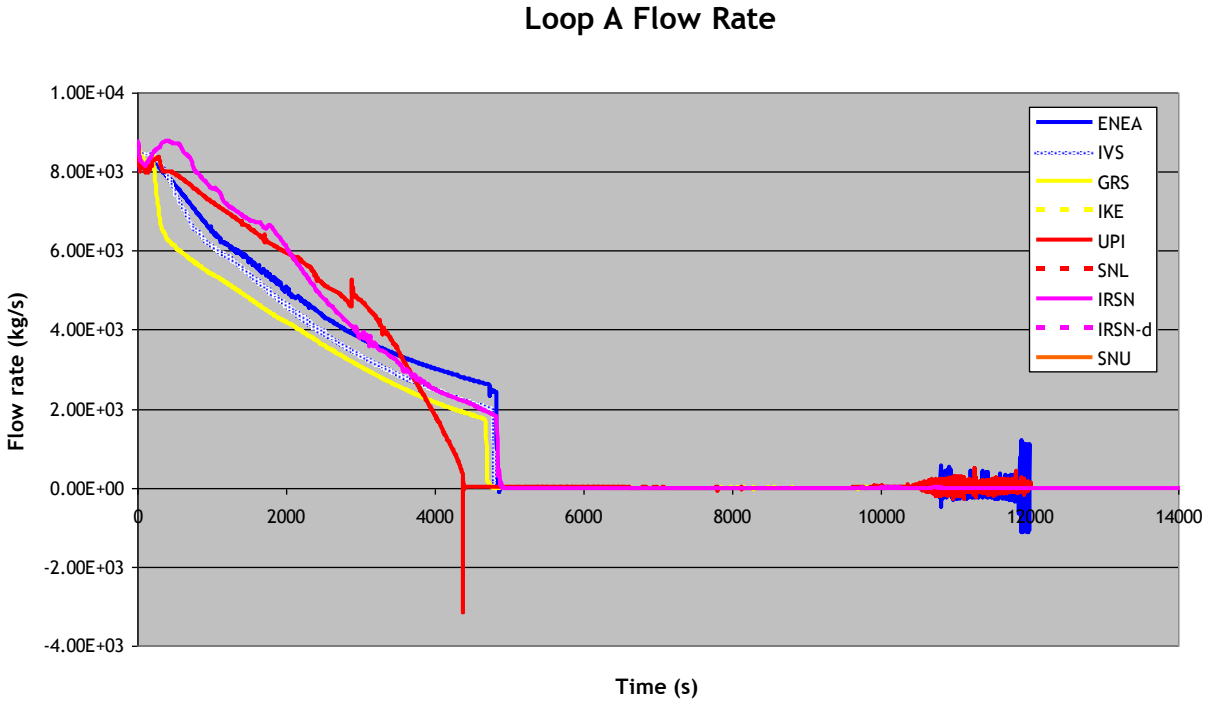

Fig. 10 Loop A mass flowrate

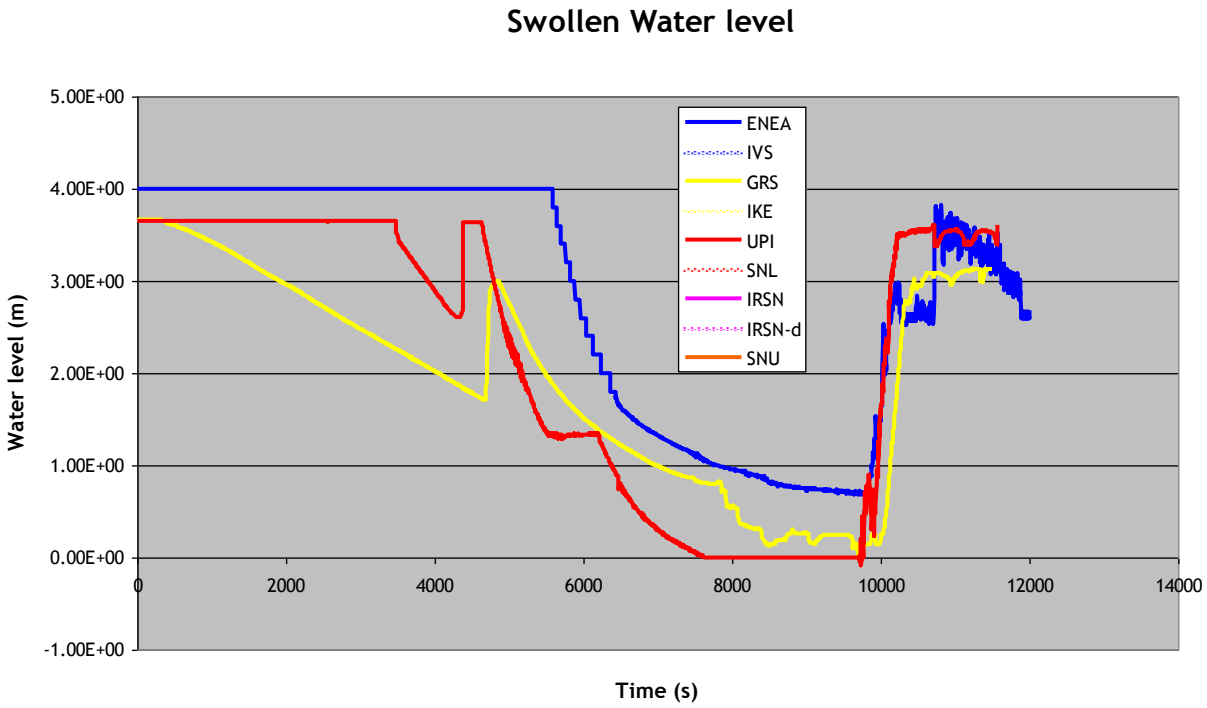

Fig. 11 Core swollen water level

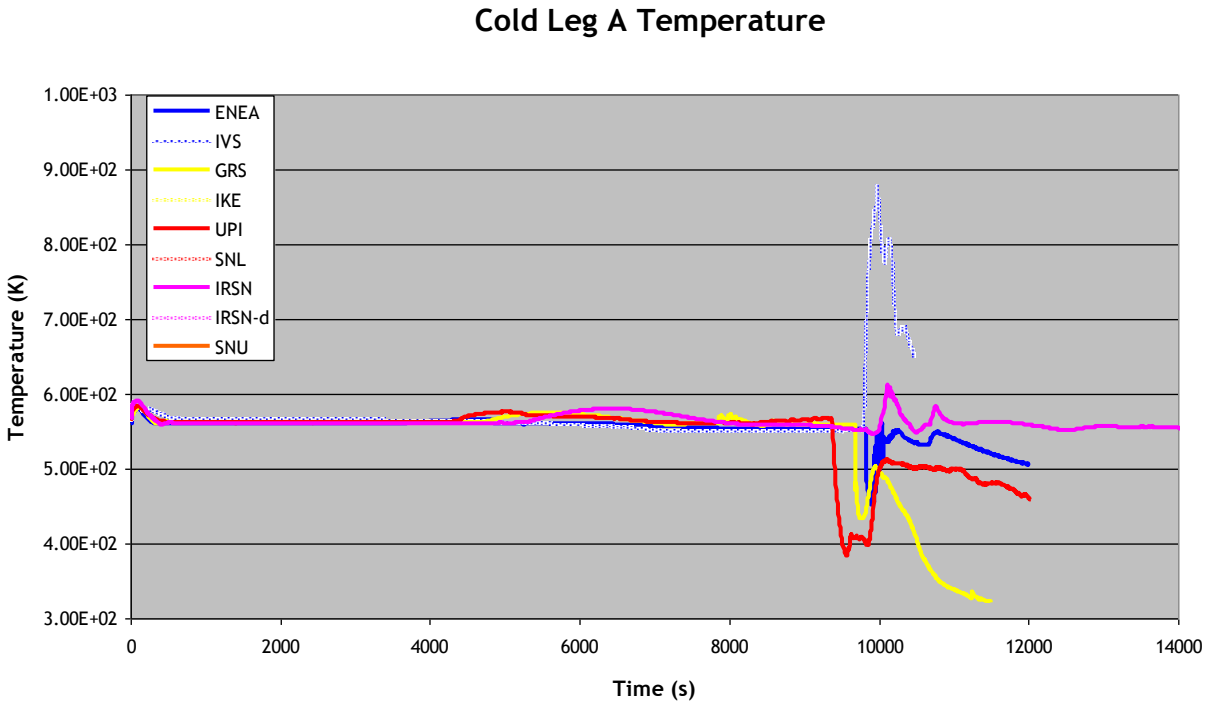

Fig. 12 Cold leg A temperature

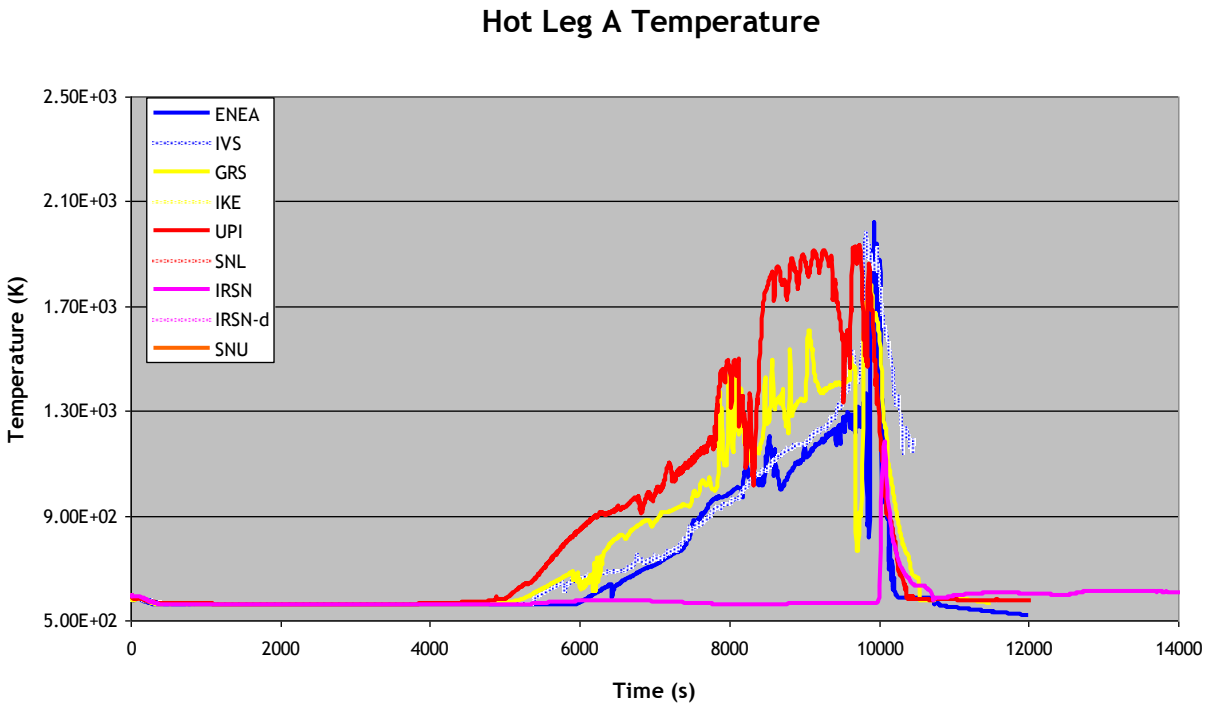

Fig. 13: Hot leg A temperature

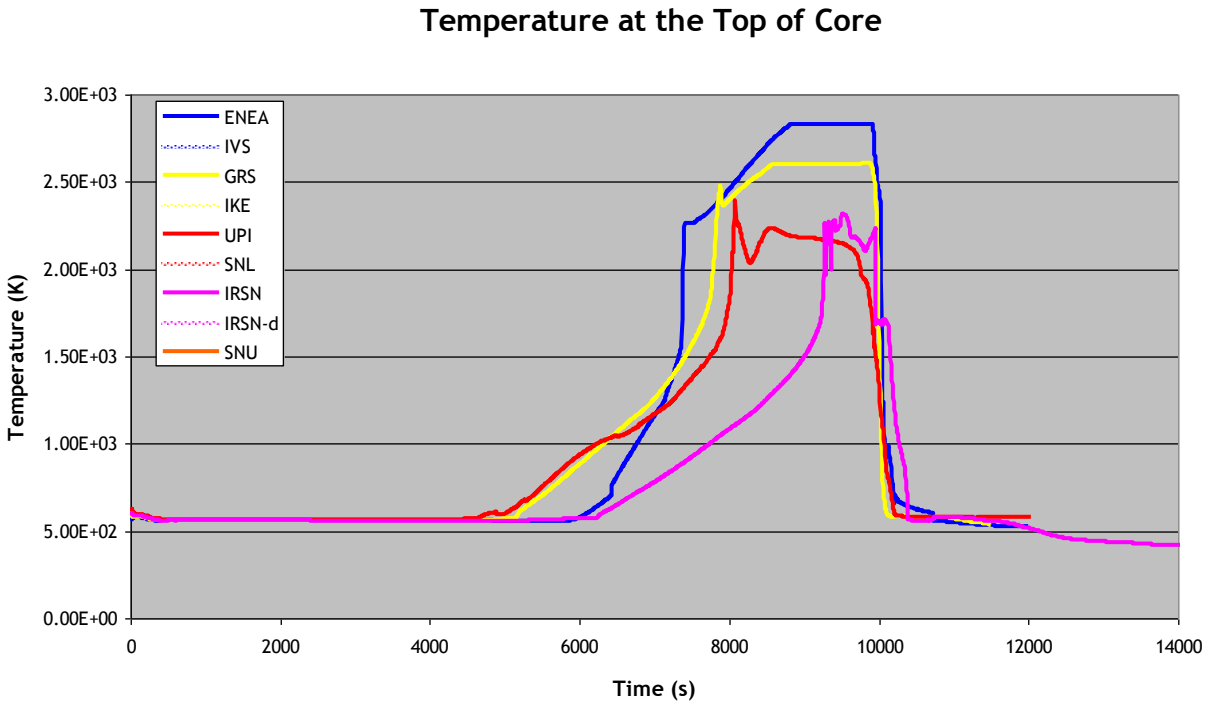

Fig. 14: Fuel rod temperature at the top of the core

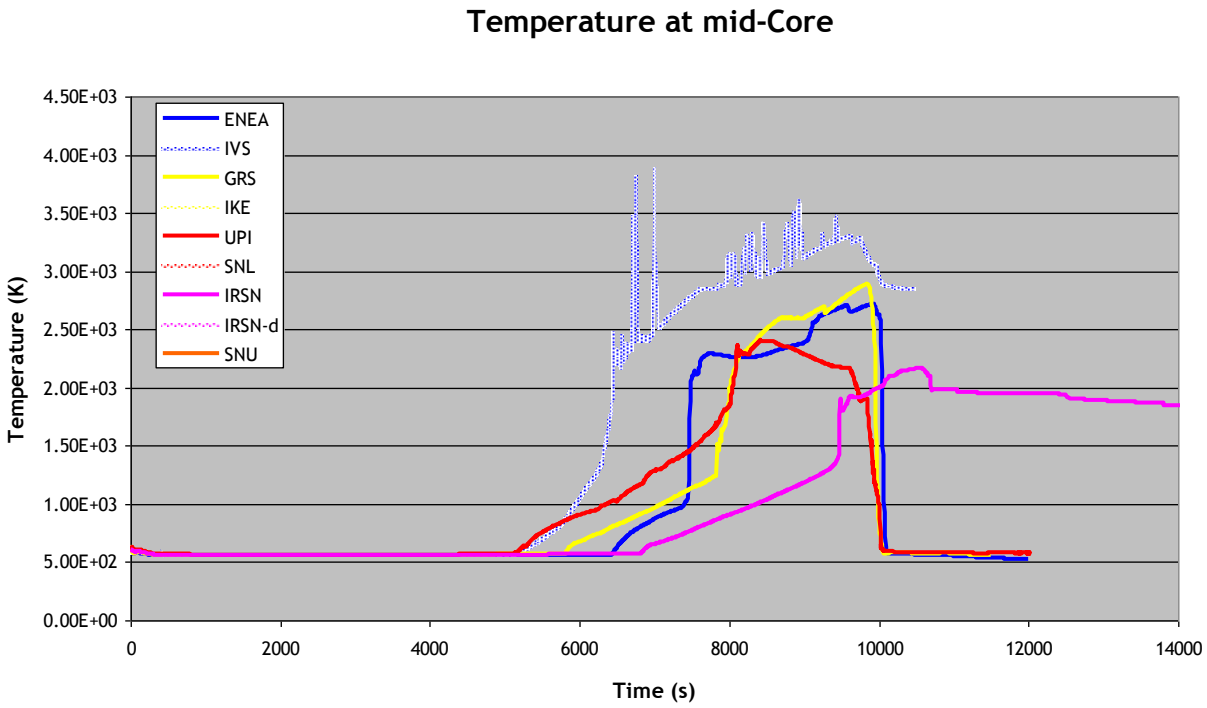

Fig. 15: Fuel rod temperature at the middle of the core

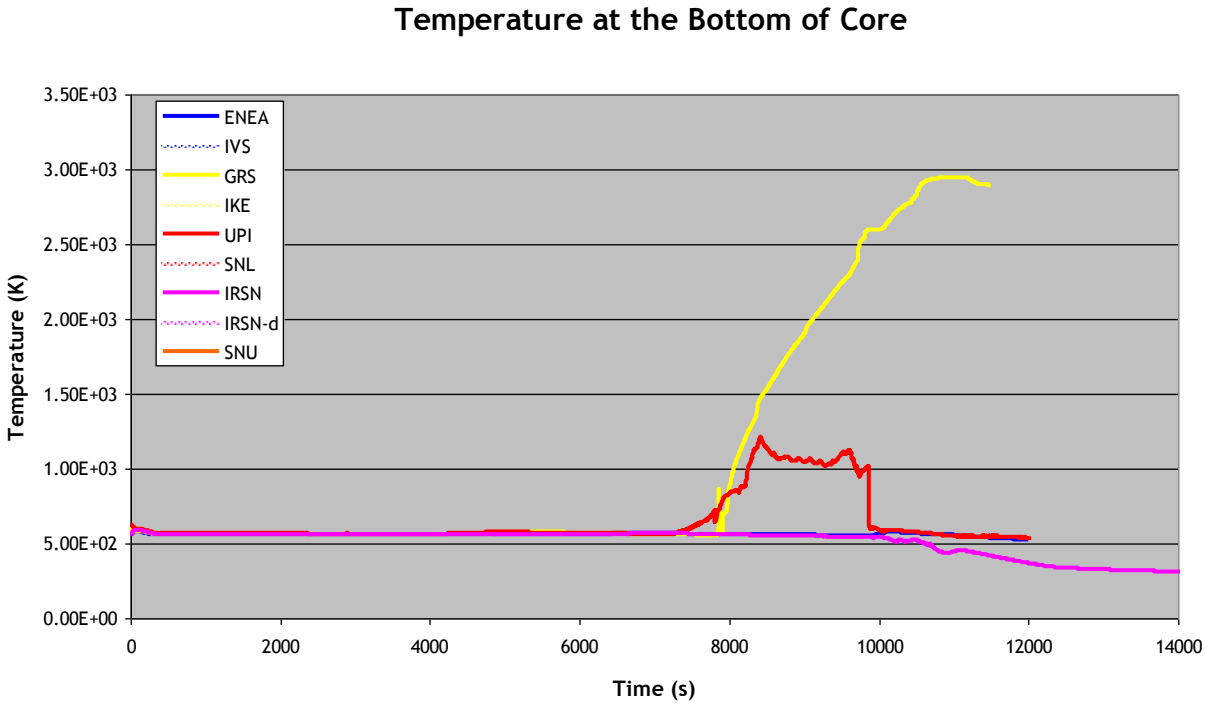

Fig. 16 Fuel rod temperature at the bottom of the core

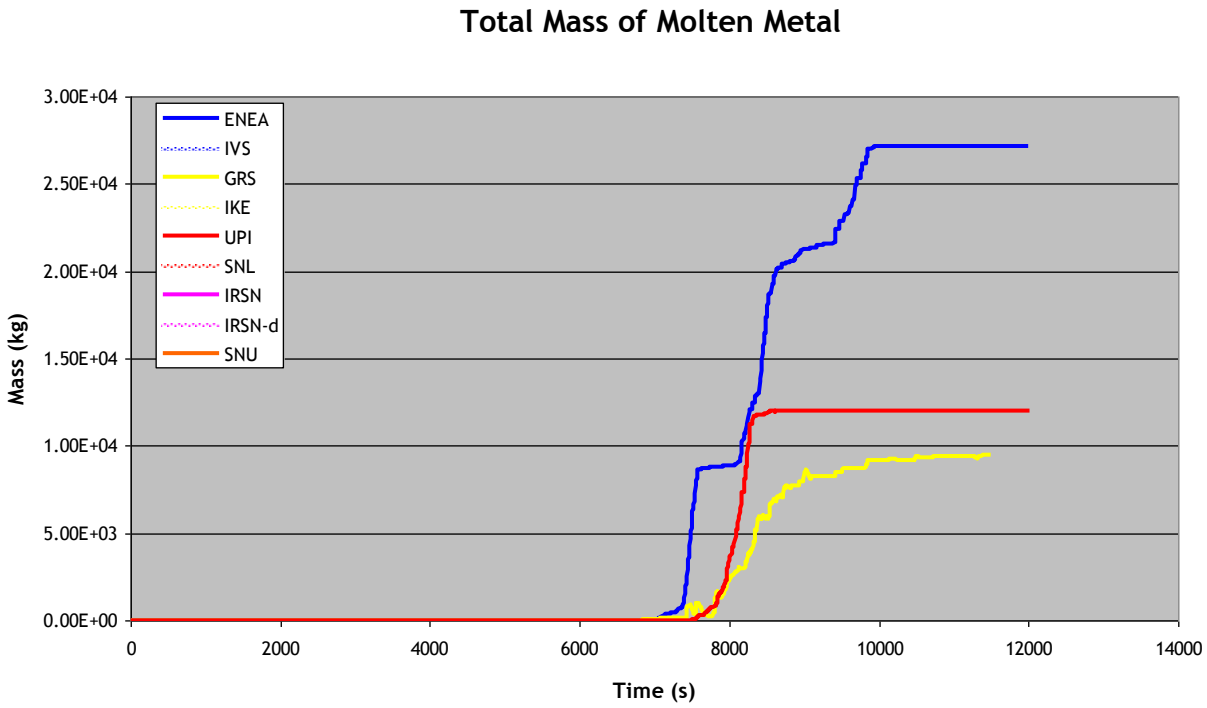

Fig. 17: total mass of molten metals

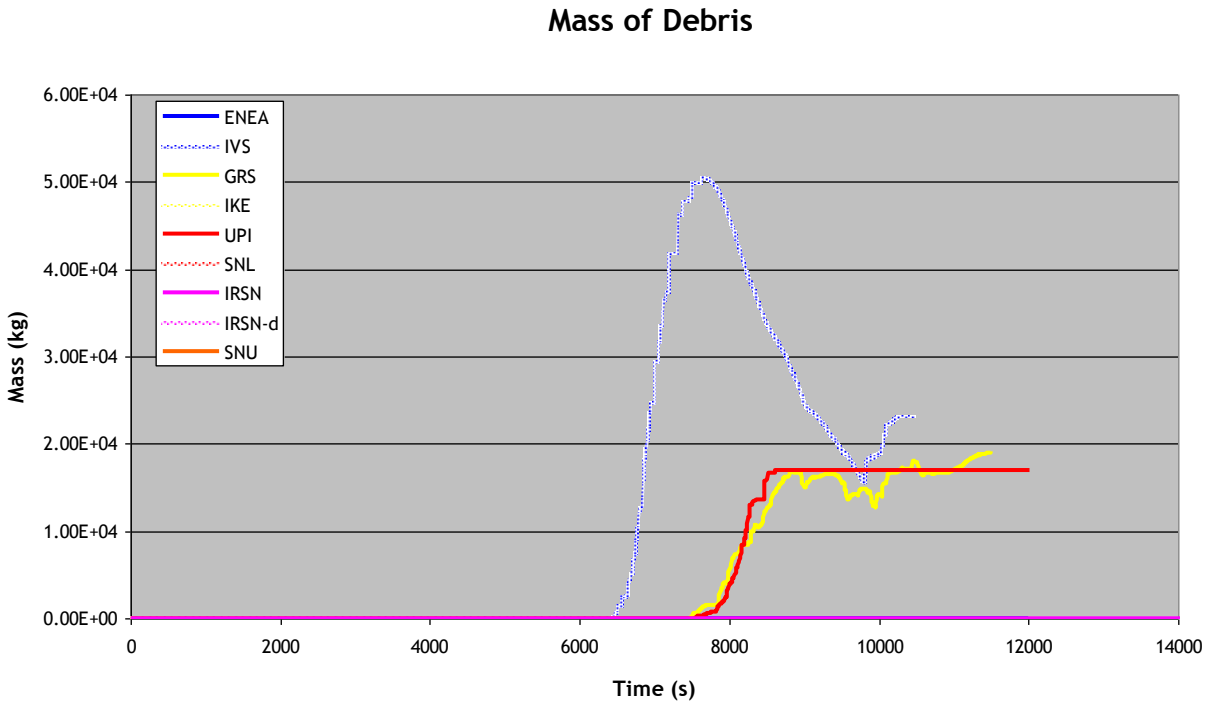

Fig. 18: total mass of debris

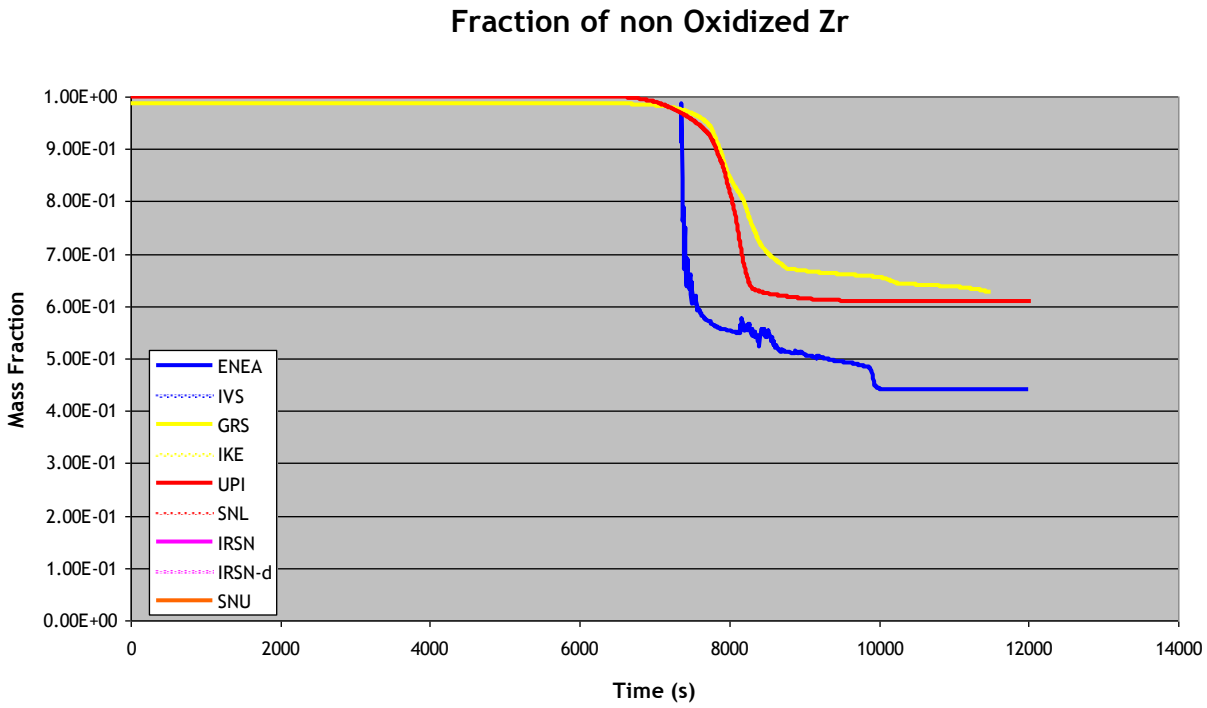

Fig. 19 Fraction of non oxidised Zr

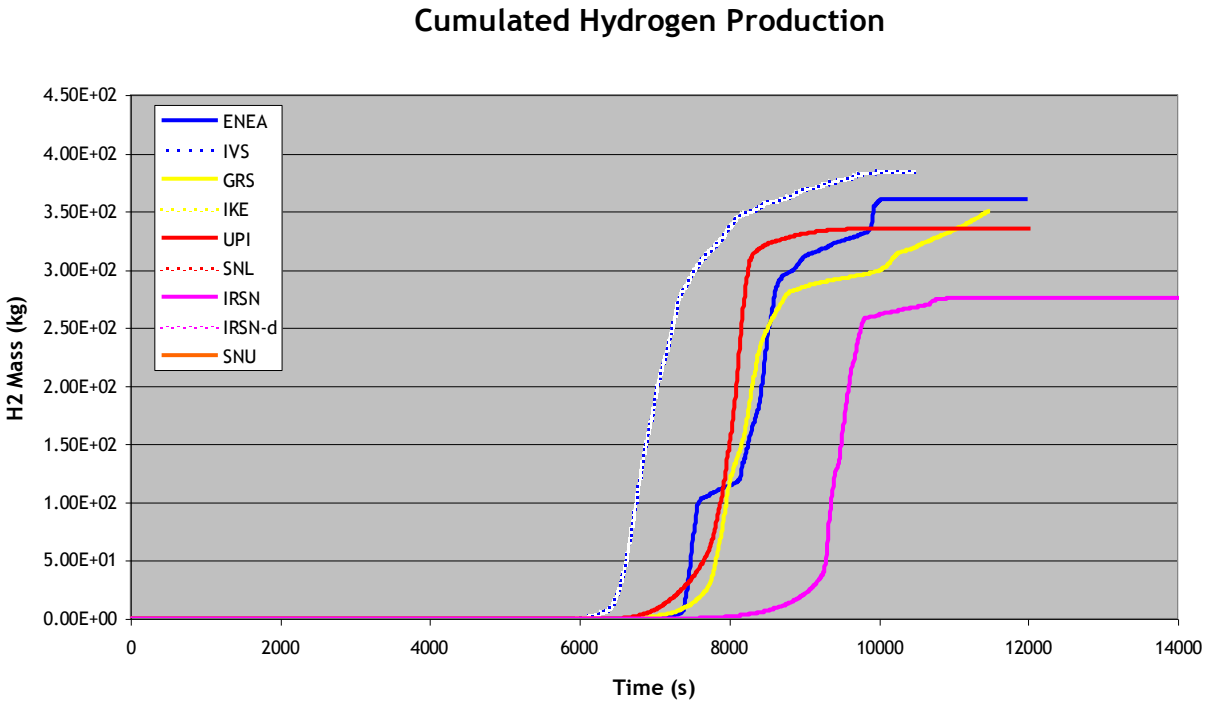

Fig. 20 Cumulated mass of Hydrogen

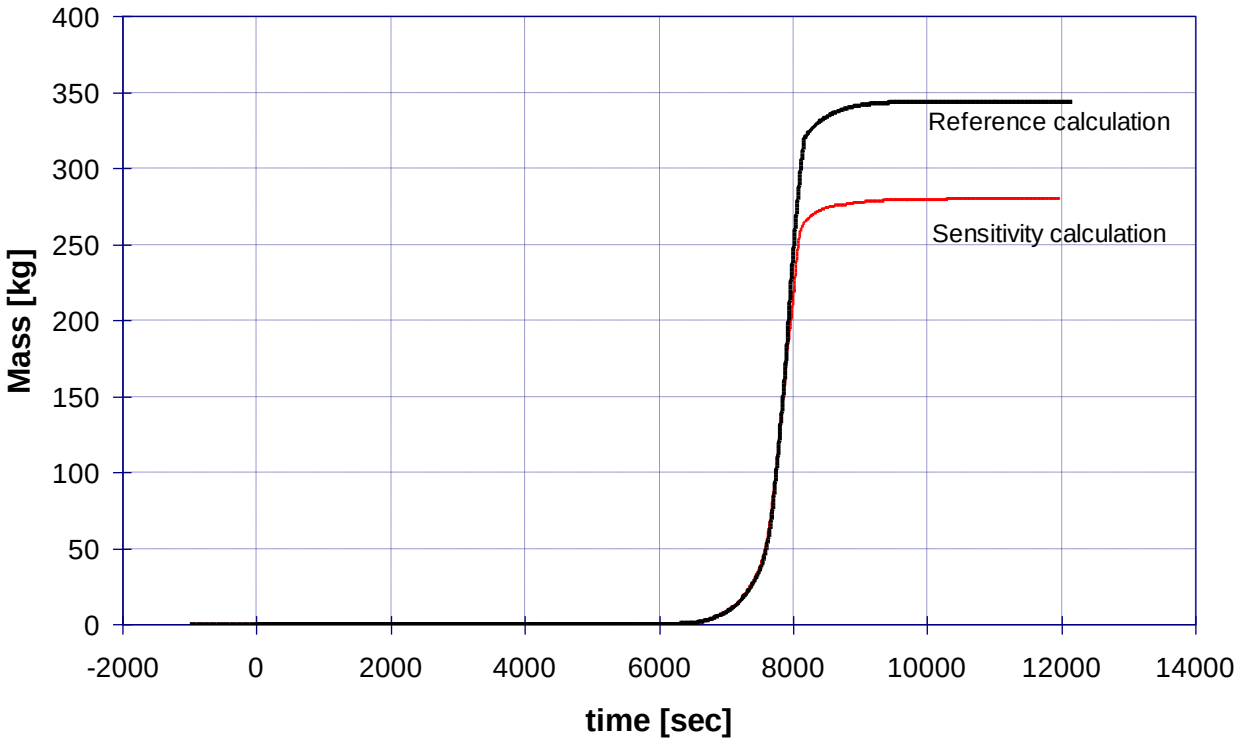

Fig. 21 Hydrogen production comparison

Synthetic Views of the Core at Selected Instants

Standard case

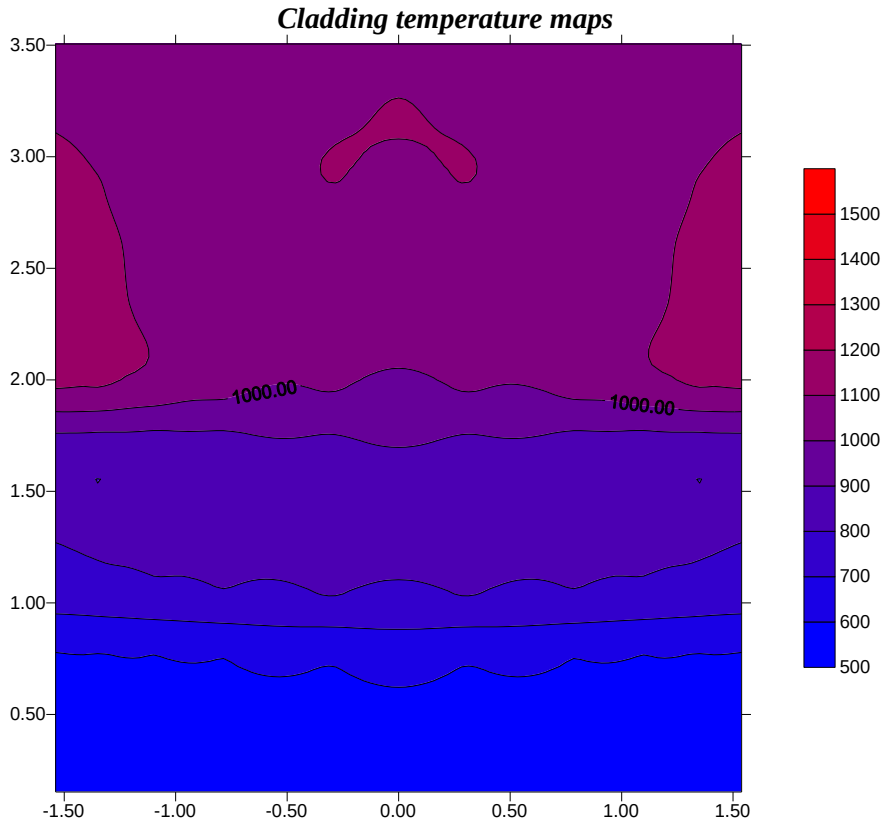

Fig. 22: Cladding temperature (t = 6600. s)

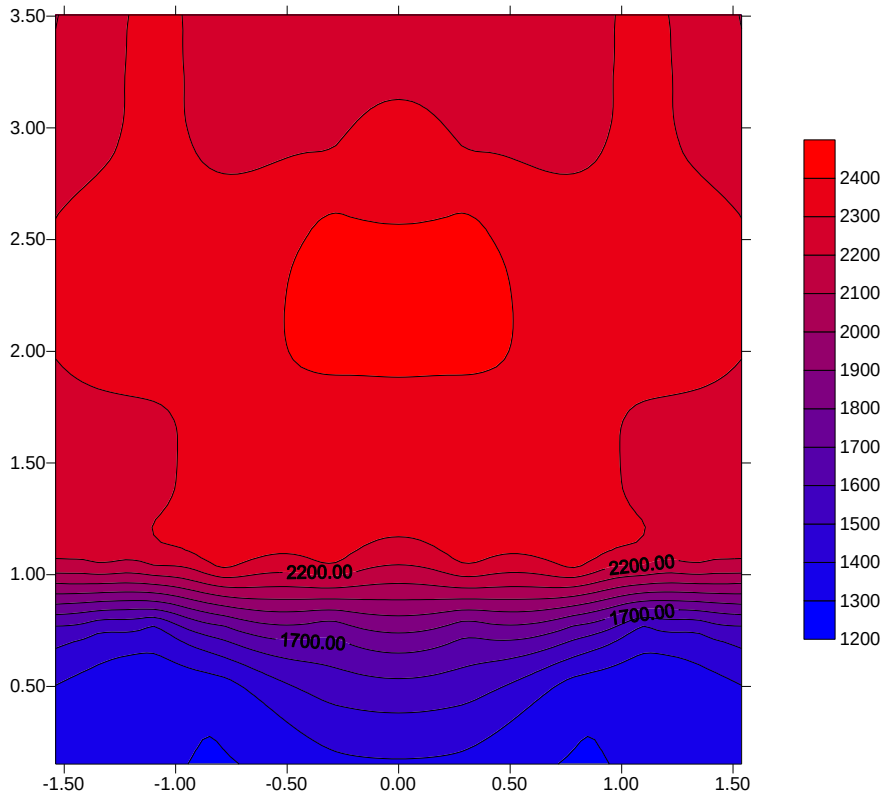

Fig. 23: Cladding temperature (t = 8200. s)

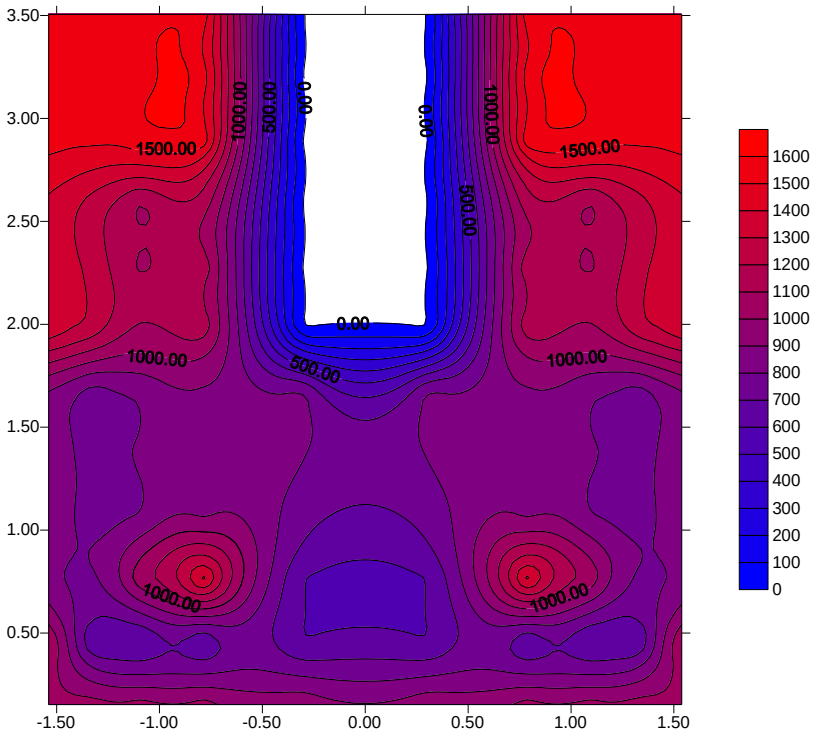

Fig. 24: Cladding temperature (t = 10000. s)

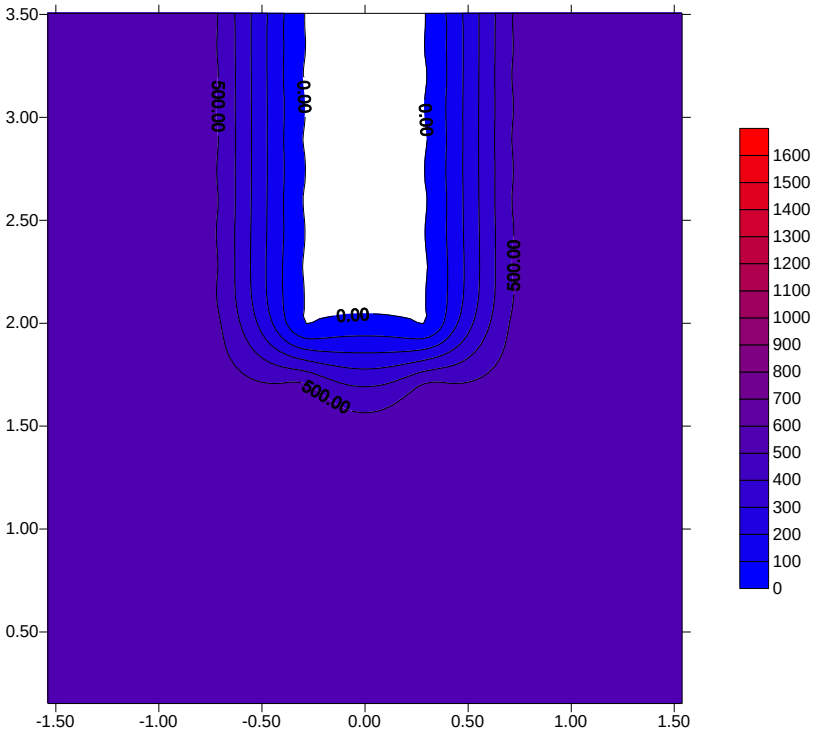

Fig. 25: Cladding temperature (t = 12000. s)

Linear mass of oxidised Zircalloy

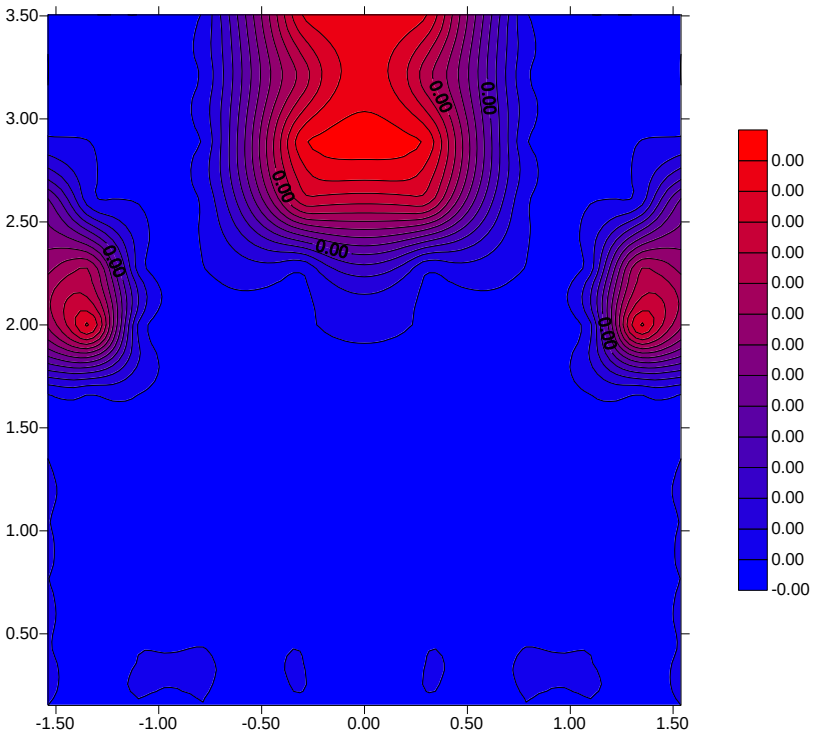

Fig. 26: ZrO_2 linar mass (t = 6600. s)

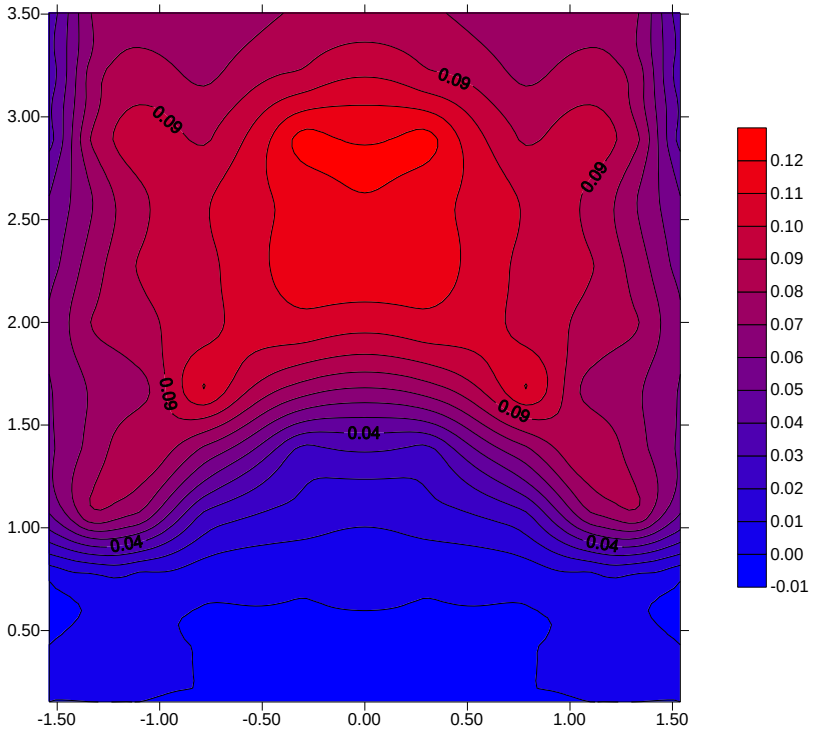

Fig. 27: ZrO_2 linar mass (t = 8200. s)

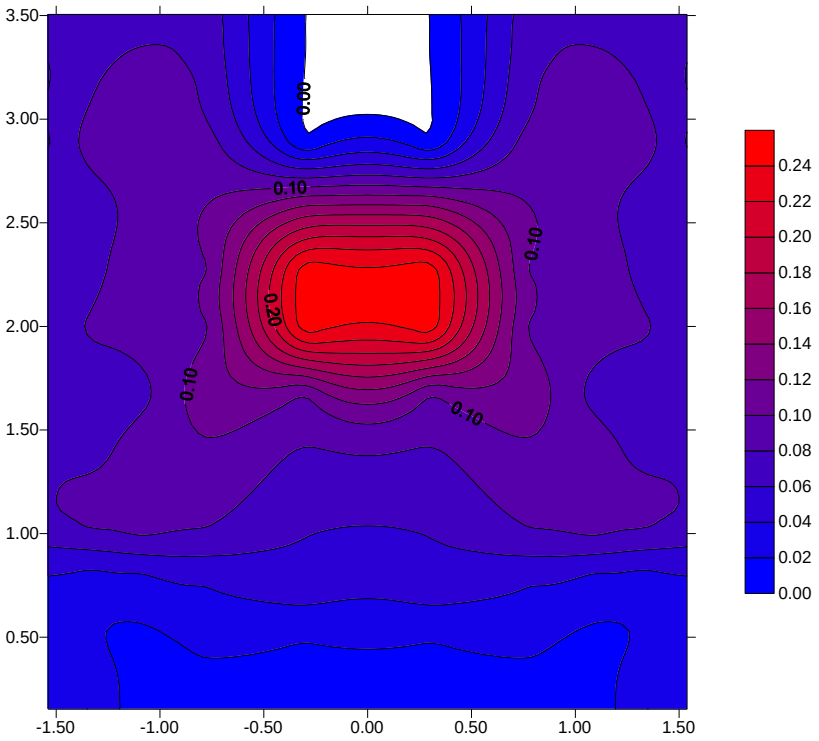

Fig. 28: ZrO_2 linar mass (t = 10000. s)

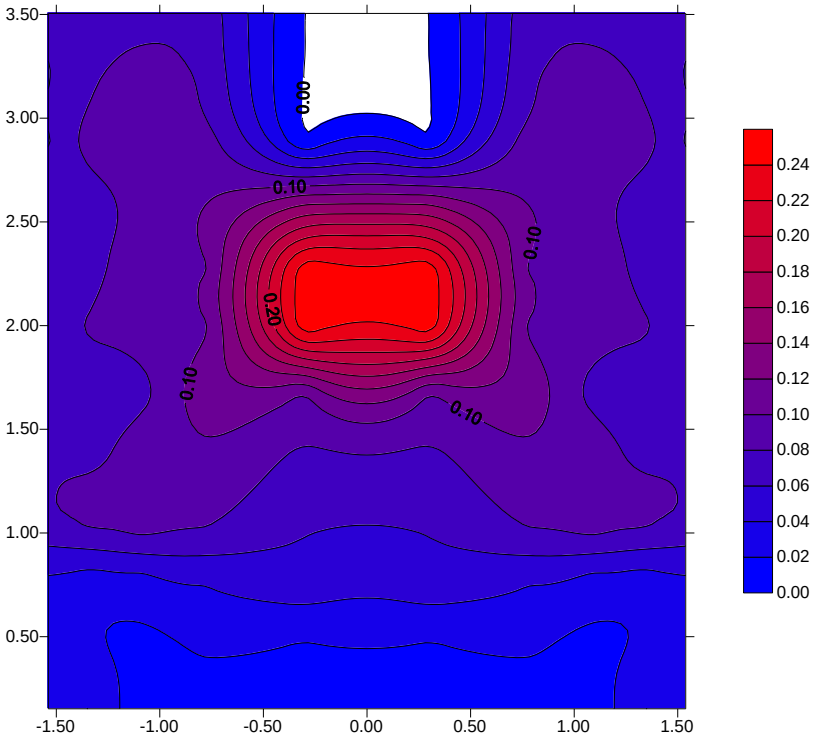

Fig. 29: ZrO_2 linar mass (t = 12000. s)

Molten Zircalloy mass

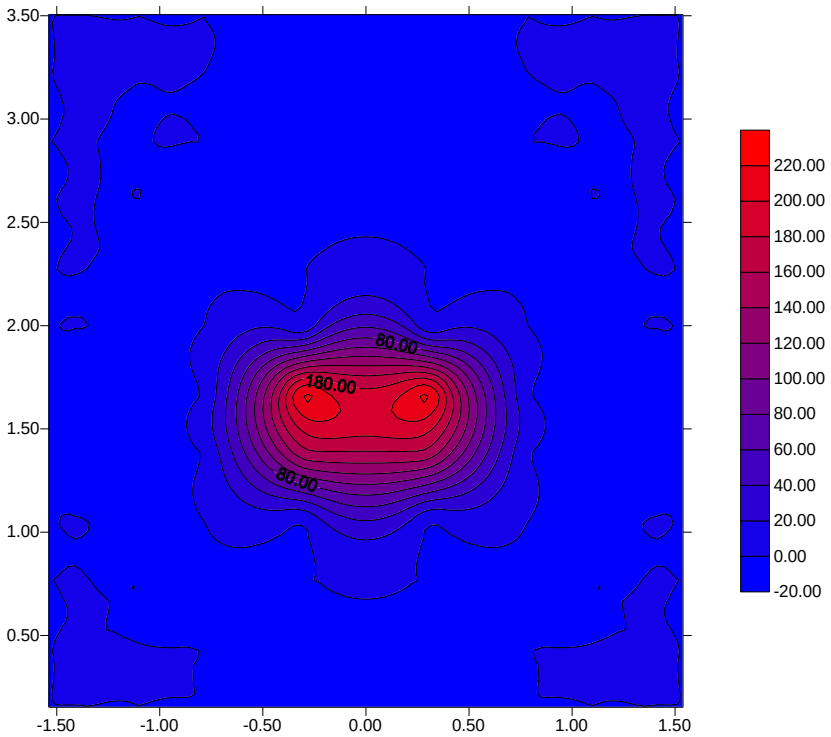

Fig. 30: Molten Zircalloy mass (t = 7900. s)

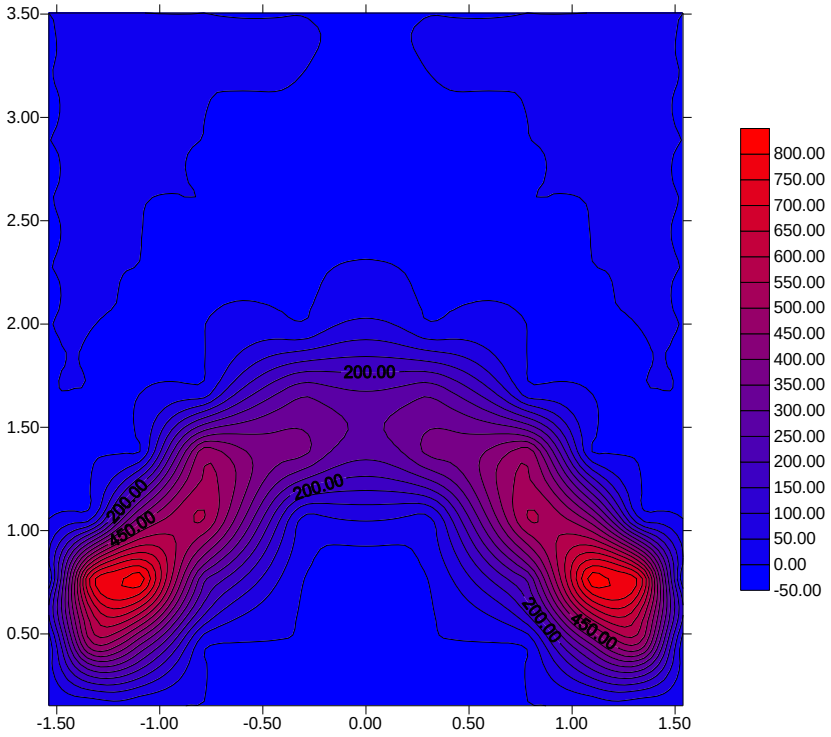

Fig. 31: Molten Zircalloy mass (t = 8200. s)

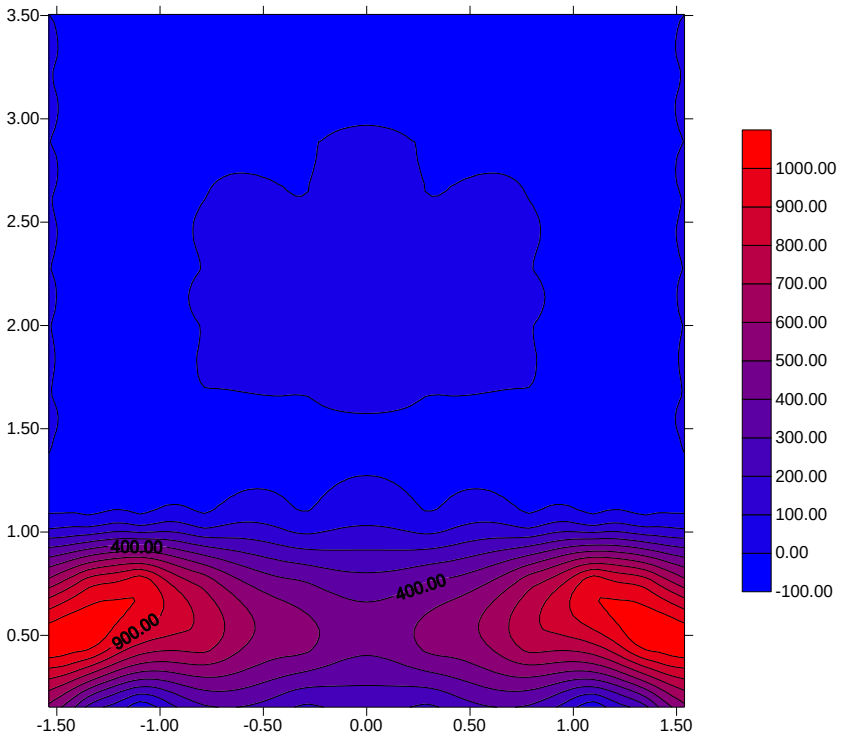

Fig. 32: Molten Zircalloy mass (t = 12000. s)

Sensitivity case

Cladding temperature maps

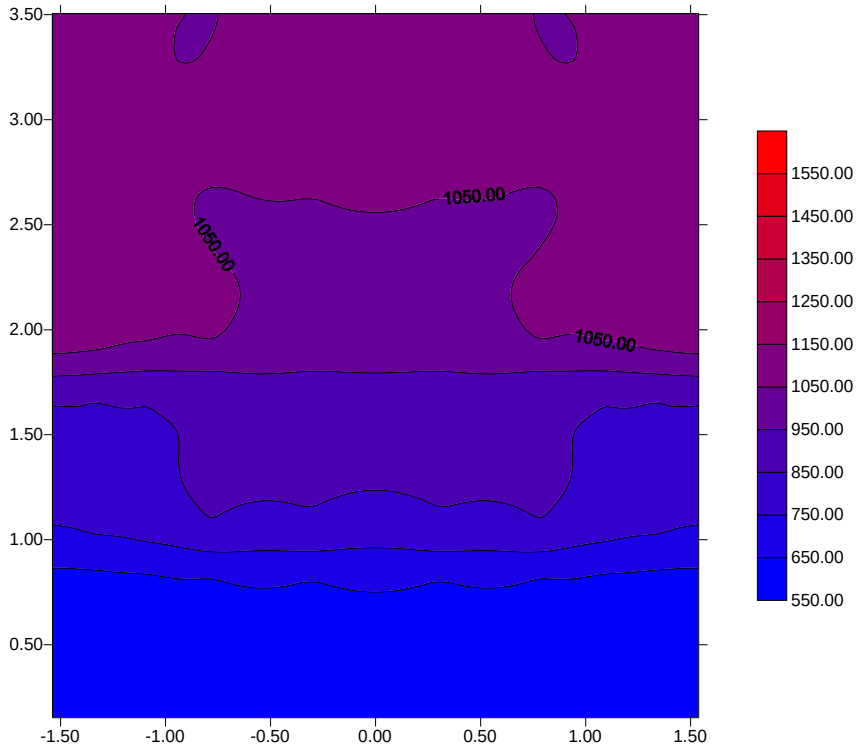

Fig. 33: Cladding temperature (t = 6600. s)

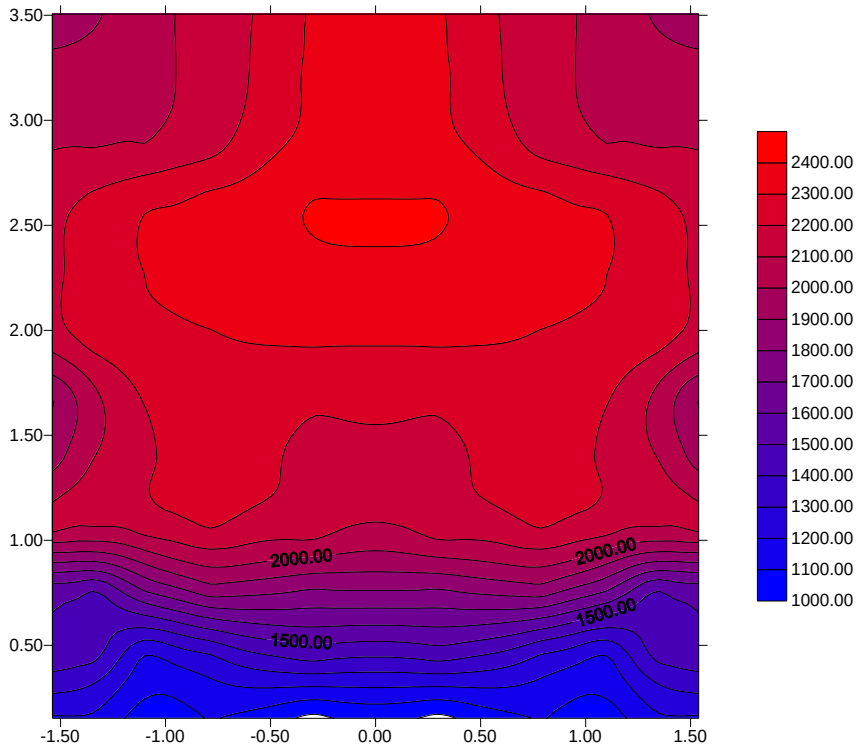

Fig. 34: Cladding temperature (t = 8200. s)

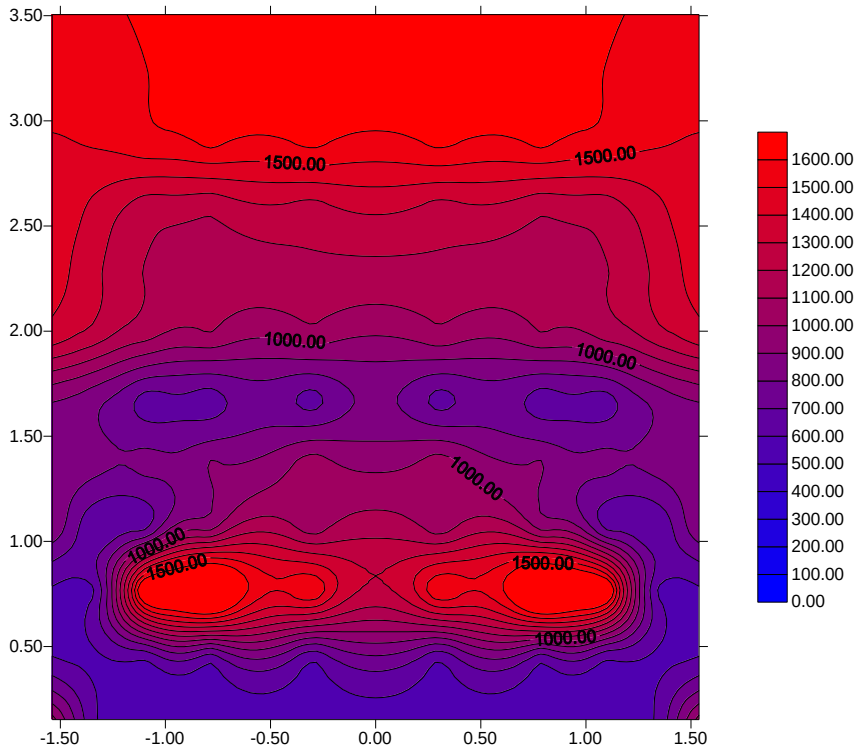

Fig. 35: Cladding temperature (t = 10000. s)

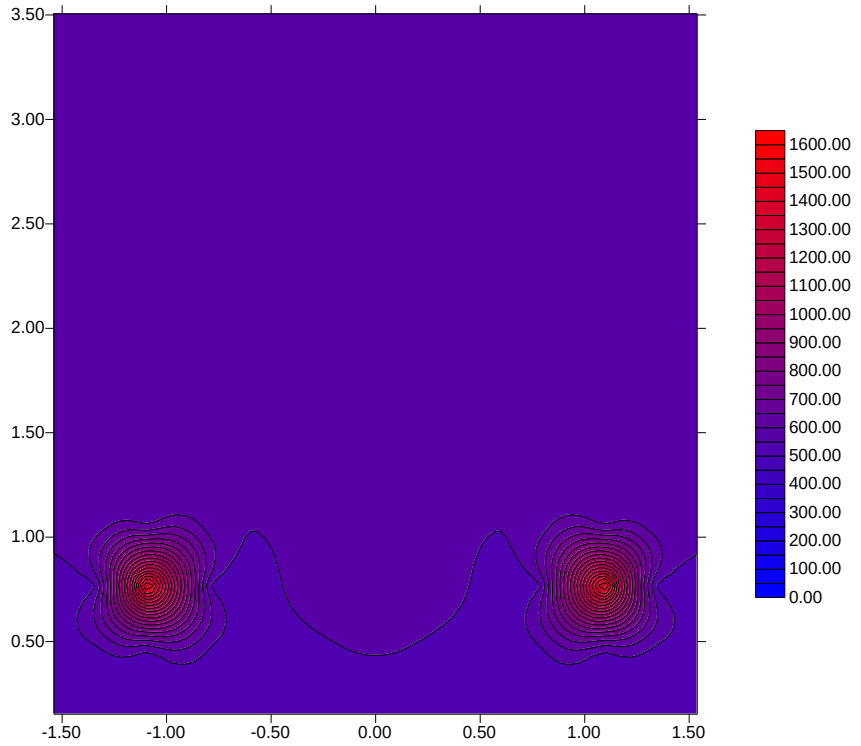

Fig. 36: Cladding temperature (t = 12000. s)

Linear mass of oxidised Zircalloy

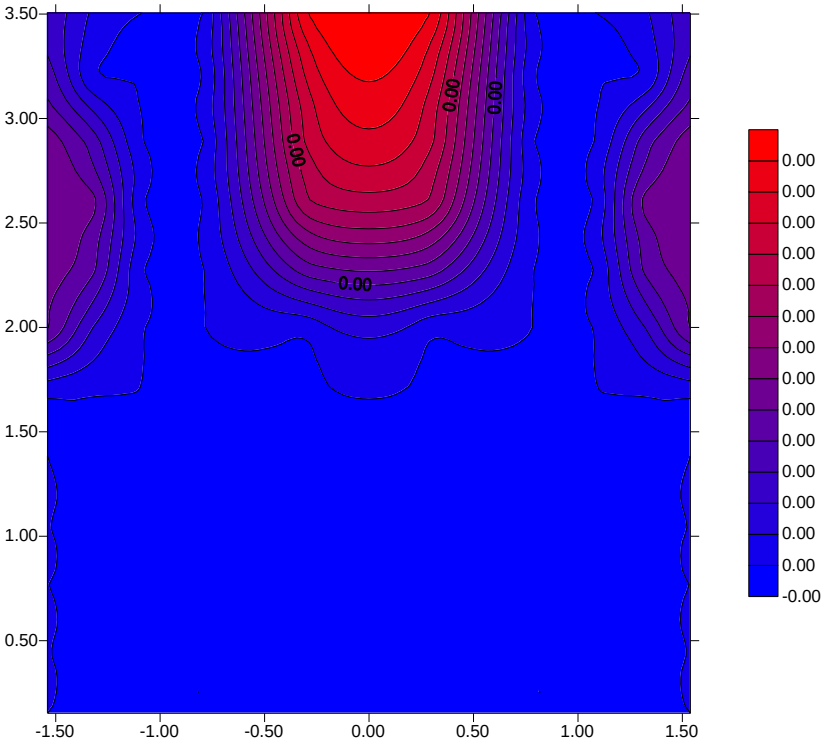

Fig. 37: ZrO_2 linar mass (t = 6600. s)

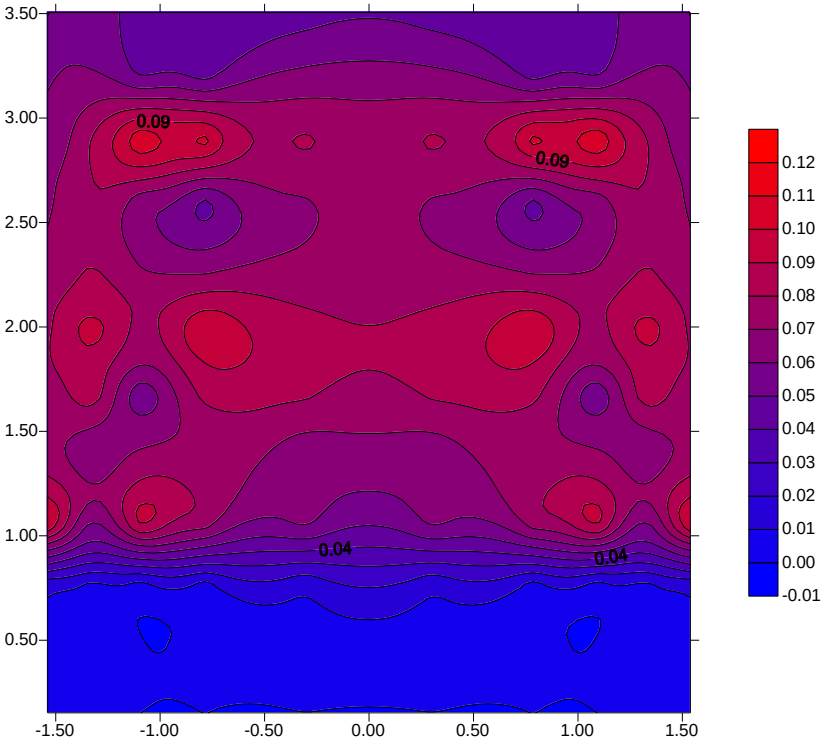

Fig. 38: ZrO_2 linar mass (t = 8200. s)

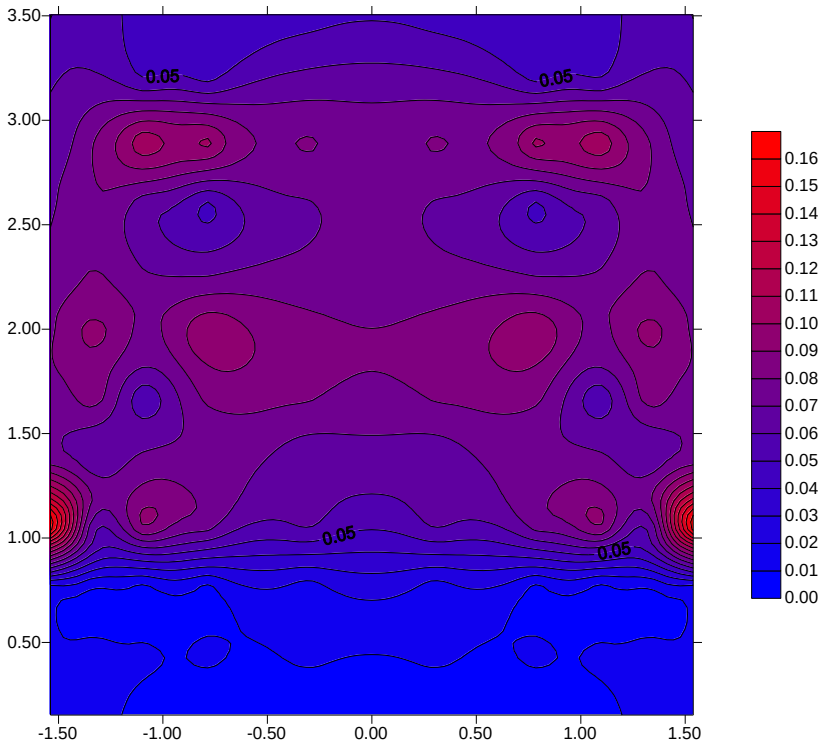

Fig. 39: ZrO_2 linar mass (t = 10000. s)

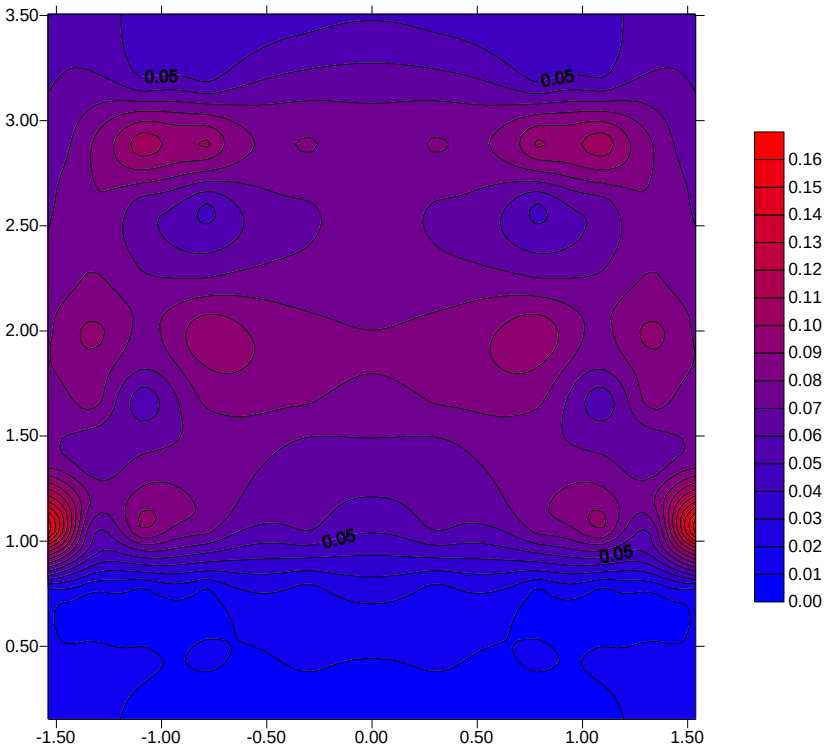

Fig. 40: ZrO_2 linar mass (t = 12000. s)

Molten Zircalloy mass

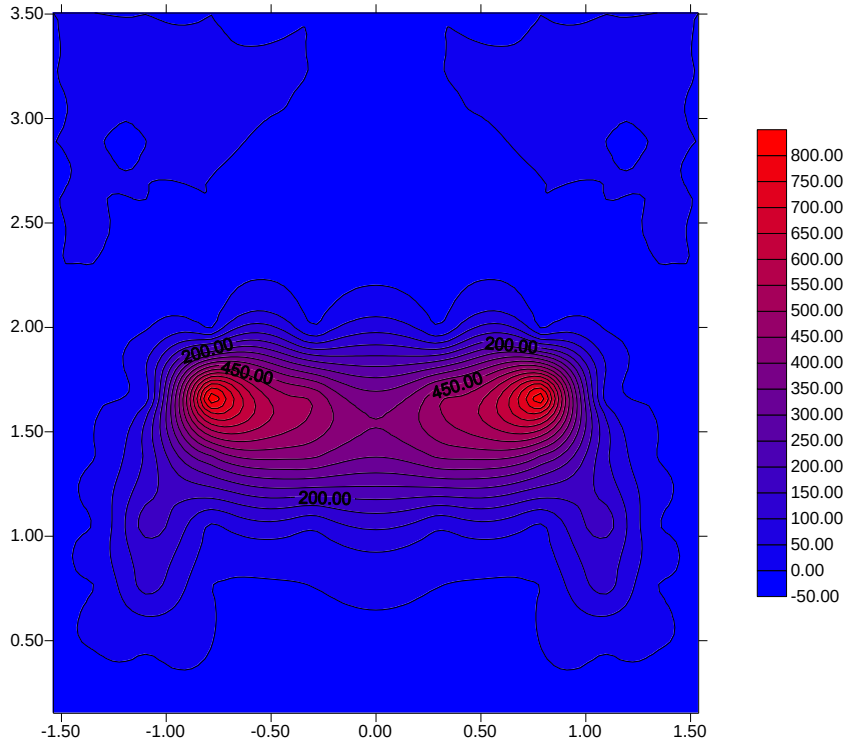

Fig. 41: Molten Zircalloy mass (t = 7900. s)

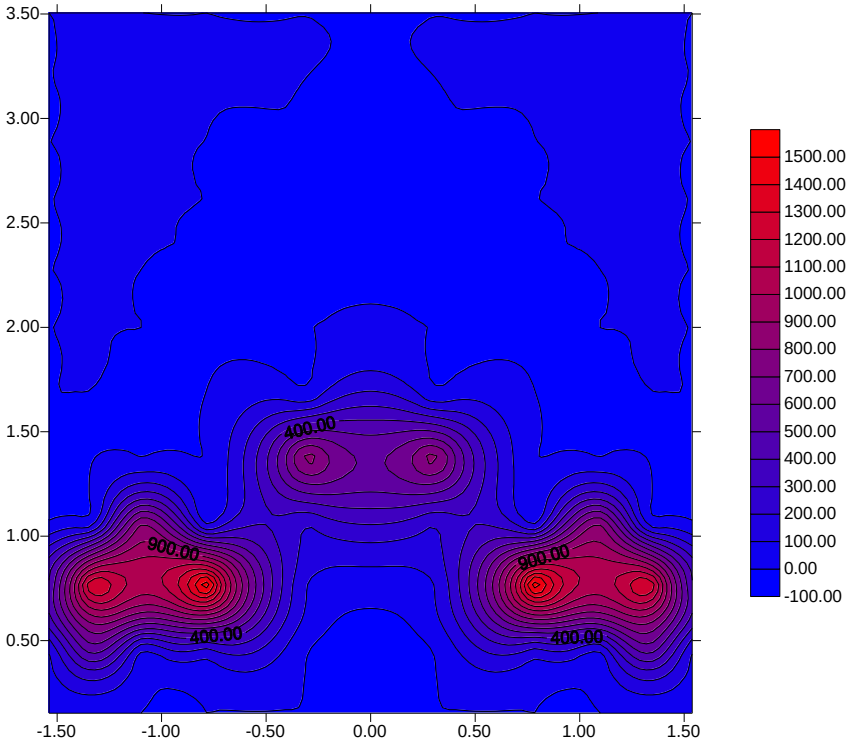

Fig. 42: Molten Zircalloy mass (t = 8200. s)

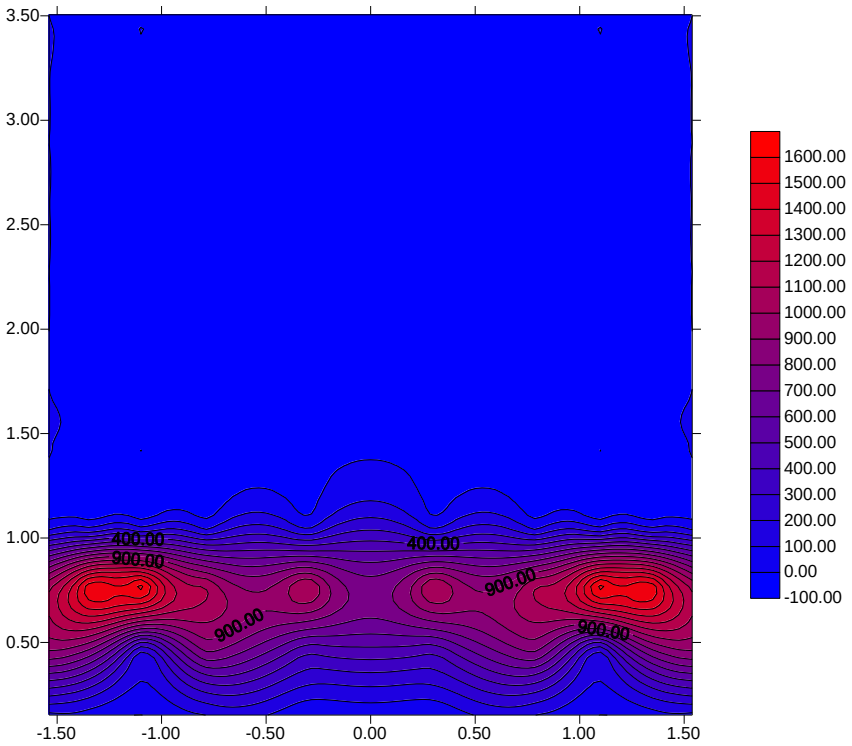

Fig. 43: Molten Zircalloy mass (t = 12000. s)

18. APPENDIX : IVS CALCULATION WITH ASTEC V1.3

18.1 TMI-2 Plant Modelling

The two previously described ASTEC modules were used in the coupled mode. The front-end thermal-hydraulic part of the transient was performed by CESAR module and the DIVA module was activated later, when the core heat-up takes place. The TMI-2 plant nodalization scheme is shortly described below.

18.1.1 Reactor vessel:

- PRIMARY data (core, bypass, lower plenum and downcomer) automatically created from VESSEL_D data by ASTEC;
- VENT valve was modelled between the reactor downcomer and upper plenum;
- Double junctions to reactor vessel upper head with slightly different elevations were used in order to prevent the flow stagnation in this volume;
- All junctions were of type 0 (standard two-phase flow junction);
- Volumes of type 0 (standard homogeneous volumes) were used preferably. Volumes of type 1 (volumes with swollen level) were used in upper part of the reactor vessel. Volumes of type –1 (axial elements) were used to model fuel assemblies;
- All characteristic features of vessel (e.g. vessel vent valves) modelled;
- Default value of tau_long parameter (time return to thermal equilibrium) for volumes of type 1 were used.

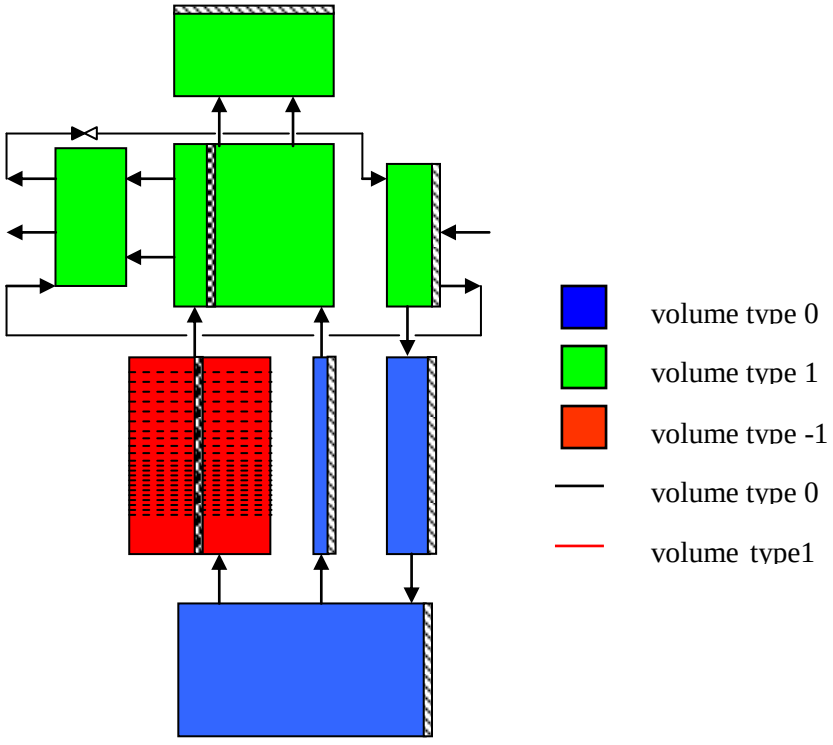

Fig. 1. Nodalization of reactor vessel

18.1.2 Circulation loops:

- Two identical loops were modelled (loop with pressurizer and break is shown);
- Two parallel cold legs were modelled in each loop;
- Volumes of type 0 (standard volumes) were used preferably. Volumes of type 1 (volumes with swollen level) were used only in pressurizer and SG cold collector, volumes of type –1 (axial elements) used only in SG tubes;
- Junctions of type 0 (standard two-phase flow junction) preferred, some junctions of type 1 used in order to enable proper phase separation;
- SG tubing was split into 2 parallel bundles (90% - inner channel and 10% - outer channel cooled by EFW spray) in accordance with nodalisation of secondary side;
- Reactor coolant pumps were modelled using shaft equation, respecting the pump inertia, friction, motor and hydraulic torque.

18.1.3 Pressurizer and surge line:

- Pressurizer was modelled using 3 volumes of type 1 (volumes with swollen level);
- RRZ surge line was modelled by 2 volumes of type 0 (standard volumes) connected by junction in their bottom part (loop seal shape).

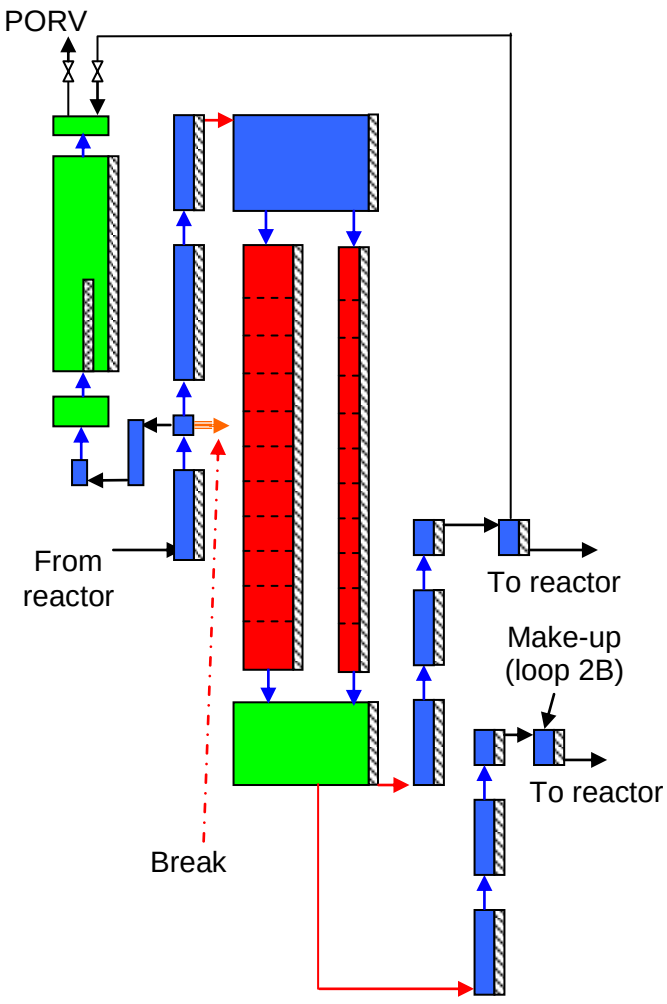

Fig. 2. Nodalization of loop with pressurizer

18.1.4 Steam generator – secondary side:

- Two identical SGs modelled;
- SG tubes bundle was split into 2 parallel nodes (90% - inner channel and 10% - outer channel);
- Volumes of type 0 (standard volumes) were used preferably. Volumes of type 1 (volumes with swollen level) were used only in parallel bundle channel (10% of SG tubes) for EFW injection;
- High value of tau_long parameter was used for volumes of type 1 (20000 s);
- All junctions are of type 0;
- EFW injected into upper part of outer channel.

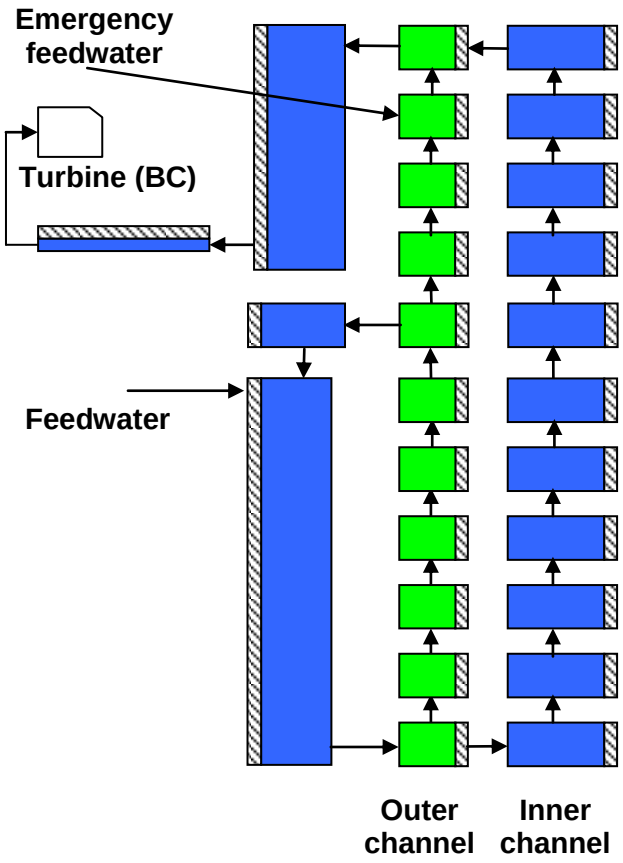

Fig. 3. Nodalization of SG secondary side

18.1.5 Core, lower plenum and downcomer model:

- Meshing: 6 parallel channels (core rings) + bypass, downcomer and lower plenum;
- Fuel assemblies split into 24 axial meshes;
- Core is assumed only as a region containing fuel;
- The following solid macro components were defined:
- Fuel and cladding;
- Control rods and gain tubes;
- Core baffle and shield;
- Reactor vessel with thermal insulation;

- Lower plenum;
- Model of the molten pool formation used (=> macro components DEBRIS and MAGMA were defined).

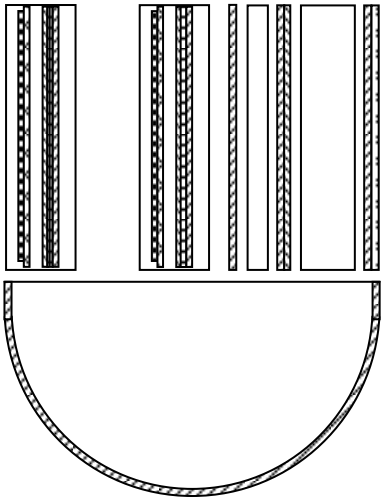

Fig. 4. Nodalisation of reactor core, lower plenum and downcomer

18.2 Initial Steady-State Conditions

The initial "steady-state" conditions were obtained running the calculation (with $t < 0$) on nominal TMI-2 plant conditions using the simplified form of most important plant controllers. This includes simple FW controllers, cycling of PRZ heaters and turbine modelled as pressure boundary condition. The obtained stabilised parameters and their comparison with nominal TMI-2 values at the start of transient ($t = 0$) is given in the table below.

TABLE I: Comparison of ASTEC steady-state conditions with TMI-2 data

Parameter	Unit	ASTEC V1.3	TMI-2
Reactor Power	W	2700	2700
Primary Pressure	MPa	15.32	15.2
Temperature Hot Leg A	K	592.9	592
Temperature Hot Leg B	K	592.9	592
Temperature Cold Leg A	K	565.1	548-561
Temperature Cold Leg B	K	565.1	565
Mass Flow Rate – Loop A	kg/s	8501	8280
Mass Flow Rate – Loop B	kg/s	8498	8560
Pressurizer Level	M	5.69	5.77
Total Primary Mass	ton	221515	-
Pressure SG A	MPa	6.247*	7.31
Pressure SG B	MPa	6.246*	7.24
Steam Temperature SG A	K	578.8	586

Steam Temperature SG B	K	578.0	586
Collapsed Level SG A	M	3.81	-
Collapsed Level SG B	M	3.65	-
Liquid Mass SG A	Kg	15303	-
Liquid Mass SG B	Kg	14409	-
Feedwater Flow SG A	Kg/s	746.5	723
Feedwater Flow SG B	Kg/s	737.2	717
SG Feedwater Temperature	K	513	-

* according to benchmark scenario, pressure boundary condition 6.2 MPa was used on the secondary side .

18.3 Physical Parameters Used in the Analysis

Main core degradation physical parameters used in the base case calculation with ASTEC are given in the table below. Only the base case calculation with Urbanic-Heidric Zr oxidation kinetic model was performed for final benchmark scenario. The sensitivity analysis with FZK correlation for oxidation kinetics was performed only in previous stage of benchmark exercise.

TABLE II: Main physical parameters used in the base case and sensitivity analysis

Parameter	ASTEC V1.3 Rev. 0
Zr Oxidation correlation	Urbanic-Heidric
Cladding failure criteria [1]	T > 2260K and e(ZrO2) < 160 μm T > 2280K and e(ZrO2) < 200 μm T > 2340K and e(ZrO2) < 220 μm T > 2380K and e(ZrO2) < 240 μm T > 2450K and e(ZrO2) < 300 μm
UO2-ZrO2 melting temperature	default values from material database of the code
Debris formation criteria	code default criteria, DEBRIS macro component and reflooding model in ASTEC are still under development
Debris diameter	5 % of 2 mm diameter 15 % of 4 mm diameter 60 % of 6 mm diameter 15 % of 8 mm diameter 5 % of 10 mm diameter
Debris porosity [2]	0.7 / 0.6

Remarks:

1. This is not cladding failure criterion (cladding failure is function of temperature, internal pressure, ...) but criteria for change of the status from COMPACT to DISLOCAT (i.e. relocation).
2. The first value is porosity used for collapsing of free debris, the second parameter is porosity for collapsing of debris bed.

18.4 The results of the analysis

The chronology of major events calculated by ASTEC is presented in the Table III below and illustrated on the attached figures.

After reactor scram the primary pressure starts to decrease. The primary pressure first reached saturation pressure and later further decreases and approaches to the secondary pressure. The core is cooled via two-phase forced circulation in primary system. The core decay power and RCPs heat are removed by the steam generators. The total heat removed by both SGs is clearly higher than the decay heat. The mass-flow-rate through the loops is monotonously decreasing due to increased void fraction in primary coolant.

The void primary coolant mass drops below 85 t at t = 4789 s. At this time all RCPs were tripped. Since this time, phase separation occurs in primary system and the core decay heat is removed in natural circulation boiler-condenser mode through loops A and B (in loop A the steam is also escaping through the break into containment). However, the total heat transfer from primary to secondary side is about 50% of the decay heat and later decreases due to decrease of primary pressure and even heat flux reversal occurs in both SGs when the primary pressure drops below the secondary pressure.

TABLE III: Chronology of main events during the accident

Event	Time [s]
Break opening and loss of feedwater	0
SG B level drops below 1 m	12.6
PRZ spray valve opening	13.5
SG A level drops below 1 m	14.0
PRZ PORV opening	15.2
Reactor scram	19.4
PRZ spray valve closing	23.3
PRZ PORV closing	23.3
SGs are nearly dry (water mass in SG B/ SG A < 100 kg)	26.6/29.9
Pressurizer is nearly empty (water level < 0.5 m)	150
Primary coolant mass (water + steam) < 85 t => all RCPs are tripped	4314
Onset of core heatup	5149
Max. cladding temperature > 550°C (DIVA start)	5759
First fuel rod clad burst	6306
First debris and magma in the core	6402
Melting pool formation in the core	7925
Start of HP injection	9789
End of calculation (code crash in DIVA module)	10478

The break opening and FW trip was considered as initiating event at time t = 0. The loss of FW results in rapid decrease of secondary side SG water level followed by increase of primary pressure (neither the break flow nor PRZ spray and PORV opening were sufficient to prevent further primary pressure increase). The pressure rise activated reactor scram (P > 16.34 MPa) at t = 19.4 s.

The initial coolant leak through the break exceeds 90 kg/s. After the reactor scram dropped below 40 kg/s and later further slowly decreases below 30 kg/s. Up to the RCPs trip the leak is prevailingly in the water phase. After the RCPs are tripped, phase separation occurs in primary system, practically pure steam is escaping from primary system and mass-flow-rate drops below 10 kg/s and further decreases in the later course of the accident. Shortly after RCP trip the leaking steam is saturated. Later, when the core heatup takes place, the steam is overheated.

When the maximum core temperature exceeds 550 °C at t = 5759 s, the DIVA module of ASTEC was activated to compute in-vessel core degradation and melt relocation. Since this time the oxidation of the claddings is calculated by DIVA module. First fuel rod clad burst due to overpressure is calculated by ASTEC at 6306 s. Since the t ~ 6500 s an intensive oxidation take place and the maximum chemical power for certain period even exceeded the decay heat. Since t ~ 7500 s the oxidation rate slows down significantly and the chemical power is only fraction of decay heat.

At t = 9789 high-pressure injection into horizontal part of all cold legs starts. The primary pressure, leak flow-rate and heat transfer from primary to secondary side increase due to core quenching and intensive steam production here. However, this injection was followed only with minor hydrogen production. Since this time primary coolant inventory and core water level start to rise. At t = 10478 s the calculation was terminated due to error in DIVA module. The total mass of hydrogen produced till the end of calculation is 383.5 kg.

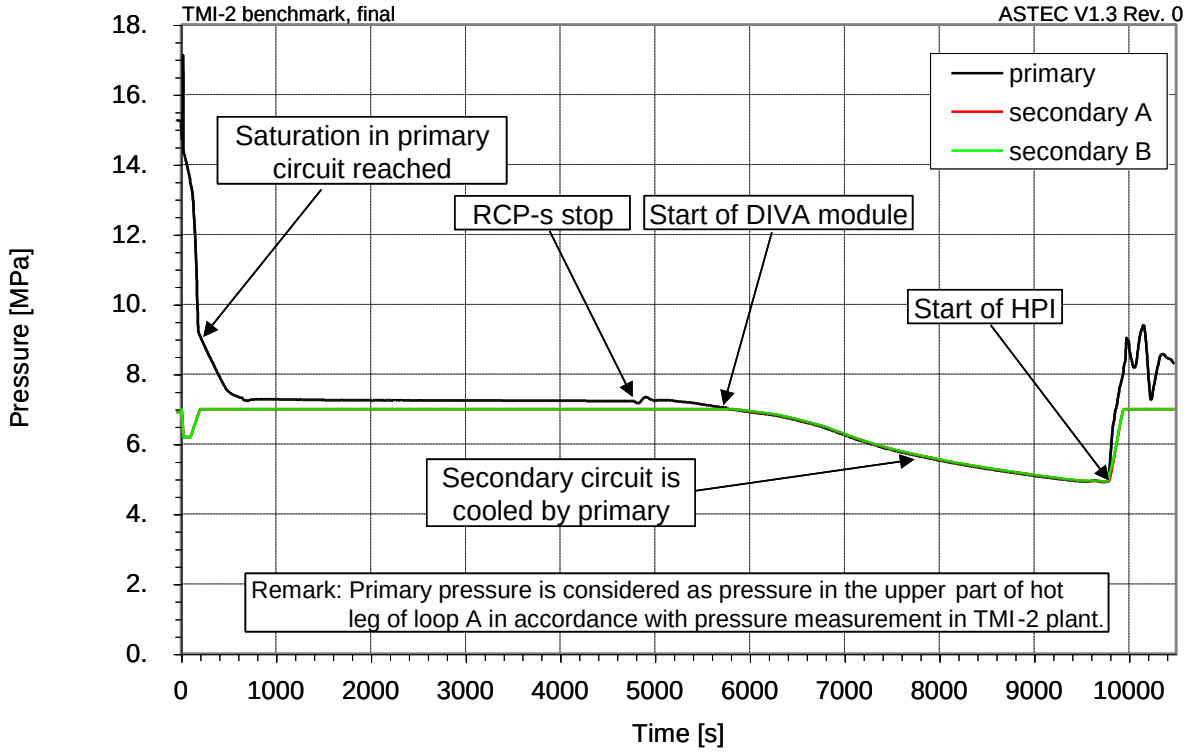

Fig 5. Pressures.

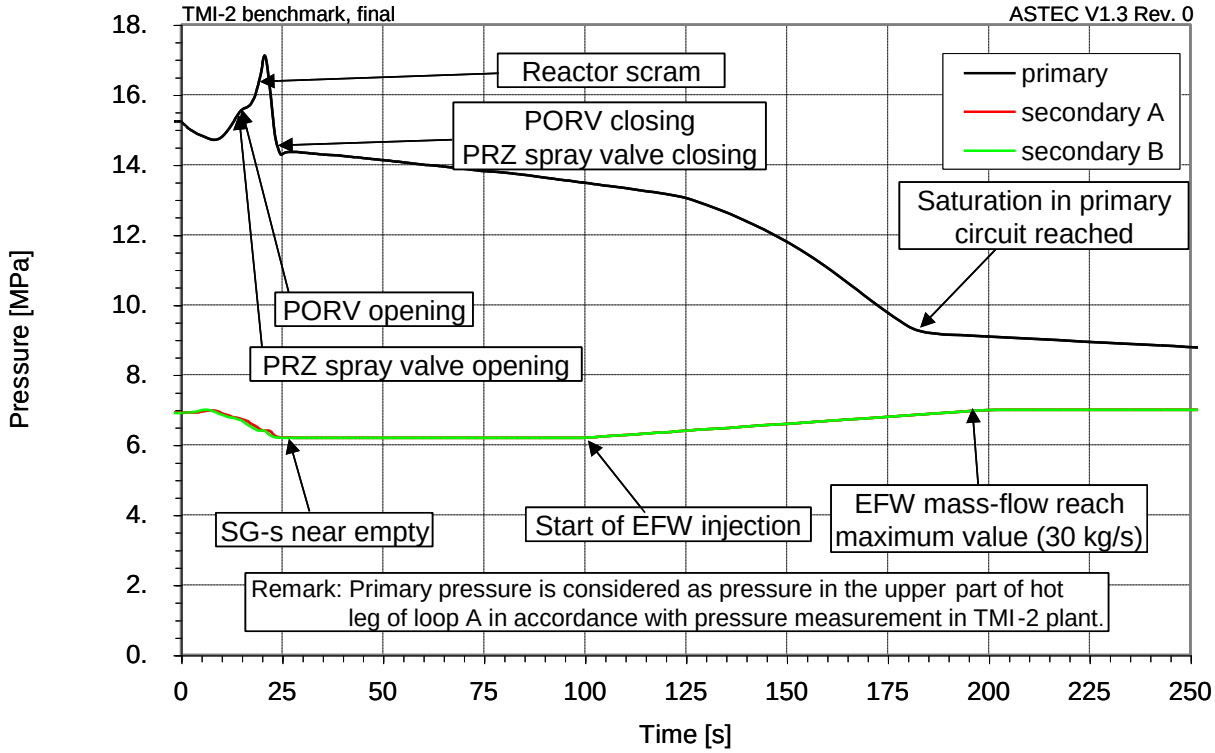

Fig 6. Pressures (fine scale).

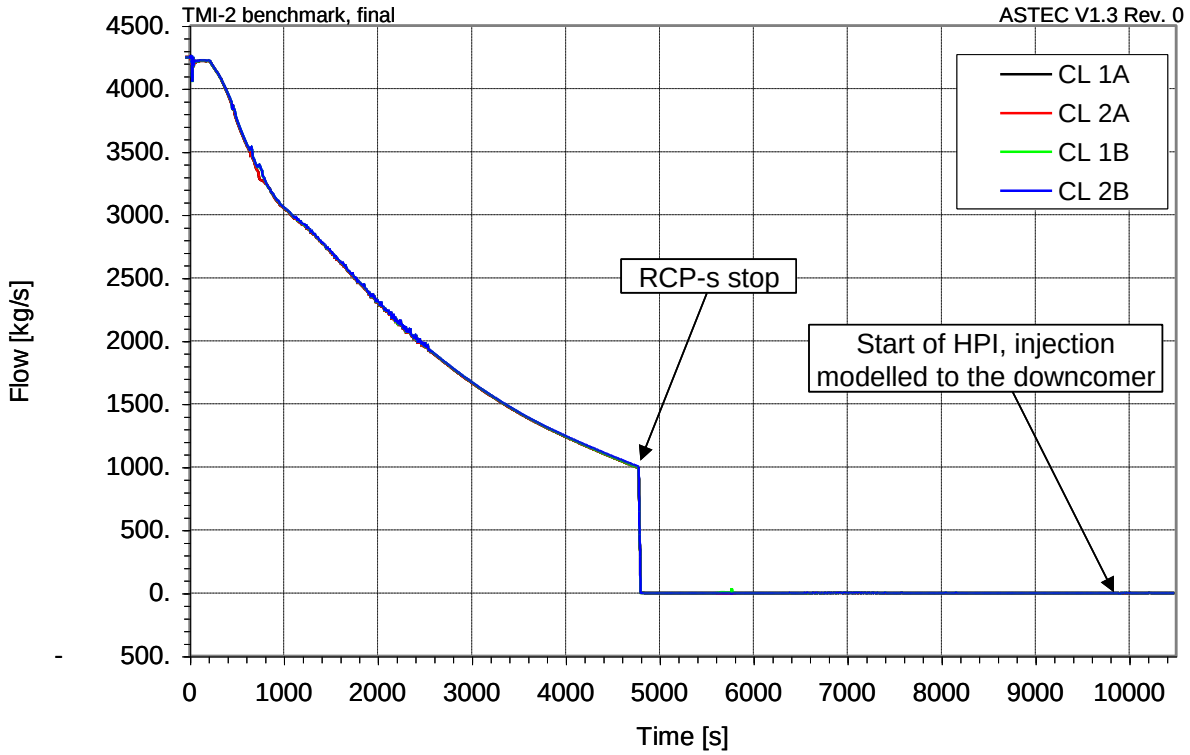

Fig 7. Cold leg mass-flows.

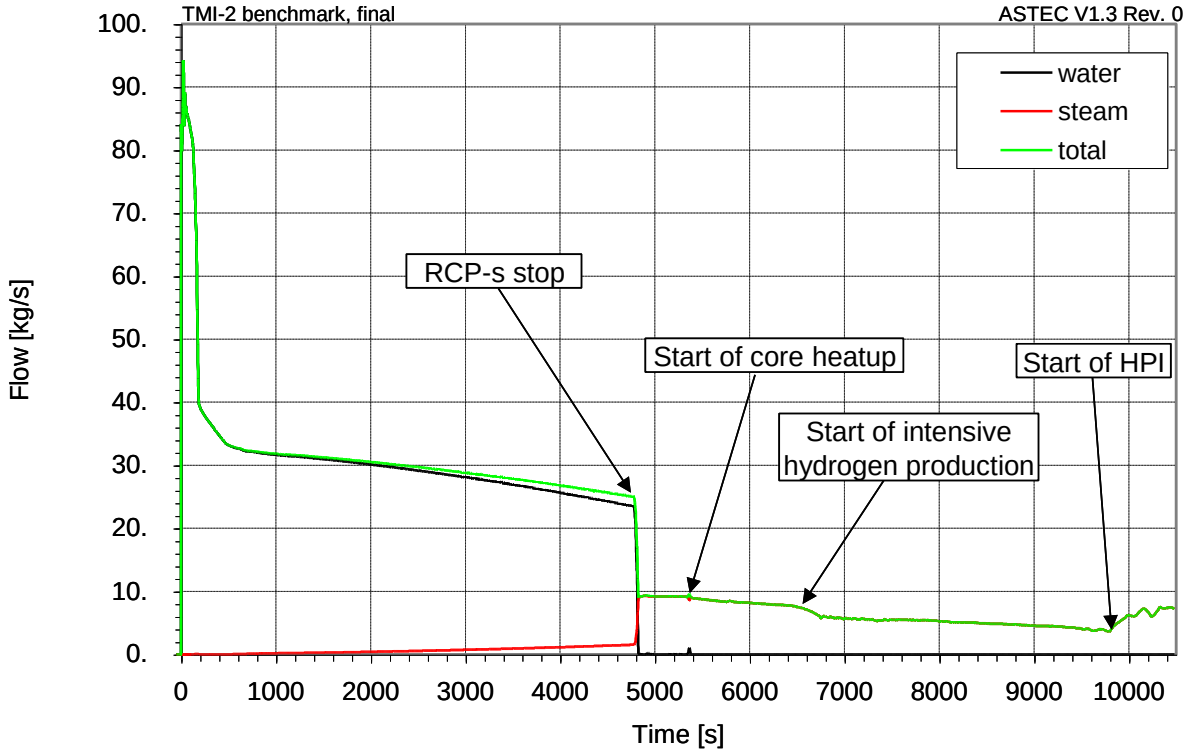

Fig 8. Break mass-flow.

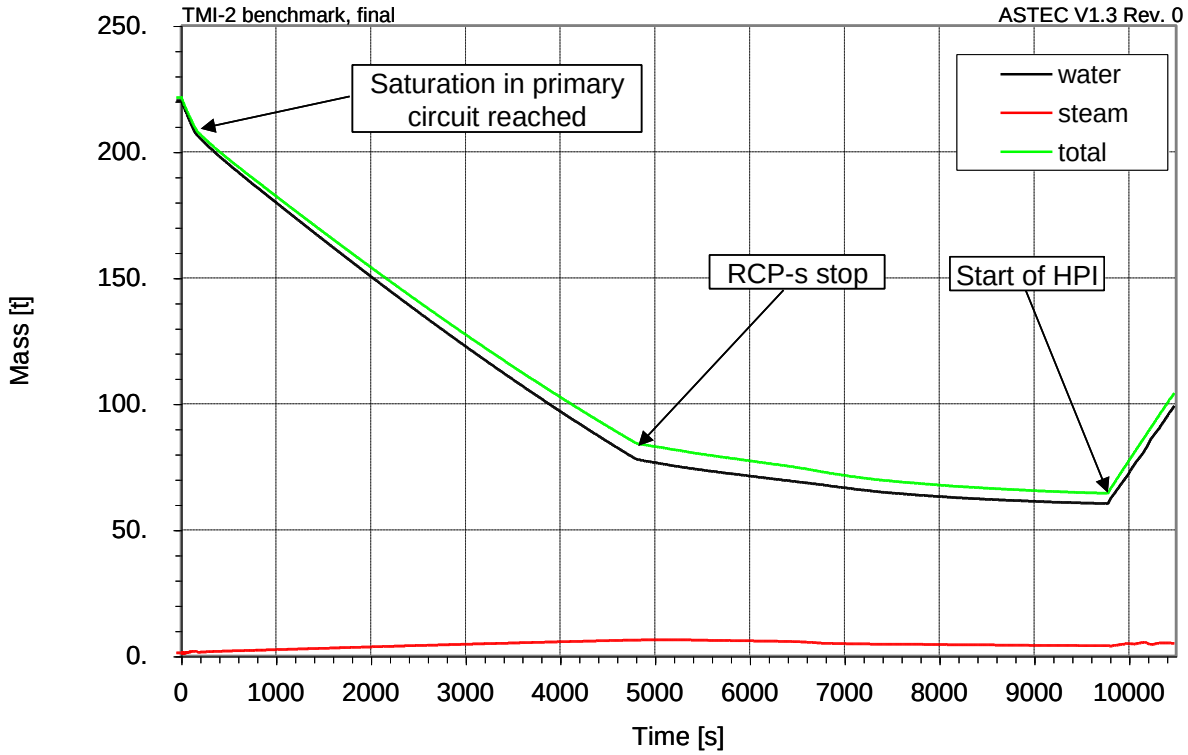

Fig 9. Primary masses.

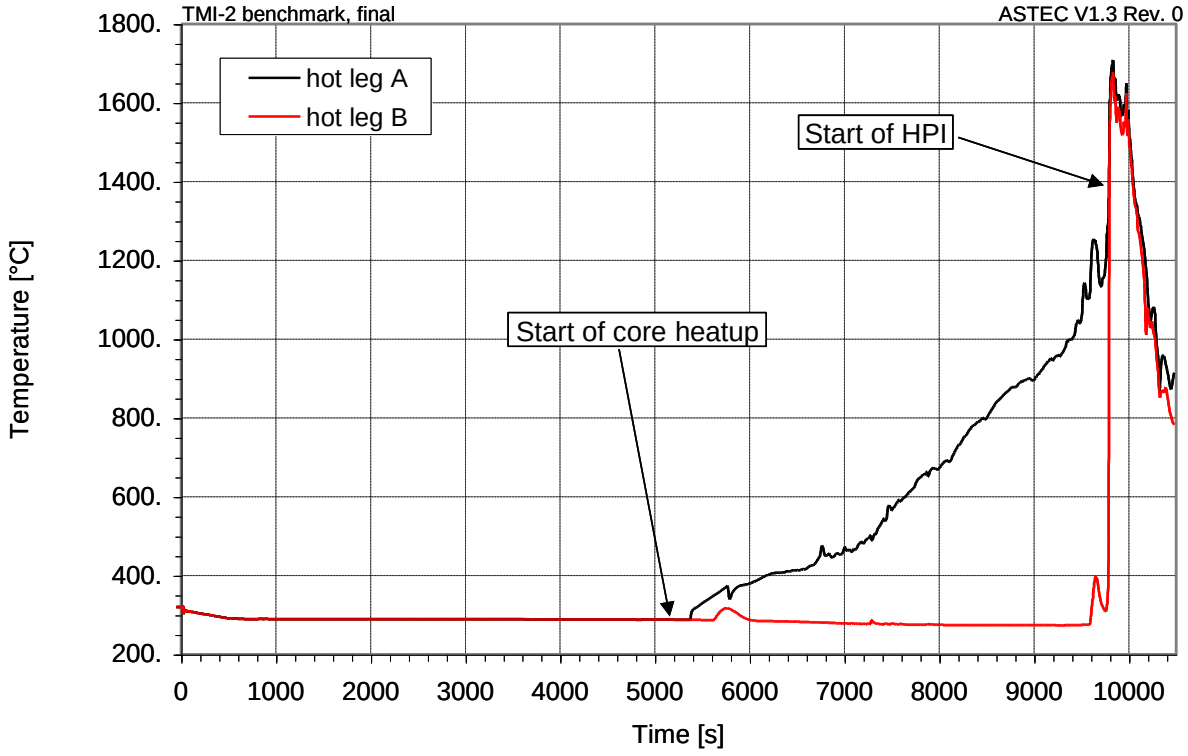

Fig 10. Reactor outlet temperatures.

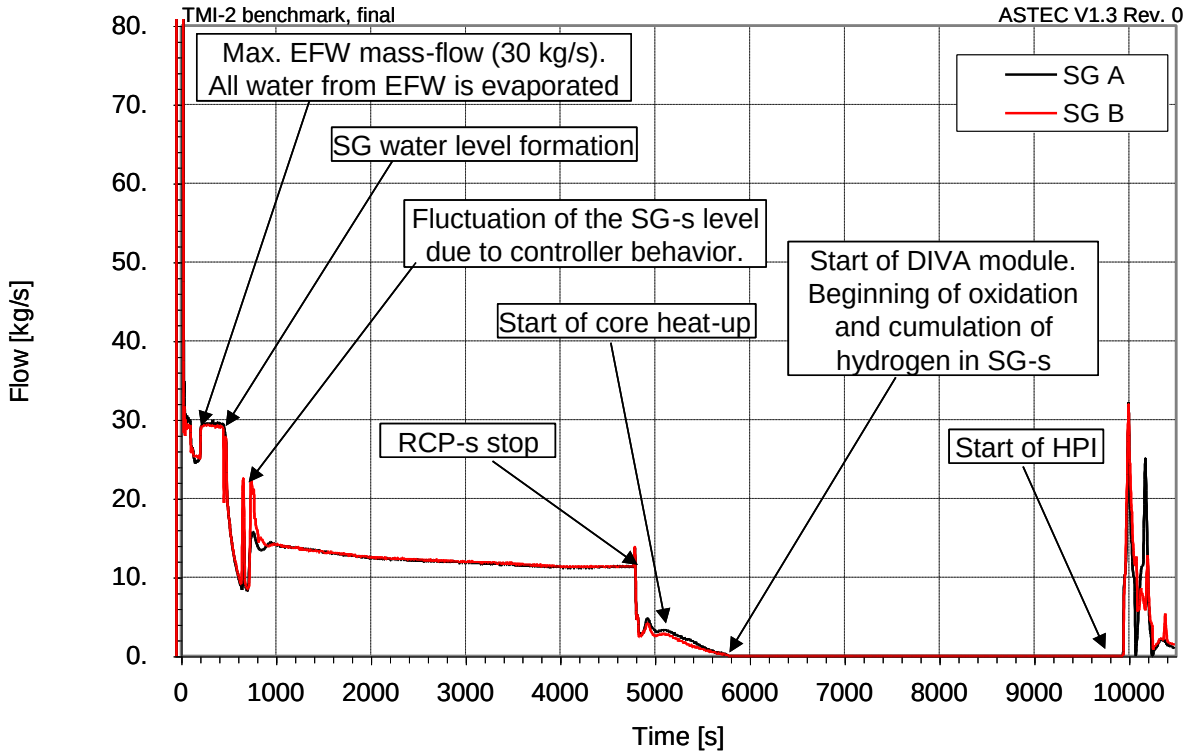

Fig 11. SG-s outlet.

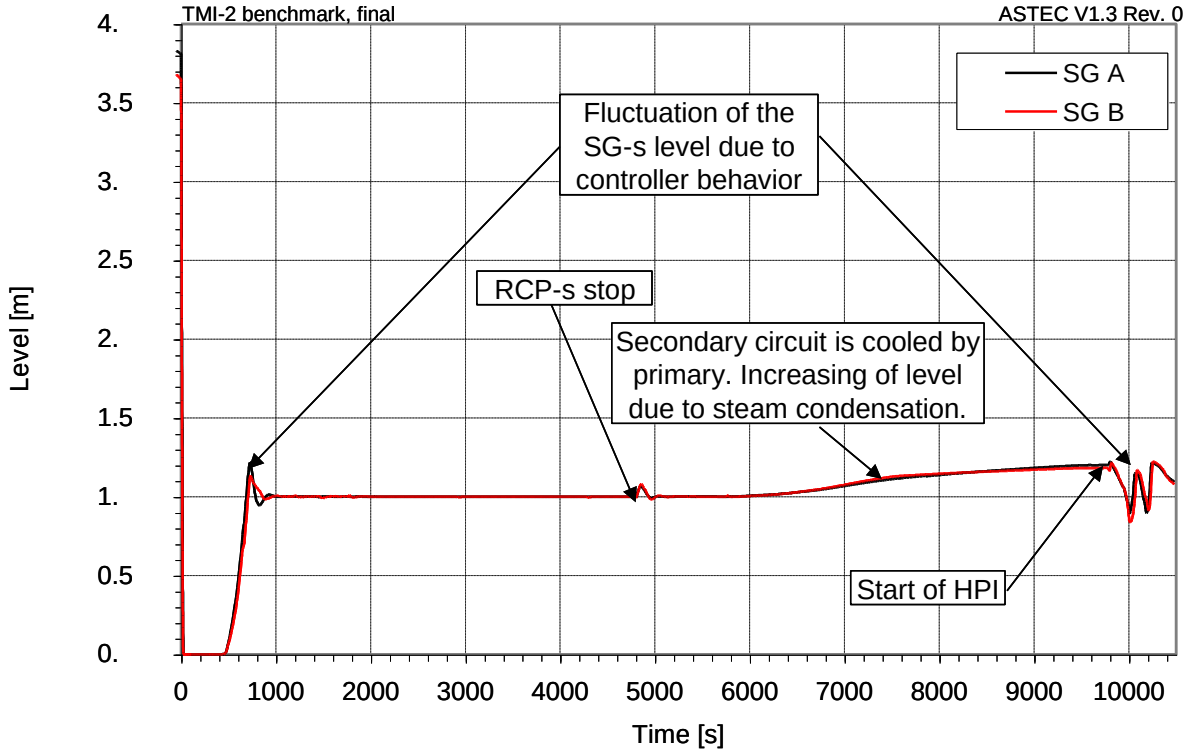

Fig 12. SG-s levels.

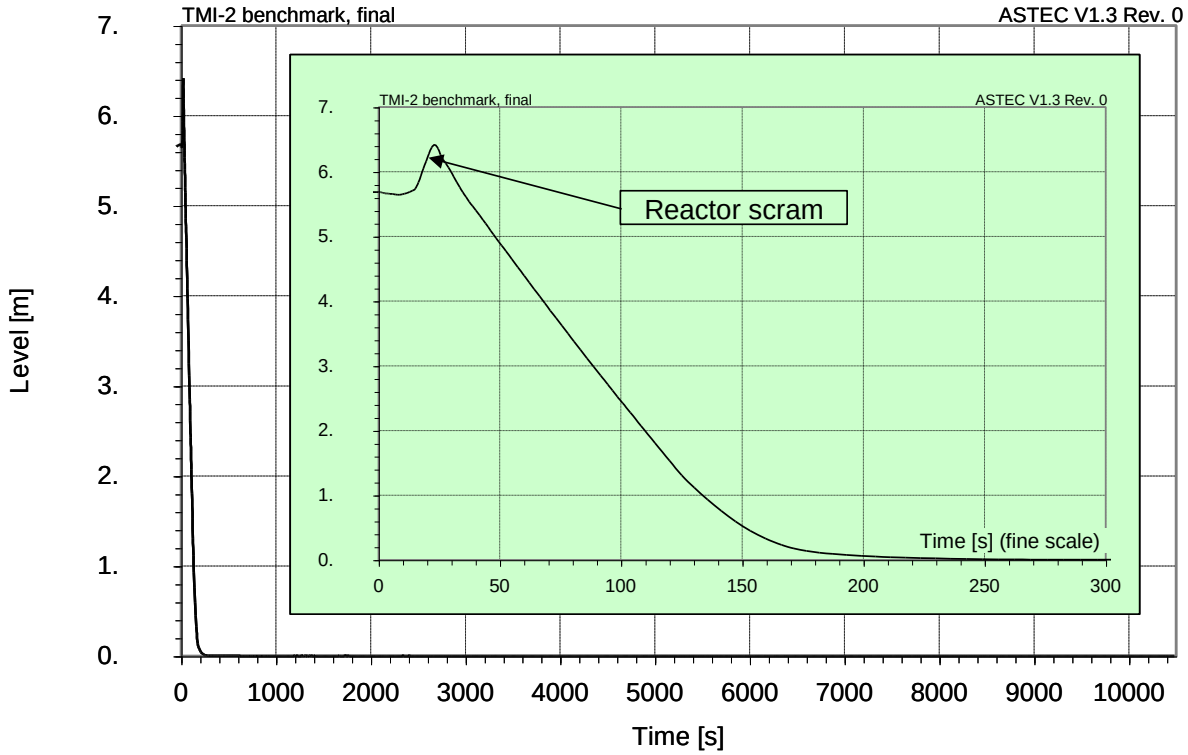

Fig 13. Pressurizer level.

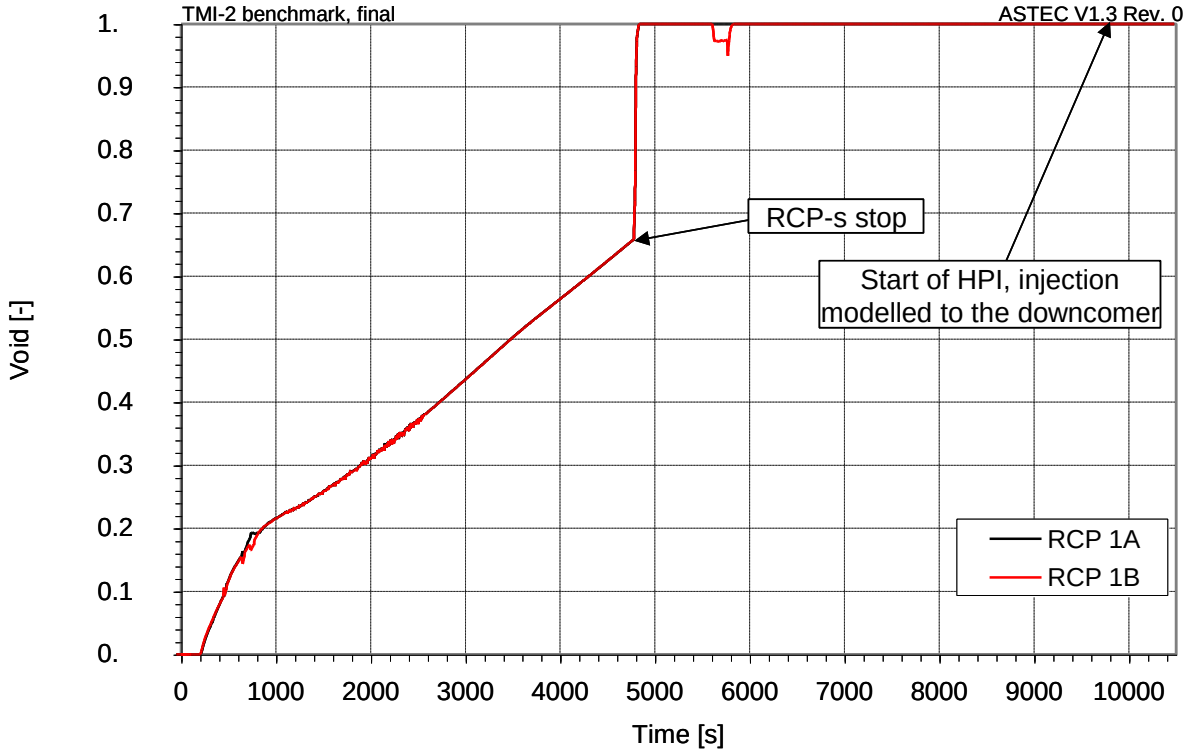

Fig 14. RCP void fractions.

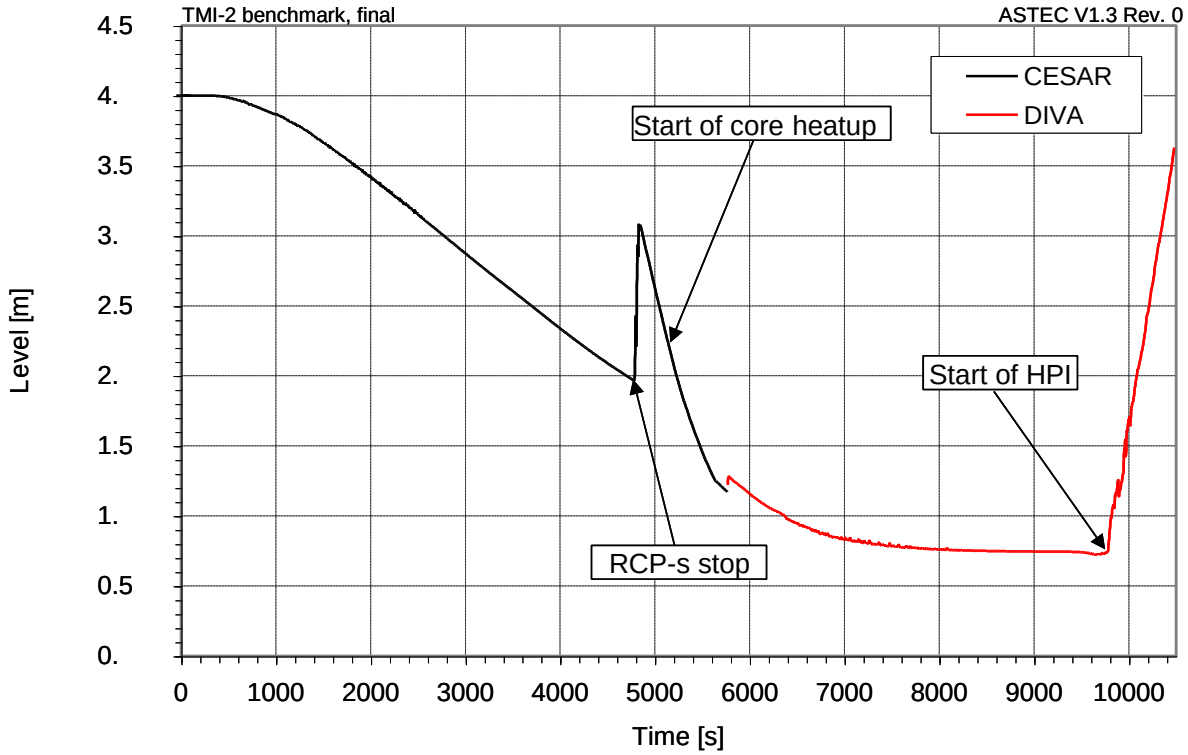

Fig 15. Core collapsed level.

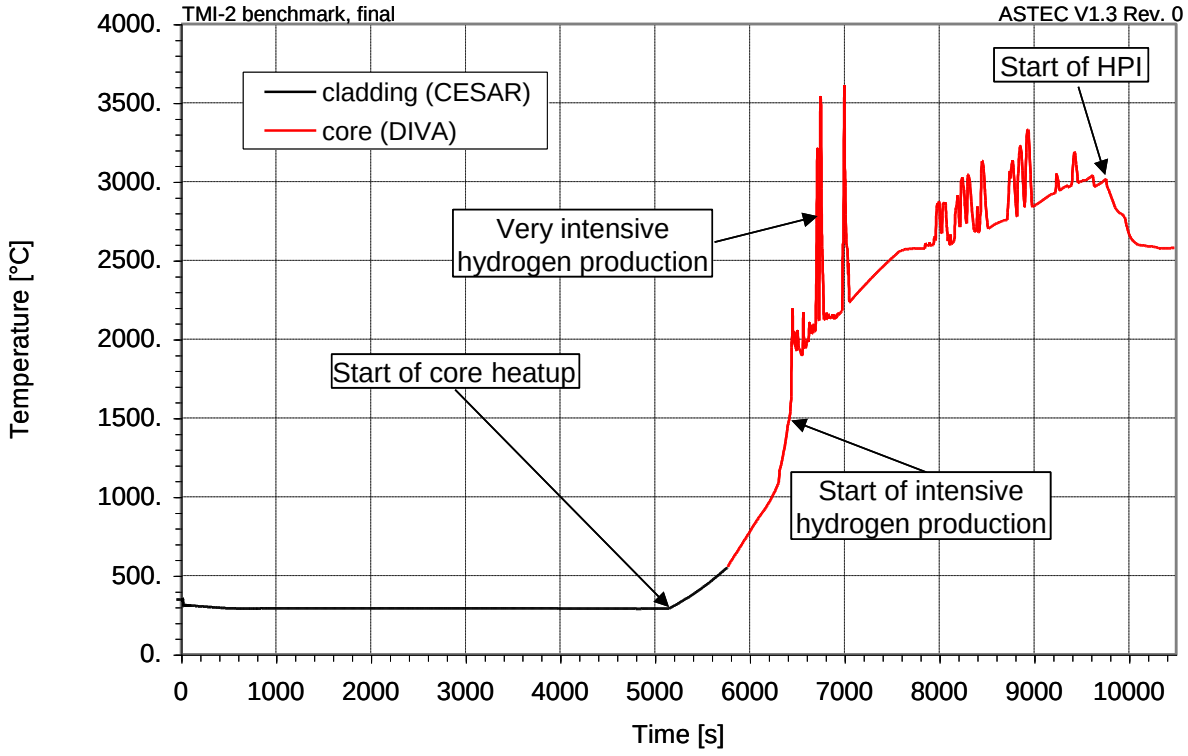

Fig 16. Maximum temperatures.

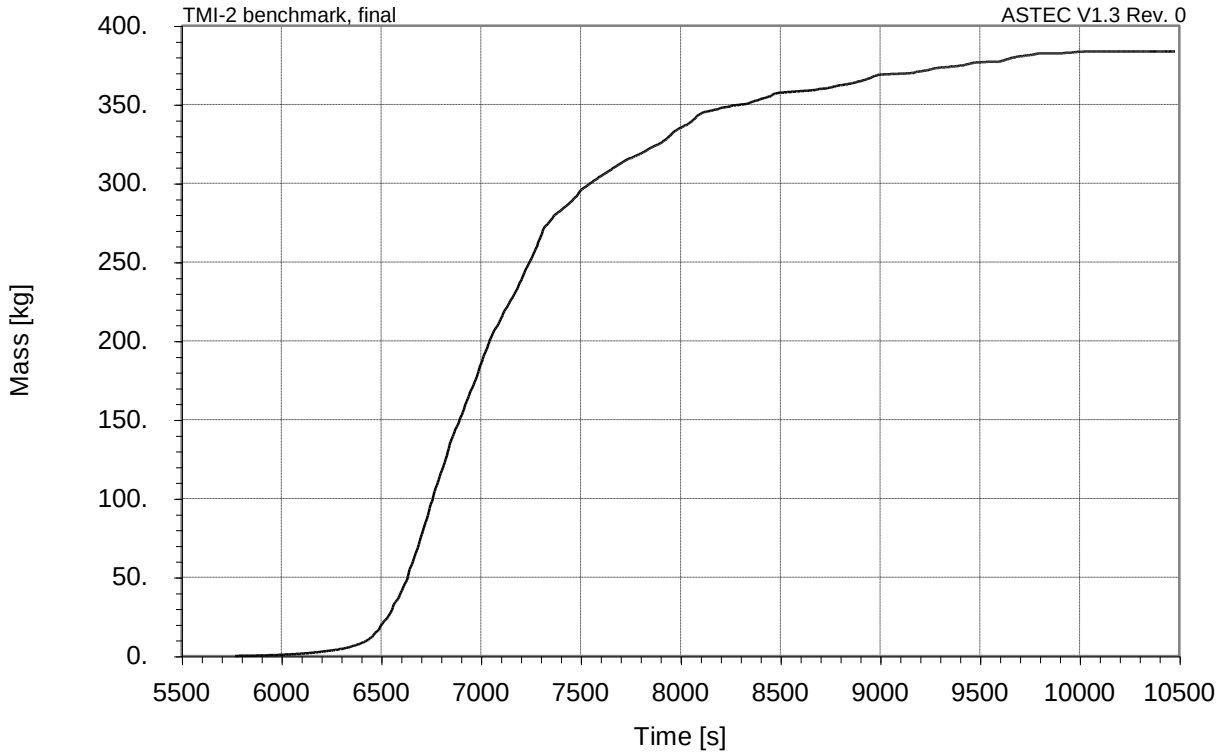

Fig 17. Hydrogen production.

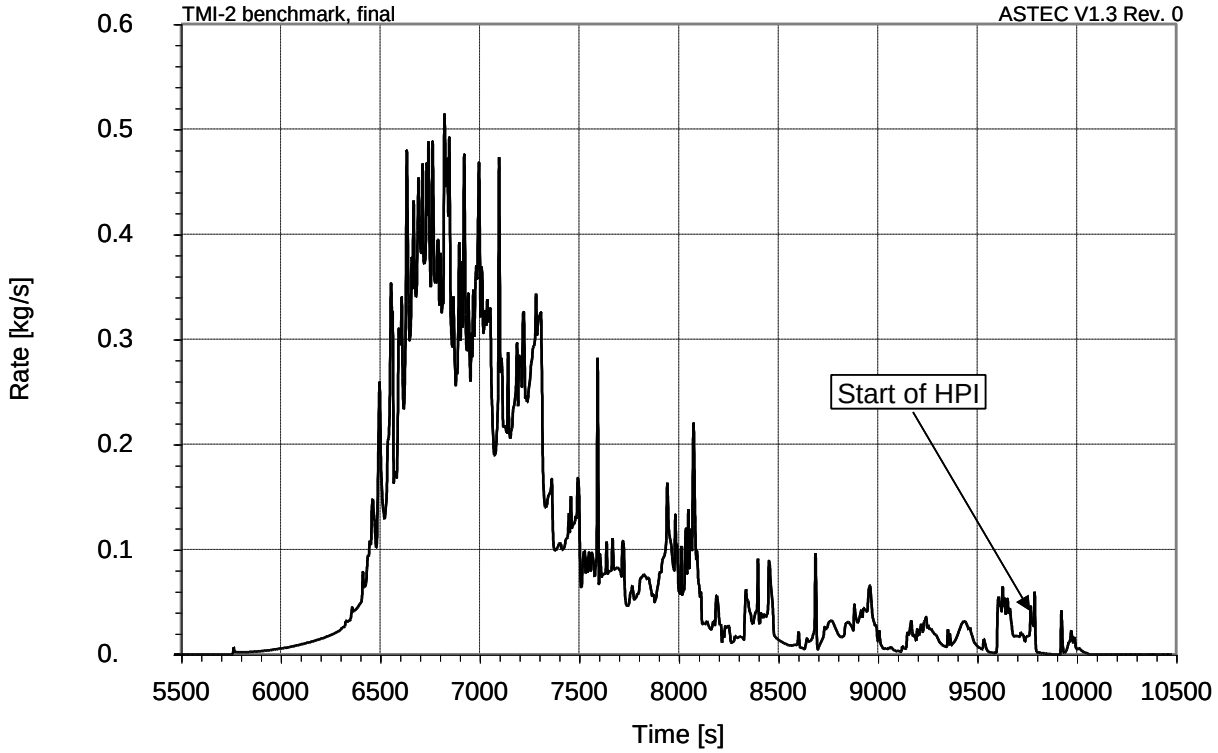

Fig 18. Hydrogen production rate.

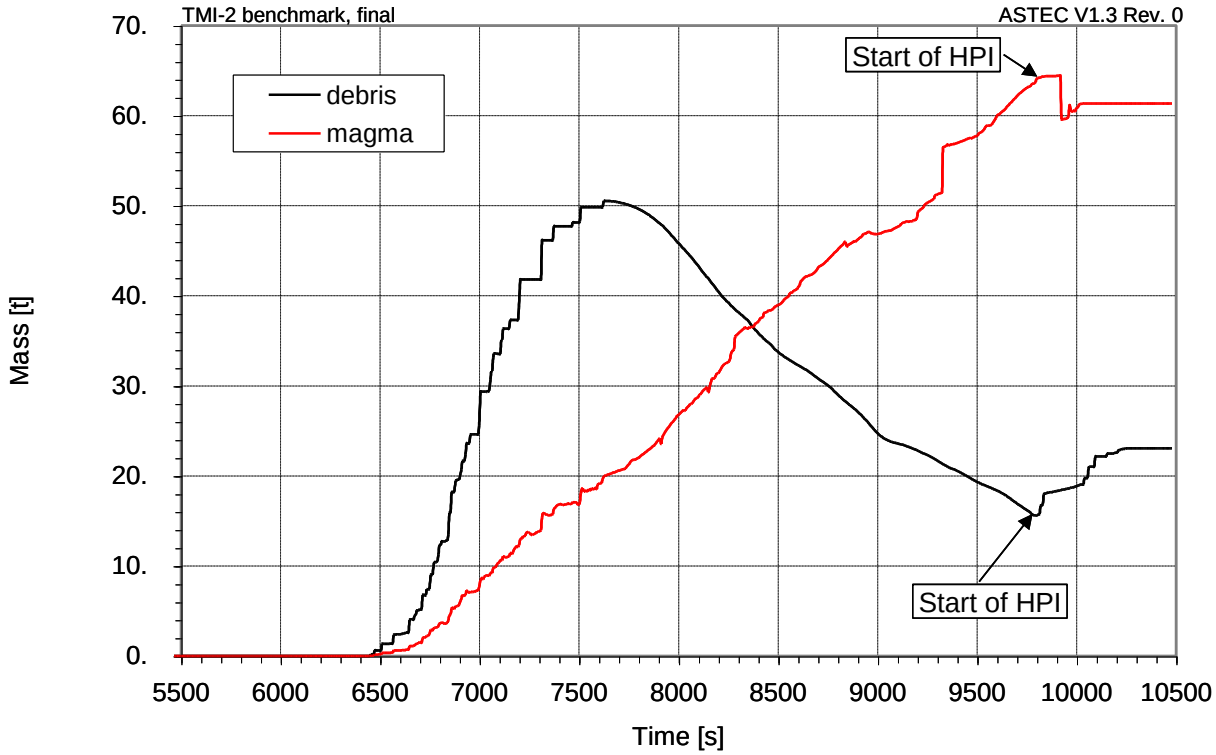

Fig 19. Masses in the core.

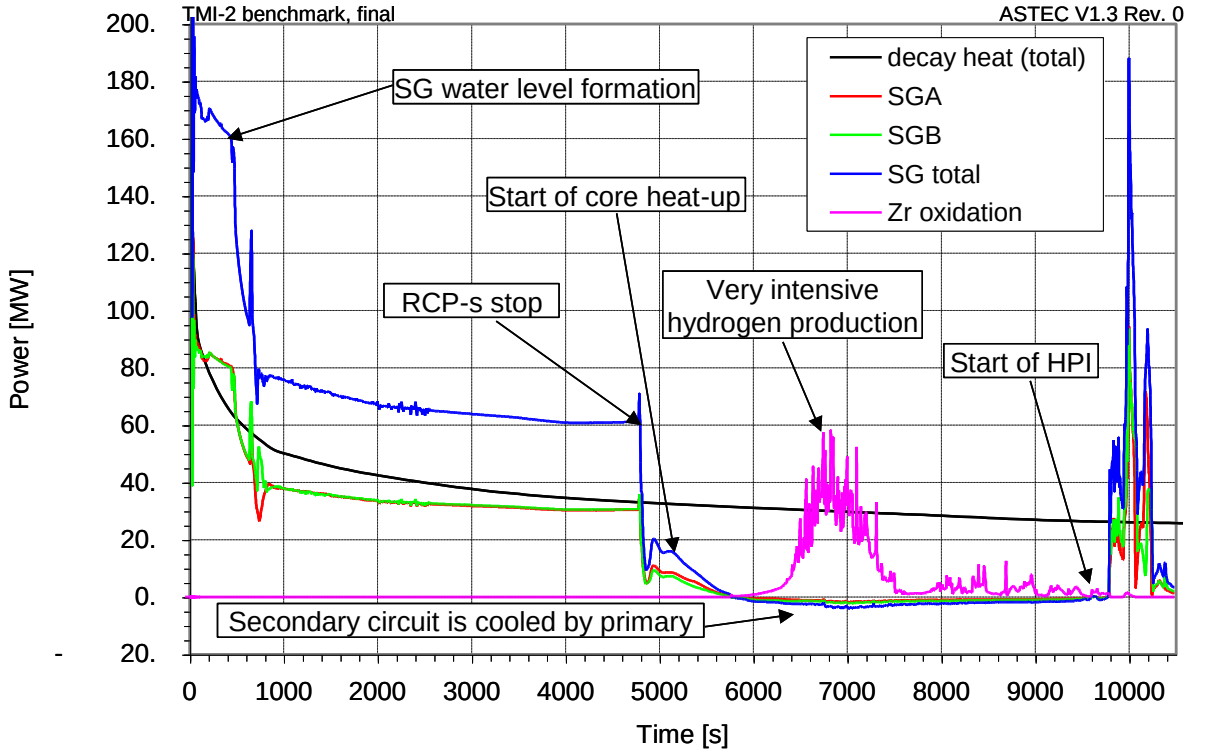

Fig 20. Powers.

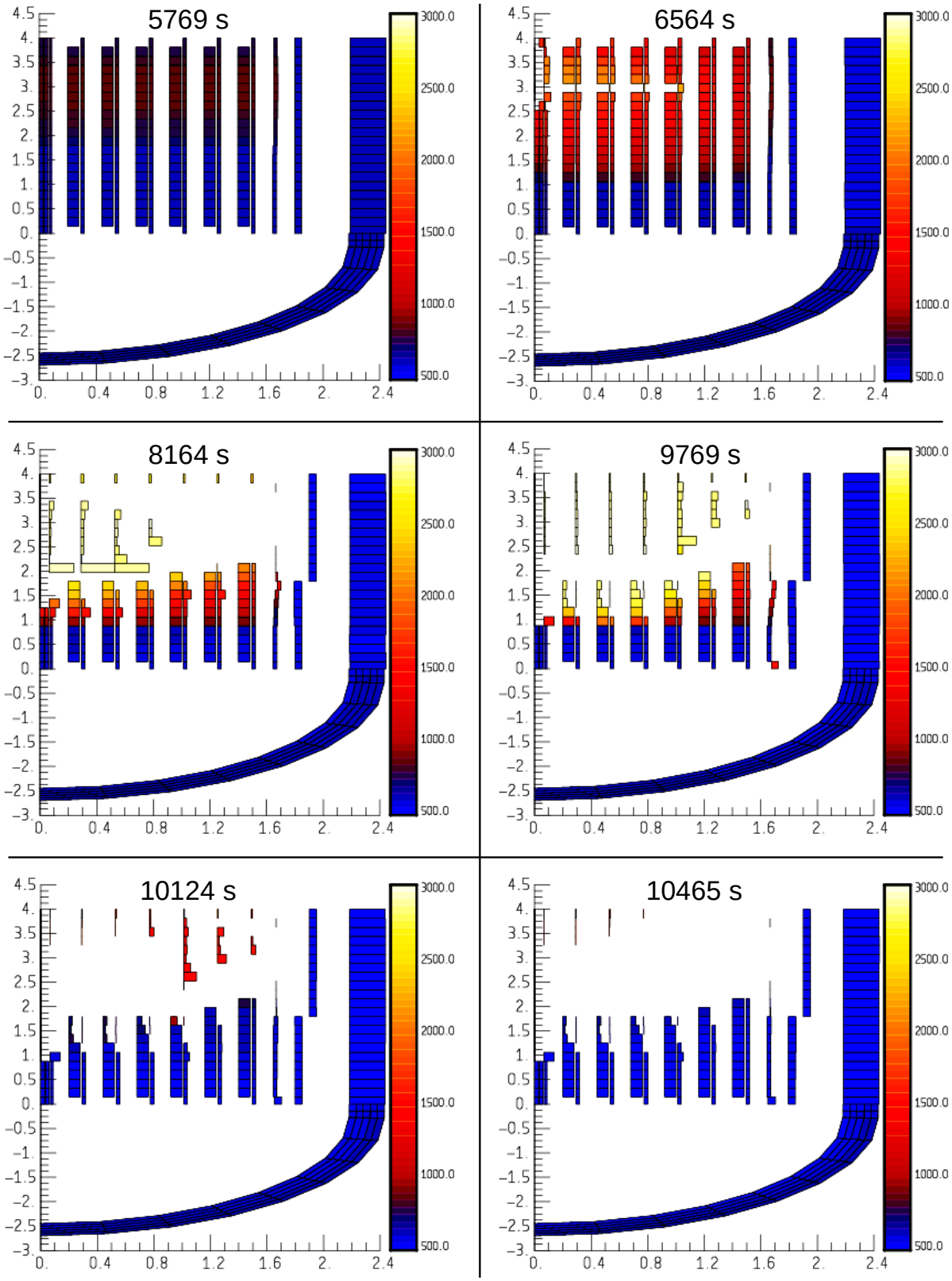

Fig. 21. Core temperature field [K].

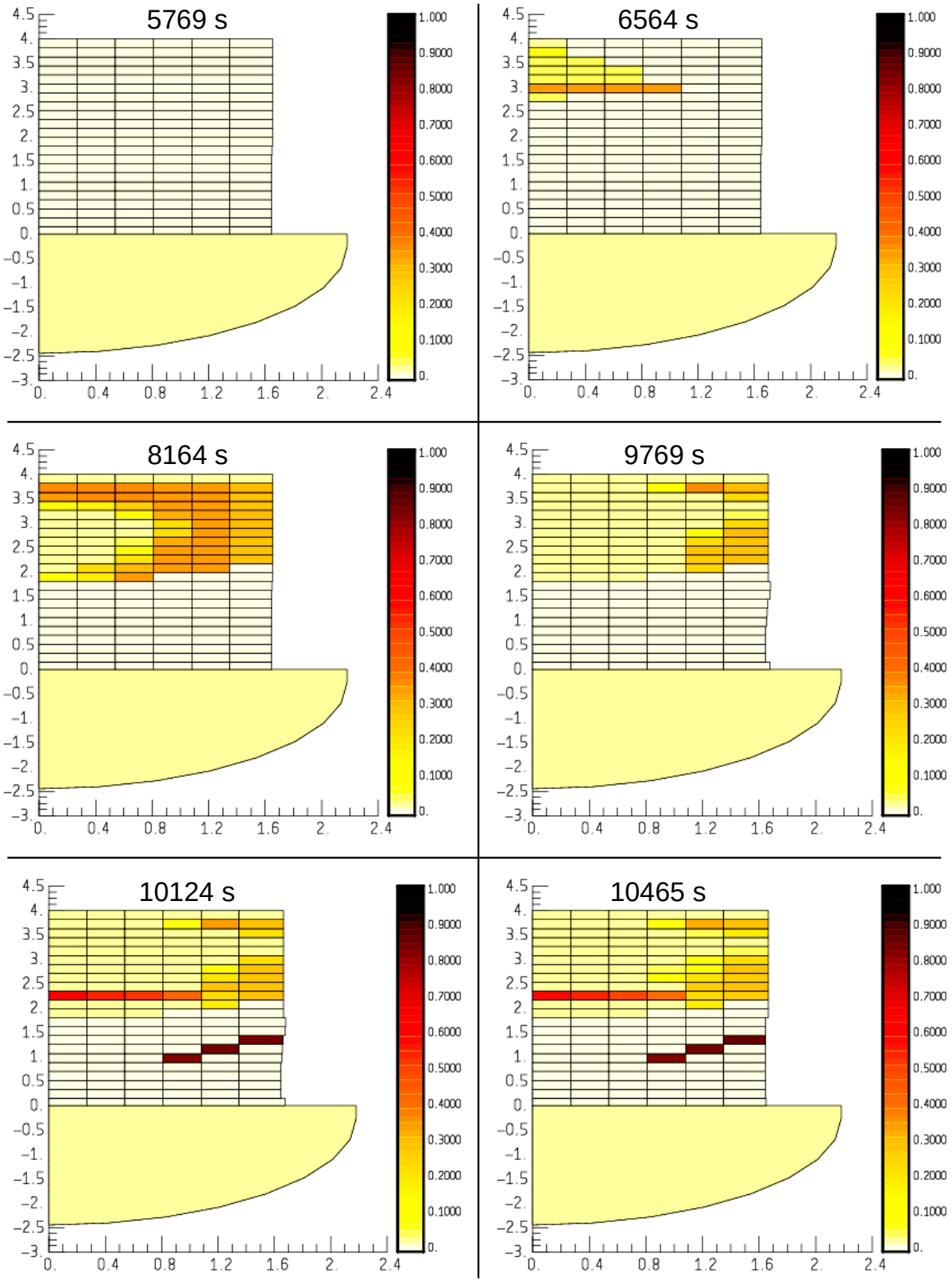

Fig. 22. Debris saturation in the core [-].

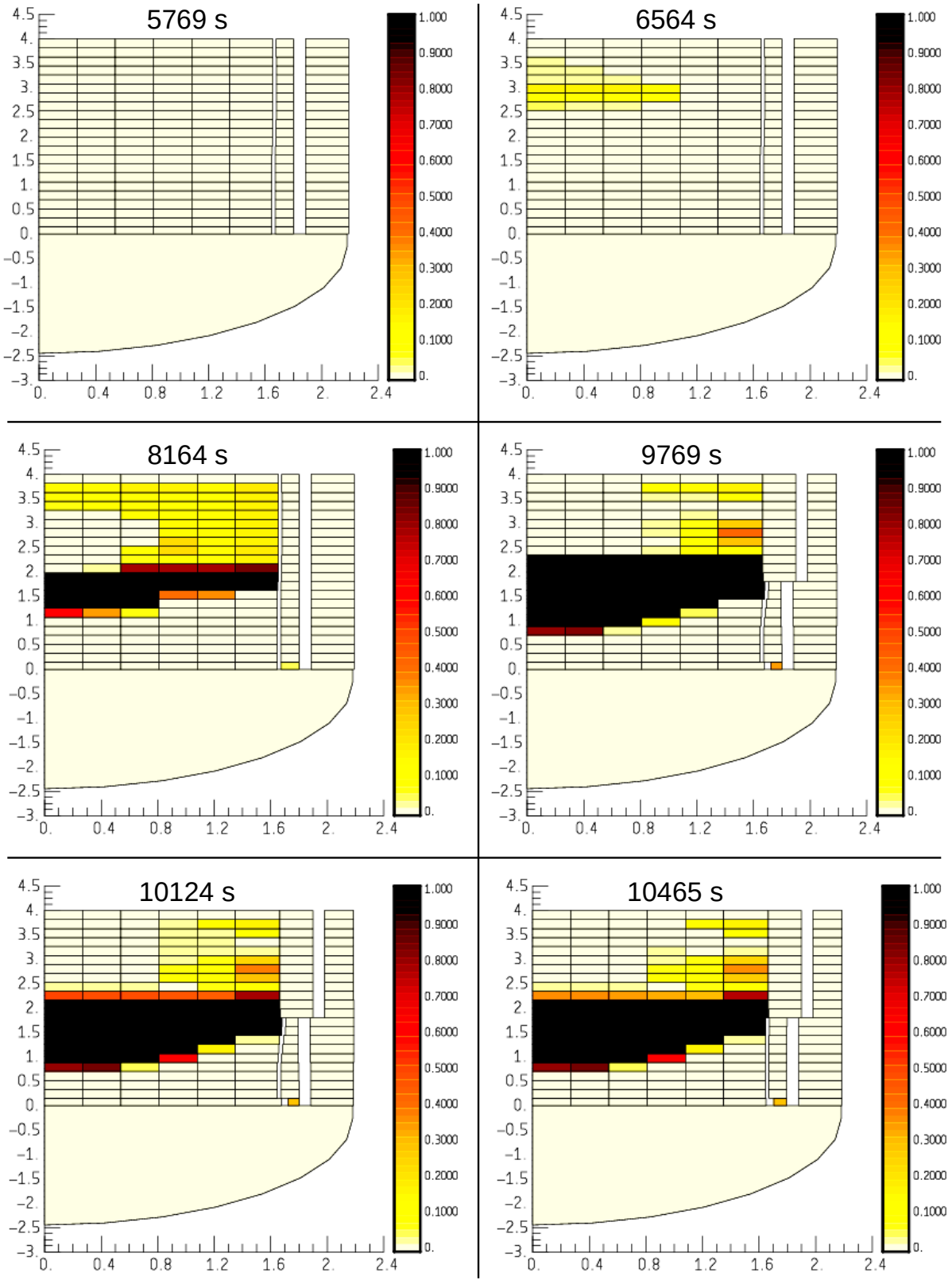

Fig. 23. Magma saturation in the core [-].

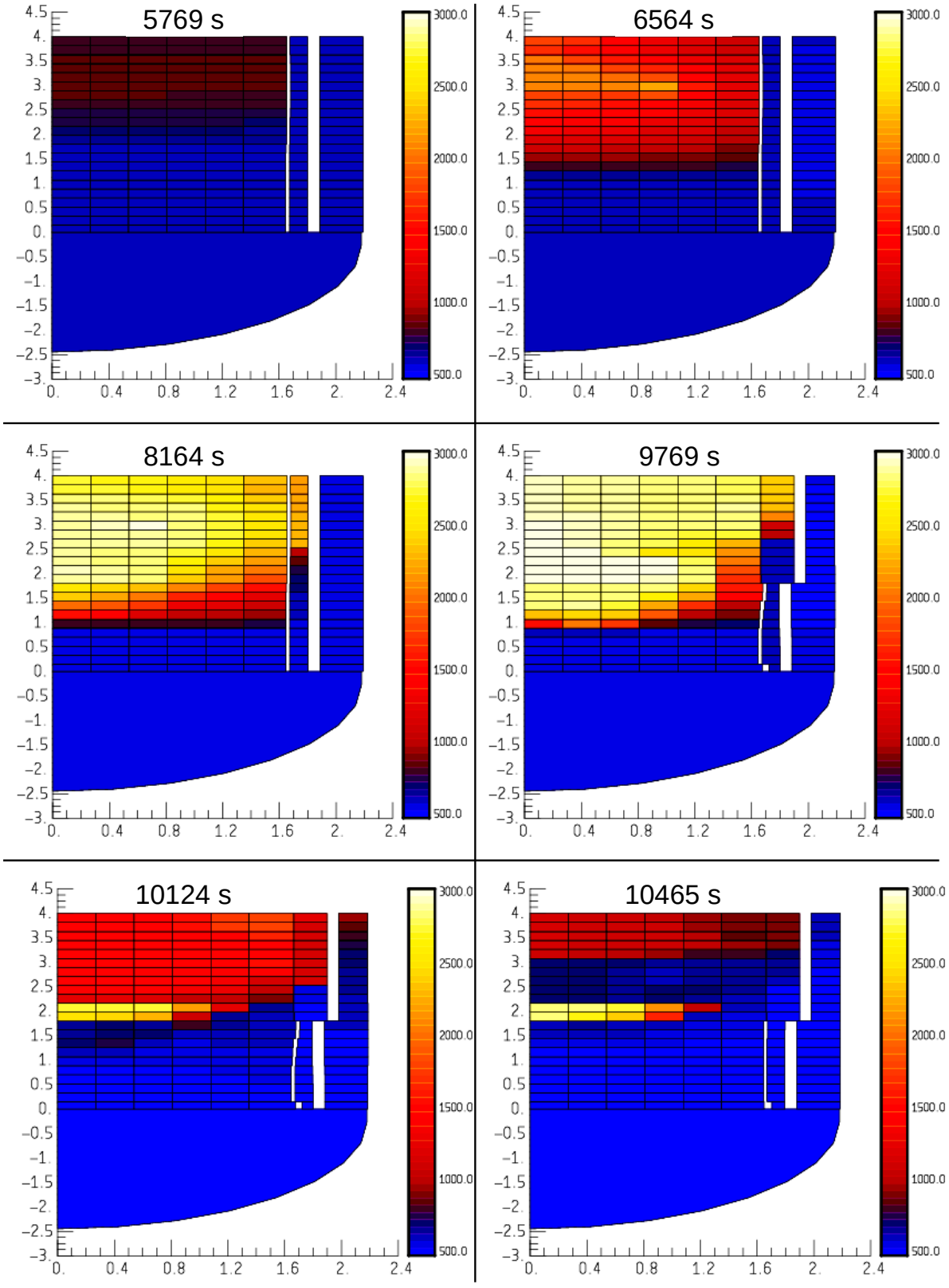

Fig. 24. Gas temperature in the core [K].

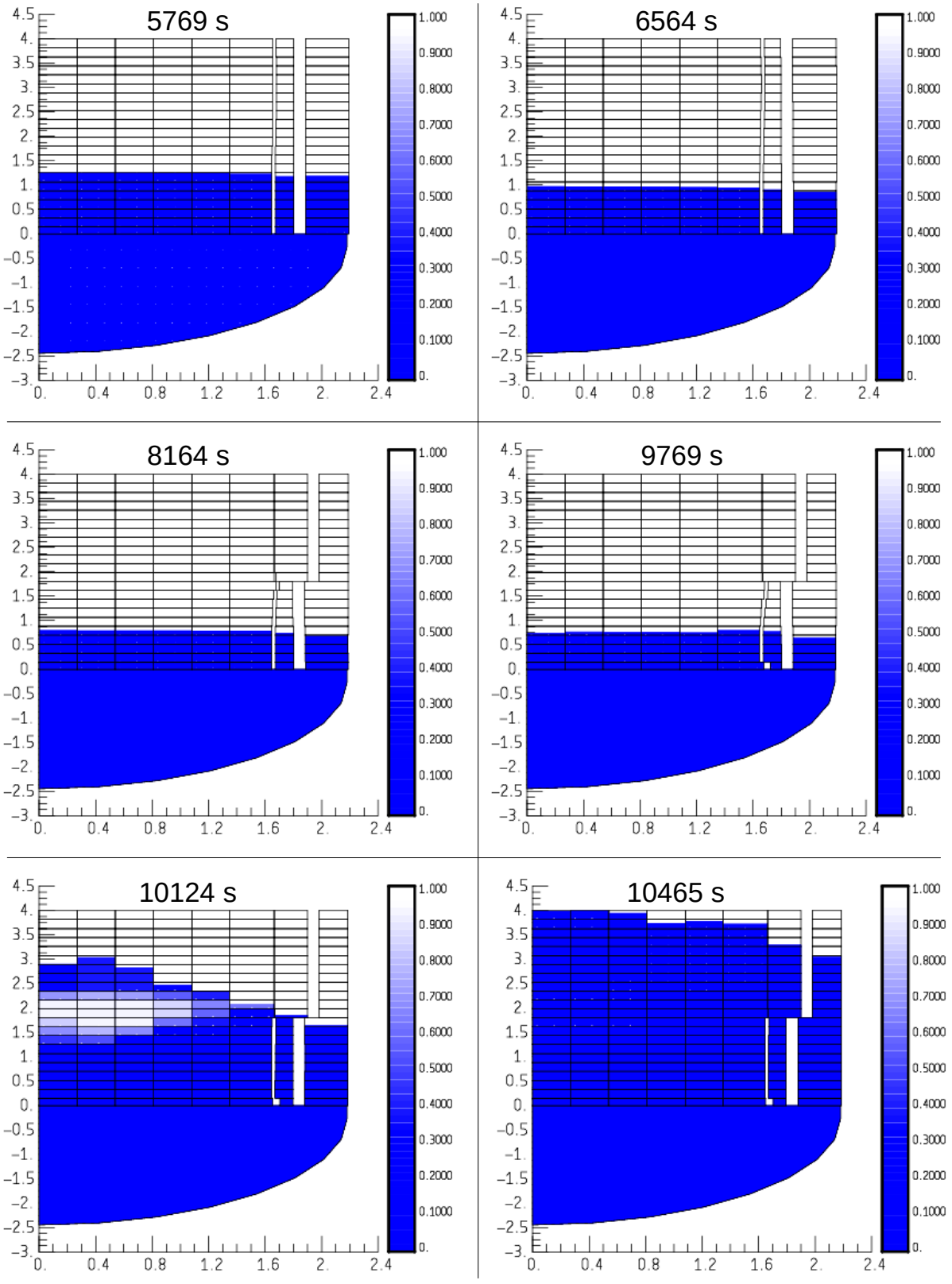

Fig. 25. Water level in the core [m].

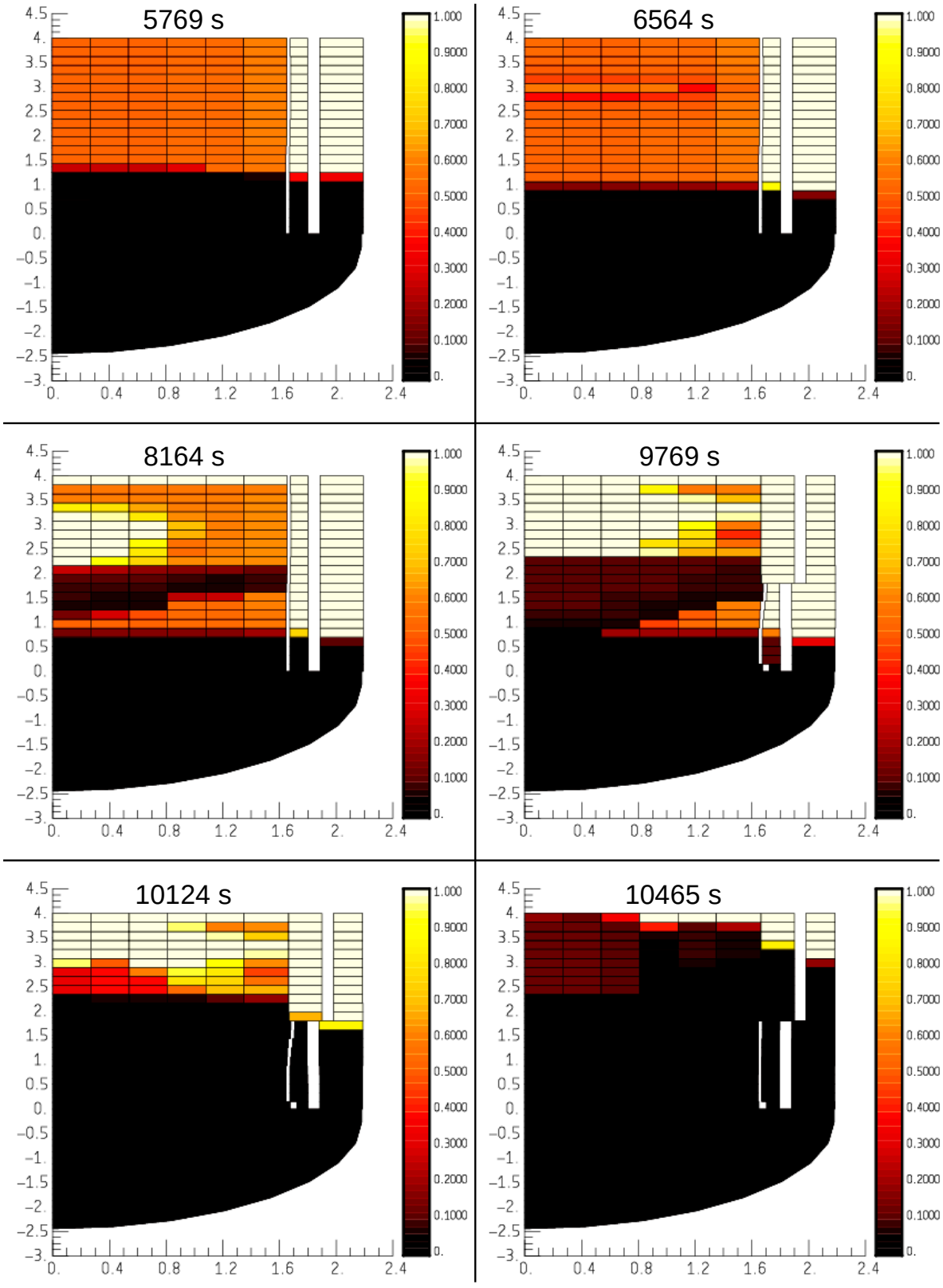

Fig. 26. Gas porositry in the core [-].

19. APPENDIX : NRC-SNL CALCULATION WITH MELCOR 1.8.6

19.1 TMI-2 Plant Modeling

MELCOR version 1.8.6 (YS) was used in this calculation. The TMI-2 plant nodalization scheme used in this calculation is depicted in the figure below. It models the reactor pressure volumes and internals, the primary loops with pressurizer, and main emergency and control systems. The model uses a total of 143 control volumes (see table), 213 flow paths, and 134 heat structures. Of the 143 control volumes, 123 are in the primary (88 in the RPV, six in the pressurizer, and 29 in the piping, pumps, and steam generator tubes) and 16 control volumes in the secondary. The remaining 4 control volumes serve as boundary conditions. Most of the heat structures, 64, are in contact with the RPV volumes, 38 are in contact with the secondary.

In the primary loop, the coolant flow and heat transfer through the A and B loops are represented as distinct flow circuits. However, the division of primary coolant flow at the exit of each SG into two parallel cold leg piping systems is neglected, and the pair of RCPs in each loop are represented as a single composite pump. The pressurizer and surge line are modeled with six control volumes and six heat structures.

Modeling of the secondary systems is limited to the secondary side of steam generators, the steam lines with isolation valves, and main feedwater and auxiliary feedwater injections.

MELCOR TMI-2 plant nodalization within the active core, fuel behavior is modeled by subdividing the core into five (plus the by-pass) radial rings and 12 axial levels. The twelve axial levels are equal in height, representing roughly 1-foot increments of the core. Two additional axial levels are defined to represent the volume below the active core, where damaged fuel can relocate. The core baffle, the barrel and the thermal shield at the core periphery are also represented. Core debris can relocate outside the baffle and down through the formers. The control rod guide tubes and drive assemblies in the upper plenum region and a flow distributor and in-core instrumentation tubes in the lower head region are also modeled.

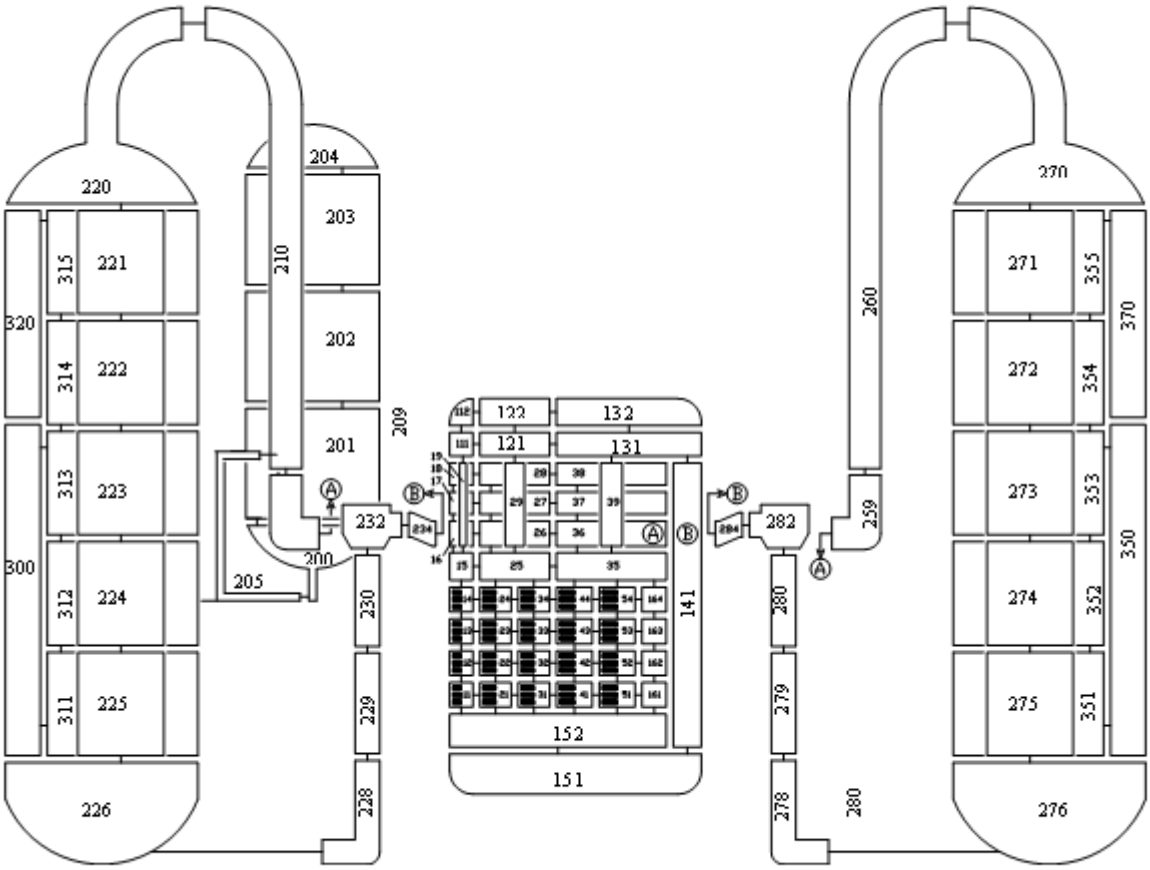

	Total	Primary	RPV	Pressurizer	etc.	Secondary
Control Volumes	143	123	88	6	29	16
Flow Paths	213	154	121	8	33	16
Heat Structures	134	114	64	6	44	38

19.2 Geometry

The geometry assumed for the MELCOR calculation is summarized in the table provided below. The input deck used in this calculation was derived from the standard TMI-2 deck used for MELCOR assessments where boundary/initial conditions were modified to conform to the problem specifications. A notable variance from the problem specification is in the axial nodalization used for the core. This calculation used 14 meshes over the total core length compared to 20 in the problem specification. Also, the total primary volume is somewhat larger than the specification. This reported difference was not resolved.

		Problem Specification	MELCOR
Free volume			
	Primary volume	337.6	351
	Primary system volumes out of pressurizer (m3)	294.6	308
	Pressurizer volume (m3)	43	43
	RPV volume (m3)	116.5	127
	Secondary side free volume of 1 SG		65
Heat transfer with the secondary side			
	SG tubes surface (secondary side) / SG	12302.5	12303.
	Number of tubes / SG	15530	15531
Initial Core Geometry			
Core Characteristics			
	Number of fuel bundles of type 15x15	177	177
	Active cor length	3.66	3.66
	Total core length	4	4
	Type of fuel lattice	square	Square
	Rod pitch	0.01443	0.01443
	Number of fuel rods/assembly	208	208
	External diameter of fuel rod	0.0109	0.0109
	Fuel pellet radius	0.0047	0.0047
	Fuel rod cladding thickness	0.000673	0.000673
Initial core material inventory			
	UO2 mass	93650	95382.96
	Zircaloy mass	23050	23026
	(H2 total mass if converted from total zircaloy (mZr/22.8))	1011	1010
	AIC mass (Ag+In+Cd) [kg]	2750	2818.4064
	Core barrel inside diameter [m]	3.584	3.58
	Core barrel outside diameter [m]	3.683	3.683
Core Meshing			
	Radial rings	5 or 6	5
	Axial meshes (over total core length)	20	14
	Mesh size (m)	0.2	.1778, .1335, 12x.3048

19.2.1 Vent valves

These valves, between the upper plenum and the top of the downcomer, are designed to avoid a direct loss of water by the hot leg. They were modeled, as they were shown to have an influence on the transient, following the problem specifications, i.e.,

- If $\Delta p < 414$ Pa, the valves are closed.
- If $\Delta p > 1724$ Pa, the valves are fully open, which corresponds to a total section of 0.794 m^2.
- If $414 < \Delta p < 1724$, the valves are considered half-open, with a section increasing linearly with Δp.

19.3 Updated Initial Steady-State Conditions

The TMI2 plant state at transient initiation is obtained by a steady-state precursor calculationlasting 300 s and starting from plant thermal-hydraulic parameter values close to the ones specified for TMI-2. Following the initialization, the break is initiated at time t=0. The TMI2 plant initial conditions calculated by MELCOR 1.8.6 are compared with TMI2 accident data at turbine trip in the table below. A noticeable point of discrepancy between the MELCOR calculation and other contributed calculations is the total primary mass, which is ~2% higher for the MELCOR calculation. This is in part explained by the available free volume, which is larger than the problem specification by about 4%, as discussed previously.

Parameter	Unit	MELCOR 1.8.6	TMI-2
Reactor Power	W	2700	2700
Primary Pressure	MPa	15.0	15.2
Temperature Hot Leg A	K	592	592
Temperature Hot Leg B	K	592	592
Temperature Cold Leg A	K	564	548-561
Temperature Cold Leg B	K	564	565
Mass Flow Rate – Loop A	kg/s	8737	8280
Mass Flow Rate – Loop B	kg/s	8828	8560
Pressurizer Level	M	5.77	5.77
Total Primary Mass	ton	231273	-
Pressure SG A	MPa	6.42	7.31
Pressure SG B	MPa	6.27	7.24
Steam Temperature SG A	K	568	586
Steam Temperature SG B	K	567	586
Collapsed Level SG A	M	5.6	-
Collapsed Level SG B	M	5.1	-
Liquid Mass SG A	Kg	18700	-

Liquid Mass SG B	Kg	16900	-
Feedwater Flow SG A	Kg/s	750	723
Feedwater Flow SG B	Kg/s	770	717
SG Feedwater Temperature	K	513	-

19.4 Standard Physical Parameters of the Code

Oxidation of Zircaloy and stainless steel (released from control rods) is modeled with parabolic rate equation. The Urbanic-Heidrick correlation is used in MELCOR to evaluate rate constants for Zircaloy in steam. New to MELCOR 1.8.6, oxidation of unquenched Zircaloy and steel surfaces below the pool surface is also calculated. The necessary steam is assumed to come from the gas film between the hot surface and the pool and is therefore limited only by the pool mass.

Debris bed and molten pool models are modeled in version 1.8.6. Debris beds formation occurs when intact material fails. Cladding fails and fuel rods collapse when clad temperature exceeds 2300 K and unoxidized clad thickness exceed .3mm or unconditionally when clad thickness exceeds 2500K. For control rods, failure occurs when either the unoxidized thickness exceeds a criterion or the steel melt temperature is reached.

The standard best practice used by MELCOR is to define the effective UO2-ZrO2 melting temperature as 2800 K to simulate the reduction in liquefaction temperatures that results from materials interactions. Molten pools form as molten material that candles on surfaces is blocked and forms contiguous molten regions in either the core or in the lower plenum. By default, MELCOR 1.8.6 assumes that molten pools will separate into a denser oxide pool with a metallic pool above. Radionuclides are partitioned between the molten pools and convective heat transfer is calculated from Rayleigh correlations for convecting pools. Heat transfer from the molten pool to the supporting substrate is calculated using an integral Stefan model.

For the sensitivity calculation, the liquefaction temperature for UO2-ZrO2 has been reduced from the standard 2800 K to 2550 K. In addition, a new damage criterion for fuel rod collapse was implemented. This model can lead to debris bed formation at temperatures as low as 2100K and ensures rod failure at temperatures that exceed 2500 K.

<table>
<tr><td>Parameter</td><td>Standard Case</td><td colspan="2">Sensitivity</td></tr>
<tr><td>Zr Oxidation correlation</td><td>Urbanich Heidrich</td><td colspan="2">Urbanich Heidrich</td></tr>
<tr><td rowspan="2">Cladding Failure (rod collapse) criteria</td><td rowspan="2">• T > 2500 K and e(ZrO2) < 100 μm
• T > 2800 K</td><td colspan="2">In addition to the standard failure criterion, failure based damage function.
• Damage accumulates when un-oxidized clad thickness < 1 mm</td></tr>
<tr><td><u>Temperature (K)</u>
< 1000
1000≤T<2100
2100 ≤ T < 2500
T>2500</td><td><u>Time (sec)</u>
1.0e9
3600.0
1800.0
60.0</td></tr>
<tr><td>UO2-ZrO2 melting temperature</td><td>2800 K</td><td colspan="2">2550 K</td></tr>
<tr><td>Debris Formation</td><td>Debris forms when clad fails</td><td colspan="2">Debris forms when clad fails</td></tr>
<tr><td>Debris diameter</td><td>Core - 0.01 m
Lower Plenum - 0.002 m</td><td colspan="2">Core - 0.01 m
Lower Plenum - 0.002 m</td></tr>
<tr><td>Debris porosity</td><td>0.4</td><td colspan="2">0.4</td></tr>
</table>

19.5 Chronology of Major Events

The chronology of major events calculated by MELCOR is presented in the table below.

Event	Time (s)	
	Standard case	Sensitivity case
Break opening and loss of feedwater	0	0
Reactor scram	25	25
Pressurizer is empty	144	144
Primary pump void fraction > 0.6	4770	4770
Primary pump shutdown (M < 85000 kg)	4840	4840
Onset of core uncovery	4900	4900
Onset of core heatup	4910	4910
Beginning of oxidation	6500	6500
First fuel rod clad burst	6690	6710
First melt relocation (U-Zr-O)	7580	7580

First ceramic melting (UO2-ZrO2)	8200	9200
Onset of reflooding	9840	9840
End of calculation	14000	13920

19.6 Result Analysis

Thermal hydraulics

Overall, the results of the MELCOR 1.8.6 calculation are in good agreement with the other calculations in this benchmark activity. Loss of primary coolant inventory through the break was well simulated though it was noted that careful modeling of flow path junction heights in the system was necessary to avoid stratification of flow throughout the system. This stratification results from MELCOR's lack of a flow regime map and improper modeling of the flow path opening heights. Also, flow rates through the loops is significantly higher in the MELCOR calculation probably due to differences in pump models.

Core Degradation

Heat up of the core occurs at roughly the same time as other codes, though onset of core uncovery may be a bit earlier than other calculations. At about 8000 seconds, fuel rods lose integrity just above the middle of the core and the MELCOR support logic leads to failure of intact rods from the level of initial rod failure to the top of the core. As a result, the upper core slumps and there is no longer a temperature recorded for intact rods at the top of the core, though other codes continue to calculate temperature increase of fuel rods at the top of the core. Oxidation signatures predicted by MELCOR initially look similar to other codes with oxidation beginning at 6500 seconds though the total hydrogen generation predicted by MELCOR is less than other codes as oxidation diminishes when the intact rods form debris and slumps at 8000 seconds.

The standard default calculation predicts only 20 tons total of molten material, much less than the 40 tons predicted by other codes. This is explained by the relatively high default UO2/ZrO2 melting temperature of 2800 K. The sensitivity calculation predicts significantly more melted material, 33 tons, which compares more closely to the other codes. It also appears that the debris rests lower, near the core plate than predicted by other codes. Fifty-five tons of debris are predicted by the standard calculation (65 tons in the sensitivity calculation) of which about 6 tons of debris, composed mostly of steel and control rod material (with trace quantities of UO2 and ZrO2) relocates onto the lower head.

The flow blockage model has been activated for axial flow paths in the core region. However, radial blockages were not activated. Adding radial flow blockages may reduce heat removal from the debris bed and lead to additional melted material.

It is also of interest to point out that the standard MELCOR calculation predicted that the outer fuel rods remain standing throughout the calculation. However, the sensitivity calculation predicts failure of the outer fuel rods during the reflood. This may be due to the time-at-temperature criterion of failure that has become a MELCOR 'best practice' in recent time.

Lessons Learned

Important lessons learned that are being considered by the MELCOR development team as a result of this exercise include perhaps the need to reduce the default UO2/ZrO2 melting temperature to be more in line with Phebus FPT observations and the default settings for flow path opening heights in vertical flow paths.

The original input deck also specified multiple radial flow paths connecting a single control volume with an adjacent control volume in the core. This was done because a single control volume was associated with multiple COR cells and the flow paths were specified to capture flow blockage within each COR cell. This nodalization scheme led to non-physical convection cells within the core that redistributed heat from the center of the core to outer rings. This practice is highly discouraged and the final specification associated a single control volume with each COR cell and removed this nodalization problem.

19.7 Synthetic Views of the Core at Selected Times

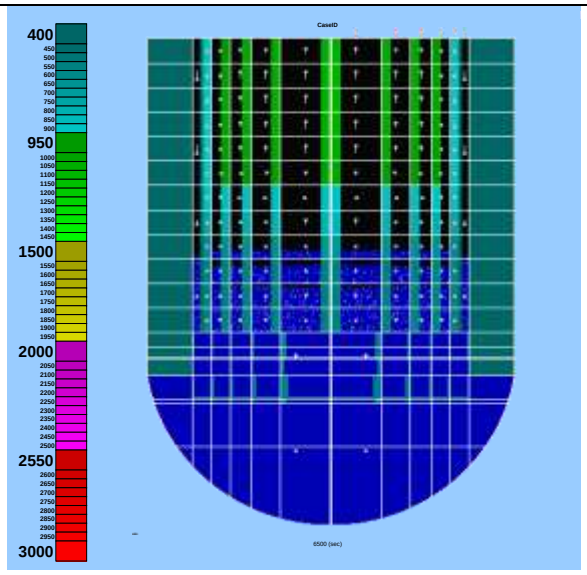

Core State at onset of oxidation for default case (6500 sec)

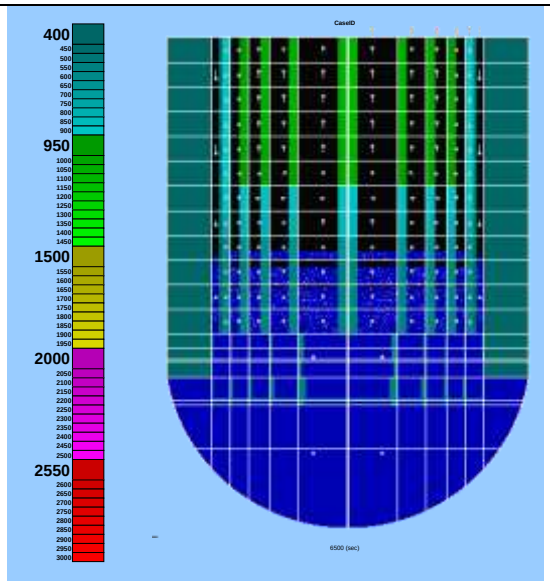

Core State at onset of oxidation for sensitivity case (6500 sec)

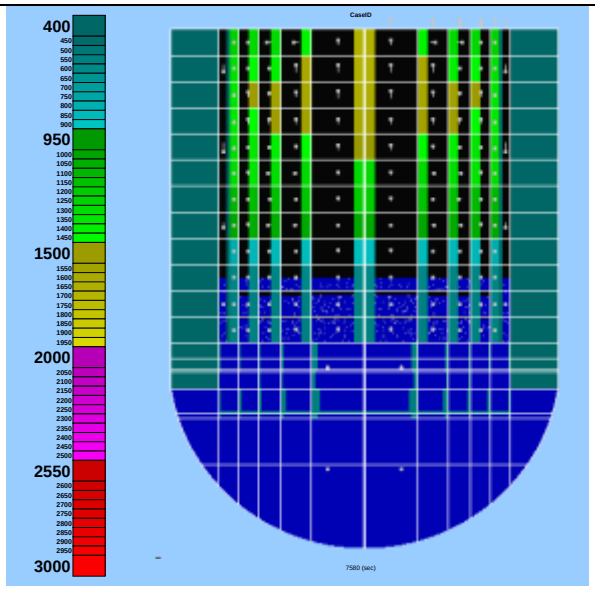

Core State at **First melt relocation** for default case (7580 sec)

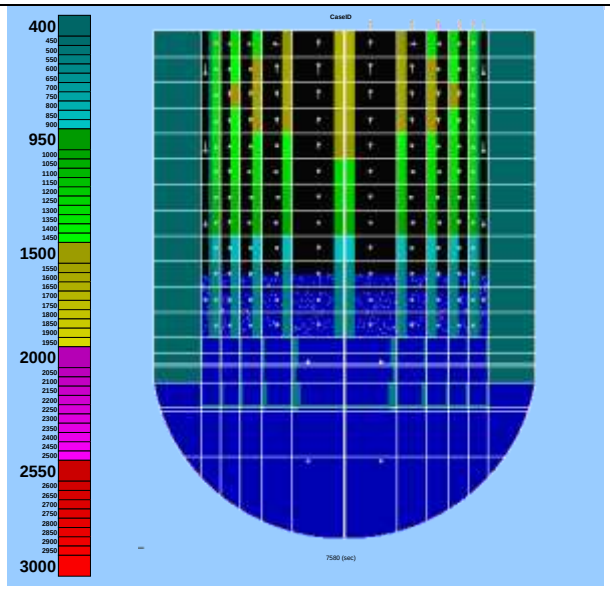

Core State at **First melt relocation** for sensitivity case (7580 sec)

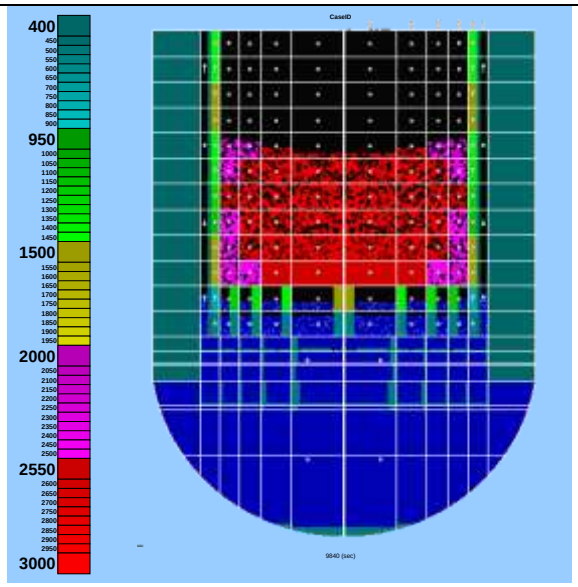

Core State at **time of reflooding** for default case (9840 sec)

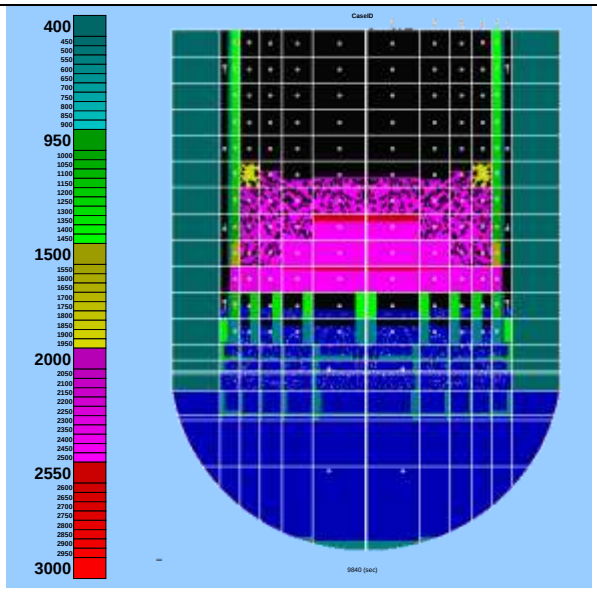

Core State at **time of reflooding** for sensitivity case (9840 sec)

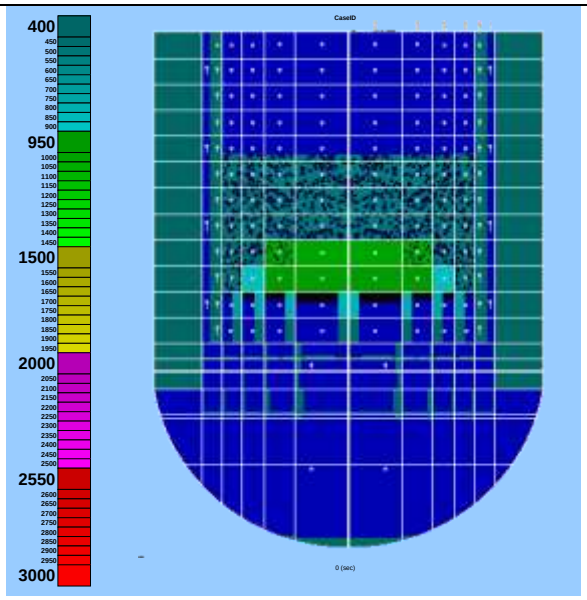

Core State at **end of calculation** for default case (14000 sec)

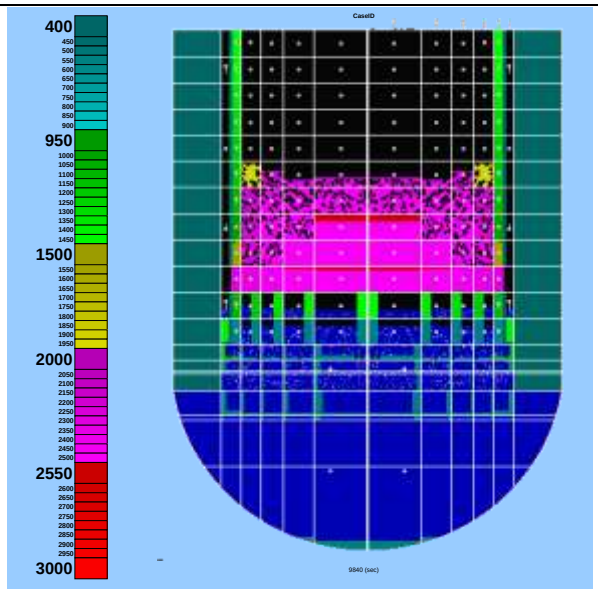

Core State at **end of calculation** for sensitivity case (13920 sec)

20. APPENDIX : IRSN CALCULATION WITH ICARE/CATHARE V2

20.1 TMI-2 Plant Modeling

The TMI-2 plant nodalization used in the Icare/Cathare benchmark calculation is shown on figure 1. This modeling includes a detailed nodalization of the primary circuit with:

- The reactor pressure vessel,
- The two primary coolant loops (with one hot leg and two cold legs for each loop) with the once-through steam generators,
- The pressurizer (with the surge-line, the heaters, the spray-line and the pilot operated relief valve),
- All the main emergency and control systems are also represented.

Concerning the secondary circuit, the modeling is limited to the secondary side of the steam generators, the steam lines with the isolation valves and of course the main and auxiliary feed waters injections.

The reactor vessel is modeled as an Icare/Cathare full 2D module (see figure 2) with the core and all the major internal structures. A total of 8x45 meshes are used. 6 radial rings and 25 axial meshes model the core. Another ring is devoted to the core bypass and another one for the vessel downcomer.

All other elements of the plant are modeled as standard Cathare 0D or 1D modules with their external walls.

Finally, all the boundaries conditions are been modeled according to the prescribed scenario:

- With a constant make-up flow,
- With regulations of the secondary side of the steam generators.

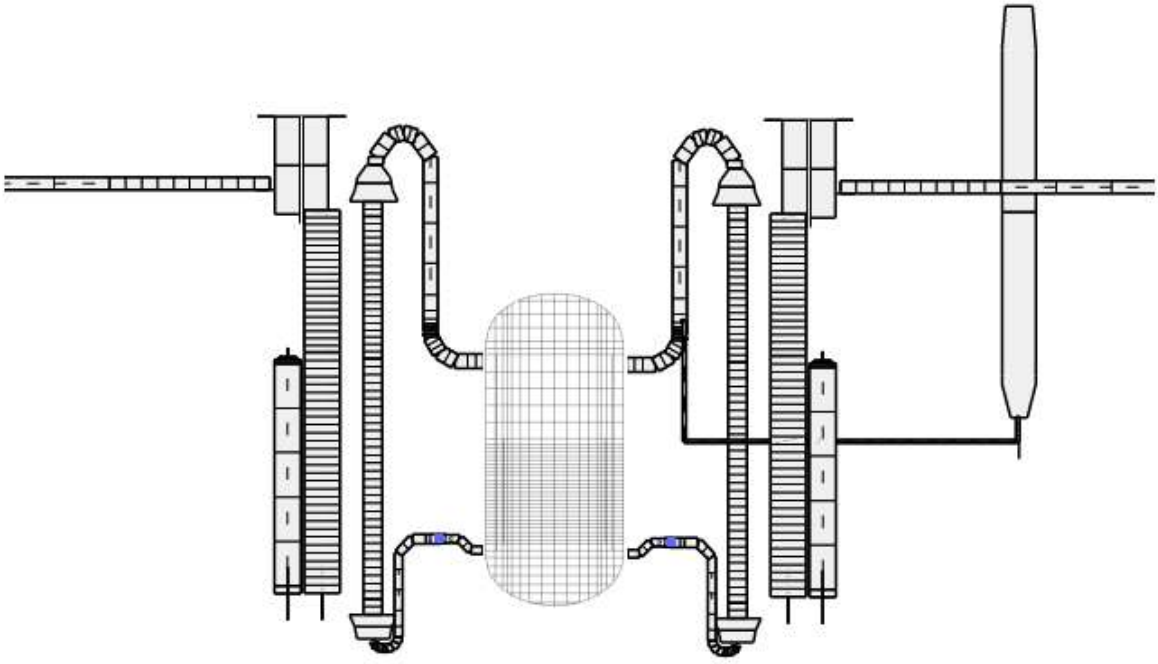

Figure 1: Reactor Plant Nodalization

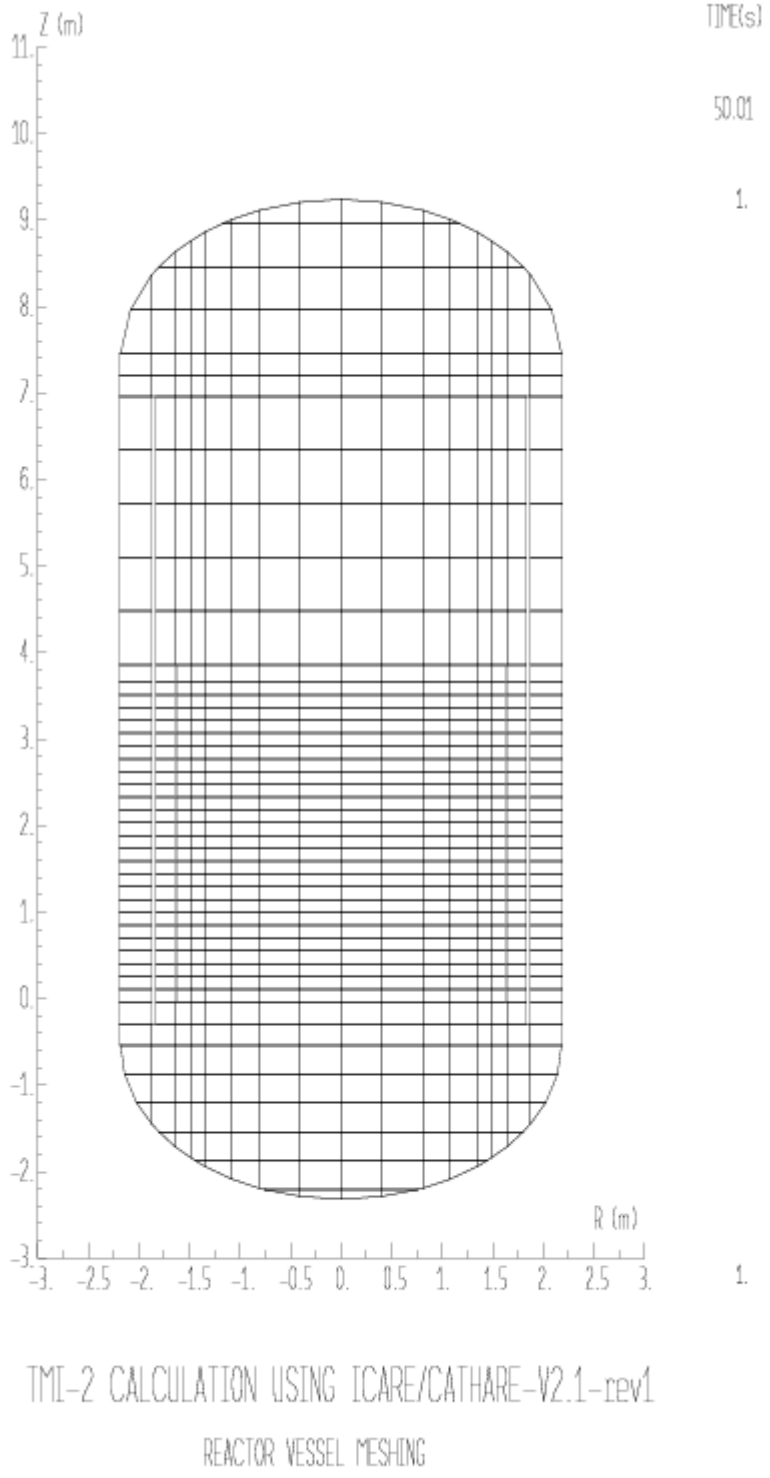

Figure 2: Reactor Vessel Meshing

20.2 Physical Parameters of the Code

The benchmark calculation has been performed with the last version of Icare/Cathare, which is the version V2.1-rev1 released in July 2007. The main core degradation physical parameters used in Icare/Cathare calculation are given in table 1. All the parameters requested in the benchmark specifications, actually correspond to the recommended values by Icare/Cathare team for reactor applications. Therefore, no sensitivity study was necessary.

The most advanced models concerning the degradation phase have been used:

- 2D molten material movement model,
- Advanced 2D radiative model in core region,
- Molten pool formation and evolution model,
- Corium oxidation model.

Finally, the Cathare 3D thermal hydraulics model has been used to calculate the thermal hydraulics in the whole reactor vessel.

Remark: According to the benchmark specifications, an alternative calculation should have been performed with different parameters. It was decided to enable the specific debris model and porous media model, but unfortunately the current Icare/Cathare version was not able to perform such calculation due to numerical instabilities in the transition phase from intact geometry to debris geometry and in the transition phase from standard hydraulic model to porous hydraulic model. This should be solved in the next Icare/Cathare version (V2.2-rev1), which is planned to be released in June 2008.Such results could be available in the nextsteps of this benchmark activity, if it continues.

Parameters	Standard Case
Zr Oxidation correlation	Correlations proposed by Schanz et al. (2001) • Cathcart correlation if T < 1800 K • Prater correlation if T > 1900 K • Linear interpolation between 1800 – 1900 K
Cladding Failure criteria	• T > 2300 K and e(ZrO2) < 300 μm • T > 2500 K
UO2-ZrO2 melting temperature	2550-2600 K
2D Corium Movement Model	enable
Corium Oxidation Model	enable
Debris model	disable

Table 1: Mains Icare/Cathare Code Parameters

20.3 Initial Steady State Conditions

The TMI2 plant state at the beginning of the transient is obtained by performing an Icare/Cathare steady state calculation of the reactor following by a transient calculation at nominal conditions with standard regulation processes. This transient lasts about 5000 s and, at the end, all the main plant parameters are stable. All those parameters are given in the following table and compared with TMI-2 accident data at turbine trip.

Parameter	Unit	ICARE/CATHARE V2	TMI-2
Reactor Power	W	2700	2700
Primary Pressure	MPa	15.02	15.2
Temperature Hot Leg A	K	592.3	592
Temperature Hot Leg B	K	592.3	592
Temperature Cold Leg A	K	566.3	548-561
Temperature Cold Leg B	K	564.7	565
Mass Flow Rate – Loop A	kg/s	8805	8280
Mass Flow Rate – Loop B	kg/s	8846	8560
Pressurizer Level	M	5.60	5.77
Total Primary Mass	ton	230389	-
Pressure SG A	MPa	6.38	7.31
Pressure SG B	MPa	6.24	7.24
Steam Temperature SG A	K	584.9	586
Steam Temperature SG B	K	583.6	586
Collapsed Level SG A	M	5.26	-
Collapsed Level SG B	M	5.39	-
Liquid Mass SG A	Kg	18425	-
Liquid Mass SG B	Kg	18989	-
Feedwater Flow SG A	Kg/s	700	723
Feedwater Flow SG B	Kg/s	742	717
SG Feedwater Temperature	K	513.0	-

Table 2: Steady State Conditions Parameters

Since the conditions in the TMI-2 plant just before the turbine trip are not very well known, it not possible to reach exactly the TMI-2 data, especially for the secondary circuit.

20.4 Analysis of code results

The chronology of major events as calculated by Icare/Cathare is presented in the table 3. Fours synthetic views of the reactor vessel state at different times are shown on figures 3 to 6.

Event	Time (s)
	Standard Case
Break opening and loss of feedwater	0
Reactor scram	16
Pressurizer is empty	240
Primary pump shutdown (M < 85000 kg)	4831
Primary pump void fraction > 0.6	4855
Onset of core uncovery	5788
Onset of core heatup	6250
Beginning of oxidation	7550
First fuel rod clad burst or perforation	8462
First melt relocation (U-Zr-O)	9272
Onset of reflooding	9831
End of calculation	15000

Table 3: Chronology of Main Events

The scenario calculation can be divided into three phases: the thermal hydraulics phase, the core degradation phase and the core reflood phase.

20.4.1 The thermal hydraulics phase (from t = 0 s to t = 6250 s)

The scenario starts with the opening of a small break on hot leg A and with the loss of main feedwater at the same initial time. The loss of feedwater induces a strong reduction of heat transfer between primary and secondary circuit. The resulting loss of heat removal causes the primary pressure to reach rapidly the high-pressure reactor trip point and the reactor scram occurs at about 16 s. After this scram, the primary pressure decreases progressively to reach a stable value near the secondary pressure value at about 450 s.

During this phase the mass inventory in the primary circuit continuously decreases due to the break on hot leg A. But as the primary pumps are still working, a forced circulation of a liquid water and steam

mixture is established. In those conditions, the core decay power is removed totally from the primary circuit by the steam generators.

According to the benchmark scenario, this behavior continues until the primary mass inventory falls below 85000 kg. This occurs at 4831 s. At this time, the primary pumps are shutdown.

After pumps stop, the forced convective circulation in primary circuit is replaced by a natural circulation. This induces a large increase of primary pressure. The heat removal from the core is progressively reduced and the core decay power is no more removed at about 5450 s. From this moment the vessel water level decreases continuously and the core uncovery starts at about 5800 s.

The degradation process starts after this moment.

20.4.2 The core degradation phase (from t = 6250 s to t = 9831 s)

Shortly after the start of core uncovery the fuel rod temperatures increase rapidly in the central zone of the upper part of the core (at about 6250 s). The temperature escalations expand radially and downwards to the bottom of the core.

The oxidation runaway occurs at about 7550 s and increases the core heat-up rate (the state of the core at this time is shown on figure 3). It is followed by the first clad failure at about 8460 s and by the first melt relocation at about 9270 s (see figure 4).

The evolution of the degradation process can be seen on figures 7. The degradation zone is limited to the upper part of the core because the total dry-out of the core is never reached.

At the time 9831 s, a total of 258 kg of hydrogen has been released and 36577 kg of corium has been formed. The state of the core is presented on figure 5).

Remark: Between t = 8000 s and t = 9831 s, it is not possible to impose the right boundary conditions on the steam generators. There is an increase of the steam generators level and at the same time a decrease of steam generators pressure because of steam condensation in the secondary side of the steam generators.

20.4.3 The core reflood phase (from t = 9831 s to 15000 s)

According to the benchmark specifications, the High Pressure Injection is enabled 5000 s after primary pumps shutdown. This occurs at 9831 s. The total flowrate injection is 60 kg/s.

The reflood of the core causes a large primary pressure increase (about 9.0 MPa) due to steam generation in the core. This reflood is very efficient and the vessel is totally refilled and cooled down in about 1200 s. During this quenching phase, the hydrogen production and the corium formation are very rapidly stopped. The hydrogen mass release is limited to 17 kg (compared to 258 kg during the degradation phase) and the corium mass production is only 3368 kg (compared to 36577 kg during the previous phase).

The evolution of reflood process is presented on figures 8 to 10. This process can be divided into 4 main phases:

- A core bypass phase (during about 300 s)
- A top core quenching phase (during about 500 s)

- A bottom core quenching phase (during about 400 s)
- A final steady state phase (from t = 11000 s to t = 15000 s)

<u>Remark:</u> After t = 12500 s, it is not possible to impose the right boundary conditions on the steam generators. There is an increase of the steam generators level and at the same time a decrease of steam generators pressure because of steam condensation in the secondary side of the steam generators.

20.5 Comparisons to other code results

In general there is a good agreement between Icare/Cathare and other codes results:

- The thermal-hydraulic behavior as calculated by Icare/Cathare is very consistent with other code results.
- There is no large discrepancy concerning total hydrogen release and total molten material formation.
- As other codes, Icare/Cathare predicts a very efficient reflood process with a rapid vessel refilling and a very limited amount of hydrogen release and corium formation during quenching phase.

The main discrepancies with other codes results are the following:

- The primary pressure evolution after pumps stop differs.
- The starts of core uncovery and core heat-up rate are different.
- The degradation process seems to be rather different between different codes.

It seems that the thermal hydraulic behavior in the steam generators just after the pump shutdown are not the same in the different calculations and it should have a non negligible impact on the beginning of degradation process and then on the conditions just before reflooding. This is not yet clearly explained.

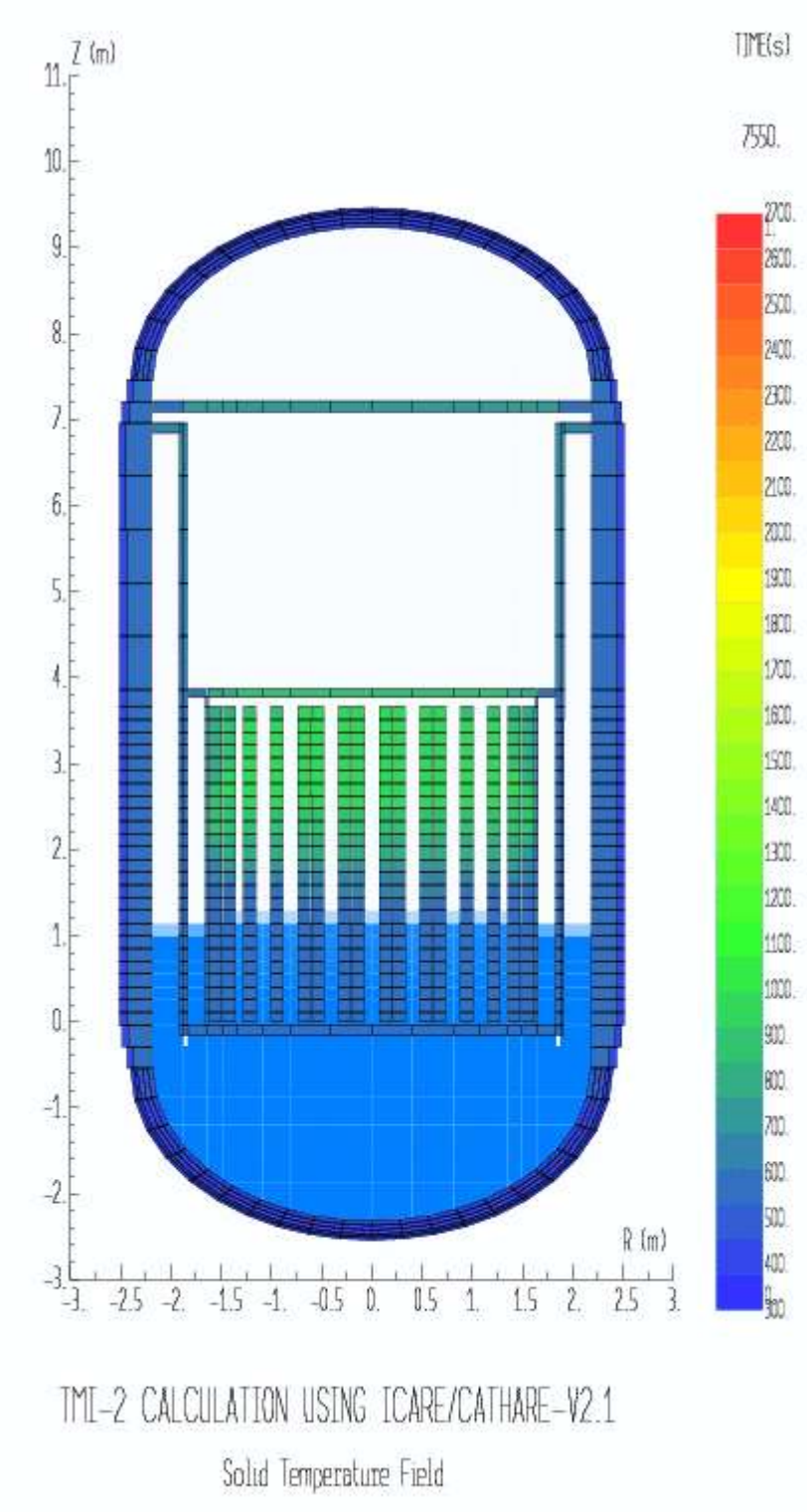

Figure 3: View of the Reactor Vessel at the beginning of oxidation

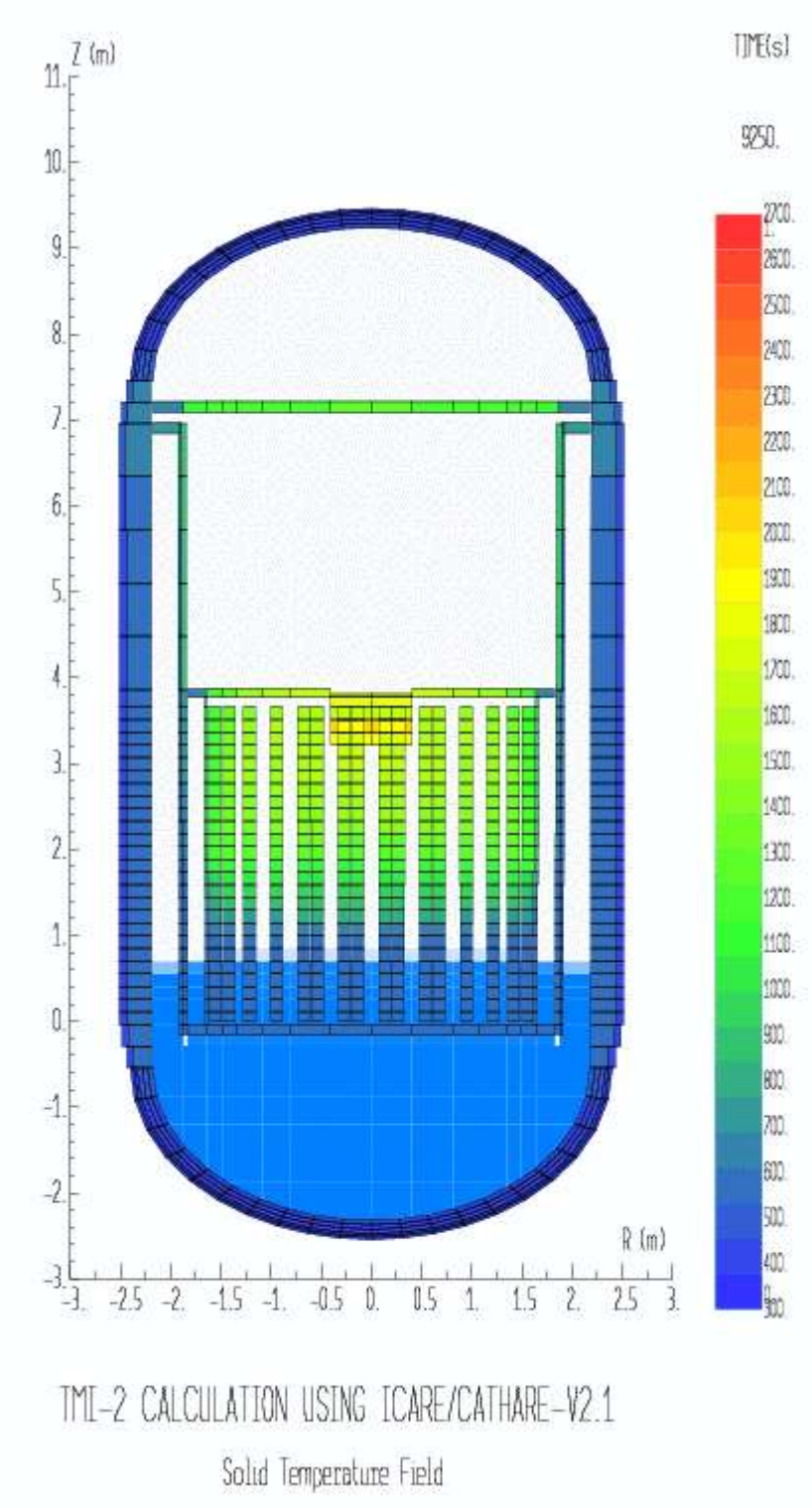

Figure 4: View of the Reactor Vessel at time of first melt relocation

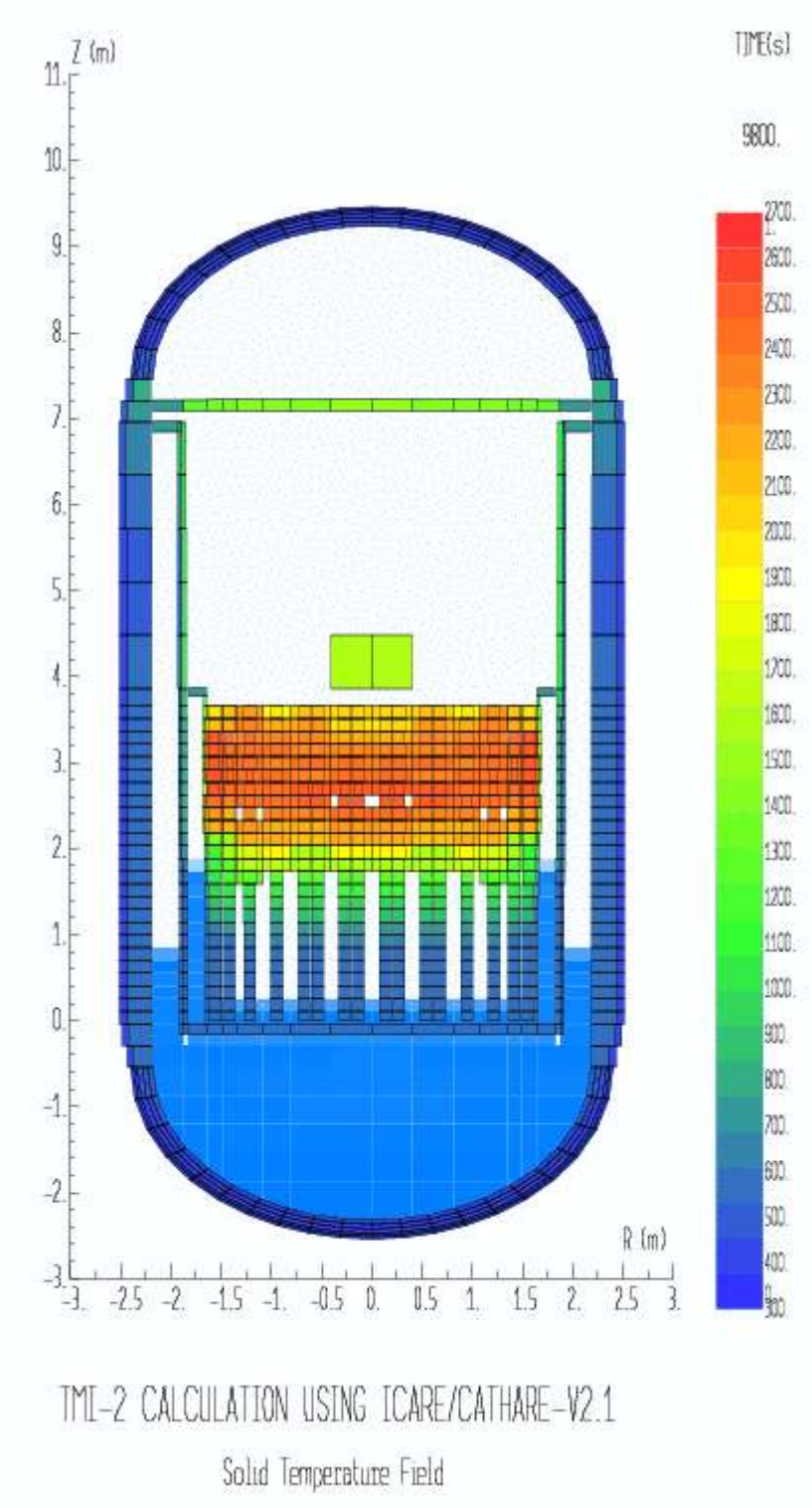

Figure 5: View of the Reactor Vessel at the start of the reflooding

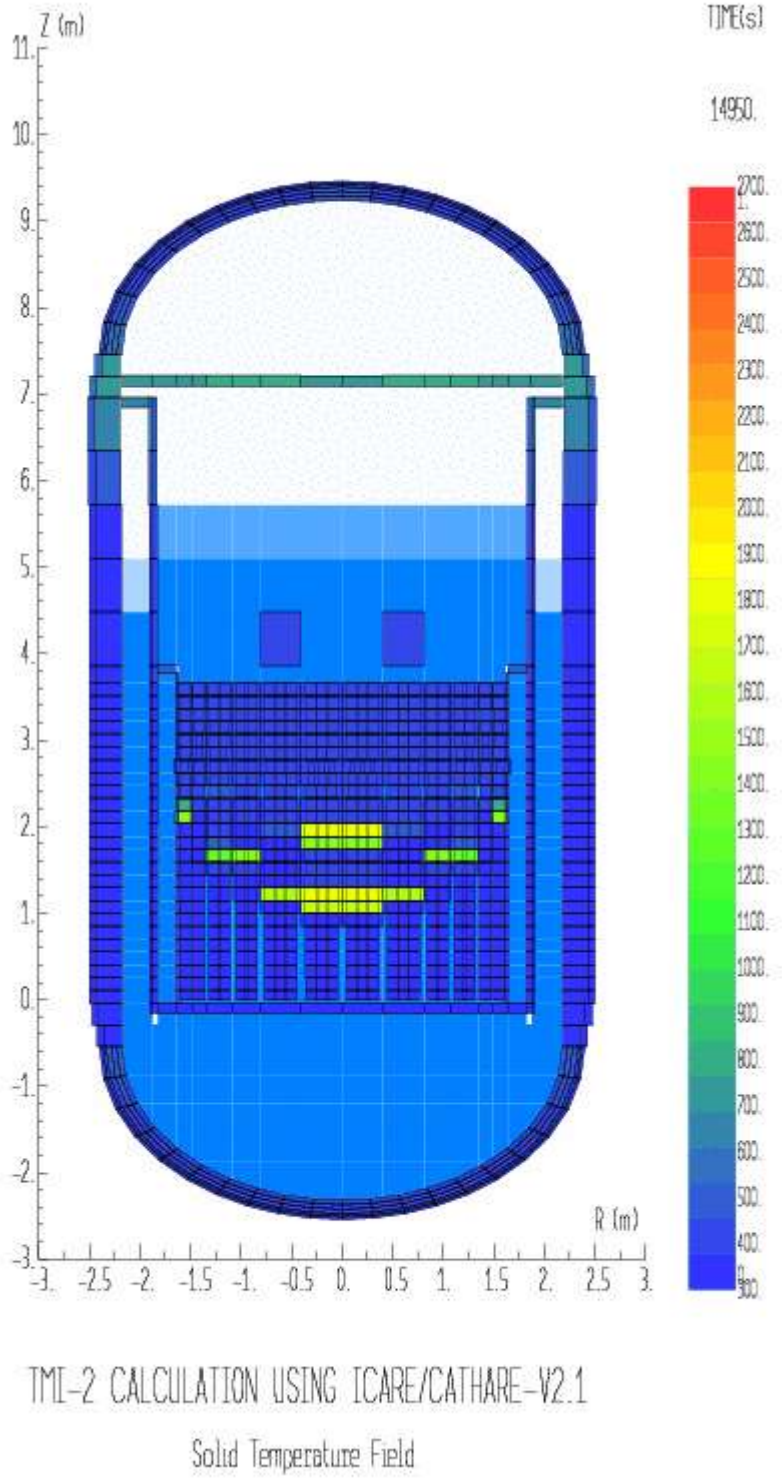

Figure 6: View of the Reactor Vessel at the end of the calculation

Figure 7: Core Degradation Phase: Relocation Process (t = 9250 s ➔ t = 9750 s)

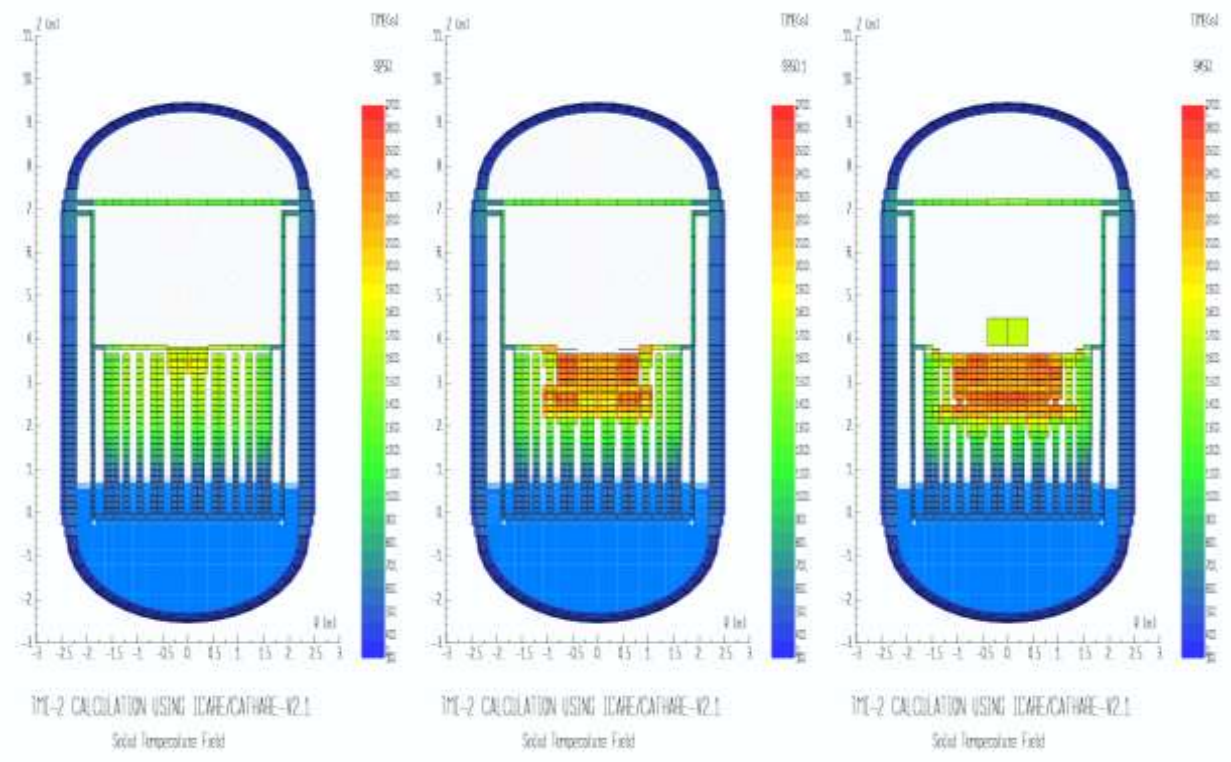

t = 9250 s **t = 9350 s** **t = 9450 s**

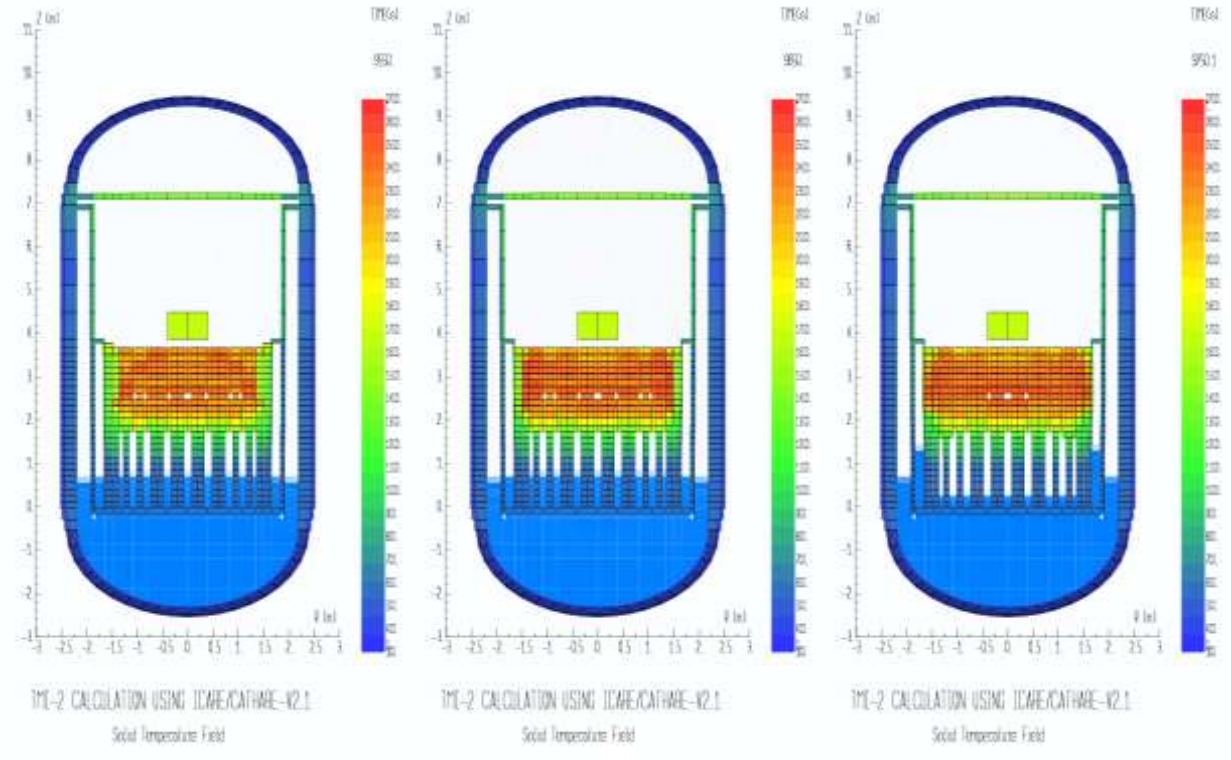

t = 9550 s **t = 9650 s** **t = 9750 s**

Figure 8: Core Reflood Phase: Core By-Pass Phase (t = 9800 s ➔ t = 10100 s)

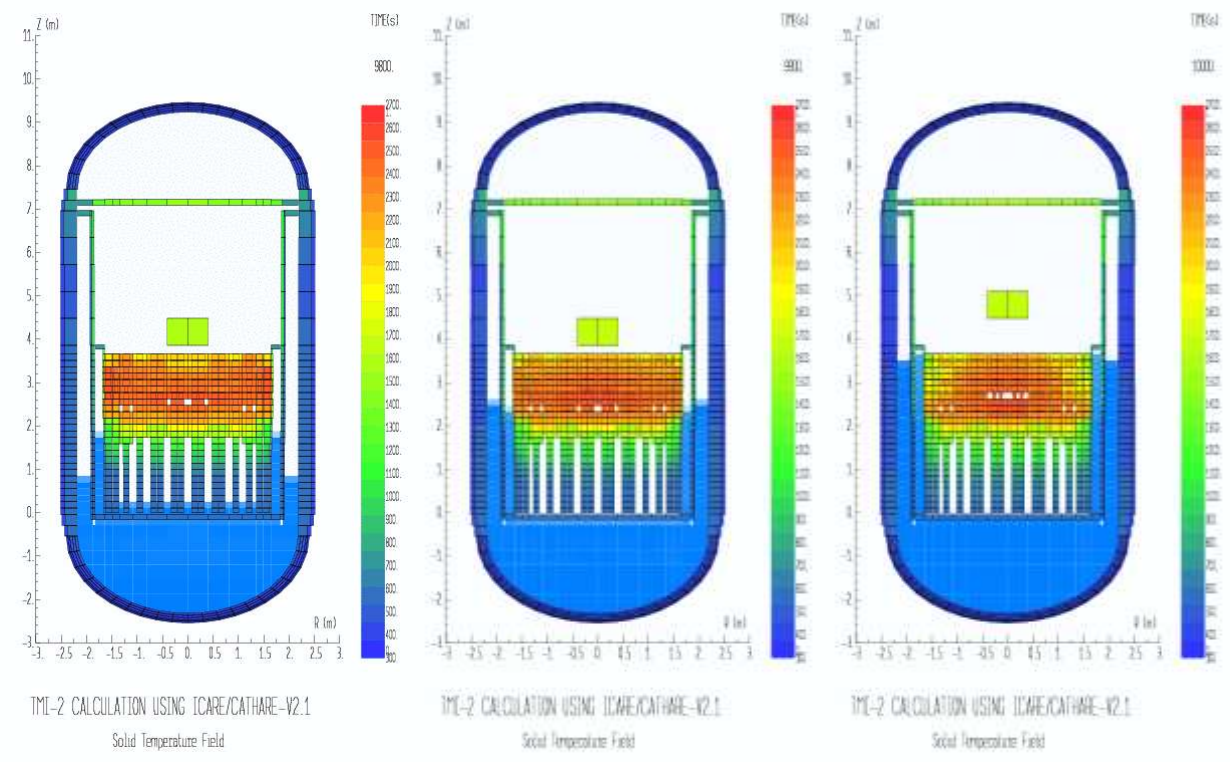

t = 9800 s **t = 9900 s** **t = 10000 s**

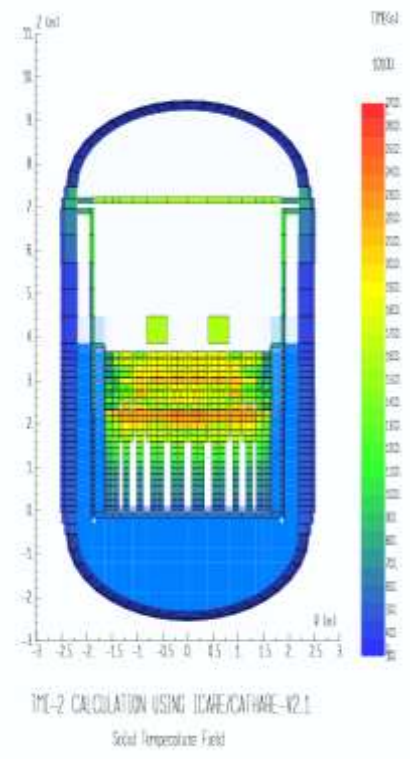

t = 10100 s

Figure 9: Core Reflood Phase: Top Core Quenching Phase (t = 10100 s ➔ t = 10600 s)

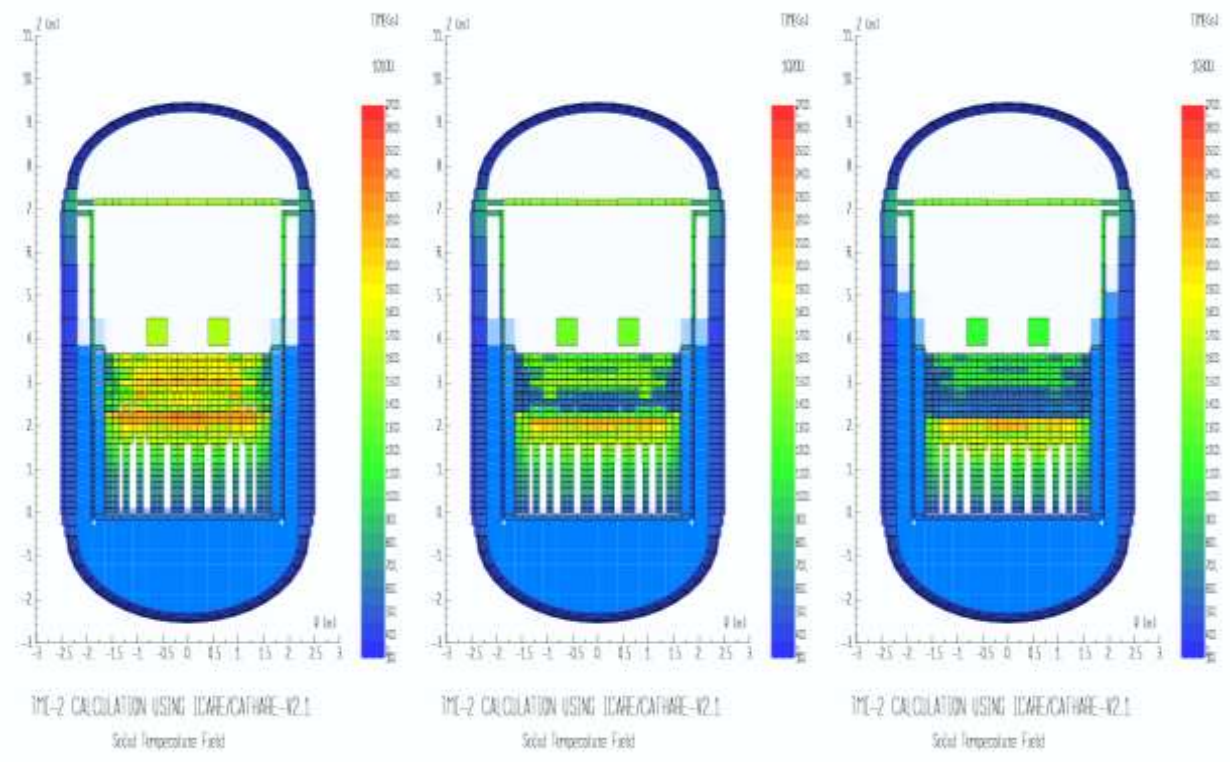

t = 10100 s **t = 10200 s** **t = 10300 s**

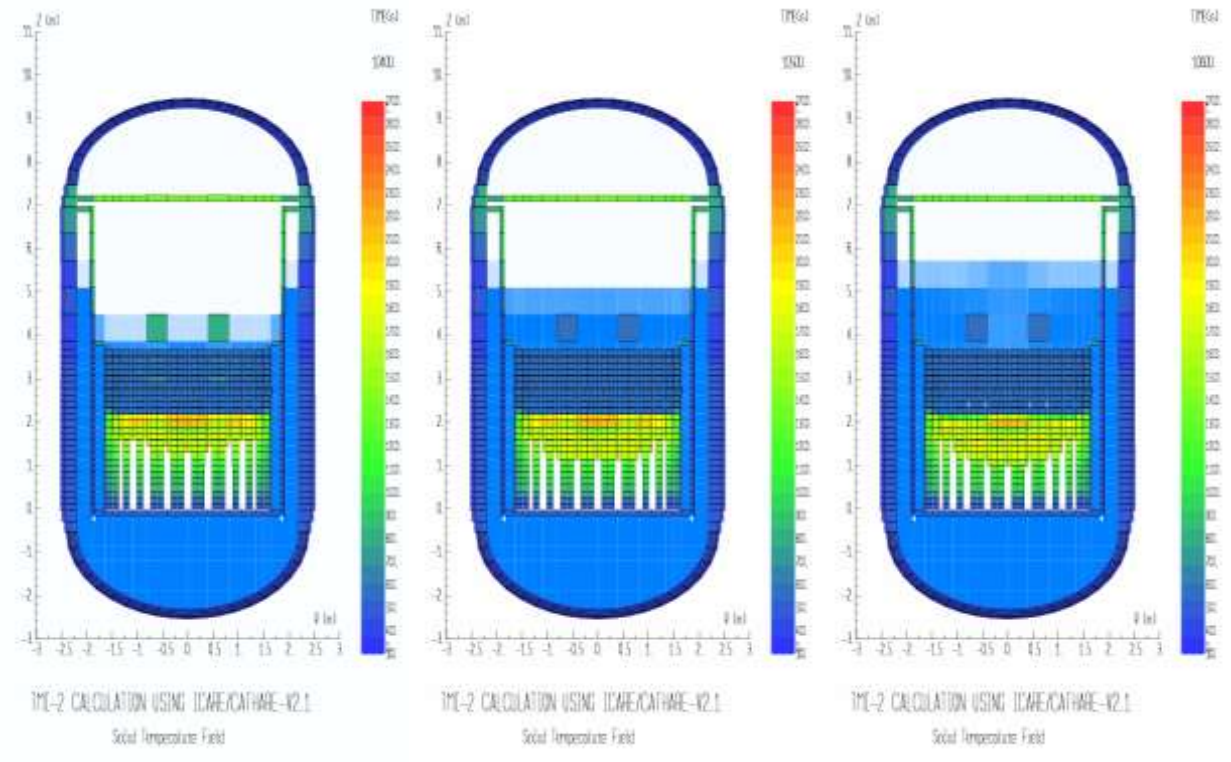

t = 10400 s **t = 10500 s** **t = 10600 s**

Figure 10: Core Reflood Phase: Bottom Core Quenching Phase (t = 10600 s ➔ t = 11000 s)

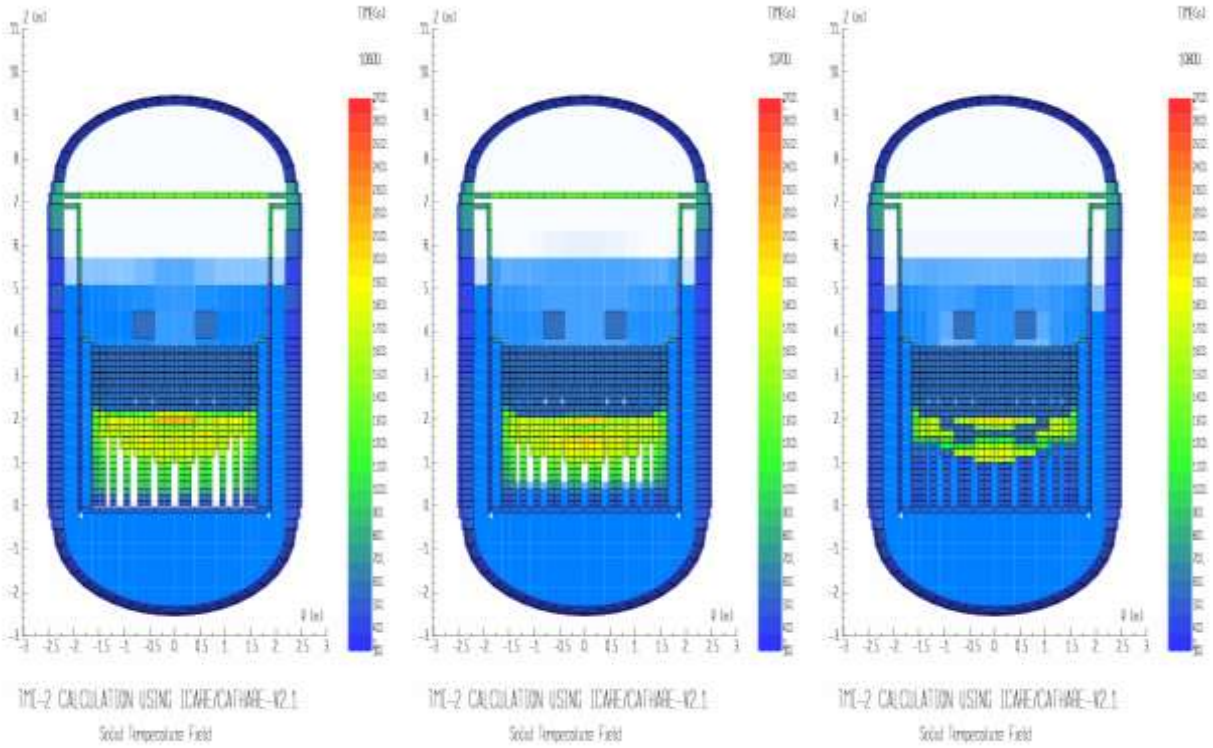

t = 10600 s **t = 10700 s** **t = 10800 s**

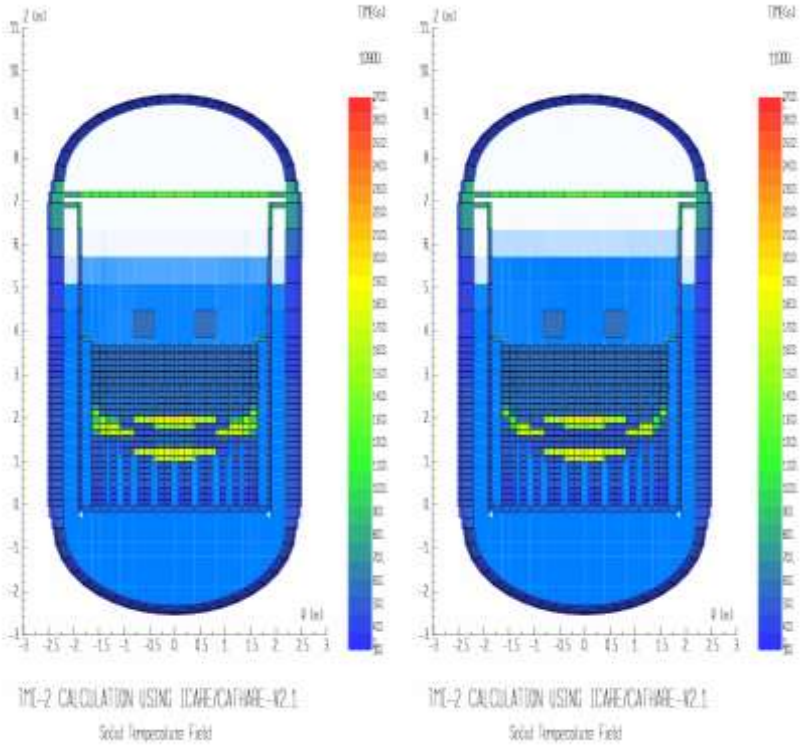

t = 10900 s **t = 11000 s**

21. APPENDIX : SNU CALCULATION WITH MAAP4

21.1 TMI-2 Plant Modelling

The MAAP4.03 primary system nodalization for tracking these quantities in a Babcock &Wilcox type plant is shown in Fig. 1. The reactor consists of four volumes: core, downcomer, upper plenum, and reactor dome. All loops except one, the broken loop, are lumped together, and the broken loop is treated separately. The broken loop refers to the loop that can contain a primary system break. The user selects whether the pressurizer is in the broken or unbroken loop. The A-loop is taken as the broken loop for analysis of the TMI-2 accident.

The reactor vessel is nodalized in the form of heat sinks and control volumes. Fig. 2 specifies the core region with the number of radial rings and axial rows. A radial peaking factor and volume fraction are fixed for each ring, and an axial peaking factor is assigned for each row. Seven rings and thirteen rows are used to nodalize the TMI-2 core for simulation of the accident.

Two input files are required to simulate the TMI-2 accident with MAAP4: the parameter file and an input deck. The user inputs various parameters for each component such as volumes or masses. The parameter file has the information on TMI-2 relevant to the plant geometry, system performance, controls and initial conditions used to perform these benchmark calculations. The input deck defines the operator actions and boundary conditions during the course of the accident.

Mass and energy rates of change for core materials are calculated for each core node. Steam and hydrogen are assumed to flow along the uncovered and unblocked flow channels, and the mass flow rates and enthalpies in channel are determined by accounting for the generation and consumption at each axial level. The core water pool is treated as a lumped mass and energy volume.

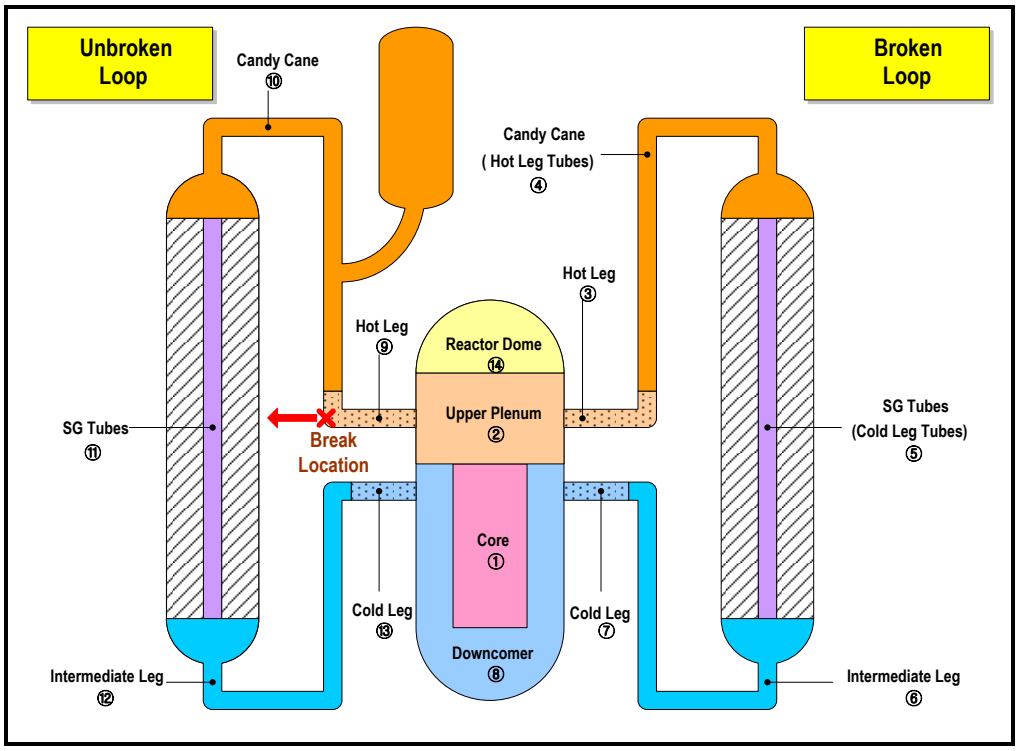

Figure 1 Primary System Nodalization

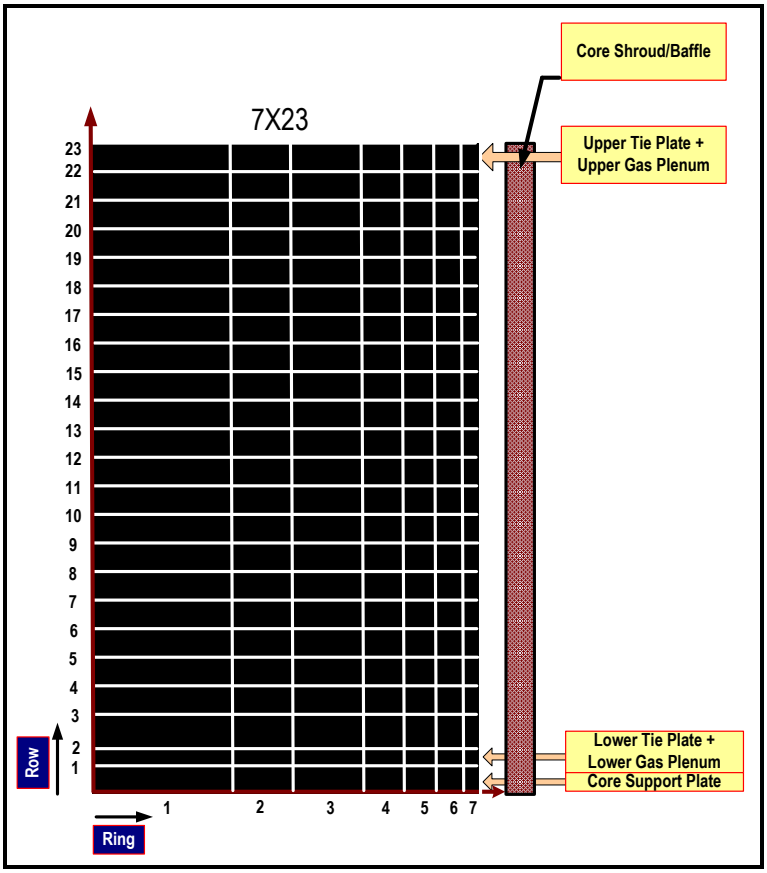

Figure 2 Primary System Nodalization

21.2 Initial Steady State Conditions and Scenarios

The accident is initiated by a small break at the bottom of hot leg A together with a loss of main feedwater for the TMI-2 nuclear power plant. The main assumptions include stopping of the primary pumps when the primary mass void fraction exceeds 0.6 and starting of the High Pressure Injection (HPI) 5000 s thence forth. There is no letdown flow nor Power Operated Relief Valve (PORV) failure. This alternative scenario was chosen because it describes a standard small-break scenario with core uncovery and core degradation and then reflood so that it could lead to good comparison without a great deal of uncertainties involved with the actual accident.

Table 1 lists the TMI-2 plant initial conditions for MAAP4. Table 2 presents the core heat flux profile according to radial ring and axial row.

Table 1. Initial Conditions

Main Parameters	Unit	MAAP4.03
Reactor Power	MW	2700
Primary pressure	MPa	15.2
Temperature Hot Leg A	K	579
Temperature Hot Leg B	K	579
Temperature Cold Leg A	K	559
Temperature Cold Leg B	K	559
Pressurizer level	m	6.78
Total primary mass	kg	211170
Pressure SG A	MPa	6.38
Pressure SG B	MPa	6.38
Steam temperature SG A (inlet)	K	508
Steam temperature SG B (inlet)	K	508
Collapsed level SG A	m	3.28
Collapsed level SG B	m	3.28
Liquid mass SG A	kg	17506
Liquid mass SG B	kg	17506
Feedwater flow SG A	kg/s	756
Feedwater flow SG B	kg/s	756
SG feedwater temp.	K	508

Table 2. Core Heat Flux Profile

Radial profile

Ring	Power factor	Area factor
1	1.162	0.0937
2	1.160	0.1123
3	1.155	0.1680
4	1.150	0.1616
5	1.130	0.1548
6	0.803	0.1548
7	0.480	0.1548

Axial profile

Row	Z (m)	Power factor
23	4.56	0
22	3.99	0.57019
21	3.81	0.81171
20	3.62	0.95979
19	3.44	1.02413
18	3.26	1.04428
17	3.08	1.05070
16	2.89	1.05660
15	2.71	1.06329
14	2.53	1.06838
13	2.34	1.07127
12	2.16	1.07435
11	1.98	1.08075
10	1.80	1.09117
9	1.61	1.10233
8	1.43	1.10843
7	1.25	1.10482
6	1.06	1.08932
5	0.88	1.05178
4	0.70	0.93659
3	0.52	0.55506
2	0.33	0
1	0.08	0

21.3 Sensitivity Study

The main core degradation physiscal parameters used in the standard calculation with MAAP4 are compared against alternative physical parameters for PHEBUS-FPT1 in Table 3.

Table 3. Core Degradation Physiscal Parameters

	PHEBUS FPT1	MAAP4
Zr Oxidation correlation	Urbanic-Heidrick model	Baker-Just model (T_{clad} > 1875 K) Cathcart model (T_{clad} < 1850 K) Interpolated inbetween
Cadding failure criteria	T > 2280 K and e(ZrO_2) < 200 mm T > 2450 K and e(ZrO_2) < 300 mm	T > 2500 K Fraction of clad reacted > 0.675
UO_2-ZrO_2 melting temperature	T > 2550K	T > 2500 K
Debris formation criteria	No debris bed and molten pool formation modelling	Melt progression model
Debris diameter	-	
Debris porosity	-	0.4 (debris bed)

21.4 Chronology of Major Events

The chronology of major events calculated by MAAP4 is presented in Table 4 and discussed in Section 6.

Table 4. Major Events Squence

Event	Time (s)	
	Standard	Alternative
Break opening and loss of feedwater	0	0
Reactor scram	18	18
Pressurizer is empty	221	221
FP models on	1497	1797
Primary pump shutdown	5342	5342
Onset of core uncovery	5682	5682
Beginning of oxidation	**6251**	**6251**
Maximum core temperature has exeeded 2499K	7638	7528
First fuel rod clad collapses	7789	7775
First melt relocation	**7794**	**7775**
HPI swich no forced off	**10342**	**10342**
Onset of reflooding	**10342**	**10342**
End of calculation	**10422**	**10422**

21.5 Results Analysis

The overall system behavior was reasonably predicted according to the hot leg break opening at 0 s, the contemporary feedwater trip with consequent loss of heat removal by the secondary side results in the primary pressure increase. Reactor scrammed due to the pressure in the primary system is higher than a MAAP4 specified high pressurizer-pressure trip point at 18 s. The primary system starts to depressurize after the reactor scram. The steam generator secondary side is dry due to loss of feedwater. The primary pressure decrease is accelerated when the pressurizer gets empty by 221 s.

Before the pump shutdown a steam-water mixture circulates in the primary circuit and through the core at the saturated condition, while the void fraction in the primary system increases due to loss of fluid (mostly liquid) from the hot leg break. During this time the core decay power and pump heat are removed by the steam generators. The primary pumps are shut down when the primary pump void fraction exceeds 0.6 after 5342 s.

After the pump shutdown, the liquid water starts to settle down in the primary circuit and inside the vessel. By this time the break flow rate quickly reduces, changing from mostly liquid to pure steam flow due to liquid stratification in the primary system with hot leg draining. The reactor core starts to uncover at 5682 s because the decay power is no longer removed by natural circulation in the primary circuit.

Cladding oxidation in core begins at 6251 s. The maximum core temperature exceeds 2499K by 7638 s in the stnadard calculation. In the sensitivity calulation, on the other hand, the maximum core temperature exceeds 2499K at 7528 s. It is followed after few seconds by clad failure and first melt relocation. First clad collapse occurs a bit earlier at 7775 s due to higher oxidation rate below 1200 K with the Urbanic-Heidrick correlation. Melt relocation is calculated later on at 7775 s in the sensitivity calculation due to HPI operation. Table 5 presents sensitivity results according to main events.

Table 5. Comparison of Sensitivity Results

Baker-Just Model					
Main Events	Time [s]	Decay Energy [J]	Oxidation Energy [J]	Hydrogen Generation [kg]	Clad Reacted Fraction [%]
Beginning of oxidation	6251	3.297E+11	2.50E+04	7.47E-05	0
Beginning of node collapses	7789	3.716 E+11	2.45E+10	84	18.18
Time of first melt relocation	7794	3.762E+11	2.49E+10	85	18.47
Time reflooding	10342	4.373E+11	6.57E+10	225	48.77
End of the calculation	10422	4.39E+11	6.58E+10	225	48.81

Urbanic-Heidrick Model					
Main Events	Time [s]	Decay Energy [J]	Oxidation Energy [J]	Hydrogen Generation [kg]	Clad Reacted Fraction [%]
Beginning of oxidation	6251	3.297E+11	8.08E+04	2.42E-04	0
Beginning of node collapses	7775	3.755E+11	3.20E+10	110	23.79
Time of first melt relocation	7775	3.755E+11	3.20E+10	110	23.79
Time reflooding	10342	4.289E+11	6.81E+10	238	51.70
End of the calculation	10422	4.38E+11	7.78E+10	292	64.30

21.6 Synthetic Views of the Core

21.6.1 Standard Case

- At the beginning of oxidation

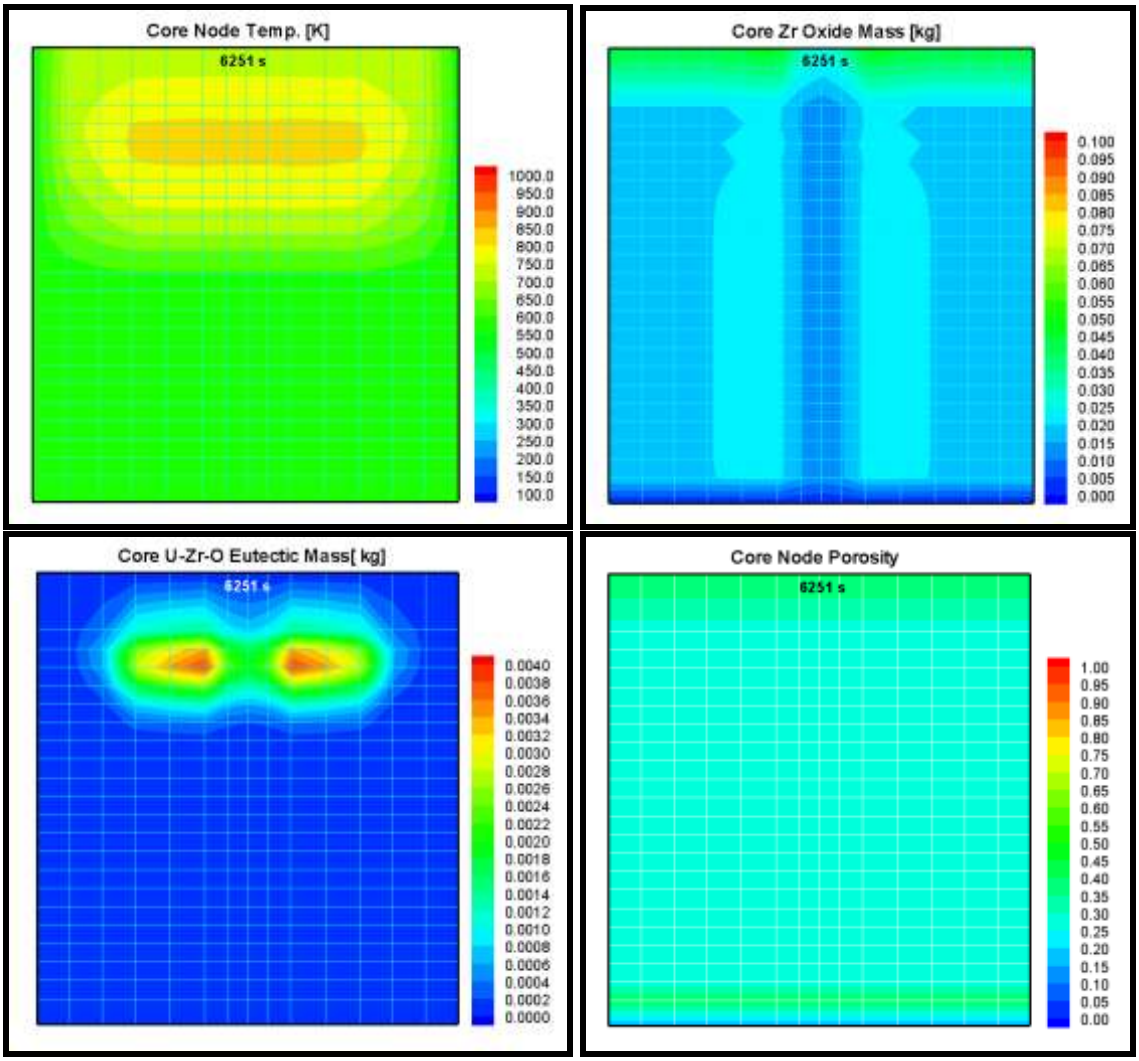

- At the time of first melt relocation

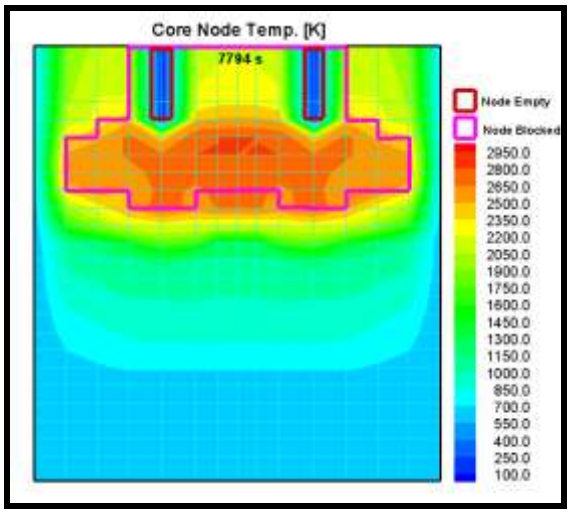

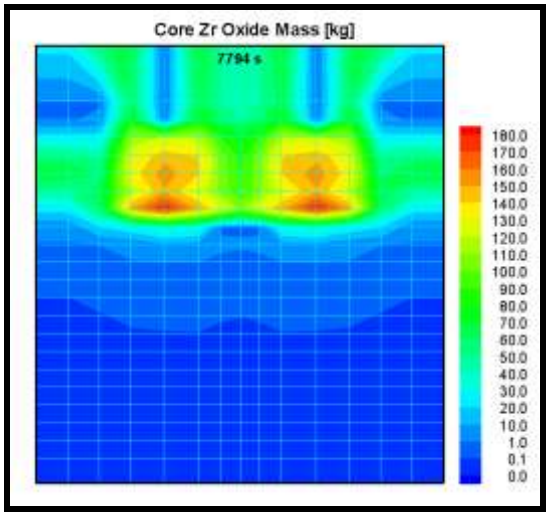

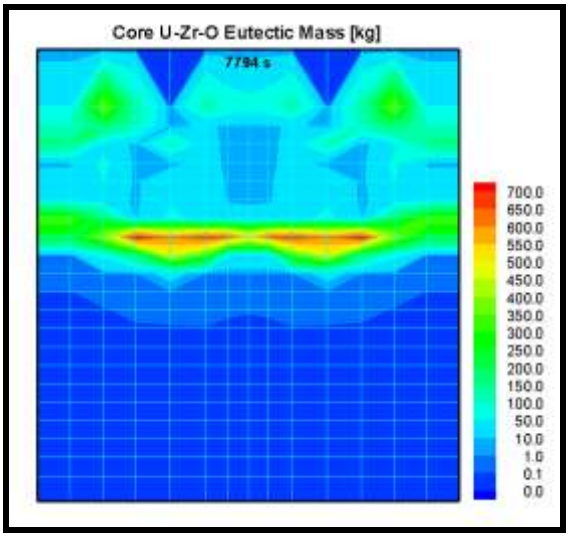

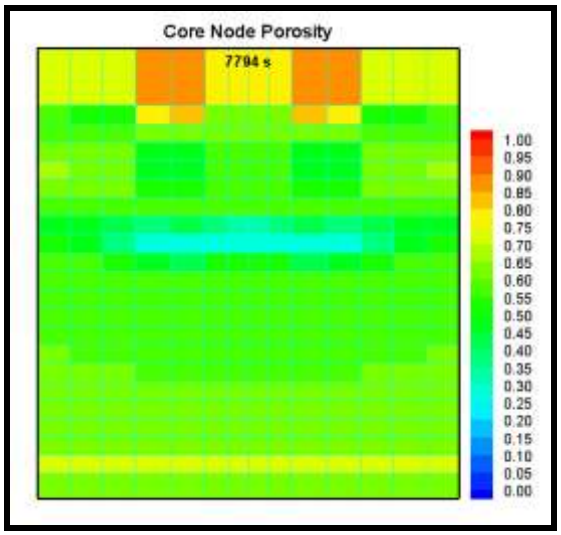

- At the time of reflooding

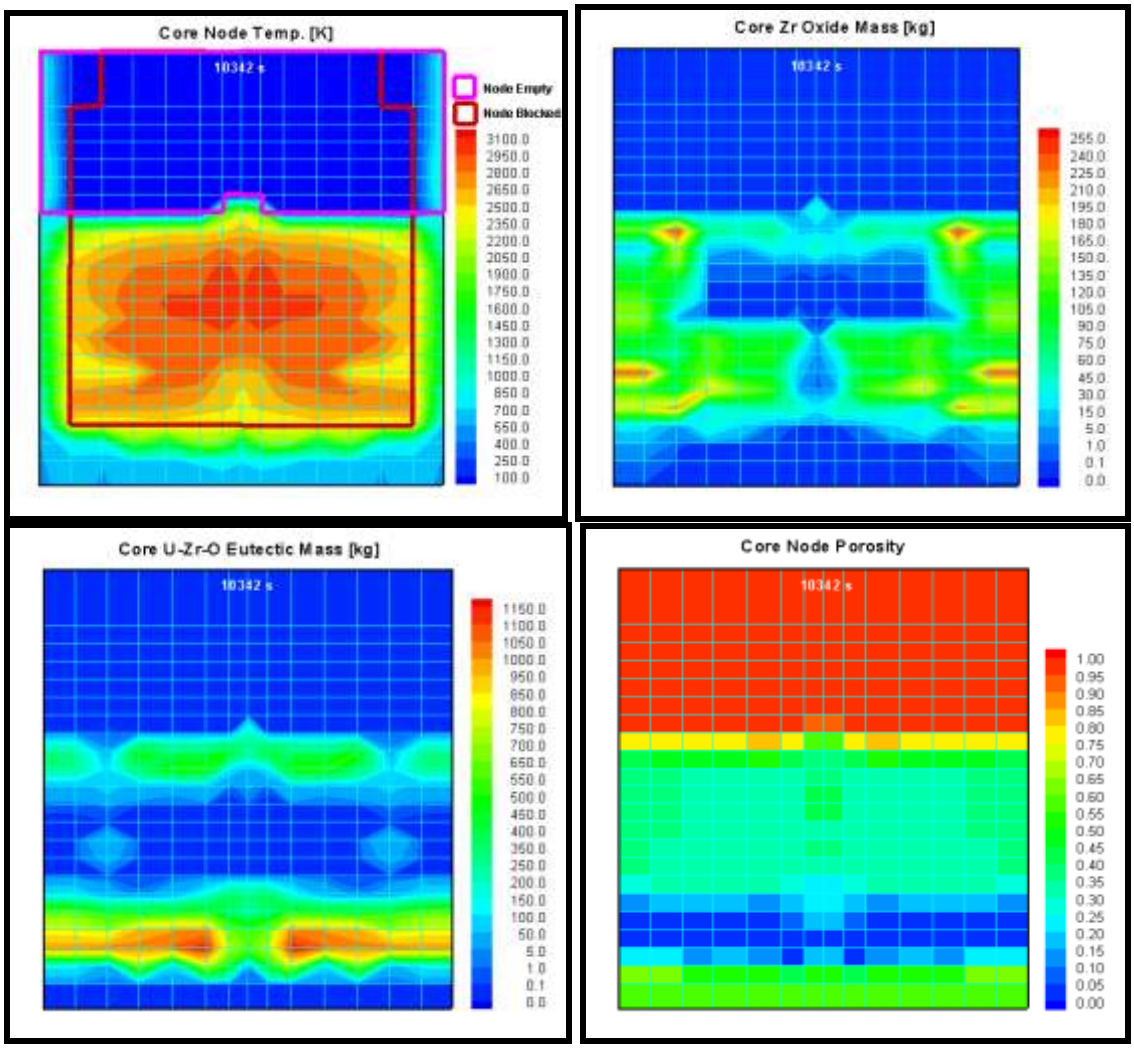

- At the end of the caculation

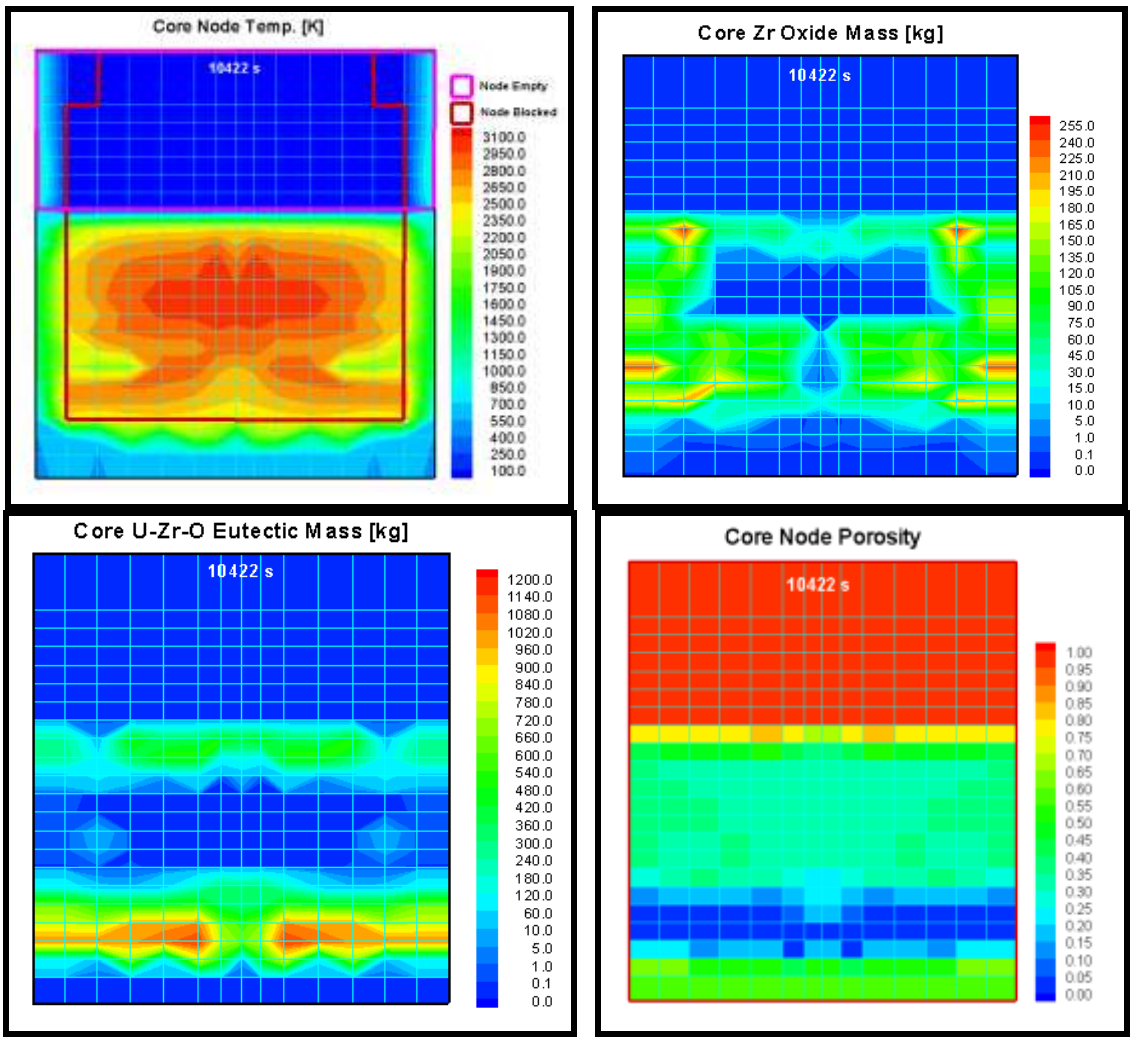

21.6.2 Sensitivity Case

- At the beiginning of oxidation

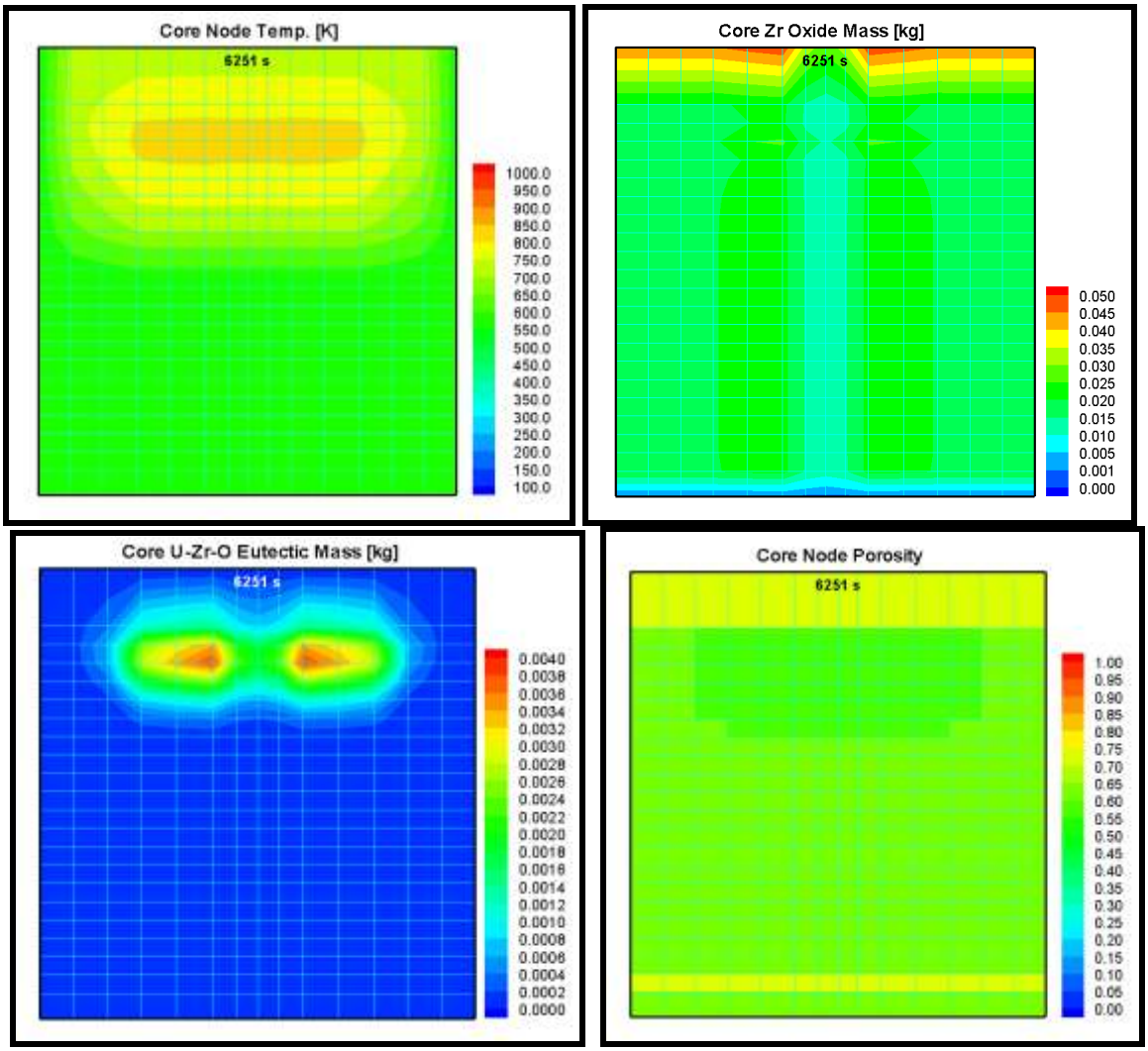

- At the time of first melt relocation

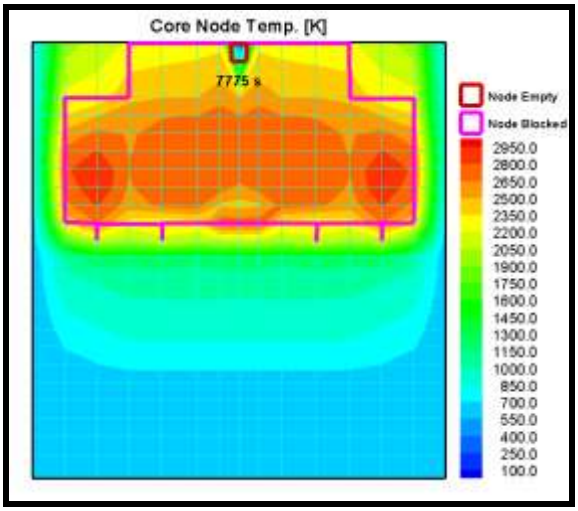

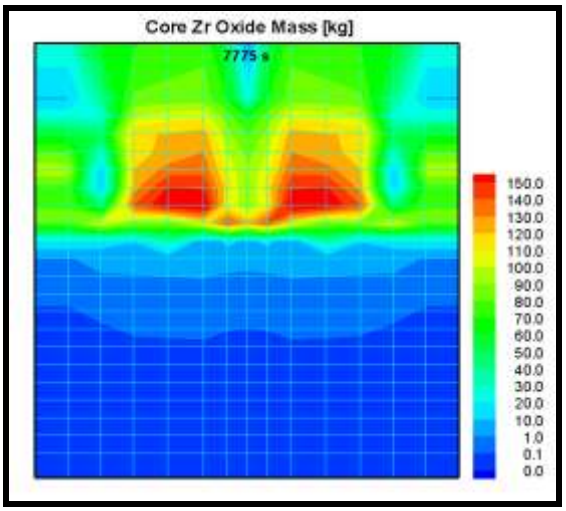

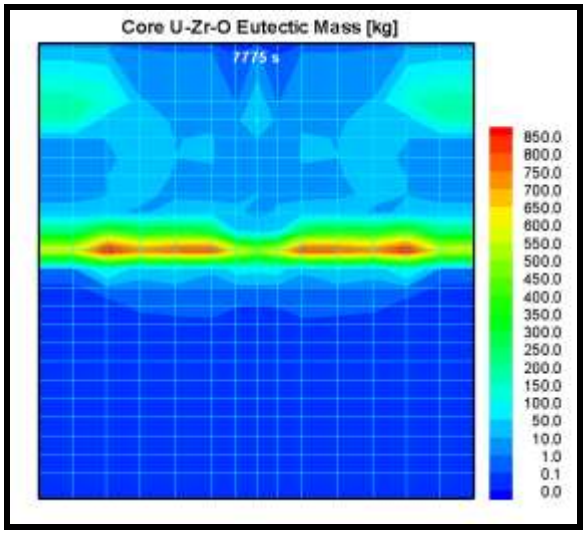

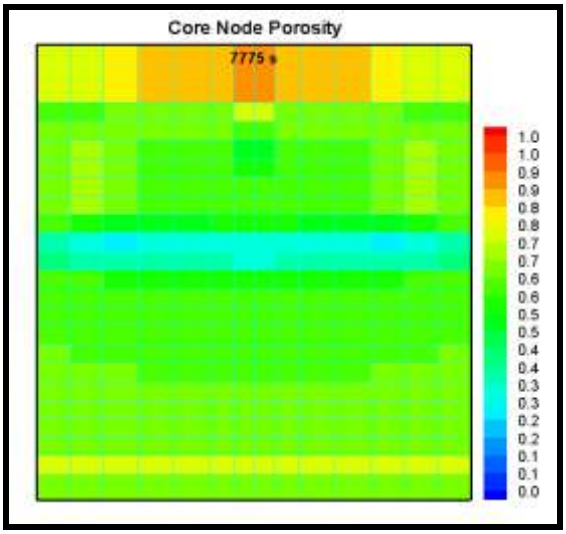

- At the time of reflooding

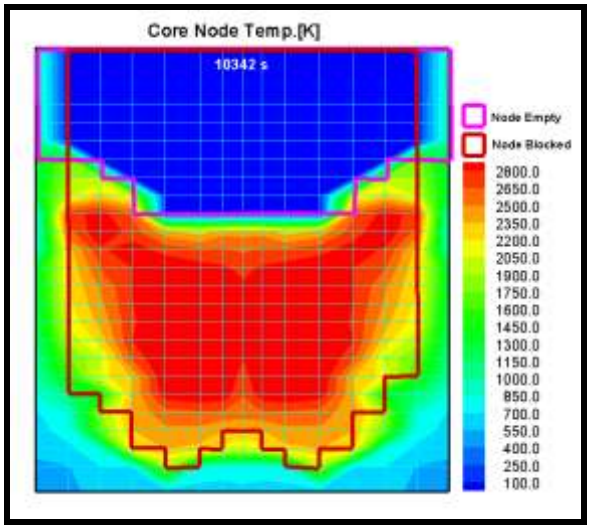

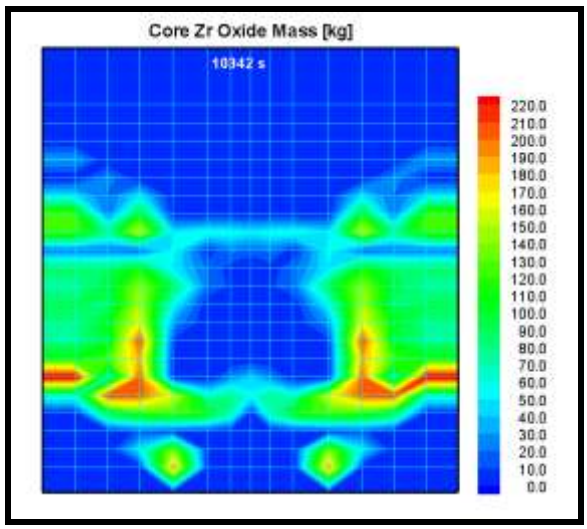

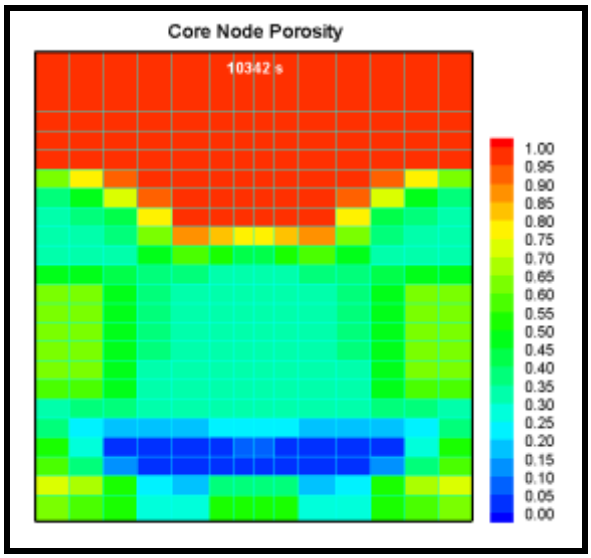

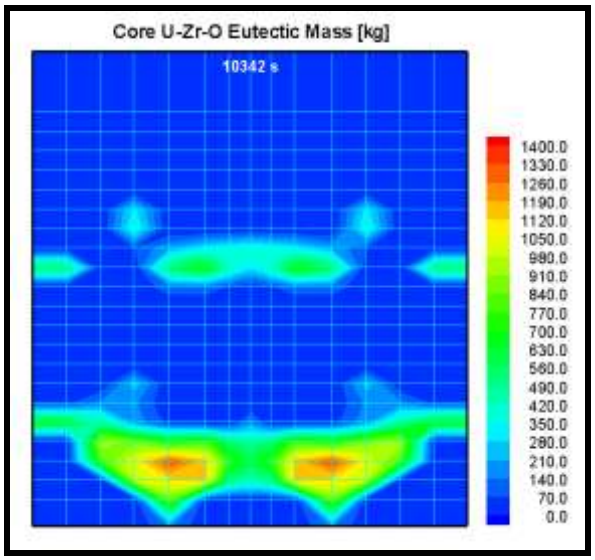

- At the end of the caculation

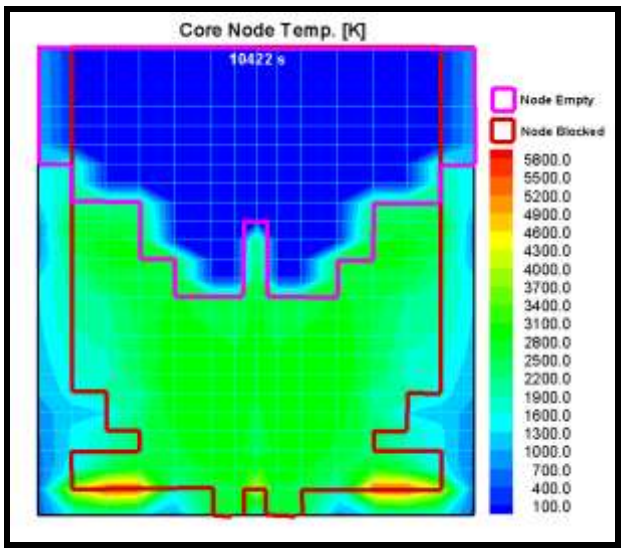

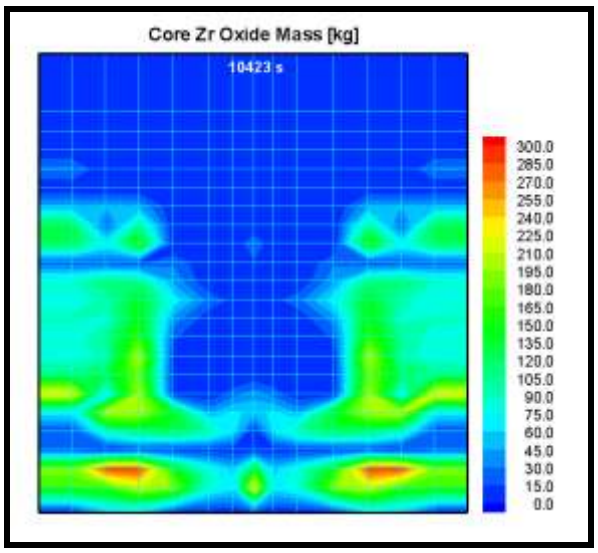

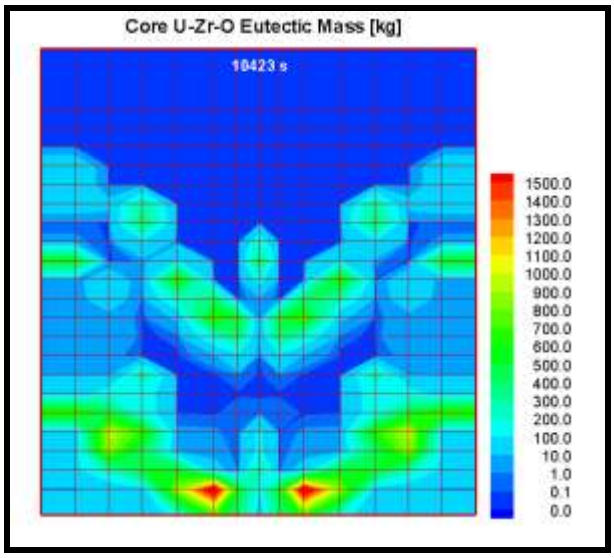

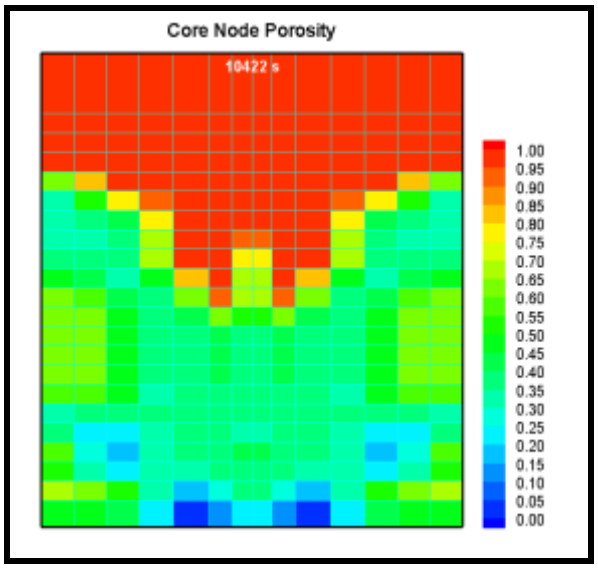

22. APPENDIX : IKE CALCULATION WITH ATHLET/MEWA

The results of the calculations of IKE could not be provided in time to be included in the general presentation of the benchmark results. Therefore, major results of the calculations with ATHLET-CD including the porous media module MEWA are briefly described here.

22.1 TMI-2 Plant Modelling

For the calculations, ATHLET-CD was run with essentially the same input that was used by GRS for the standard calculations (made available by courtesy of Henrique Austregesilo). Thus, the plant modelling ist he same as described in the GRS contribution.

22.2 Main modelling options

Up to the onset of quenching by high pressure injection 5000s after switch-off of the main coolant pump, the modelling options were the same as in the GRS calculation with ATHLET-CD for the standard case.

In the calculations of IKE, the description for the core region was switched to the MEWA model, when the quenching of the core is starting (at about 9700 s). Switching to the MEWA model was done at once, i.e. the formation of a particulate debris bed was assumed to take place instantaneously, not progressively. Temperatures, porosity and melt fractions were derived from the results of the ATHLET-CD calculation with representative rod modelling at this time. A representative particle diameter of 3 mm assumed.

22.3 Discussion of Results

The calculation of IKE with ATHLET-CD only differs from the calculation of GRS for the standard case after onset of quenching, when the MEWA module was activated. For the results up to this point, it is therefore referred to the results of GRS.

Figs. 22-1 to 22-5 show synthetic views of the core status at selected instants. It can be seen that the core is quenched with water rising in lateral, colder and more intact core regions (higher porosity), which then penetrates from the sides into the degraded parts, driven by the outer water head. This cleary demonstrates that multi-dimensional aspects decide about the success of cooling.

The quenching takes quite a long time, due to the slow water penetration into the debris bed. At the end of the calculation, still some parts of liquid metallic melt remain in the compacted region at the bottom of the core, but the temperatures in this part remain below the melting temperature of ceramic corium.Also, the melt region is not increasing in extent any more.

Fig 22-6 shows the development of the pressure in the pressurizer. Up to the onset of quenching it coincides with the respective GRS calculation for the standard case. The pressure increase after about

9700 s during quenching is less pronounced, since the steam production is limited by the water access to the hot regions of the core, which is much slower in the case of the debris bed, due to the large friction.

Concerning hydrogen production shown in Fig 22-7, the ATHLET-CD/MEWA calculation only predicts a very small additional amount of about 25 kg during the quenching phase. According to the calculation, hydrogen production in this phase is limited by steam availability, not by temperature. The low steam availability is again caused by the large friction and thus slow water penetration into the debris bed.

Fig 22-8 and Fig 22-9 show that further degradation and melting of the core is practically stopped after onset of flooding. Only some limited additional melting takes place, while the melt that was present prior to flooding is partly being solidified. The ceramic melt refreezes completely, while parts of metallic melt in a compacted region in the lower part of the core remain liquid still at the end of the calculation.

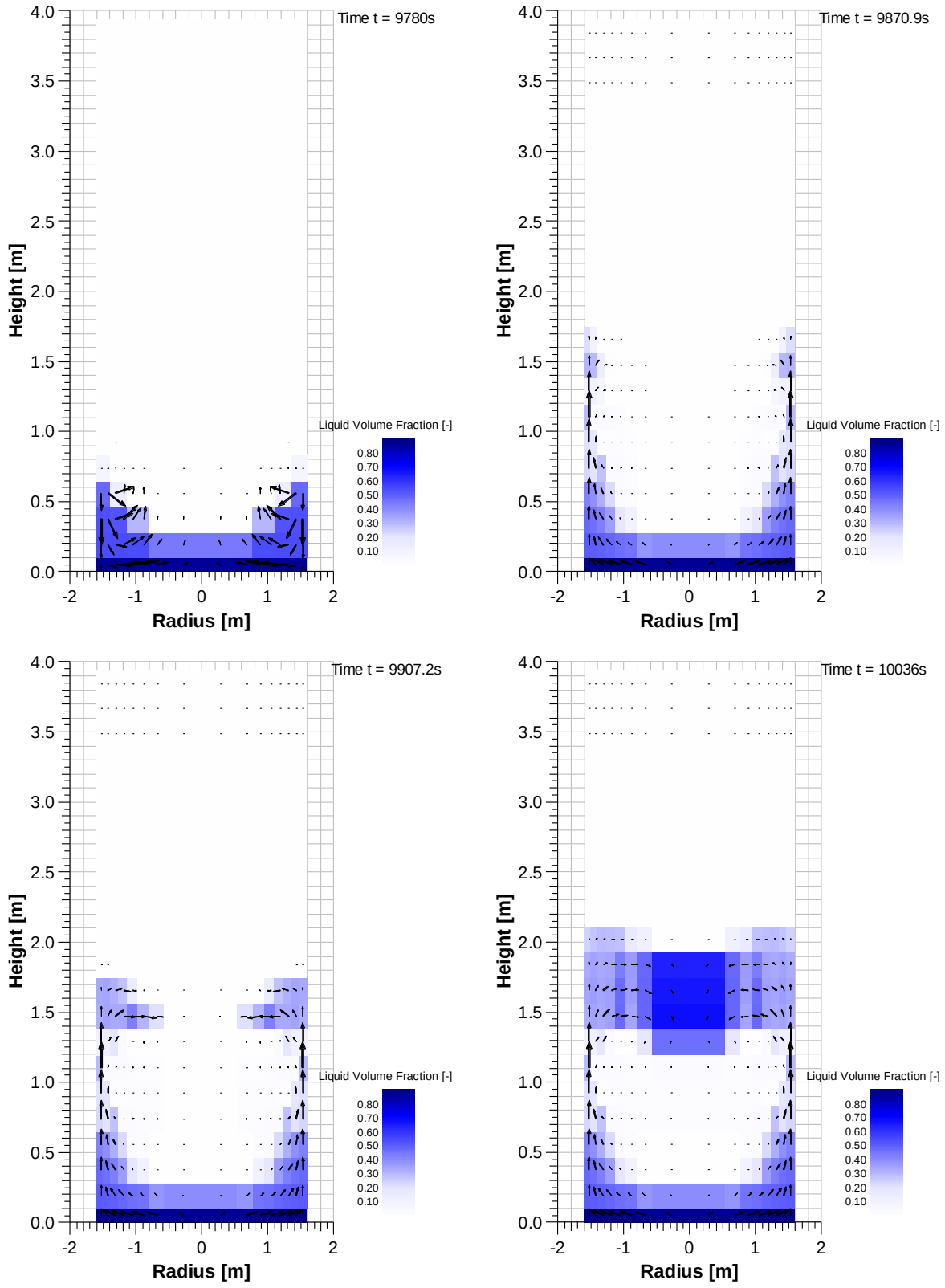

Fig 22-1: Water volume fraction in TMI core during reflooding

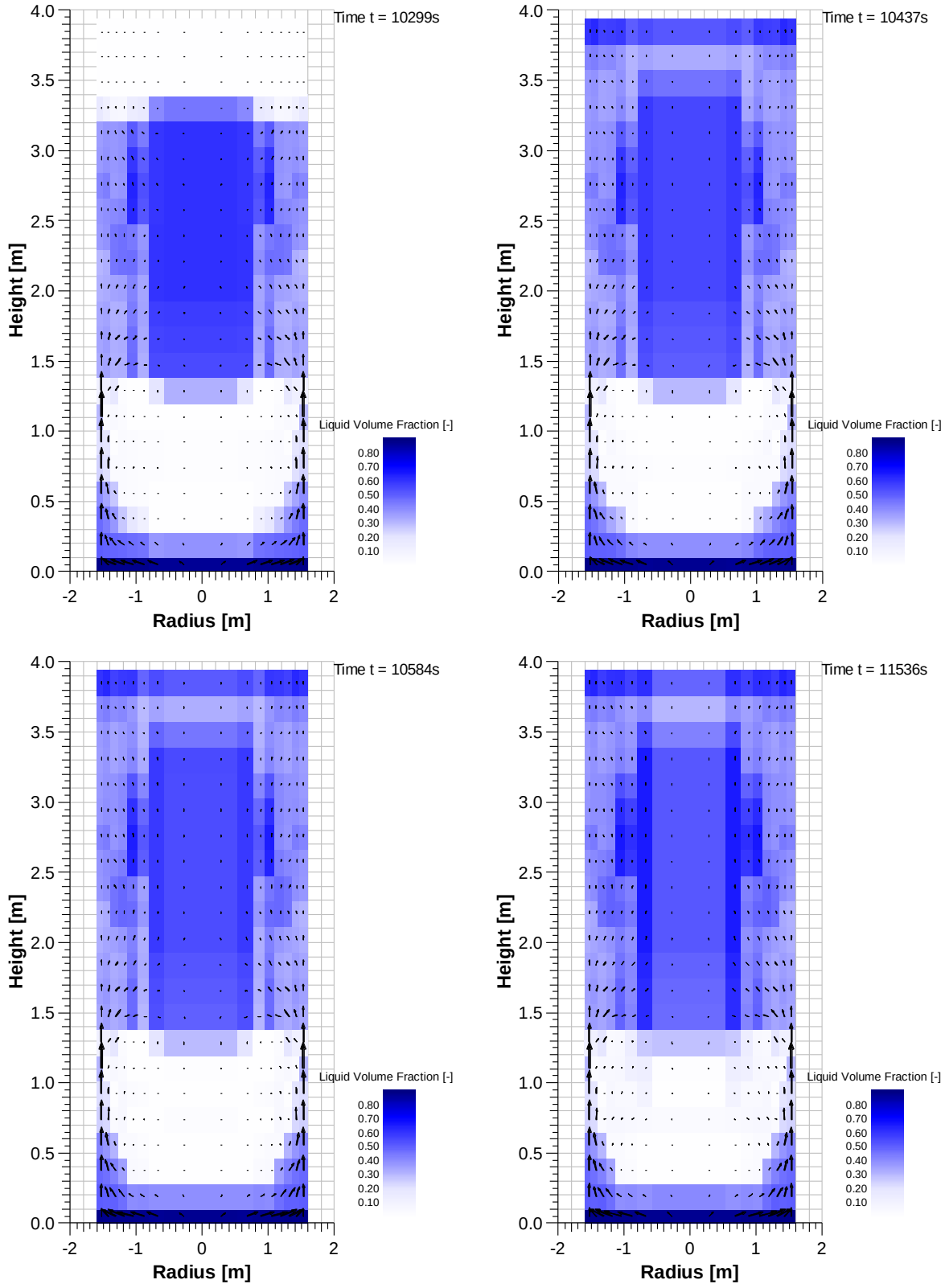

Fig 22-2: Water volume fraction in TMI core during reflooding (continued).

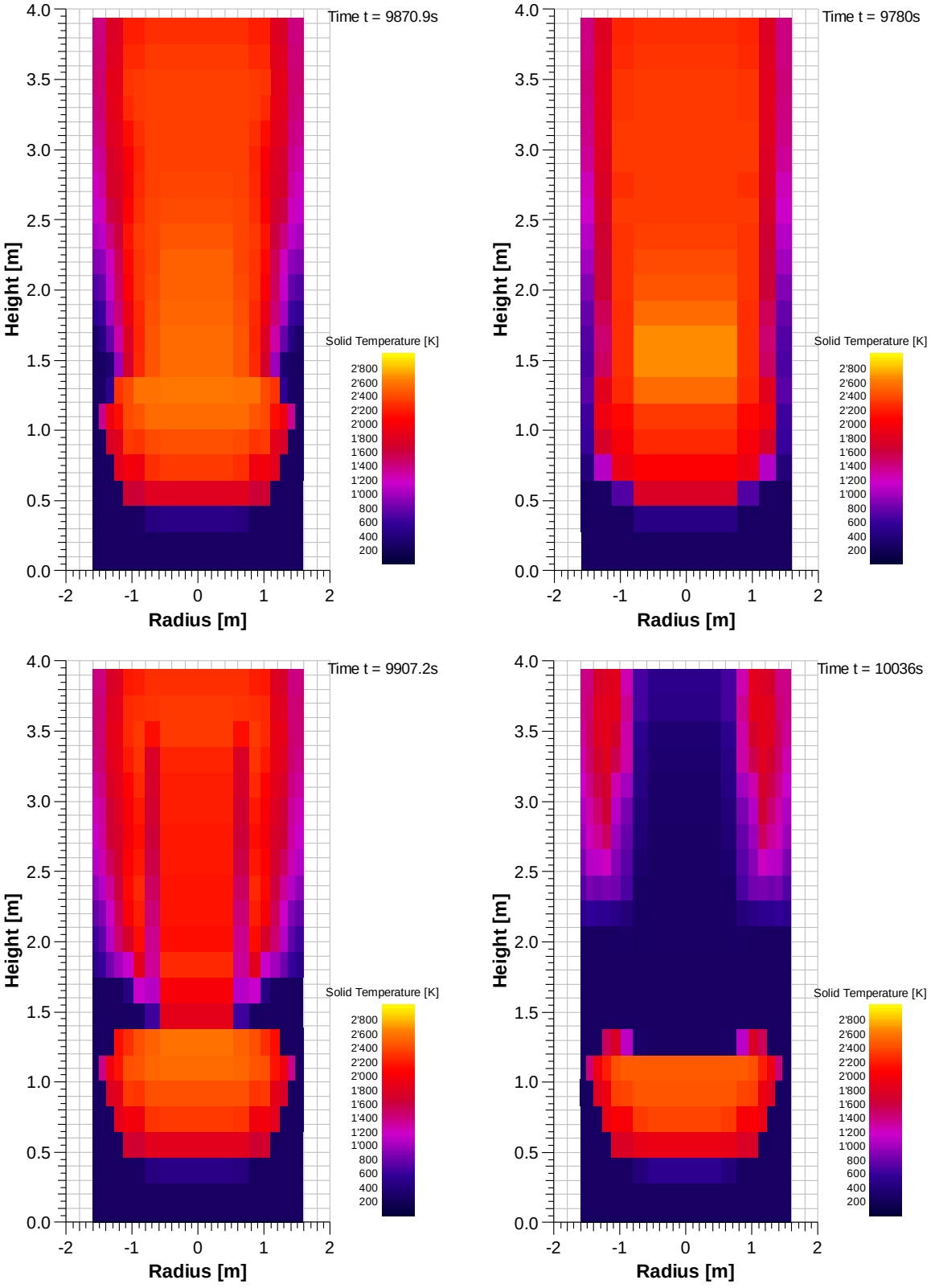

Fig 22-3: Temperature distribution in TMI core during reflooding.

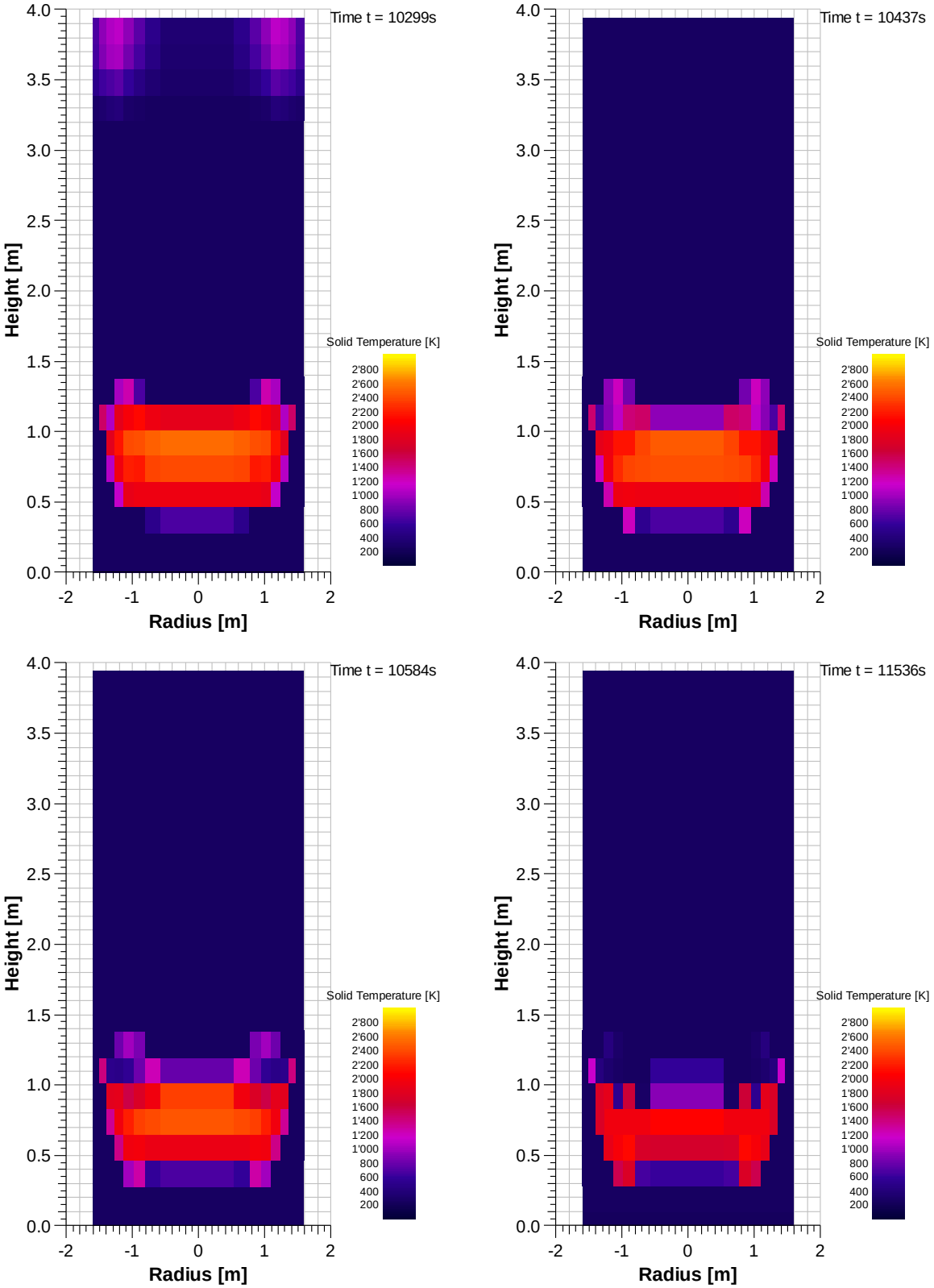

Fig 22-4: Temperature distribution in TMI core during reflooding (continued).

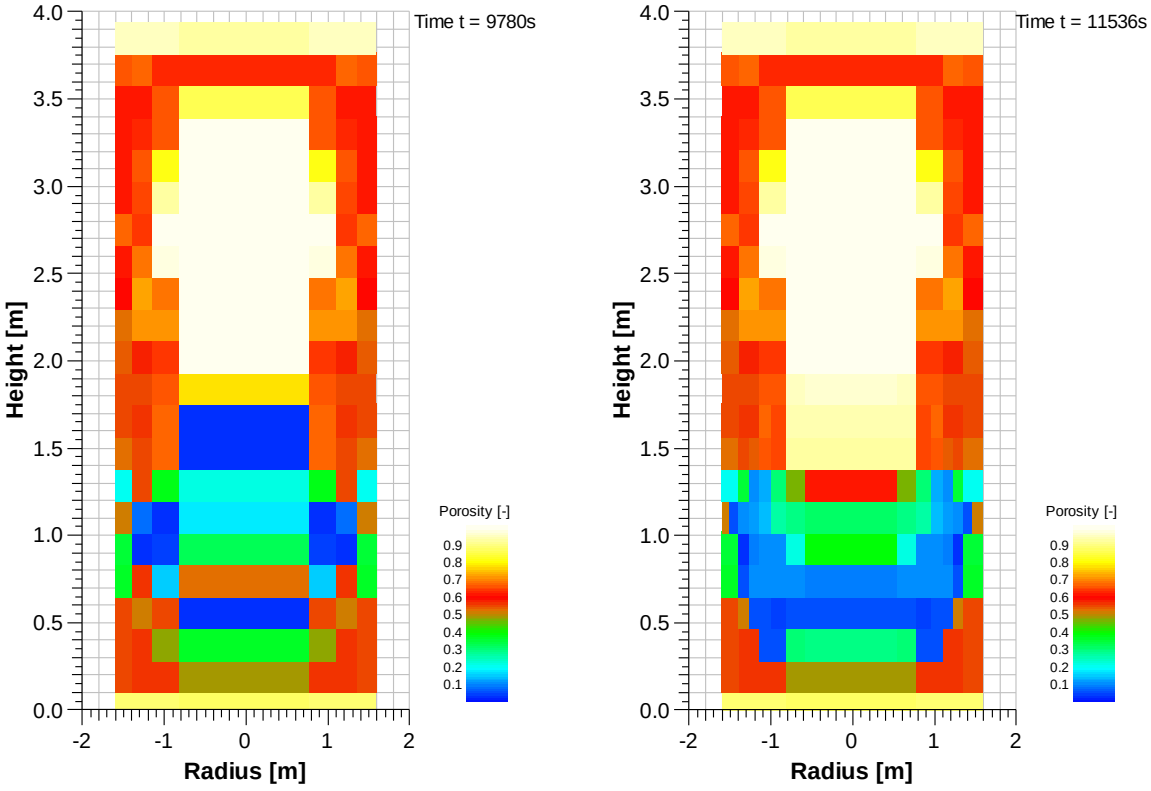

Fig 22-5: Porosity distribution in TMI core during reflooding.

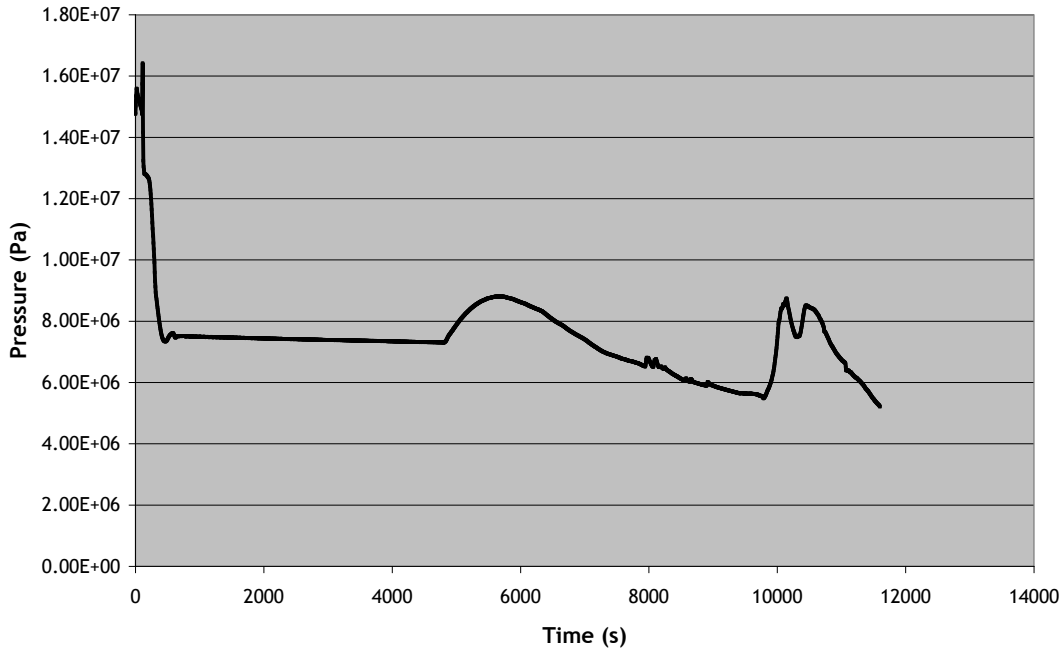

Fig 22-6: Development of pressure in the pressurizer

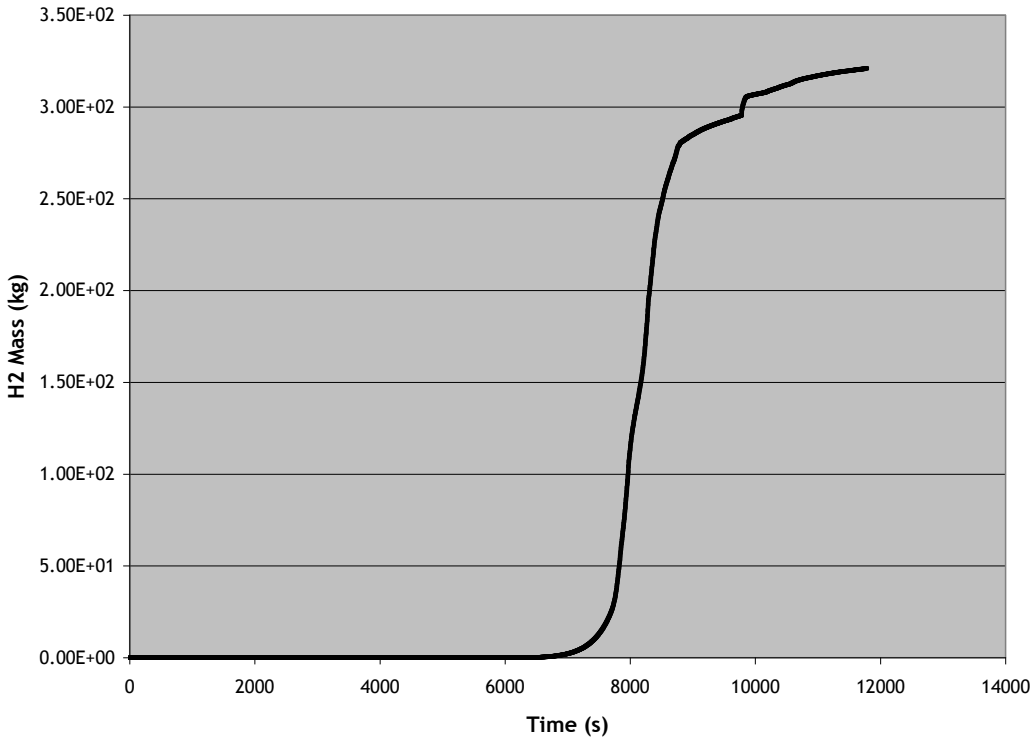

Fig 22-7: Cumulated hydrogen production

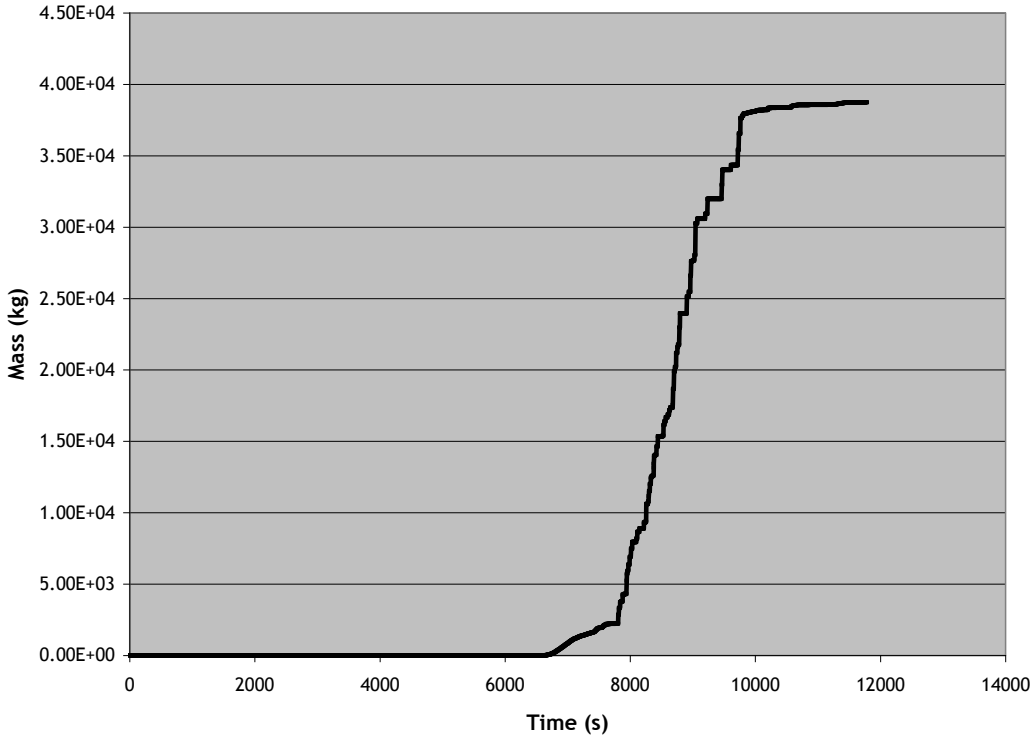

Fig 22-8: Development of total mass of molten materials (i.e. sum of liquid and refrozen melt)

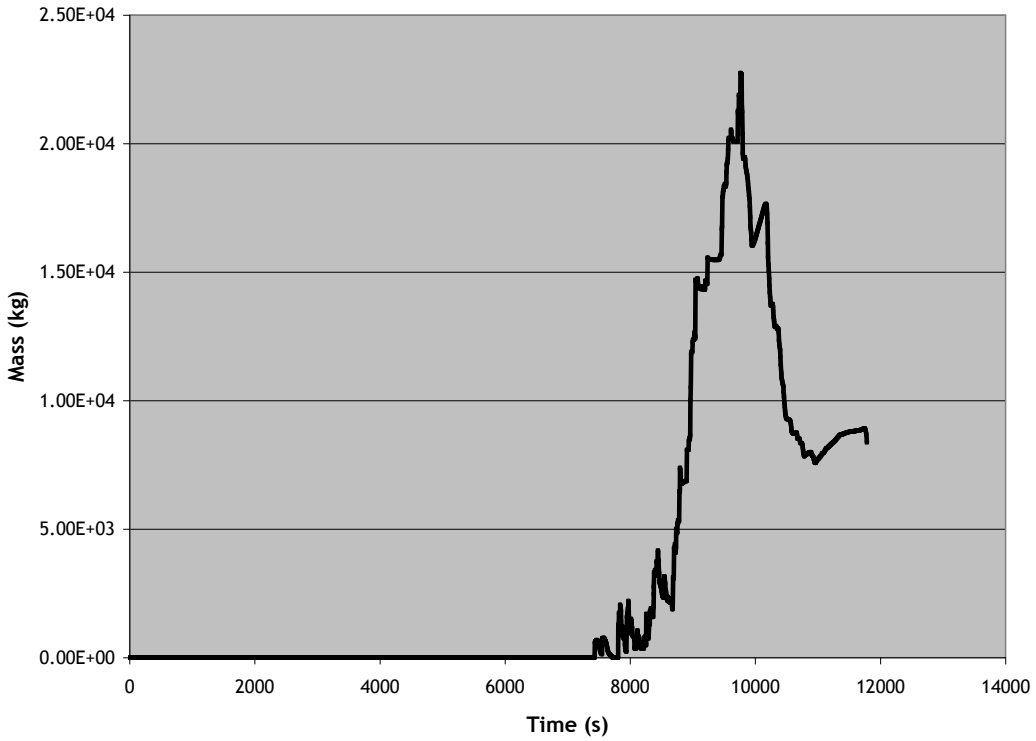

Fig 22-9: Mass of molten pool (liquid melt)

22.4 Additional calculations

In additional calculations, it was tried to evaluate the limits of coolability of the degraded core, i.e. the possibility of reflooding the core before melting further progresses such that an un-coolable situation is reached, due to too large friction in the debris bed (which impedes water access resp. vapour removal). For this, the representative particle diameter was varied. All other parameters were as in the previous calculation. For particles size smaller than 1 mm, complete quenching was not possible any more (see Fig 22-10). The heat-up of the dry parts and melting continues and a larger molten pool is obtained at the end of the calculation (Fig 22-11).

In general, the possibility to quench a particulate debris bed in the core is quite good according to the present calculations. Only in the case of very finely fragmented core (very large friction, representative particle diameter of 1 mm or below) a non-coolable situation is reached. Such core configurations are considered as relatively un-realistic. Of course, in the present case the the coolability is strongly supported by the high pressure. In similar calculations done with MEWA for reactor cases at lower pressures (2-5 bars), limits of coolability were rather obtained for average particle sizes around 2-3 mm. But, also in these cases, it was shown that 2D/3D features strongly help to reflood a strongly degraded core and to establish coolable configurations.

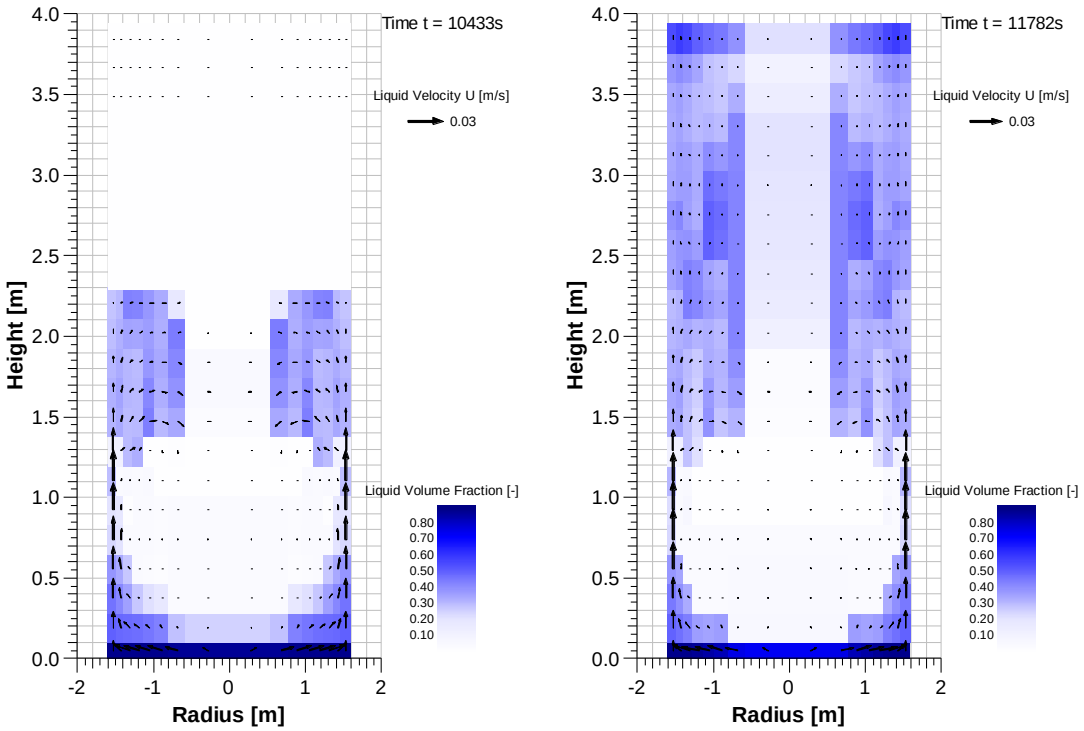

Fig 22-10: Development of water fraction in during reflooding for the case with 1 mm representative particle diameter

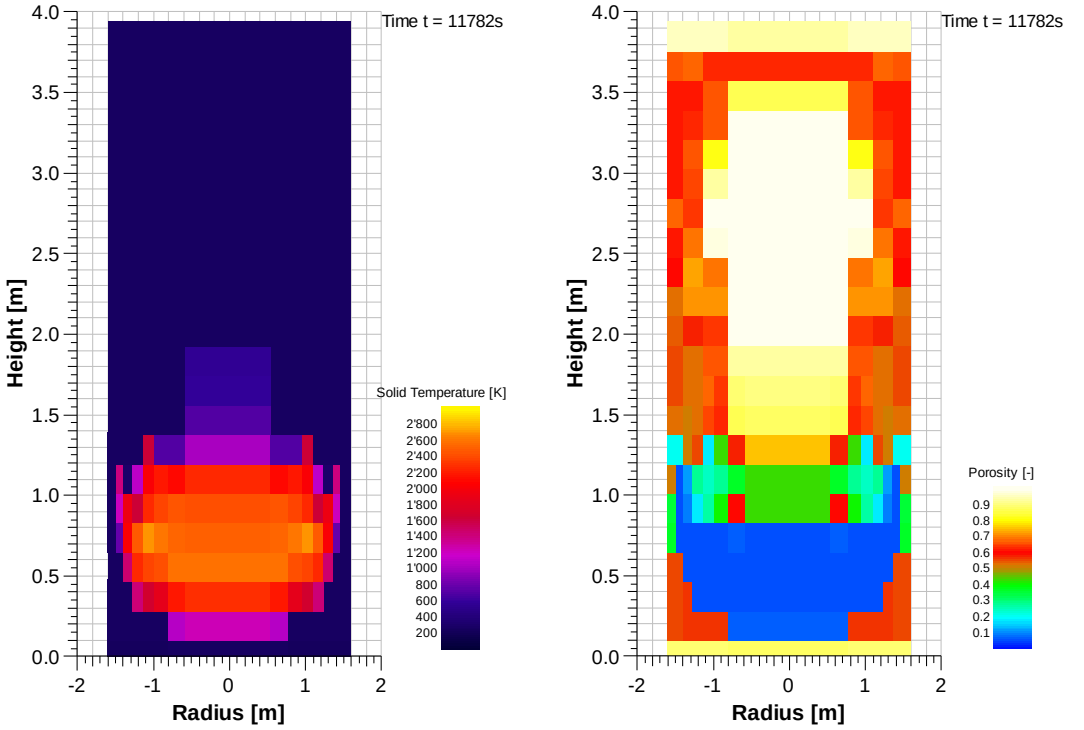

Fig 22-11: Temperature (left) and porosity distribution (right) at the end of the calculation for the case with 1 mm representative particle diameter